

Environmental Research  
of the  
Federal Ministry for the Environment, Nature Conservation and Nuclear Safety  
Chemical and Biological Safety

Final report  
FKZ (UFOPlan) 3710 65 414

**Mobility, fate and behaviour of TiO<sub>2</sub> nanomaterials  
in different environmental media**

by

Carmen Nickel<sup>1</sup>, Bryan Hellack<sup>1</sup>, André Nogowski<sup>2</sup>, Frank Babick<sup>2</sup>, Michael Stintz<sup>2</sup>,  
Hanna Maes<sup>3</sup>, Andreas Schäffer<sup>3</sup>, Thomas A.J. Kuhlbusch<sup>1, 4</sup>

<sup>1</sup> IUTA e.V., Air Quality & Sustainable Nanotechnology, Duisburg, Germany,

<sup>2</sup> TU Dresden - Mechanical Process Engineering, Dresden, Germany,

<sup>3</sup> RWTH Aachen, Biology V, Aachen, Germany,

<sup>4</sup> Center for Nanointegration Duisburg-Essen (CENIDE), Universität Duisburg-Essen,  
Duisburg, Germany

ON BEHALF OF THE

FEDERAL ENVIRONMENT AGENCY

August 2012



## Berichtskennblatt

<b>Berichtsnummer</b>	UBA-FB 001741/E
<b>Titel des Berichts</b>	Mobility, fate and behaviour of TiO <sub>2</sub> nanomaterials in different environmental media
<b>Autor(en) (Name, Vorname)</b>	Carmen Nickel <sup>1</sup> , Bryan Hellack <sup>1</sup> , André Nogowski <sup>2</sup> , Frank Babick <sup>2</sup> , Michael Stintz <sup>2</sup> , Hanna Maes <sup>3</sup> , Andreas Schäffer <sup>3</sup> , Thomas A.J. Kuhlbusch <sup>1,4</sup>
<b>Durchführende Institution (Name, Anschrift)</b>	1 IUTA e.V., Luftreinhaltung & Nachhaltig Nanotechnologie, Duisburg 2 TU Dresden - Mechanische Verfahrenstechnik, Dresden, 3 RWTH Aachen, Biologie V, Aachen, 4 Center for Nanointegration Duisburg-Essen (CENIDE), Universität Duisburg-Essen, Duisburg
<b>Fördernde Institution</b>	Umweltbundesamt Postfach 14 06 06813 Dessau-Roßlau
<b>Abschlussdatum</b>	März 2013
<b>Forschungskennzahl (FKZ)</b>	3710 65 414
<b>Seitenzahl des Berichts</b>	219
<b>Zusätzliche Angaben</b>	
<b>Schlagwörter</b>	TiO <sub>2</sub> Nanomaterialien, Umweltverhalten und Verbleib, Mobilität, Carrier Effekt, Coating Stabilität, Oberflächenfunktionalisierung

## Report Cover Sheet

<b>Report No.</b>	UBA-FB 001741/E
<b>Report Title</b>	Mobility, fate and behaviour of TiO <sub>2</sub> nanomaterials in different environmental media
<b>Author(s) (Family Name, First Name)</b>	Carmen Nickel <sup>1</sup> , Bryan Hellack <sup>1</sup> , André Nogowski <sup>2</sup> , Frank Babick <sup>2</sup> , Michael Stintz <sup>2</sup> , Hanna Maes <sup>3</sup> , Andreas Schäffer <sup>3</sup> , Thomas A.J. Kuhlbusch <sup>1,4</sup>
<b>Performing Organisation (Name, Address)</b>	1 IUTA e.V., Air Quality & Sustainable Nanotechnology, Duisburg, Germany, 2 TU Dresden - Mechanical Process Engineering, Dresden, Germany, 3 RWTH Aachen, Biology V, Aachen, Germany, 4 Center for Nanointegration Duisburg-Essen (CENIDE), Universität Duisburg-Essen, Duisburg, Germany
<b>Funding Agency</b>	Umweltbundesamt Postfach 14 06 06813 Dessau-Roßlau
<b>Report Date</b>	March 2013
<b>Project No. (FKZ)</b>	3710 65 414
<b>No. of Pages</b>	219
<b>Supplementary Notes</b>	
<b>Keywords</b>	TiO <sub>2</sub> nanomaterials, environmental fate and behaviour, mobility, carrier effect, coating stability, surface functionality

## Abstract

In this study two different topics were analysed. The first part dealt with the development of a methodological approach testing the stability of ENM coatings. The methodological approach was tested with two functionalised TiO<sub>2</sub> nanomaterials. The nanomaterials were NM103 (trade name: UV Titan M262) coated with aluminium oxide and dimethicone and NM104 (trade name: UV Titan M212) coated with aluminium oxide and glycerol. The coating stability was analysed under different stress factors like energy input for the suspension preparation as well as different environmental conditions like pH, ionic strength and dissolved organic carbon (DOC) concentration. The second part of this study analysed the carrier function of an uncoated TiO<sub>2</sub> nanomaterial P25 for two different substances, copper and <sup>14</sup>C triclocarban (TCC) in three different soil types. The coating stability of the two coated TiO<sub>2</sub> nanomaterials was measured in different ways: a) by quantifying the released coating material, b) by quantifying the coating material on the nanomaterial prior and after exposure to stress conditions, and c) indirectly by determining changes in the behaviour of the ENM. Based on the results of the different measurements it is concluded that the outer coating dimethicone of NM103 and the glycerol coating of NM104 is mostly released from the surface of the materials. The aluminium oxide layer stays intact even after severe stress conditions. Consequently it presents the surface of the tested TiO<sub>2</sub> ENMs which interacts with the environment. An influence of the ionic strength as well as DOC (here AHA - Aldrich humic acid) on the zeta potential was clearly shown. It seems that especially DOC is of importance and leads to a (steric) stabilisation of the ENMs and a negative zeta potential. In the second part the mobility of copper and TCC and the carrier effect of P25 for these substances was analysed. The added P25 showed a low mobility in the soil types and only with SEM / EDX a transport of single agglomerates was detectable. It was also shown that by trend P25 reduced the transport of copper and TCC through soil columns. The reduced mobility of the substances could lead to accumulation in upper soil layers. This is important for organisms that especially live in these layers like earthworms. Ecotoxicological tests with *Eisenia fetida* conducted in the framework of this study show that the presence of TiO<sub>2</sub> leads to higher fractions of TCC in the gut but also to lower negative effects of the compound towards this organism. Nevertheless, it was shown that ENMs, here TiO<sub>2</sub> might have a significant influence on the fate of environmentally important pollutants.

## Kurzbeschreibung

In dieser Studie wurden zwei verschiedene Fragestellungen bearbeitet. Die erste Untersuchung betraf die Entwicklung einer Prüfmethode zur Beurteilung der Stabilität von Beschichtungen auf TiO<sub>2</sub>-Nanopartikeln. Dazu wurden zwei verschiedenen funktionalisierte TiO<sub>2</sub>-Nanomaterialien untersucht, NM103 (Handelsname: UV Titan M262) mit einer Aluminiumoxid und einer hydrophoben Dimethicone Beschichtung und NM104 (Handelsname: UV Titan M212) mit einer Aluminiumoxid und einer hydrophilen Glycerin Beschichtung. Die Stabilität der Beschichtung wurde in Abhängigkeit von verschiedenen Einflussfaktoren, wie dem Energieeintrag zur Herstellung der Suspension und den Umgebungsbedingungen wie pH-Wert, Ionenkonzentration und dem gelösten organischen Kohlenstoff (DOC), getestet. Im zweiten Teil der Studie wurde die „Carrier“-Funktion von P25 für Kupfer sowie <sup>14</sup>C Triclocarban (TCC) in drei verschiedenen Bodenarten untersucht.

Die Stabilität der Beschichtung der zwei beschichteten TiO<sub>2</sub> Nanomaterialien wurde auf verschiedene Arten getestet: a) durch die quantitative Bestimmung des freigesetzten Beschichtungsmaterials, b) durch die quantitative Bestimmung des Beschichtungsmaterials auf dem Trägermaterial vor und nach dem Belastungstest sowie c) indirekt durch die Untersuchung der Änderungen im Verhalten der ENMs. Die Messergebnisse zeigen, dass die Dimethicone und Glycerol Beschichtungen größtenteils von der Oberfläche des Materials freigesetzt wurden. Die Aluminiumoxid-Schicht bleibt hingegen bei beiden ENMs intakt auf der Oberfläche. Des Weiteren wurde gezeigt, dass sowohl die Ionenstärke als auch die DOC Konzentration einen Einfluss auf das Zeta-Potential der ENMs haben. Speziell der Einfluss des DOC (hier Aldrich humic acid - AHA), welcher in dieser Studie zu einer (sterischen) Stabilisierung der ENMs führte, scheint für das weitere Verhalten in der Umwelt von Bedeutung zu sein.

Im zweiten Teil dieser Studie wurde die Mobilität von Kupfer und TCC und der „Carrier“-Effekt von P25 auf diese Substanzen analysiert. Das P25 zeigte eine geringe Mobilität in den getesteten Böden und nur mittels REM / EDX konnte ein Transport einzelner P25 Agglomerate nachgewiesen werden. Tendenziell zeigten die mit P25 beaufschlagten Bodensäulen einen geringeren Transport der beiden Substanzen als die Säulen ohne P25 und können daher zur Ausbildung von Akkumulationschichten im oberen Bodenbereich führen. Dieses ist bedeutsam für Bodenorganismen welche sich vornehmlich in diesen Schichten aufhalten, wie zum Beispiel Regenwürmer. Ökotoxikologische Untersuchungen mit *Eisenia fetida*, welche im Rahmen dieser Studie durchgeführt wurden, zeigten, dass, bei Anwesenheit von P25 mehr TCC in den Darm der Organismen aufgenommen wurde, dieses aber einen geringeren negativen Effekt zeigte. Nichtsdestotrotz wurde gezeigt, dass ENMs hier speziell TiO<sub>2</sub> einen Einfluss auf das Verhalten von Schadstoffen haben.

## List of Content

Symbols and abbreviations.....	XXV
1 Introduction.....	1
2 Methods, characterisation techniques and measurands.....	3
2.1 Measurements techniques.....	5
2.1.1 Dynamic light scattering (DLS) .....	6
2.1.2 Electrophoretic zeta potential measurement.....	7
2.1.3 Chemical analysis (LC-MS, ICP-OES).....	9
2.1.4 Scanning electron microscopy coupled with energy dispersive X-ray spectroscopy (SEM / EDX).....	10
2.1.5 Electron Paramagnetic Resonance (EPR) Spectroscopy.....	11
2.1.6 Nuclear magnetic resonance (NMR) spectroscopy .....	12
2.1.7 Radioanalytics.....	12
3 Surface coating stability.....	14
3.1 Background .....	14
3.2 Materials .....	14
3.2.1 Preliminary remarks on surface coating stability.....	16
3.3 Suspension preparation .....	16
3.4 Results.....	17
3.4.1 Stock suspension preparation .....	17
3.4.2 Results – Surface coating stability NM104 (UV Titan M212).....	20
3.4.3 Results – Surface coating stability of NM103 (UV Titan M262).....	26
3.4.4 Further surface properties of NM103 & NM104.....	30
3.5 Summary and conclusion stability surface coating .....	33
3.6 Influence of pH, ionic strength and natural organic matter concentration on the interfacial properties.....	34
3.6.1 NM in CaCl <sub>2</sub> solutions.....	35
3.6.2 Aging of suspensions in CaCl <sub>2</sub> solutions .....	39
3.6.3 NM in DOC solutions .....	40
3.6.4 Aging of suspensions in DOC-solutions .....	43
3.7 Résumé for the environmental behaviour .....	43
4 Soil experiments.....	45
4.1 Background .....	45
4.2 Materials and Method.....	45
4.3 Selection of pollutant.....	46
4.4 Titanium dioxide nanomaterial selection .....	47
4.5 Nanomaterial suspension.....	48

4.6	Soils.....	48
4.6.1	Soil spiking.....	49
4.7	Study design .....	49
4.8	Results.....	51
4.8.1	Physical-chemical properties of P25 suspension.....	51
4.8.2	Mobilisation of copper sulphate by P25.....	52
4.8.3	Titanium dioxide.....	54
4.8.4	Mobilisation of Triclocarban by P25.....	56
4.9	Bioavailability for Lumbricidae.....	59
4.10	Discussion - Mobility of TCC and copper affected by P25.....	64
5	Summary and conclusion .....	66
6	Literature.....	70
7	Annex.....	75
	Annex I Measurement techniques .....	76
AI.1	Dynamic Light Scattering.....	76
AI.2	Zeta potential.....	77
	Annex II - Standard operation procedure - SOPs .....	80
AII.1	Standard operation procedure - Preparing titanium dioxide (stock) suspension .....	80
AII.2	Standard operation procedure - Particle size and zeta potential measurements by using Dynamic Light Scattering (DLS).....	84
AII.3	Standard operation procedure - zeta potential measurements using microelectrophoresis (μEP).....	91
AII.4	Standard operation procedure - Liquid chromatography measurements.....	94
AII.5	Standard operation procedure - enzymatic UV Tests .....	98
AII.6	Standard operation procedure - radioanalytics.....	102
AII.7	Standard operation procedure - inductively coupled plasma optical emission spectrometry (ICP-OES).....	105
AII.7.1	Standard operation procedure (SOP) - ICP-OES measurements of applied substances in natural soils .....	105
AII.7.2	Standard operation procedure (SOP) - ICP-OES measurements in the eluate of natural soils.....	109
AII.7.3	Standard operation procedure (SOP) - ICP-OES measurements of Aluminium and Silicon in solid samples.....	113
AII.7.4	Standard operation procedure (SOP) - ICP-OES measurements of Aluminium and Silicon in liquid samples.....	117
AII.8	Standard operation procedure - Carrier effects of nanoscale particles in soil columns.....	121



Annex III Results of the Coating Characterisation .....	127
AIII.1 Basic characterisation of NM104 and NM103.....	127
AIII.1.1 Fourier transform infrared spectroscopy (FTIR) measurements of the powder of both coated titanium dioxide nanomaterials .....	127
AIII.1.2 Low energy ion scattering (LEIS) measurements of the two materials.....	127
AIII.1.3 Time of Flight Secondary Ion Mass Spectrometry (ToF SIMS) analysis of the powder of both coated titanium dioxide nanomaterials.....	128
AIII.2 Comparison measurement and validation of the enzymatic UV test and the LC-MS analysis .....	134
AIII.3 Dispersibility tests of NM104 and NM103 .....	135
AIII.4 Stability of the stock suspensions from NM103 & NM104 .....	137
AIII.5 Zeta potential measurements of NM103 and NM104 .....	138
AIII.5.1 Hysteresis of ELS measurements.....	138
AIII.6 EPR measurements of the two coated TiO <sub>2</sub> nanomaterials NM104 and NM103	140
AIII.7 NMR measurements of NM104 and NM103 .....	142
AIII.8 Zeta potential measurements of NM104 and NM103 as function of pH in deionised water as basic characterisation .....	145
AIII.9 Zeta potential measurements in environmental like media.....	146
AIII.9.1 Zeta potential measurements of NM103 and NM104 in environmental like media – variation of ionic strength .....	146
AIII.10 Agglomeration in environmental media – DLS.....	154
AIII.11 Zeta potential measurements of NM104 and NM103 in environmental like media – variation of dissolved organic carbon (DOC) concentration .....	157
Agglomeration in environmental media – DLS .....	164
AIII.12 Zeta potential measurements of NM104 and NM103 in environmental like media – in a mixture of CaCl <sub>2</sub> and dissolved organic carbon (DOC) .....	166
Annex IV Results of the soil experiments .....	167
AIV.1 Detailed analysis data of the employed soils .....	167
AIV.2 Quality assurance ICP-OES measurements of the soil samples.....	168
AIV.3 Breakthrough curves of the tested soil types .....	169
AIV.4 Background concentration of Ti and Cu in the tested soil types.....	171
AIV.5 Results Zeta potential measurements different TiO <sub>2</sub> materials in DI water, 0.01M CaCl <sub>2</sub> solution and soil eluate.....	172
AIV.6 Results carrier function triclocarban.....	175
AIV.6.1 Soil Type A01 .....	175
AIV.6.2 Soil Type A02 .....	175
AIV.6.3 Soil Type G03 .....	176

AIV.7 Results carrier function copper sulphate.....	177
AIV.7.1 Soil type A01 .....	177
AIV.7.2 Soil type A02.....	178
AIV.7.3 Soil type G03.....	179
AIV.7.4 Eluate .....	180
AIV.8 Results titanium transport ICP-OES and SEM / EDX scans.....	181
AIV.8.1 Soil type A01 .....	181
AIV.8.2 Soil type A02.....	181
AIV.8.3 Soil type G03.....	182
AIV.8.4 Eluate .....	183
AIV.9 SEM / EDX scans of different soil segments.....	184
AIV.9.1 Soil type A01 .....	184
AIV.9.2 Soil type A02.....	188
AIV.9.3 Soil type G03.....	190

## List of Figures

Figure 1: Number of total products listed, by date of inventory update, with regression analysis (left), number of listed products associated with specific ENMs (right), Woodrow Wilson Database, 2012. ....	1
Figure 2: Triclocarban (TCC) with <sup>14</sup> C label (*) at the monochlorinated phenyl ring.....	12
Figure 3: Average size ( $x_{Cum}$ ) and polydispersity index from dynamic light scattering measurements, when prepared according to SOP – evolution with time, left: NM103, right: NM104; n = 10 (repeated measurements).....	19
Figure 4: Quantitative measurements of the glycerol content of 100 mg/L NM104 suspension preparation using an enzymatic UV test and LC-MS measurements. The dashed lines indicate the glycerol content based on the manufactures data and based on own OC (organic carbon) measurements (incl. 75er and 25er percentile) using a sunset EC/OC (elemental and organic carbon) analyser; n = 3. ....	22
Figure 5: Zeta potential measurements of 100 mg/L NM104 in DI water, suspension preparation based on SOP; two measurement techniques were applied ELS and $\mu$ EP; n = 3.....	24
Figure 6: SEM / EDX scan of the dry powder of NM104.....	25
Figure 7: SEM / EDX scan of the NM104 suspension (preparation based on SOP). Background C-Tab and Cu mesh. The scan of Area 1 (upper diagram) shows the EDX analysis of titanium agglomerates, whereas area 2 showed the EDX results for an area close to the agglomerate (background).....	26
Figure 8: Average of ICP-OES measurements of the silicon content of 100 mg/L NM103 after dispersion by mixing and after standard operation procedure (SOP - 1 min sonication, 60 min stirring). The line indicate the silicon concentration based on ICP-OES measurements of the dry powder of the material; error bars = standard deviation, n = 3. ....	27
Figure 9: Two zeta potential test series of 100 mg/L NM103 in DI water, suspension preparation based on SOP, error bars = standard deviation; n = 3.....	28
Figure 10: SEM / EDX scan of the dry powder of NM103.....	29
Figure 11: SEM / EDX scan of the NM103 suspension (preparation based on SOP). Background C-Tab and Cu mesh. The scan of Area 1 (upper diagram) showed the EDX results for an area close to the agglomerate (background). Area 2 (lower diagram) shows the EDX analysis of a titanium agglomerate. ....	30

Figure 12: Hydroxyl radical generation of the coated titanium dioxide material NM104, NM103 and the uncoated P25 with and without UV irradiation, suspension preparation based on SOP, pH 5; mean values of n = 3.....33

Figure 13: Zeta potential for NM103 and NM104 in CaCl<sub>2</sub> solution, ELS (continuous titration from acid to basic); n = 3. ....37

Figure 14: Zeta potential as function of pH for NM103 (left) and NM104 (right) dispersed according to the SOP in DI-water, measured with ELS (continuous titration: acid → basic → acid), 3 independent sample preparations.....37

Figure 15: Zeta potential as function of pH for NM104, dispersed according to the SOP in DI-water (left) and in 0.001 M CaCl<sub>2</sub>, measured with μEP (discrete titration), 3 independent sample preparations..... 38

Figure 16: Zeta potential as function of pH for NM104 in 0.0001 M CaCl<sub>2</sub> (left) and 0.01 M CaCl<sub>2</sub> (right), ELS (continuous titration acid → basic (upper measurements points) and back from basic → acid (lower measurement points) μEP (discrete titration), n = 3. ....39

Figure 17: Zeta potential as function of pH for NM104 in 0.001 M CaCl<sub>2</sub>, measured with ELS (continuous titration acid → basic → acid; left) and μEP (discrete titration; right) on a freshly prepared and an aged suspension, n = 3. ....39

Figure 18: Zeta potential measurements of NM104 in DOC solution with 0.001 M CaCl<sub>2</sub> background, ELS (continuous titration from acid to basic); error bars = standard deviation; n = 3. ....43

Figure 19: Texture of the tested soil types; [www.refesol.de](http://www.refesol.de).....49

Figure 20: Cumulative intensity (left diagram) and particle size distribution (right diagram) of the particle diameter weighted in scattering intensity measured with DLS for P25 suspended in DI water at pH 5 directly after dispersion and 24 h later; error bars = standard deviation; mean value of n = 9. ....51

Figure 21: Average Copper concentration of the different segments of the three different soil types, without P25; n = 3. An average amount of 186 mg Cu (SD: 270) were applied to the soils, all presented values are background corrected.....53

Figure 22: Average copper concentration of the different segments of the three different soil types, with P25; n = 3. An average amount of 186 mg Cu (SD: 270) were applied to the soils, all presented values are background corrected.....54

Figure 23: SEM and EDX Scan of segment 7 of column one of soil type A01.....55

Figure 24: SEM and EDX Scan of segment 7 of column two of soil type A02.....55

Figure 25: SEM and EDX Scan of segment 7 of column two of soil type G03..... 56

Figure 26: Triclocarban (TCC) concentration in the middle (core) of five segments (0-1, 1-2, 2-3, 3-4, and 5-11 cm) of columns filled with three different soil types (A01, A02, and G03) in absence of P25 (n = 1) upper figure and presence of P25 (Ti; n = 2) lower figure, after application of TCC to the upper segment and 48 h of surface sprinkling; error bars = SD of 3 sub samples of the corresponding segment. .... 57

Figure 27: Triclocarban (TCC) concentration at the border (outer cm) of five segments (0-1, 1-2, 2-3, 3-4, and 5-11 cm) of columns filled with three different soil types (A01, A02, and G03) in absence of P25 (n = 1) upper figure and presence of P25 (Ti; n = 2) lower figure, after application of TCC to the upper segment and 48 h of surface sprinkling; error bars = SD of 3 sub samples of the corresponding segment. .... 58

Figure 28: Survival (bars) and dry weight (dw, round data points) of earthworms (*Eisenia fetida*) exposed to triclocarban (TCC) for 14 days in soil systems spiked via different methods: via the soil water (TCC susp), via a fraction of the soil (TCC soil), and via the diet (TCC food). Treatments, in which uncontaminated food was supplied to the worms, are indicated with “+ F”. The presence of P25 is indicated with “+ Ti”. The whiskers represent the standard deviation on the mean weight of five replicates. The standard deviation of TC soil + F is covered by the data point; n = 5. .... 61

Figure 29: Bioaccumulation factors (BAF) calculated using soil and organism dry weight (dw) after exposure of earthworms (*Eisenia fetida*) to triclocarban (TCC) for 14 days in soil systems that were spiked via different methods: via the soil water (TCC susp), via a fraction of the soil (TCC soil), and via the diet (TCC food). Treatments, in which uncontaminated food was supplied to the worms, are indicated with “+ F”. The presence of P25 is indicated with “+ Ti”. The whiskers represent the standard deviation on the mean of five replicates. .... 62

Figure 30: Percentage of the total amount of radioactivity found in earthworms (*Eisenia fetida*) and their faeces, after they were exposed to triclocarban (TCC) for 14 days in soil systems that were spiked via different methods: via the soil water (TCC susp.), via a fraction of the soil (TCC soil), and via the diet (TCC food). Treatments, in which uncontaminated food was supplied to the worms, are indicated with “+ F”. The presence of P25 is indicated with “+ Ti”. The whiskers represent the standard deviation on the mean of five replicates. .... 63

Figure 31: Dynamic light scattering: instrumental technique and time signals ..... 76

Figure 32: electrophoresis and double layer polarisation .....	78
Figure 33: Calibration curve for quantitative estimation of glycerol within aqueous solutions. ....	96
Figure 34: Simplified graphic description of the segment sampling for the copper experiments left, 14C TCC experiments in the middle.....	124
Figure 35: FTIR spectrum of the dry powder of the two coated titanium dioxide nanomaterials.....	127
Figure 36: Detailed 3 keV He <sup>+</sup> Leis spectrum of NM103 and NM104.....	128
Figure 37: Details of the 3 keV He <sup>+</sup> Leis spectrum of the Al, Si (left diagram) and Ti region (right diagram) for NM103 and NM104. In the Ti region a Ti reference spectrum (with K contamination) is shown. ....	128
Figure 38: Detail TOF SIMS spectrum of positive secondary Ions .....	131
Figure 39: Detail TOF SIMS spectrum of negative secondary Ions.....	132
Figure 40: Typical TOF SIMS spectrum of positive secondary Ions .....	133
Figure 41: Normalised intensity particle distribution of NM103 and NM104 after 10 min stirring directly (solid line) and after 96 h (dashed line). ....	135
Figure 42: Normalised Intensity particle distribution of NM103 and NM104 after 10 min sonication using a waterbath (UB) directly (solid line) and after 96 h (dashed line). ....	136
Figure 43: Normalised Intensity particle distribution of NM103 and NM104 after 10 min sonication using an ultrasonic homogeniser (UH) directly (solid line) and after 96 h (dashed line). ....	136
Figure 44: EPR measurements of 100 mg/L NM104, NM103 and P25 as positive control. Suspension preparation based on established SOP, with and without 5 min UV irradiation; n =3. Note: Exemplarily one measurement is shown (n = 3 was tested and no differences were detected).....	140
Figure 45: EPR measurements of 100 mg/L NM104 after suspension preparation using an ultrasonic homogenizer (pulse 0.2/0.8, 200 W) with and without 5 min UV irradiation; n =3. ....	140
Figure 46: EPR measurements of 100 mg/L P25 as positive control. Suspension preparation based on established SOP and 1 min vortexing, with 5 min UV irradiation; n =3.....	141
Figure 47: Zeta potential measurements three seperat measurmenets of NM103 in DI water. The pH was varied in a first step from 4.5 to pH 10 (measurements 1 - 3) and in a second step back from pH 10 to pH 4.5 (measurements 1.2 - 3.2). ....	145
Figure 48: Zeta potential measurements of three seperat measurmenets of NM104 in DI water. The pH was varied in a first step from 4.5 to pH 10	

(measurements 1 - 3) and in a second step back from pH 10 to pH 4.5 (measurements 1.2 - 3.2).....	145
Figure 49: Zeta potential measurements of three separate measurements for NM104 in DI water (top left) with 0.0001M CaCl <sub>2</sub> solution (top right), 0.001M CaCl <sub>2</sub> solution (bottom left) and 0.01M CaCl <sub>2</sub> solution (bottom right). The pH was varied in a first step from 4.5 to pH 10 (measurements 1 - 3) and in a second step back from pH 10 to pH 4.5 (measurements 1.2 - 3.2). .....	146
Figure 50: Zeta potential measurements of three separate measurements of NM103 in DI water (top left), with 0.0001M CaCl <sub>2</sub> solution (top right), 0.001M CaCl <sub>2</sub> solution (bottom left) and 0.01M CaCl <sub>2</sub> solution (bottom right). The pH was varied in a first step from 4.5 to pH 10 (measurements 1 - 3) and in a second step back from pH 10 to pH 4.5 (1.2 - 3.2). .....	147
Figure 51: Evolution of zeta potential values for NM103 in 0.0001 M CaCl <sub>2</sub> and 0.01 M CaCl <sub>2</sub> , measured with $\mu$ EP. ....	148
Figure 52: Evolution of zeta potential values for NM104 in 0.0001 M CaCl <sub>2</sub> and 0.01 M CaCl <sub>2</sub> , measured with $\mu$ EP. ....	148
Figure 53: Evolution of zeta potential values for NM104 in DI-water and 0.001 M NaCl, measured with $\mu$ EP.....	148
Figure 54: Evolution of average particle size ( $x_{Cum}$ ) for NM103 in 0.0001 M CaCl <sub>2</sub> and 0.01 M CaCl <sub>2</sub> , measured with DLS. ....	149
Figure 55: Evolution of average particle size ( $x_{Cum}$ ) for NM104 in 0.0001 M CaCl <sub>2</sub> and 0.01 M CaCl <sub>2</sub> , measured with DLS. ....	149
Figure 56: Evolution of average particle size ( $x_{Cum}$ ) for NM104 in DI-water and 0.001 M NaCl, measured with DLS.....	149
Figure 57: Zeta potential vs. pH for NM103 (left) and NM104 (right) in DOC solution, ELS (continuous titration from acid to basic). ....	157
Figure 58: Zeta potential of three separate NM104 measurements in DI water (top left), with 2.5 mg/L DOC solution (top right), 5 mg/L DOC solution (bottom left) and 10 mg/L DOC solution (bottom right). The pH was varied in a first step from 4.5 to pH 10 (measurements 1 - 3) and in a second step back from pH 10 to pH 4.5 (measurements 1.2 - 3.2). .....	157
Figure 59: Zeta potential of three separate NM103 measurements in DI water (top left) with 2.5 mg/L DOC solution (top right), 5 mg/L DOC solution (bottom left) and 10 mg/L DOC solution (bottom right). The pH was varied in a first step from 4.5 to pH 10 (measurements 1 - 3) and in a second step back from pH 10 to pH 4.5 (measurements 1.2 - 3.2). .....	158
Figure 60: Evolution of zeta potential values for NM103 (left) and NM104 (right) in aqueous solution of 5 mg/L DOC, measured with $\mu$ EP.....	159

Figure 61: Evolution of average particle size ( $x_{Cum}$ ) for NM103 (left) and NM104 (right) in aqueous solution of 5 mg/L DOC, measured with DLS. ....	159
Figure 62: Zeta potential measurements of NM104 in 5 mg/L NOM and 0.001M CaCl <sub>2</sub> solution. The pH was varied in a first step from 4.5 to pH 10 and in a second step back from pH 10 to pH 4.5.....	166
Figure 63: Zeta potential measurements of NM103 in 5 mg/L NOM and 0.001M CaCl <sub>2</sub> solution. The pH was varied in a first step from 4.5 to pH 10 and in a second step back from pH 10 to pH 4.5.....	166
Figure 64: Measured (full bars) and default values (dashed bars) of Ti concentration and Cu concentration of two reference soils: error bars = standard deviation; n = 8. The certified value for Ti is 3360 mg/kg and for Cu 33.9 mg/kg for San Joaquin soil 2709a and 2700 mg/kg for Ti and 69.7 mg/kg for Cu for BCR.....	168
Figure 65: Determination of the reproducibility of the digestion method and ICP-OES measurements of the copper concentration in one segment of the three soil types. ....	169
Figure 66: Determination of the reproducibility of the digestion method and ICP-OES measurements of the copper (full bars) and Ti (dashed bars) concentration in the eluate of the three soil types. ....	169
Figure 67: Breakthrough curve of soil type A01 – Dystric Cambisol normalized to the initial conductivity in percent conducted in both laboratories (IUTA and RWTH).....	170
Figure 68: Breakthrough curve of soil type A02 – Stagnic Luvisol normalized to the initial conductivity in percent conducted in both laboratories (IUTA and RWTH).....	170
Figure 69: Breakthrough curve of soil type G03 – Eutric Cambisol normalized to the initial conductivity in percent conducted in both laboratories (IUTA and RWTH).....	171
Figure 70: Background concentration of Ti diamonds and Cu triangle for the three tested soil types, n = 2. ....	171
Figure 71: Triclocarban (TCC) concentration at the wall (outer cm, left) and in the core (right) of 1 cm soil segments taken from columns filled with soil of type A01 in absence of TiO <sub>2</sub> (n = 1) and presence (n = 2) of TiO <sub>2</sub> (P25). Analyses were performed 48 h after the upper segment of the soil column had been spiked with TCC and had been subjected to continuous surface sprinkling in that time frame. The whiskers represent the standard deviation on the mean of replicates and soil subsamples (3). ....	175



Figure 72: Triclocarban (TCC) concentration at the wall (outer cm, left) and in the core (right) of 1 cm soil segments taken from columns filled with soil of type A02 in absence of TiO<sub>2</sub> (n = 1) and presence (n = 2) of TiO<sub>2</sub> (P25). Analyses were performed 48 h after the upper segment of the soil column had been spiked with TCC and had been subjected to continuous surface sprinkling in that time frame. The whiskers represent the standard deviation on the mean of replicates and soil subsamples (3). ..... 175

Figure 73: Triclocarban (TCC) concentration at the wall (outer cm, left) and in the core (right) of 1 cm soil segments taken from columns filled with soil of type A02 in absence of TiO<sub>2</sub> (n = 1) and presence (n = 2) of TiO<sub>2</sub> (P25). Analyses were performed 48 h after the upper segment of the soil column had been spiked with TCC and had been subjected to continuous surface sprinkling in that time frame. The whiskers represent the standard deviation on the mean of replicates and soil subsamples (3). ..... 176

Figure 74: ICP-OES results of the copper concentration of the five different segments of the three columns. Reference system without P25 and test system with P25, soil type A01; n = 3. .... 177

Figure 75: ICP-OES results of the copper concentration of the eluate at the five different time points of soil type A01, of the test system with P25, the reference system without P25 and the background; n = 3. An average amount of 186 mg Cu (SD 270) were applied to the soils..... 177

Figure 76: ICP-OES results of the copper concentration of the five different segments of the three columns. Reference system without P25 and test system with P25, soil type A02..... 178

Figure 77: ICP-OES results of the copper concentration of the eluate at the five different time points of soil type A02, of the test system with P25, the reference system without P25 and the background; n = 3. An average amount of 186 mg Cu (SD: 270) were applied to the soils..... 178

Figure 78: ICP-OES results of the copper concentration of the five different segments of the three columns. Reference system without P25 and test system with P25, soil type G03..... 179

Figure 79: ICP-OES results of the copper concentration of the eluate at the five different time points of soil type G03, of the test system with P25, the reference system without P25 and the background; n = 3. An average amount of 186 mg Cu (SD: 270) were applied to the soils..... 179

Figure 80: Ti concentration of the different segments of the soil type A01. The blue line shows the background concentration of the soil type; n = 3..... 181

Figure 81: Ti concentration of the different segments of the soil type A02. The blue line shows the background concentration of the soil type; n = 3.....	182
Figure 82: Ti concentration of the different segments of the soil type G03. The blue line shows the background concentration of the soil type; n = 3.....	182
Figure 83: Titanium concentration in the eluate of the test and the background sample for soil type G03. Background, n = 2, test n = 3, error bars = min and max.....	183
Figure 84: Soil type A01, column three, segment one.....	184
Figure 85: Soil type A01, column two, segment one.....	185
Figure 86: Soil type A01, column one, segment one. ....	185
Figure 87: Soil type A01, column one, segment one. ....	186
Figure 88: Soil type A01, column one, segment two.....	187
Figure 89: Soil type A01, column two, segment two.....	187
Figure 90: Soil type A01, column one, segment seven. ....	187
Figure 91: Soil type A02, column one, segment one. ....	188
Figure 92: Soil type A02, column two, segment one.....	188
Figure 93: Soil type A02, column two, segment one. ....	188
Figure 94: Soil type A02, column three, segment one.....	189
Figure 95: Soil type A02, column one, segment two.....	189
Figure 96: Soil type A02, column two, segment two.....	189
Figure 97: Soil type A02, column two, segment seven. ....	190
Figure 98: Soil type G03, column one, segment one. ....	190
Figure 99: Soil type G03, column one, segment one, negative control. ....	190
Figure 100: Soil type G03, column two, segment one. ....	191
Figure 101: Soil type G03, column three, segment one.....	191
Figure 102: Soil type G03, column three, segment one.....	192
Figure 103: Soil type G03, column one, segment two. ....	192
Figure 104: Soil type G03, column three, segment two.....	193
Figure 105: Soil type G03, column two, segment seven. ....	193

## List of Tables

Table 1: Manufacturers data (Sachtlen Chemie GmbH, Germany) for the used coated titanium dioxide nanomaterials.....	15
Table 2: DLS results for differently prepared NM suspensions; powders suspended in deionised water and dispersed with a sonication probe (200 W), with overhead stirrer (~350 rpm) and with sonication in a waterbath (150 W, stirred, fixed position of the sample); statistics for 5 independent samples, ± = standard deviation; n = 10, (repeated measurements).....	18
Table 3: Hydroxyl radical generation (OH·) potential in arbitrary unit (AU) of the coated titanium dioxide nanomaterials NM103 and NM104 and the uncoated P25 as photocatalytic material, suspension preparation based on SOP, pH 5; ± standard deviation of n = 3.....	31
Table 4: Surface reactivity in arbitrary unit (AU) of the coated titanium dioxide nanomaterials NM103 and NM104 and the uncoated P25 as photocatalytic material, suspension preparation based on SOP; n = 3.....	32
Table 5: Surface reactivity in arbitrary unit (AU) of the coated Titan materials NM103 and NM104, suspension preparation with 1 min mixing, n = 3.....	32
Table 6: Zeta potential measurements of NM103 suspensions with varying pH (4.5 – 10) and CaCl <sub>2</sub> concentration (0.0001M, 0.001M and 0.01M); IEP = isoelectric point; n = 3.....	36
Table 7: Zeta potential measurements of NM104 suspensions with varying pH (4.5 - 10) and CaCl <sub>2</sub> concentration (0.0001M, 0.001M and 0.01M); IEP = isoelectric point; n = 3.....	36
Table 8: Zeta potential measurements of NM103 (UV Titan M262) suspensions with varying pH (4.5 – 10) and DOC content (2.5 mg/L, 5mg/L and 10 mg/L); IEP = isoelectric point; n = 3.....	41
Table 9: Zeta potential measurements of NM104 (UV Titan M212) suspensions with varying pH (4.5 – 10) and DOC content (2.5 mg/L, 5 mg/L and 10 mg/L); IEP = isoelectric point; n = 3.....	41
Table 10: Zeta potential measurements of NM104 (UV Titan M212) suspensions in 5 mg/L DOC and 0.001M CaCl <sub>2</sub> solution with varying pH (4.5 – 10); IEP = isoelectric point; n = 3.....	42
Table 11: Overview of the study and experiment design.....	50
Table 12: Averages and standard deviation of zeta potential measurements of P25 (2.5 g/L) in 100 mL DI water; 10 min sonication (ultrasonic homogeniser); n = 3.....	51

Table 13: Prepared setups to exposure the earthworm <i>Eisenia fetida</i> to 14C-labelled triclocarban (TCC) in absence or presence of nano-TiO <sub>2</sub> (P25), with five replicates for one tests. ....	60
Table 14: MRM parameter settings for glycerol. ....	95
Table 15: Overview of parameters/values required to calculate the concentration of glycerol. ....	99
Table 16: Relative intensities of the detected substances, - = no detection, + = detection in the range of LOD, ++ = low, +++ = medium and ++++ = high intensity. ....	130
Table 17: Overview of validation results for the enzymatic UV test and the LC-MS/MS method. ....	134
Table 18: Median, Minimum and Maximum of the z-average and zeta potential; n = 3. ....	135
Table 19: DLS results for differently prepared NM suspensions; powders suspended in deionised water and dispersed with sonication using a probe (200 W), with overhead stirrer (~350 rpm) and with sonication in a waterbath (120 W, stirred, fixed position of the sample); measurement precision: n = 10 measurements per sample. ....	137
Table 20: Evolution of the size distribution of stock suspensions (1000 ppmw) over a period of 30 days as measured with DLS. ....	137
Table 21: Zeta potential of NM103 in deionised water, measured with ELS, titration from acid → basic → acid, 3 independent samples and average result. ....	138
Table 22: Zeta potential of NM104 in deionised water, measured with ELS, titration from acid → basic → acid, 3 independent samples and average result. ....	138
Table 23: Zeta potential of NM104 in 0.001 M CaCl <sub>2</sub> , measured with ELS, titration from acid → basic → acid, 3 independent samples and average result. ....	139
Table 24: Zeta potential of NM103 in aqueous CaCl <sub>2</sub> solutions, measured with ELS, titration from acid → basic → acid, averages from 3 independent samples. ....	150
Table 25: Zeta potential of NM104 in aqueous CaCl <sub>2</sub> solutions, measured with ELS, titration from acid → basic → acid, averages from 3 independent samples. ....	150
Table 26: Zeta potential of NM103 in 0.0001 M CaCl <sub>2</sub> , measured with μEP, independent samples for each pH value, averages from 3 repeated measurements. ....	151
Table 27: Zeta potential of NM103 in 0.001 M CaCl <sub>2</sub> , measured with μEP, independent samples for each pH value, averages from 3 repeated measurements. ....	151

Table 28: Zeta potential of NM103 in 0.01 M CaCl <sub>2</sub> , measured with $\mu$ EP, independent samples for each pH value, averages from 3 repeated measurements. ....	151
Table 29: Zeta potential of NM103 in 0.001 M CaCl <sub>2</sub> , dispersed with 10 min us-homogenizer instead of 1 min as in SOP, measured with $\mu$ EP, independent samples for each pH value, averages from 3 repeated measurements. ....	151
Table 30: Zeta potential of NM104 in 0.0001 M CaCl <sub>2</sub> , measured with $\mu$ EP, independent samples for each pH value, averages from 3 repeated measurements. ....	152
Table 31: Zeta potential of NM104 in 0.001 M CaCl <sub>2</sub> , measured with $\mu$ EP, independent samples for each pH value, averages from 3 repeated measurements, series A.....	152
Table 32: Zeta potential of NM104 in 0.001 M CaCl <sub>2</sub> , measured with $\mu$ EP, independent samples for each pH value, averages from 3 repeated measurements, series B.....	152
Table 33: Zeta potential of NM104 in 0.001 M CaCl <sub>2</sub> , measured with $\mu$ EP, independent samples for each pH value, averages from 3 repeated measurements, series C.....	152
Table 34: Zeta potential of NM104 in 0.01 M CaCl <sub>2</sub> , measured with $\mu$ EP, independent samples for each pH value, averages from 3 repeated measurements. ....	153
Table 35: Zeta potential of NM104 in 0.001 M NaCl, measured with $\mu$ EP, independent samples for each pH value, averages from 3 repeated measurements. ....	153
Table 36: Zeta potential of NM104 in 0.001 M CaCl <sub>2</sub> , dispersed with 10 min us-homogenizer instead of 1 min as in SOP, measured with $\mu$ EP, independent samples for each pH value, averages from 3 repeated measurements. ....	153
Table 37: Mean particle size ( $x_{Cum}$ ) of NM103 in 0.0001 M CaCl <sub>2</sub> , measured with DLS, independent samples for each pH value, averages from 3 repeated measurements. ....	154
Table 38: Mean particle size ( $x_{Cum}$ ) of NM103 in 0.001 M CaCl <sub>2</sub> , measured with DLS, independent samples for each pH value, averages from 3 repeated measurements. ....	154
Table 39: Mean particle size ( $x_{Cum}$ ) of NM103 in 0.01 M CaCl <sub>2</sub> , measured with DLS, independent samples for each pH value, averages from 3 repeated measurements. ....	154

Table 40: Mean particle size ( $x_{Cum}$ ) of NM103 in 0.001 M CaCl <sub>2</sub> , dispersed with 10 min us-homogenizer instead of 1 min as in SOP, measured with DLS, independent samples for each pH value, averages from 3 repeated measurements. ....	155
Table 41: Mean particle size ( $x_{Cum}$ ) of NM104 in 0.0001 M CaCl <sub>2</sub> , measured with DLS, independent samples for each pH value, averages from 3 repeated measurements. ....	155
Table 42: Mean particle size ( $x_{Cum}$ ) of NM104 in 0.001 M CaCl <sub>2</sub> , measured with DLS, independent samples for each pH value, averages from 3 repeated measurements, series A.....	155
Table 43: Mean particle size ( $x_{Cum}$ ) of NM104 in 0.001 M CaCl <sub>2</sub> , measured with DLS, independent samples for each pH value, averages from 3 repeated measurements, series B.....	155
Table 44: Mean particle size ( $x_{Cum}$ ) of NM104 in 0.001 M CaCl <sub>2</sub> , measured with DLS, independent samples for each pH value, averages from 3 repeated measurements, series C.....	156
Table 45: Mean particle size ( $x_{Cum}$ ) of NM104 in 0.01 M CaCl <sub>2</sub> , measured with DLS, independent samples for each pH value, averages from 3 repeated measurements. ....	156
Table 46: Mean particle size ( $x_{Cum}$ ) of NM104 in 0.001 M NaCl, measured with DLS, independent samples for each pH value, averages from 3 repeated measurements. ....	156
Table 47: Mean particle size ( $x_{Cum}$ ) of NM104 in 0.001 M CaCl <sub>2</sub> , dispersed with 10 min us-homogenizer instead of 1 min as in SOP, measured with DLS, independent samples for each pH value, averages from 3 repeated measurements. ....	156
Table 48: Zeta potential of NM103 in aqueous solutions of DOC, measured with ELS, titration from acid → basic → acid, averages from 3 independent samples. ....	160
Table 49: Zeta potential of NM104 in aqueous solutions of DOC, measured with ELS, titration from acid → basic → acid, averages from 3 independent samples. ....	161
Table 50: Zeta potential of NM103 in 2.5 ppmw DOC, measured with $\mu$ EP, independent samples for each pH value, averages from 3 repeated measurements. ....	161
Table 51: Zeta potential of NM103 in 5 ppmw DOC, measured with $\mu$ EP, independent samples for each pH value, averages from 3 repeated measurements. ....	161

Table 52: Zeta potential of NM103 in 10 ppmw DOC, measured with $\mu$ EP, independent samples for each pH value, averages from 3 repeated measurements. ....	162
Table 53: Zeta potential of NM104 in di-water, measured with $\mu$ EP, independent samples for each pH value, averages from 3 repeated measurements.....	162
Table 54: Zeta potential of NM104 in 2.5 ppmw DOC, measured with $\mu$ EP, independent samples for each pH value, averages from 3 repeated measurements. ....	162
Table 55: Zeta potential of NM104 in 5 ppmw DOC, measured with $\mu$ EP, independent samples for each pH value, averages from 3 repeated measurements. ....	162
Table 56: Zeta potential of NM104 in 10 ppmw DOC, measured with $\mu$ EP, independent samples for each pH value, averages from 3 repeated measurements. ....	163
Table 57: Mean particle size ( $x_{cum}$ ) of NM103 in 2.5 ppmw DOC, measured with DLS, independent samples for each pH value, averages from 3 repeated measurements. ....	164
Table 58: Mean particle size ( $x_{cum}$ ) of NM103 in 5 ppmw DOC, measured with DLS, independent samples for each pH value, averages from 3 repeated measurements. ....	164
Table 59: Mean particle size ( $x_{cum}$ ) of NM103 in 10 ppmw DOC, measured with DLS, independent samples for each pH value, averages from 3 repeated measurements. ....	164
Table 60: Mean particle size ( $x_{cum}$ ) of NM104 in di-water, measured with DLS, independent samples for each pH value, averages from 3 repeated measurements. ....	164
Table 61: Mean particle size ( $x_{cum}$ ) of NM104 in 2.5 ppmw DOC, measured with DLS, independent samples for each pH value, averages from 3 repeated measurements. ....	165
Table 62: Mean particle size ( $x_{cum}$ ) of NM104 in 5 ppmw DOC, measured with DLS, independent samples for each pH value, averages from 3 repeated measurements. ....	165
Table 63: Mean particle size ( $x_{cum}$ ) of NM104 in 10 ppmw DOC, measured with DLS, independent samples for each pH value, averages from 3 repeated measurements. ....	165
Table 64: Detailed analysis data of the used soils – Soil A01 Dystric Cambisol – AV = Average, COV = coefficient of variation. A = field. ....	167

Table 65: Detailed analysis data of the used soils – Soil A02 Stagnic Luvisol – AV = Average, COV = coefficient of variation. A = field. ....	167
Table 66: Detailed analysis data of the used soils – Soil G03 Eutric Cambisol – AV = Average, COV = coefficient of variation. A = field. ....	167
Table 67: Zeta potential of TiO <sub>2</sub> in deionised Water as function of time after dilution of the stock suspension. Measurements were conducted 1 day after suspension preparation, zeta potential was analysed with μEP. NM101 = Hombikat UV100, NM102 = PC105. ....	172
Table 68: Zeta potential of TiO <sub>2</sub> in deionised water. Measurements were conducted 1 day after suspension preparation and 1 h after dilution, zeta potential was analysed with μEP. NM101 = Hombikat UV100, NM102 = PC105 .....	173
Table 69: Zeta potential of TiO <sub>2</sub> in 0.01 M CaCl <sub>2</sub> -solution as function of time after dilution of the stock suspension with 0.01 M CaCl <sub>2</sub> -solution. NM101 = Hombikat UV100, NM102 = PC105. Measurements were conducted 1 day after suspension preparation, zeta potential was analysed with μEP. ....	174
Table 70: Detection of Cu in the reference system without P25. Values are presented as percent of the added copper. The eluat was collected at different time points. Sample 1 = after 1h, sample 2 = after 2 h, sample 3 = after 3 h, sample 4 = after 18 h, sample 5 = after 48 h, ± = Standard Deviation; n = 3. ....	180
Table 71: Detection of Cu in the test system with P25. Values are presented as percent of the added copper. The eluat was collected at different time points. Sample 1 = after 1h, sample 2 = after 2 h, sample 3 = after 3 h, sample 4 = after 18 h, sample 5 = after 48 h, ± = Standard Deviation; n = 3. ....	180
Table 72: Detection of P25 in the eluate of the three different soil types, Values are presented as percent of the added TiO <sub>2</sub> , The eluat was collected at different time points. Sample 1 = after 1h, sample 2 = after 2 h, sample 3 = after 3 h, sample 4 = after 18 h, sample 5 = after 48 h, ± = Standard Deviation; n = 5. ....	183



### Symbols and abbreviations

$C_{\text{ext}}$	$\text{m}^2$	extinction cross section
$C_{\text{psca}}$	$\text{m}^2$	partial scattering cross section
$C_{\text{sca}}$	$\text{m}^2$	total scattering cross section
$C_{n,i}^{\infty}$	$\text{mol}/\text{m}^3$	molar bulk concentration of ionic species $i$
$\mathbf{E}$	$\text{V}/\text{m}$	electric field strength
$F$	$\text{C}/\text{mol}$	Faraday's constant
$k$	$\text{m}^{-1}$	wave number
$M_{k,r}$		$k$ -th moment of the distribution $q_r$
$m$	-	relative refractive index
$PDI$	-	polydispersity index for $q_{\text{int}}(x_h, \text{eff})$ , eq. (2)
$Q_0$	$\text{m}^{-1}$	number weighted cumulative function
$Q_{\text{ext/int}}$	$\text{m}^{-1}$	extinction/intensity weighted cumulative function
$R$	$\text{J}/\text{mol}/\text{K}$	universal gas constant
$S_m$	$\text{m}^2/\text{g}$	mass specific surface area
$S_{\text{int,ext}}$	$\text{m}$	standard deviation of $q_{\text{int}}/q_{\text{ext}}$
$T$	$\text{K}$	absolute temperature
$V_p$	$\text{m}/\text{s}$	particle velocity
$X_{\text{BET}}$	$\text{m}$	BET equivalent diameter
$X_{\text{Cum}}$	$\text{m}$	harmonic mean of $q_{\text{int}}(x_h, \text{eff})$
$X_g$	$\text{m}$	diameter of gyration
$X_{h,\text{eff}}$	$\text{m}$	effective hydrodynamic diameter
$X_{h,t}$	$\text{m}$	translational hydrodynamic diameter
$X_p$	$\text{m}$	diameter of the primary particles
$X_{\text{Stokes}}$	$\text{m}$	Stokes diameter
$\epsilon_r$	-	relative permittivity
$\epsilon_0$	$\text{F}/\text{m}$	electric field constant
$\zeta$	$\text{V}$	zeta potential
$\eta$	$\text{Pa}\cdot\text{s}$	dynamic viscosity of the liquid phase
$\theta$	-	scattering angle
$\kappa$	$1/\text{m}$	Debye-Hückel parameter, inverse Debye length
$\mu_{\text{ek}}$	$\text{m}^2/\text{s}/\text{V}$	electrokinetic mobility
$\nu_i$	-	valency of ionic species $i$
$\sigma_{\text{ln}}$	-	scale parameter of a log-normal distribution
$\phi_s$	-	solid volume fraction in the suspension

AHA	Aldrich Humic Acid
DI	Deionised water
DLS	Dynamic light scattering
DOC	Dissolved organic carbon
DUM	Dynamic ultramicroscopy
EC	Elemental carbon
EDL	Electric double layer
EDX	Energy dispersive X-ray spectroscopy
ELS	Electrophoretic light scattering
ENM	Engineered nanomaterials
EPR	Electron paramagnetic resonance spectroscopy
ESR	Electron spin resonance spectrometry
FTIR	Fourier transform infrared spectroscopy
ICP-OES	Inductively coupled plasma optical emission spectrometry
IS	Ionic strength
LC-MS	Liquid chromatography mass spectrometry
LEIS	Low energy ion scattering
LOD	Limit of detection
NOM	Natural organic matter
NM	Nanomaterial
NMR	Nuclear magnetic resonance spectroscopy
OC	Organic carbon
PDI	Polydispersity index
SEM	Scanning electron microscopy
SD	Standard Deviation
SOP	Standard operation procedure
TC	Total carbon
Tof SIMS	Time of Flight Secondary Ion Mass Spectrometry

## 1 Introduction

Engineered nanomaterials (ENM) are already used in many technologies and consumer products like e.g. electrical engineering, computer displays, rotor blades of wind energy plants, paints, textiles, sport equipment or cosmetics (Gottschalk et al. 2009; Woodrow Wilson Database 2012, Figure 1). Consequently also a release of ENMs into the environment can not be excluded (Nowack & Bucheli, 2007) and was already shown in recent studies (Hsu & Chein, 2007; Benn & Westerhoff, 2008; Kaegi et al., 2008 & 2010).

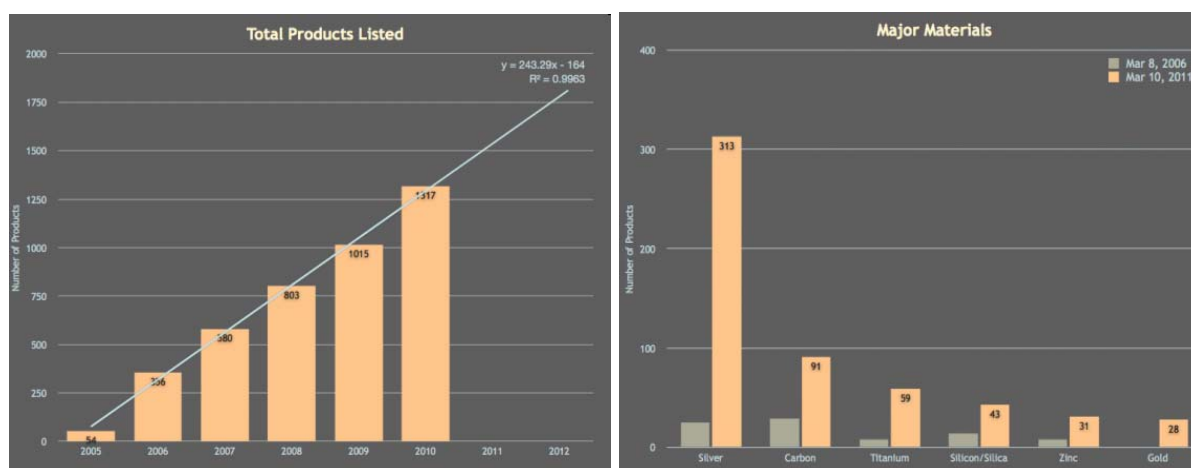


Figure 1: Number of total products listed, by date of inventory update, with regression analysis (left), number of listed products associated with specific ENMs (right), Woodrow Wilson Database, 2012.

Silver, carbon based materials and titanium dioxide (TiO<sub>2</sub>) are currently the most used nanomaterials (Figure 1). At the nanoscale TiO<sub>2</sub> nanomaterials are transparent, highly UV absorbent and photo catalytic active. These properties lead to a widespread use in consumer products like paints, cosmetics or self cleaning materials (Auffan et al., 2010). A release of TiO<sub>2</sub> nanomaterials from products during their life cycle was already shown in recent studies (Kaegi et al, 2008; Hsu & Chein, 2007). Due to the mode of application, the released materials can - directly or indirectly via sewage treatment plants - reach the surface water or the soil ecosystem. Information about the fate and behaviour in these ecosystems are scarce, but very important for a risk assessment. A recently published study indicated for example that ENMs which were applied on soils were taken up by agricultural plants and led to a reduced growth and nitrogen fixation (Priester et al., 2012). In a previous study by Kuhlbusch et al. (2012) – the mobility of three different TiO<sub>2</sub> nanomaterials, one coated (UV Titan M262) and two uncoated materials (P25 and PC105), were analysed in soil columns – based on the OECD Guideline 312. It was shown that based on bulk chemical analyses a (low) transport was only indicated for the coated material (UV Titan M262). For the other two materials no transport was detected. However with microscopic analysis a transport of isolated TiO<sub>2</sub> agglomerates for all three nanomaterials was

shown. The tested materials in this study showed a positive zeta potential which could have affected the mobility due to adsorption to negatively charged soil minerals. In contrast to these results of low to no mobility, Fang et al. (2009) and Duester et al. (2011) detected a transport of applied TiO<sub>2</sub> nanomaterials in different natural soils. The main and presumably crucial contrasts of both studies compared to the UBA study (Kuhlbusch et al. 2012), is the use of negatively charged and smaller nanomaterials at higher pH values of the soils. Recent studies also indicated that the transport of nanomaterials is, aside from the nanomaterial characteristic, also affected by the soil properties (ionic strength, pH, dissolved organic carbon content (Lecoanet et al., 2004; Guzman et al. 2006; Nowack & Bucheli, 2007; Fang et al., 2009; Petosa et al., 2010). As it was shown for metal based and carbonaceous nanomaterials (Zhang, 2003, Fang et al. 2011, Hofman & von der Kammer 2009) other substances as well as pollutants can be adsorbed to nanomaterials and it is conceivable that if these nanomaterials are mobile they can act as carrier for pollutants.

Some mobile nanomaterials are used in contaminated areas for remediation (Fe<sup>0</sup> nanoparticles) (Zhang, 2003). This carrier function was also shown for TiO<sub>2</sub> ENMs reaching the surface water or the soil ecosystems. In these studies the mobility of pollutants and also the bioavailability was increased if TiO<sub>2</sub> ENM were present (Zhang et al., 2006; Sun et al., 2009; Fan et al., 2011; Fang et al., 2011).

The release of ENMs (from consumer products) does usually not occur in form of isolated untreated primary nanoparticles. In fact, such released particles are frequently embedded in a matrix, have typically functionalised surfaces and usually exist only in aggregated state, respectively and are consequently different in their fate and behaviour (Nowack & Bucheli 2007). Therefore the detection of surface characteristics after the particles where released from a matrix into the environment is necessary.

In this study two different topics were considered, the development and evaluation of test methods and the investigation about the fate and behaviour of TiO<sub>2</sub> nanomaterials in the environment based on these new test methods:

a) Surface characterisation (coating stability testing) of two different functionalised TiO<sub>2</sub> nanomaterials (hydrophilic and hydrophobic) – NM103 (UV Titan M262) and NM104 (UV Titan M212) – considering different environmental conditions like pH or ionic strength (salt concentration in the media). This topic was analysed in two different approaches. Firstly a method development how the coating stability could be analysed was established.

Secondly exemplarily results on the coating stability were analysed with the new approach.

b) Analysis of the carrier function of a selected TiO<sub>2</sub> ENM in soils which are treated with two different substances (copper sulphate and <sup>14</sup>C triclocarban).

## 2 Methods, characterisation techniques and measurands

Three different TiO<sub>2</sub> nanomaterials were used in this study, two coated materials NM103 (UV Titan M262) coated with aluminium oxide and dimethicone and NM104 (UV Titan M212) coated with aluminium oxide and glycerol and one uncoated TiO<sub>2</sub> material, P25.

### Approach testing coating stability

The two coated materials chosen for the test of coating stability were NM103 and NM104. Both materials are firstly coated with aluminiumoxid; NM103 is additionally coated with a hydrophobic dimethicone and NM104 with a hydrophilic glycerol coating. These materials were tested in order to understand and predict the stability of the surface coatings under environmental conditions. Their reaction to changes in pH and/or additive concentration was investigated. Transformations of the surface may occur very rapidly or on long time scales. For that reason it is inevitable to monitor relevant suspension properties as a function of time and to examine the impact of dispersion. The main task of this study was to study and answer following questions:

- Is the dimethicone / glycerol coating damaged by the established standard operation procedure (SOP) for the suspension preparation (Annex AII.1)?
- Is the Al<sub>2</sub>O<sub>3</sub> coating damaged by the SOP?
- Is the respective coating damaged by sample preparation with high and/or low energy inputs?
- How do the coated surfaces interfere with the suspension medium?
- How does a coating damage change the behaviour of the material?
- Is the change in the behaviour reversible or irreversible?
- What can be derived from this behaviour for the coating stability?

Changes of the surface modification – their quality and their extent – can be either detected directly or indirectly. However, low-cost routine analyses are essentially indirect methods, i.e. they are based on metrics that indicate such changes, yet may be not very sensitive or may be affected by bulk changes (e.g. electrolyte concentration), too. This study, therefore, uses a combination of different characterisation techniques for routine analysis and the changes of the surface coating were determined in different ways:

- a) by quantifying the released coating material in e.g. the suspension media,
- b) by quantifying the coating material on the nanomaterial prior and after exposure to stress conditions, and
- c) indirectly by determining changes in the behaviour of the ENM, e.g. changes in particle size distributions, the isoelectric point (IEP).

The combination of the different quantitative and qualitative information then allows the evaluation of the different characterisation techniques and their usefulness, especially

when compared to results obtained from more elaborated and expensive techniques. Following techniques were applied in this study:

- Dynamic light scattering (DLS) for the detection of the agglomeration of the materials (cf., section 2.1.1)
- Electrophoretic techniques: yielding the zeta potential (distribution) of the particles (cf. section 2.1.2)
- ICP-OES (inductive coupled plasma - optical emission spectrometry): concentration of selected elements in the bulk liquid (cf. section 2.1.3)
- LC-MS (liquid chromatography mass spectrometry) and UV-absorption: concentration of selected molecules in the bulk liquid (cf. section 2.1.3)
- EDX (energy dispersive X-ray spectroscopy): qualitative composition of nanoparticles (cf. section 2.1.4)
- EPR (electron paramagnetic resonance spectroscopy) techniques: degree of surface reactivity or of photo-catalysis (cf. section 2.1.5)
- NMR (nuclear magnetic resonance spectroscopy): (specific) surface area of the particles (cf. section 2.1.6)
- FTIR, LEIS and TOF-SIMS analysis of the ENM were made complementary before and FTIR and TOS-SIMS analysis also after different treatments to determine directly the chemistry of the surface coating (cf. section Annex AIII.1)

Approach testing possible enhanced pollutant transport by ENM in soils

The other TiO<sub>2</sub> nanomaterial used in this study was the non coated P25. The carrier effect of this material on two different substances was analysed in soil column experiments using natural soils. The test design was adopted from a prior study (Kuhlbusch et al., 2012) and is based on the OECD test guideline 312. The only change introduced was the use of a wider column to minimise possible wall effects in this transport study. The following questions were addressed during this study:

- Can TiO<sub>2</sub> nanomaterials act as carrier for other substances in soils?
- Does TiO<sub>2</sub> lead to an accumulation of substances in the upper soil layer?
- How mobile is the tested TiO<sub>2</sub> nanomaterial?
- Does TiO<sub>2</sub> have an effect on the bioavailability of other substances in soil ecosystems?

The carrier effect of TiO<sub>2</sub> was quantitatively analysed by:

- ICP-OES (inductive coupled plasma - optical emission spectrometry): concentration of selected elements in the soil and in the liquid / eluate (cf. section 2.1.3)
- SEM / EDX (scanning electron microscopy / energy dispersive X-ray spectroscopy): qualitative composition of the P25 nanoparticles in the soil columns (cf. section 2.1.4)

- Radioanalytics using a scintillation counter for the quantification of the radio-labeled substance (cf. section 2.1.7).

Additionally, all stock suspensions and all processed samples were characterised with regard to the particle size distribution and zeta potential (cf. section 2.1.1 and 2.1.2). That facilitated a validation of the sample preparation, which should yield a constant, SOP specific size distribution and zeta potential. Time dependent measurements of the size and the zeta potential of a suspension were conducted to observe agglomeration, which serves as a further indicator for interfacial properties.

## 2.1 Measurements techniques

The evaluation of the nanomaterials' behaviour in aqueous solutions and in soil columns required the determination of a number of characteristics. These are:

- the particle size distribution, where “particle” refers to all mobile individuals – here the submicron aggregates of the nanosized primary particles
- the zeta potential of the particles (again measured at the mobile individuals),
- the release of dimethicone / glycerol from the surface into the bulk liquid (i.e. their concentration in the supernatant)
- the degradation of the Al<sub>2</sub>O<sub>3</sub> layer (i.e. the Al<sup>3+</sup>-concentration in the supernatant or its presence on the surface)
- the (photocatalytic) surface reactivity
- the local concentration of the nanomaterial or test substance (in soils)
- the specific surface area of the nanomaterials.

These characteristics and metrics were determined in this study.

Additionally the reproduction and mortality of soil organisms, Lumbricidae, was analysed in this study.

The principle of the mainly used instruments for the detection of the surface coating stability as well as for the carrier effect experiments were described in more detail in the following section below.

## 2.1.1 Dynamic light scattering (DLS)

### Principle

Dynamic Light Scattering (DLS) measures the fluctuation of light, which is scattered by a liquid dispersion. In the case of colloidal particles in a quiescent liquid this fluctuation is due to the particles' Brownian motion. For very low particle concentrations the signal fluctuation can be related to the effective diffusion coefficient  $D_{\text{eff}}$  of the particles or equivalently to the effective hydrodynamic diameter  $x_{\text{h,eff}}$  (Xu 2000).

The instruments used for this study quantify the signal fluctuation via a time-correlation function, which can be numerically analysed in terms of the particle size ( $x_{\text{h,eff}}$ ) distribution. These distributions are intrinsically weighted by the fractional scattering intensity ( $Q_{\text{int}}$ ). Alternatively, the correlation functions can be analysed by the method of cumulants (Koppel, 1972), which directly yields an average particle size ( $x_{\text{Cum}}$ ) and a polydispersity index (PDI). For details of the analysis the reader is referred to appendix AI.1.

### Instruments

DLS instruments used in this study were mainly the HPPS and the Delsa-Nano C (from Malvern Instruments and Beckmann Coulter, respectively). The two instruments are very similar with respect to the DLS measurement setup: They detect the fluctuation of back-scattered light (173° HPPS and 165° Delsa-Nano C) and possess a moveable sample holder. Both features reduce the effect of multiple scattering on the correlation function. The instruments use a polarised Helium-Neon-Laser with 632.8 nm wavelength. The samples are filled in closed cuvettes (4 mL), which are placed in the temperature controlled sample holder at least 15 minutes before the measurements. The instrument software used is Dispersion Technology Software 4.20 and Delsa-Nano C UI Software Version 3.73, respectively. For the P25 characterisation also a Zetasizer ZS (from Malvern Instruments) was used.

### Data interpretation

All data interpretation was done with the instrument software. The software based on a data base where each measured correlation functions is stored. These correlation functions were analysed in two ways: with the method of cumulants (Koppel, 1972) and with an inversion algorithm. The former is a robust algorithm that yields a mean particle diameter ( $x_{\text{Cum}}$  or z-average) and an index of polydispersity (PDI). The  $x_{\text{Cum}}$  can be interpreted as the harmonic mean of the intensity weighted size distribution:

$$x_{\text{cum}}^{-1} = \int x_{\text{h,eff}}^{-1} dQ_{\text{int}} \quad (1)$$



whereas the polydispersity index is a normalised parameter for the variation of the effective hydrodynamic diameter:

$$PDI/x_{cum}^2 = \int (x_{h,eff}^{-1} - x_{cum}^{-1})^2 dQ_{int} = \int x_{h,eff}^{-2} dQ_{int} - x_{cum}^{-2} \quad (2)$$

The method of cumulants gives average size distribution parameters only. In order to resolve the shape of an intensity weighted size distribution from the correlation functions an inversion algorithm is used. Even though the manufacturers often do not reveal the details of the employed inversion algorithms they certainly use harmonised procedures that smooth the shape of the size distribution and impose a non-negative least square (NNLS) constraint (Lawson & Hanson, 1995). A typical example of such a data analysis is the CONTIN algorithm proposed by Provencher (1982). The Delsa-Nano C uses the CONTIN algorithm for the size distribution calculation in this study.

### **Evaluation of the measurement technique**

DLS is a mature particle sizing technique, which is found in many research laboratories and commonly used for the characterisation of nanoparticle dispersions. Interlaboratory comparisons with reference materials have shown, that DLS guarantees a consistent determination of particle size for stable colloidal systems (Nickel et al., in preparation). Problems occur, when the optical concentration (turbidity) is too high or when few coarse particles are present (e.g. dust particles), because their erratic, but intensive scattering signals impair the signal evaluation. In general, the method is not suited to the characterisation of coarse particles > 1 µm, because they leave the measuring zone due to sedimentation or because they do not contribute significantly to the signal fluctuation. Problems with turbidity and coarse size are particularly relevant for instable, agglomerating dispersions. Apart from this, there are restrictions to the resolution of this characterisation technique (i.e. detectability of the multiple size modes), to the applicability of multi-component suspensions (such as natural aqueous media) and to the signal interpretation in the case of non-spherical particles. These restrictions are irrelevant for coating experiments in this study, since the DLS particle sizes are only used as relative indicator for particle stability in the corresponding suspension.

#### **2.1.2 Electrophoretic zeta potential measurement**

##### **Principle**

The zeta potential is a characteristic parameter of the electric double layer (EDL), which is formed at any charged surface in a liquid. It is defined as the electric potential at the shear plane, which separates the mobile oppositely charged counter-ions (ion cloud) from solvent molecules and ions that adhere to the particle surface. The zeta potential can thus

be probed by imposing a relative motion between bulk solvent and particle (Delgado et al., 2007).

Such a relative motion can be induced by an external electric field, which causes opposite motions of counter ions and of the charged particle (electrophoresis). The velocity of the electrophoretic motion is proportional to the strength of the electric field and to the zeta potential. The particle size has only a second order impact (cf. appendix A1.2).

## **Instruments**

In this study two instruments were employed for the zeta potential measurement, which differ in the way of the velocity measurement. The ZetaView PMX100 (Particle Metrix, Germany) measures the electrophoretic motion of single particles microscopically (micro-electrophoresis –  $\mu$ EP) and yields a number weighted distribution of zeta potential. The DELSA-NANO C (Beckmann Coulter) essentially measures the phase shift (Doppler effect) of a light signal that is scattered at all – moving – particles (Electrophoretic Light Scattering – ELS). From the spread of the phase shift one can derive an intensity weighted distribution of the zeta potential.

## **Evaluation of the zeta potential measurement techniques**

The two electrophoretic methods,  $\mu$ EP and ELS, rely on optical detection of the particle motion in an electric field. That requires a sufficiently high sample dilution and the absence of coarse contaminant particles (e.g. dust). It has to be noted that large agglomerates of nanoobjects may cause similar problems. Besides, electrophoretic measurements encounter principal difficulties when the ion concentration is high (electrolysis) and the zeta potentials are low (Brownian motion superposes electrophoretic motion).

Apart from these general remarks, there are some specific problems that are related to the instruments and to the material systems used in this study. One refers to the ELS measurements with the DELSA-NANO C, which includes an automatic titration regime that adjusts the pH of the sample to pre-defined values by adding an acid or a base. The maximum equilibration time of the instrument is 15 min after each pH switch.

The  $\mu$ EP instrument was operated without a titrator mode. In contrast to ELS the sample cannot be left in the  $\mu$ EP measurement cell, which has to be carefully rinsed after each measurement. Any replicate measurement is conducted with a new sample from the respective suspension. This additional effort reduces the number of pH values looked at in the experiments.

Due to the different procedures of the ELS and  $\mu$ EP measurements one cannot expect that the results of both instruments perfectly agree. However the magnitudes of the zeta potential and the isoelectric points (IEPs) are very similar

Both instruments can be likewise used for the zeta potential characterisation. For practical reasons, the ELS results are subsequently used to report the pH dependency, whereas the  $\mu$ EP results are employed to reveal temporal changes of the zeta potential.

The results of both instruments are highly repeatable (i.e. good agreement between repeated measurements of one suspension sample). The reproducibility (repeated measurements of independently prepared suspension samples) of the  $\mu$ EP was acceptable and only slightly lower than the reproducibility of the ELS results.

### **2.1.3 Chemical analysis (LC-MS, ICP-OES)**

#### **Liquid chromatography-mass spectrometry (LC-MS)**

For the characterisation of the surface stability of the glycerol coating of the NM104, LC-MS measurements of the solvent of the ENM were conducted. It is conceivable that the glycerol of the NM104 particles are released when the particles are suspended in water. Consequently, a quantitative detection of the desorbed glycerol can be done by liquid chromatography with mass spectrometric detection (LC-MS) of the suspensions liquid phase. Before LC-MS measurements the liquid and solid phase of the suspension was separated by centrifugation (10 min, 2700G). Afterwards, the supernatant was taken, filtered (0.22  $\mu$ m nylon filter) and analysed.

For LC-MS measurements, a Shimadzu Prominence HPLC system which consists of a CBM-20A controller, a DGU-20A3 degasser, two LC-20AD pumps, an SIL-20AC auto sampler, and a CTO-20A column (Shimadzu, Duisburg, Germany) was coupled to a linear ion trap quadrupole mass spectrometer (API 3200 QTrap, Applied Biosystems, Darmstadt, Germany). Data acquisition and analysis were performed with Analyst Software version 1.5.2. The chromatographic separation was done on a Phenomenex Luna Amino column (150  $\times$  2.0 mm, 3  $\mu$ m) at 35°C. The mobile phase consisted of 20/80 (v/v) water/acetonitrile with 40  $\mu$ mol/L Cesium acetate as complexing agent. The flow rate and the injection volume were set to 0.2 mL/min and 10  $\mu$ L, respectively.

This method was developed, adapted to the requirements of this study, verified and realized by S. Wiese, T. Teutenberg and J. Türk (IUTA).

#### **Inductively coupled plasma optical emission spectrometry (ICP-OES)**

For the surface characterisation and the analysis of the carrier function quantitative inductively coupled plasma optical emission spectrometry (ICP-OES) measurements were conducted for aluminium, silicon, copper and titanium. The measurements were conducted according to the tasks and the TiO<sub>2</sub> material for the powders, suspensions, supernatant, soil matrix and eluate. Detailed information about the method can be found in Annex AII.7. All samples were digested by different methods prior to the ICP-OES analysis.

### **Digestion method aluminium content**

100 mg – 200 mg of the solid materials was mixed with 9 mL HNO<sub>3</sub> (65% ROTH) and 1 mL H<sub>2</sub>O<sub>2</sub> (30% ROTH) followed by a microwave digestion (temperature program - 3 min from 20 °C to 130 °C, 5 min from 130 °C to 210 °C and 7 min at 210 °C). Afterwards the samples were filled up to a volume of 25 mL. Six millilitres of the supernatant were mixed with 0.8 mL HNO<sub>3</sub> (69% ROTH) followed by microwave digestion (temperature program - 3 min from 20 °C to 130 °C, 5 min 130 °C to 210 °C and 7 min at 210 °C) and subsequent sample down-cooling to room temperature for 90 min.

### **Digestion method silicon content**

To avoid a contamination of the samples by glass materials another digestion method was used for the quantification of silicon in the samples. Furthermore the sample preparation was done in platinum cups to avoid any silicon contamination of the glass vessels.

100 mg – 200 mg of the solid materials were mixed with 1000 mg NaOH. Afterwards the mixture was heated for 20 min at 600°C and 50 mL ultrapure water was added to the sample.

### **Digestion method copper and titanium content of the soil and eluate / suspension samples**

Six millilitres of the liquid sample (eluate and suspensions) or 150 mg of the soil was mixed with 0.8 mL HF (48%), 0.8 mL HNO<sub>3</sub> (69%) and 2.4 mL HCl (38%) followed by microwave digestion (temperature program - 3 min 20 to 130 °C, 5 min 130 °C to 210 °C and 7 min at 210 °C). Afterwards the samples were cooled for 90 minutes. After the samples were cooled they were mixed with 1 mL H<sub>3</sub>BO<sub>3</sub> (5%) followed by a second temperature program in the microwave (8 min 20 °C to 180 °C with 3 min at 180 °C).

Before the samples were analysed using ICP-OES the samples were diluted (1:5).

## **2.1.4 Scanning electron microscopy coupled with energy dispersive X-ray spectroscopy (SEM / EDX)**

### **Surface coating**

For the characterisation of the surface coating stability of the two coated TiO<sub>2</sub> nanomaterials SEM / EDX scans were conducted. With SEM / EDX a qualitative detection of the silicon (dimethicone) and aluminium is possible. For the measurements a sub sample of the dry powder or 10 µL of the suspensions were placed on a sample holder.

### **Carrier function soil experiments**

A qualitative detection of TiO<sub>2</sub> nanomaterials from different segments of the soil columns was conducted by representative SEM and EDX analysis. For the detection of TiO<sub>2</sub> nano-

materials the soil grains of different subsamples of the segments were analysed. Identification of transported TiO<sub>2</sub> included always both, morphological and chemical analysis, to differentiate between background and nanomaterials.

### **2.1.5 Electron Paramagnetic Resonance (EPR) Spectroscopy**

The detection of particle induced reactive oxygen species (ROS) and/or “surface reactivity” was done by spin trap/probe based electron paramagnetic resonance (EPR) spectroscopy technique (EPR 300 Spectrometer Mini Scope, Fa Magnettech, Berlin). Two different complementary approaches were used. The first approach is mainly sensitive to metal induced hydroxyl radical generation (OH $\cdot$ ), while the second approach is detecting a kind of “surface reactivity”. Additionally to these two approaches the photo catalytic activity of the NMs was studied as impact of UV irradiation on the hydroxyl radical generation (OH $\cdot$ ) potency.

#### **Hydroxyl radical generation**

Regarding to the method of Shi et al., (2003) in the presence of hydrogen peroxide (H<sub>2</sub>O<sub>2</sub>) and 5,5-dimethyl-1-pyrroline-N-oxide (DMPO) this method is especially sensitive for the detection of hydroxyl radicals (OH $\cdot$ ) generated via Fenton-type reactions. Briefly, 50  $\mu$ L of the particle suspension is mixed with 100  $\mu$ L DMPO (0.05 M) and 50  $\mu$ L of H<sub>2</sub>O<sub>2</sub> (0.5 M), incubated in a dark, shaking water bath for 15 min at 37 °C before analysed by EPR.

#### **(Surface) reactivity**

A possible (surface) reactivity of the material, caused by particle surfaces bound components and / or physical-chemical particle properties, was established by measurements using the spin probe 1-hydroxy-3-carboxy-2,2,5,5-tetramethylpyrrolidine hydrochloride (CPH) mixed with the chelator desferroxamin (0.1 mM) according to Papageorgiou et al. (2007), who used not the same but similar spin probe 1-hydroxy-4-phosphono-oxy-2,2,6,6-tetramethylpiperidine hydrochloride (PPH). The (surface) reactivity is expressed by splitting of the H<sup>+</sup> of the CPH molecule or by generating an electron delocalisation via binding. This effect is driven probably by directly active surfaces of the material. The preparation was done by mixing 50  $\mu$ L of particle suspensions with 50  $\mu$ L CPH (1 mM) and incubating for 10 min at 37 °C before analysing by EPR.

#### **UV irradiation (photo catalytic activity)**

Hydroxyl radical generation after UV-irradiation was measured according to Lipovsky, et al. (2012) in the presence of 5,5-dimethyl-1-pyrroline-N-oxide (DMPO). This method is especially sensitive for the detection of hydroxyl radicals (OH $\cdot$ ) after UV-irradiation. For the measurement 30  $\mu$ L of the particle suspension (final conc. 5 mg/L) is mixed with 30  $\mu$ L

DMPO (final conc. 0.05 M) and analysed by EPR after irradiation with UV-light (UV Energy saving lamp Omnilux 25 Watt E27 3U 230V/50Hz AC, 6000 UV K, 22000 lm) for 10 min and compared to not irradiated samples. In addition to the analysis with NM104 the photo catalytic active P25 (not coated) was used as positive control.

### 2.1.6 Nuclear magnetic resonance (NMR) spectroscopy

The detection of the particle surface area is assumed to be one crucial parameter for particle characterisation. The reason is that the surface area as the interface of the particle self and the surrounding media gives information about the available contact area e.g. for subsequent reactions (e.g. desorption of dimethicone, glycerol). For the detection of the “reactive” material surface area in suspensions a new instrument was used in this study, a low resolution NMR (US Patent, 7,417,426, 2008 - Acorn Area™). In principle, this technique is detecting the response of adsorbed and freely diffusing liquid molecules to an alternating/HF magnetic field.

However, the surface area determination by NMR has certain limitations – in particular for ENMs - that have to be considered and became evident in this study. The main prerequisite for successfully conducting surface area measurements with NMR is that a sufficiently high particle concentration remains homogeneously distributed in the measuring zone throughout the NMR-analysis. For the nanomaterials used in this study a minimum particle concentration of 1 weight-% was required. However, at this concentration the nanomaterial suspensions were not stable and agglomerated rather quickly. As a result the dispersed particles settled rather quickly and thus left the measuring zone. It was therefore not feasible to perform reliable measurements (ANNEX AIII.7).

### 2.1.7 Radioanalytics

For the carrier function soil experiments <sup>14</sup>C-labelled triclocarban (<sup>14</sup>C-TCC) with a specific radioactivity of 3.5 MBq/mg was purchased from American Radiolabeled Chemicals Inc. (St-Louis, US) via Hartmann Analytic GmbH (Braunschweig, Germany) (Figure 2).

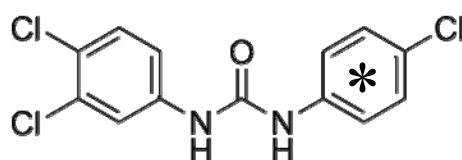


Figure 2: Triclocarban (TCC) with <sup>14</sup>C label (\*) at the monochlorinated phenyl ring

Liquid samples (eluate and eluate extracts) were transferred to scintillation vials (polyethylene vials of 20 mL, Perkin Elmer, Germany) and mixed with an adequate volume of scintillation cocktail (LumaSafe Plus™, Perkin Elmer, Germany). The maximum capacity of this cocktail for both aqueous and organic samples is a 1:1 (v/v) mixture. Therefore, no less than the same volume of cocktail was added. The number of disintegrations per min-

ute (dpm) of radioactive atoms was determined in a liquid scintillation counter (LSC; LS 5000 TD, Beckman Instruments GmbH, Germany) and recalculated to the number of disintegrations per second (dps or Bq). The detection limit (LOD) of the LSC amounts to 60 dpm or 1 Bq. For the test compound, <sup>14</sup>C-TCC with a specific radioactivity of 3.5 MBq/mg, this means a LOD of 0.28 ng/sample, i.e. 28 ng/L considering the maximal sample volume of 10 mL.

Dry solid samples (soil and organism) of maximum 0.3 g were combusted in a biological oxidizer (OX500; RJ Harvey Instruments Corporation, USA) after being collected in pre-dried and pre-weighed paper cones (Perkin Elmer, Germany) or self-formed aluminium vessels. The <sup>14</sup>CO<sub>2</sub> produced during oxidizing was trapped in a scintillation vial containing 15 mL of scintillation cocktail (Oxysolve C-400; Zinsser Analytic GmbH, Germany) that was subsequently subjected to LSC. The recovery of this process was determined by comparing the known radioactivity of 10 µL of a standard solution (SV) with the radioactivity measured after combusting paper cones filled with cellulose spiked with 10 µL of this standard (CV). The amount of radioactivity in samples was then calculated by subtracting blank values (BV), obtained by combusting clear cellulose, from the measured values (MV), and multiplying the result by the combustion factor, i.e.  $(SV-BV)/(CV-BV)$ , to correct for losses during the combustion process. BV, CV and SV are the mean values of at least three replicates. Given the maximal mass of 0.3 mg of organic material that can react with O<sub>2</sub> in the oxidizer and be trapped as CO<sub>2</sub> in the cocktail, an LOD of 0.28 ng <sup>14</sup>C-TCC /0.3 g solid sample (1 µg/kg) can be derived.

### 3 Surface coating stability

#### 3.1 Background

In this study two functionalised TiO<sub>2</sub> nanomaterials were analysed, which are used in sunscreens (manufacturer, [www.sachtleben.de](http://www.sachtleben.de)). Both materials consist of TiO<sub>2</sub> nanoparticles that are coated with aluminium oxide (Al<sub>2</sub>O<sub>3</sub>) (around 6 weight-%) to avoid light induced photo-oxidation reactions or / and the generation of reactive oxygen species (ROS) at the TiO<sub>2</sub> surface (Auffan et al., 2010). A further coating with dimethicone (NM103) (around 2 weight-%) or glycerol (NM104) (around 1 - 2 weight-%) is to ensure hydrophobic and hydrophilic behaviour, respectively. The materials were coated for better dispersability, thus widens the applicability of the nanomaterials to different types of creams (Table 1). The aim of this investigation is to study the possible degradation or change of this surface functionalisation. Any change of the coating may affect the fate and behaviour of the studied nanomaterial in the environment. The strategy, developed and pursued to test and identify possible changes of the surface coating, was to vary dispersion energy and environmental parameters like pH, ionic strength (CaCl<sub>2</sub>) or dissolved organic carbon content (DOC), as part of natural organic matter (NOM). Changes in the behaviour were used as indicators for possible aging of the coating. Furthermore the coating material was also tried to be determined in the dispersion media.

#### 3.2 Materials

The two nanomaterials examined in this study are the OECD nanomaterials NM103 (trade name: UV Titan M262) and NM104 (trade name: UV Titan M212), which are commercial products of Sachtleben Chemie GmbH (Germany). The TiO<sub>2</sub> core of the particles is rutile, the Al<sub>2</sub>O<sub>3</sub> shell is not specified. Dimethicone, which is used for hydrophobisation of NM103, is a polymeric organic silicone ((C<sub>2</sub>H<sub>6</sub>OSi)<sub>n</sub>) and frequently called polydimethylsiloxane (PDMS). It is considered practically insoluble in water. Glycerol (C<sub>3</sub>H<sub>8</sub>O<sub>3</sub>), which is used for the hydrophilisation of NM104, is a polyhydric alcohol and entirely mixable with water. There is no information on how the coating with dimethicone and the glycerol is realised (by physical adsorption or covalent bonds). Both nanomaterials consist of nanosized primary particles: XRD yields an average TiO<sub>2</sub> crystallite size of 20 nm. Sizing techniques that are based on the dynamic or optical behaviour therefore measure particle sizes (equivalent diameters) that are much larger than the primary particles (see manufacture data Table 1). The size of the primary particles and the total Al<sub>2</sub>O<sub>3</sub> content allows a calculation of the thickness of Al<sub>2</sub>O<sub>3</sub> shell (0.20 nm - 0.25 nm). These results were confirmed by LEIS (Low Energy Ion Scattering) measurements of the materials (Annex AIII.1).



With LEIS measurements a maximum thickness of the aluminium oxide and PDMS or Glycerol coating of 1.5 nm could be observed.

Table 1: Manufacturers data (Sachtleben Chemie GmbH, Germany) for the used coated titanium dioxide nanomaterials

	NM104 (UV Titan M212)	NM103 (UV Titan M262)
TiO <sub>2</sub> content	90% - 93%	89% - 92%
Al <sub>2</sub> O <sub>3</sub> content	6%	6%
Dimethicone content	-	2%
Glycerol content	1%	-
Primary particle size (agglomerate size in suspension)	20 nm (670 nm - 1270 nm)	20 nm (180 nm - 720 nm)
Crystal form	rutile	rutile

The stability of the surface coating in aqueous media, which were always prepared from deionised, filtered water (specific conductivity: 18 MΩ·cm; particle filter: 0.2 µm membrane) as function of the pH, ranging from pH 4.5 to pH 10, was tested. In order to adjust a defined electrolyte background the following salts were employed:

- CaCl<sub>2</sub> (pro analysis, MERCK and FLUCKA): 0.0001 M, 0.001 M and 0.01 M
- NaCl (pro analysis, J.T. Baker): 0.001 M

The two lower electrolyte concentrations cover the range that can be usually expected for surface water and the highest concentration for seawater (Ottofülling et al., 2011), which has less than 1000 mg/L electrolyte (with a global average of 120 mg/L) and in which Ca<sup>2+</sup> are the dominant cationic species (i.e. the Ca-concentration is less than appr. 0.0125 M) (Wetzel, 1983). Just for comparison: In artificial freshwater (dilution water according to DIN 38412-30) the Ca-content is adjusted to 0.002 M.

In surface water a high background of natural organic matter exists which could influence the fate and behaviour of the nanomaterials. In natural soils, e.g. in soil water of Podzol, varying concentrations of DOC ranging from 2.6 – 23.5 mg/L were detected (Löfgren et al., 2011). Therefore the possible effect of dissolved organic carbon (DOC) was investigated.

The variability of organic compounds in environmental media is huge. One ubiquitous organic component class present in the environment are humic and fulvic acids. We decided to use in this study a humic acid (AHA Sigma Aldrich) as a representative and reproducibly obtainable organic material. The concentrations were chosen to be 2.5 mg/L, 5 mg/L and 10 mg/L, concentrations which also can be found in environmental media. The pH was adjusted by aqueous solutions of HCl (pro analysis, MERCK and Roth 0.1 M) and NaOH (pro analysis, MERCK and Roth 0.1 M).

### 3.2.1 Preliminary remarks on surface coating stability

The tested materials are produced with two layers of coatings: an Al<sub>2</sub>O<sub>3</sub> layer for averting photo-oxidation and a second layer of dimethicone / glycerol molecules for ensuring hydrophobic / hydrophilic behaviour. The fate and behaviour of the material is affected by the actual surface coating (e.g. IEP, adsorption capacity and repulsion) and therefore the stability of the coating of the two coated TiO<sub>2</sub> nanomaterials was tested under different conditions. Hence different endpoints and their possible changes were analysed. The following tests were conducted:

- qualitative and quantitative detection of the released coating material (section 2.1.3). The analysis of the supernatant or dispersion media for the coating material allows for the direct detection of changes in the surface coating (section 2.1.3). A qualitative analysis about the surface composition of the solid material was analysed with ToF SIMS, LEIS and FTIR (section Annex AIII.1).
- zeta potential, iso electric point (IEP) (section 2.1.2) and
- size distribution of the nanomaterial in suspensions (section 2.1.1)
- changes of the zeta potential and size distribution of the nanomaterial dispersion after different treatment are an indication of changes in the surface properties and hence coating of the nanomaterial.
- hydroxyl radical generation potential (section 2.1.5)
- this is a specific test on the stability of the Al<sub>2</sub>O<sub>3</sub> coating of the TiO<sub>2</sub> particles. Titanium dioxide produces hydroxyl radicals when irradiated while this formation is not possible when the TiO<sub>2</sub> is coated by aluminiumoxide (Al<sub>2</sub>O<sub>3</sub>). Testing the potential of hydroxyl formation of the suspensions after different stress tests allows for the indirect detection of losses in Al<sub>2</sub>O<sub>3</sub> coating.
- morphology, aluminium and silicon content of single agglomerates by SEM / EDX
- these analyses were also conducted after different treatment steps to determine any changes in the chemical composition of the nanomaterials.

The above endpoints are analysed as direct and indirect indicator for a change of the surface. The stability of a surface coating is a matter of chemistry, thermodynamics and mechanical processes and depends on the suspension medium and on the applied dispersion procedure. Different test conditions were chosen to simulate different stress conditions for surface coatings.

### 3.3 Suspension preparation

A major question of this study is how the surface functionalisation of the suspended nanomaterials is affected by environmental parameters, like ionic strength, pH or DOC concentration. This can be answered by measuring relevant / characteristic properties of the suspension under defined variation of these parameters. By doing this, one has to

ensure that i) the surface functionalisation is not impaired by suspending the nanomaterials and that ii) the same state of dispersion is reproduced after each primary suspension preparation. This was achieved by a minimal invasive procedure standardised in a standard operating procedure (SOP), which comprises the two steps of suspending powder and dispersing agglomerates. The aim of the standardised SOP is also to yield a stock suspension, in which the nanomaterial is homogeneously distributed and does not agglomerate significantly for at least 24 hours. The former condition is necessary for several characterisation techniques and the latter is required because the time periods for preparation and measurement differ considerably for the different characterisation techniques. One important task in suspension preparation is also the detection of possible losses of the coating already due to the preparation of the suspension.

While the development of an appropriate SOP is subject to the scientific task and experimental method chosen, its main features can be derived from previous studies e.g. Kuhlbusch et al. (2012):

- stock suspension is prepared by suspending the nanomaterials in deionised water for environmental testing
- the particle concentration in the stock suspension is higher than required for some characterisation techniques
- suspending powders in water may require time for wetting the particle surfaces
- in order to achieve a reproducible state of dispersion the nanomaterial suspensions require ultrasonic treatment
- energy input by ultrasonication should be kept low and suspensions should be cooled during sonication
- after ultrasonic treatment the interfaces need time for equilibration.

The prepared stock suspensions were diluted to the target concentration for the  $\mu$ EP (c.f. section 2.1.2). For measurements with ELS no dilution was necessary. For the further experiments with  $\mu$ EP the stock suspension was also diluted with the electrolyte or DOC solution. For ELS the material was directly dispersed with the target DOC or CaCl<sub>2</sub> concentration. The pH was adjusted with 0.1 M HCl and 0.1 M NaOH.

## **3.4 Results**

### **3.4.1 Stock suspension preparation**

The need for a uniform preparation of the stock suspensions has already been discussed in section 3.3. Beside, the principles for an appropriate preparation method were derived from a previous study on TiO<sub>2</sub> nanomaterials. However, the details of the preparation SOP – in particular the sonication energy input – have to be determined and validated for each nanomaterial separately. Therefore different dispersion procedures were tested for

the two nanomaterials (NM103 and NM104). The results are summarised in Table 2. In each case the powders (solid material) were suspended in deionised water and the particle size distributions of the final suspensions were probed by DLS. An appropriate dispersion procedure should avoid high energy input and simultaneously guarantee a high reproducibility of the size distribution and a low polydispersity. If possible, the sedimentation of the dispersed phase should be negligible and DLS characterisation should yield reliable results. Stable suspensions can be achieved for particle sizes up to the micrometer range, but the results also vary dependent on the material type and properties. Measured with DLS the typical average particle diameters are in the range 1 nm to about 1000 nm (ISO 22412).

Table 2: DLS results for differently prepared NM suspensions; powders suspended in deionised water and dispersed with a sonication probe (200 W), with overhead stirrer (~350 rpm) and with sonication in a waterbath (150 W, stirred, fixed position of the sample); statistics for 5 independent samples,  $\pm$  = standard deviation; n = 10, (repeated measurements).

suspension technique	NM104		1000 ppmw		NM103	
	100 ppmw		1000 ppmw		1000 ppmw	
	$x_{Cum,r}$ nm	PDI	$x_{Cum,r}$ nm	PDI	$x_{Cum,r}$ nm	PDI
1 min probe	207 $\pm$ 4.1	0.302 $\pm$ 0.025	204 $\pm$ 1.2	0.271 $\pm$ 0.009	248 $\pm$ 2.9	0.381 $\pm$ 0.010
2 min probe	202 $\pm$ 5.8	0.305 $\pm$ 0.014	194 $\pm$ 0.95	0.258 $\pm$ 0.007	216 $\pm$ 3.0	0.359 $\pm$ 0.008
4 min probe	187 $\pm$ 5.0	0.279 $\pm$ 0.023	181 $\pm$ 1.2	0.239 $\pm$ 0.003	189 $\pm$ 3.9	0.344 $\pm$ 0.008
10 min probe	169 $\pm$ 3.8	0.251 $\pm$ 0.012	163 $\pm$ 0.53	0.214 $\pm$ 0.006	160 $\pm$ 2.1	0.304 $\pm$ 0.010
1 h overhead stirrer	616 $\pm$ 25.3	0.410 $\pm$ 0.057	-	-	-	-
30 min waterbath + overhead stirrer	318 $\pm$ 80.4	0.339 $\pm$ 0.042	-	-	-	-

The results of the different dispersion procedure indicate that a slight agitation by moderate stirring produces broad size distributions (PDI > 0.3) with a substantial variation in the final size distribution and visible sedimentation within 24 hours. In contrast, all sonicated samples showed only little sedimentation. Moreover, sonication leads to particle size distributions well below the 1  $\mu$ m limit and reduces the distribution width when compared to stirring.

Based on this results the following SOP was employed for preparing the stock suspensions:

- suspend 5 mg TiO<sub>2</sub> nanomaterial in 50 mL deionised water (i.e. 100 ppmw). For few experiments a sample volume of 100 mL was required; then 10 mg of the nanomaterial were suspended.
- wait until the nanomaterial has become wetted and is completely submerged in the liquid phase (While this process is very rapid for the hydrophilic NM104, it takes approximately 15 min for the hydrophobic NM103).

- homogenise the suspended powder by slight agitation with a magnetic (350 rpm)<sup>1</sup> or overhead stirrer.
- disperse the nanomaterial by sonication of the suspension sample with a sonication probe (200 W). To minimize the effect of the sonication for the surface coating of the materials an adequate minimally invasive procedure is used with a sonication time of 1 min for 50 mL samples and 2 min for 100 mL samples. If the ultrasonic probe operates with a different nominal power output, the sonication time has to be adjusted, so that the nominal energy input is not affected. During the sonication the suspension samples are cooled in cold water.
- sonication is followed by 60 min of moderate stirring (overhead stirrer 350 rpm or magnetic stirrer).

More details on this SOP are given in Annex II.

Since the various measurements took different periods of time and could not always be conducted simultaneously for practical reasons the stock suspensions stability was checked / validated over a period of 30 days. The corresponding results (i.e. mean size  $x_{Cum}$  and polydispersity index PDI from DLS analysis) are shown in Figure 3 for both nanomaterials.

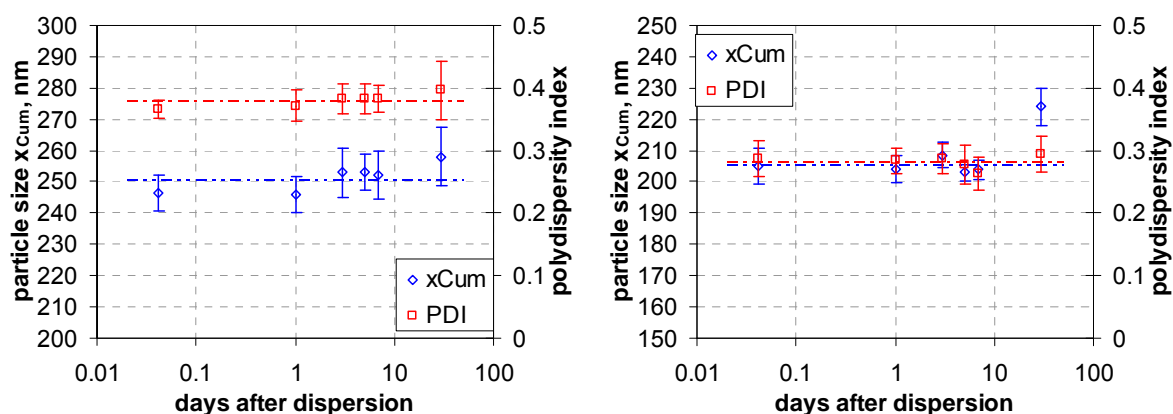


Figure 3: Average size ( $x_{Cum}$ ) and polydispersity index from dynamic light scattering measurements, when prepared according to SOP - evolution with time, left: NM103, right: NM104; n = 10 (repeated measurements).

The results clearly show no significant changes in size distribution within the first 7 days, even though a slow agglomeration process cannot be excluded (in particular when the 30 days data are considered). For the purpose of this study the stock suspensions of the two nanomaterials can be considered as stable against agglomeration.

In several cases the stock suspensions were further processed, e.g. for examining the influence of the pH value or the impact of electrolytes and solutes. For measurements with  $\mu$ EP few millilitres of the stock suspension were diluted from 100 ppmw to 2 ppmw by

<sup>1</sup> Magnetic stirrers should be avoided – in particular for long term experiments.

adding the respective solution. For measurements with ELS no dilution was necessary. The pH was adjusted with NaOH or HCl (cf. section 3.3).

### 3.4.2 Results - Surface coating stability NM104 (UV Titan M212)

#### Glycerol from NM104 in supernatant

The NM104 nanomaterial is hydrophilised by a glycerol layer. The glycerol was quantified by a total carbon analysis using a thermal-optical EC/OC analyser (Sunset dual-optics lab instrument). Therefore, around 5.4 mg of the powder were filled in an annealed quartz glass combustion boat and were analysed. The sample was incinerated by different temperature steps and the total, elemental and organic carbon (TC, EC, OC) of the sample was detected. On the basis of the organic carbon measurements (OC) in consideration of a converting factor of 2.6 an amount of 1.14% (SD < 1) glycerol (C<sub>3</sub>H<sub>8</sub>O<sub>3</sub>)<sub>n</sub> by total nanomaterial weight was observed, with an OC/TC ration of around 96%. That means, that the maximum amount of glycerol that can be released from the surface with a concentration of 100 mg/L is  $0.0114 \times 100 \text{ ppmw} = 1.140 \text{ ppmw}$ , which corresponds to 1.14 mg/L. The type of surface bonding is not disclosed by the manufacturer. However, since glycerol is completely soluble / mixable with water, it is expected that each glycerol molecule that is detached from the surface can be found in the bulk liquid.

The stability of the glycerol layer was examined for three different dispersion procedures,

- mixing – non-recurring manual shaking,
- 1 minute stirring after suspending the powder,
- 1 minute sonication (ultrasonic probe) followed by 1 hour of moderate stirring - standard operation procedure (SOP).

The glycerol concentration of different suspensions was analysed by using two independent methods, an enzymatic UV test and a LC-MS. A specific measuring protocol was applied. Briefly after suspension preparation, the suspension was centrifuged (2700G for 10 min). The supernatant was then filtered using a 0.22 µm nylon filter (Magna-Nylon, Roth) to separate the solid from the liquid phase. Afterwards, the desorbed glycerol concentration was measured in the filtrate of the suspension.

The (lower) limit of detection (LOD) of the UV method is 400 µg/L glycerol and of the LC-MS 200 µg/L; values for the deionised water employed in this study lay below this detection limit.

#### Enzymatic UV test

For this method a commercially available assay (R-BIOPHARM, Darmstadt, Germany) has been employed and the determination of glycerol takes place indirectly. First, glycerol is phosphorylated by means of adenosine-5'-triphosphate to L-glycerol-3-phosphate and adenosine-5'-diphosphate, a reaction which is catalyzed by glycerokinase. Afterwards, the

formed adenosine-5'-diphosphate is reconverted into ATP and pyruvate by phosphoenolpyruvate. Here, the reaction was catalyzed by pyruvate kinase. Finally, in the presence of the enzyme L-lactate dehydrogenase, the formed pyruvate is reduced to L-lactate by reduced nicotinamide-adenine dinucleotide (NADH) which concurrently is oxidized to NAD. Moreover, the consumption of NADH is stoichiometric to the amount of glycerol and has been detected by means of its UV absorption at a wavelength of 340 nm using a Specord 200 UV/VIS spectrometer (spectrometer (Analytik Jena, Jena, Germany). The detected amount of the NADH was employed for the calculation of the glycerol concentration. Detailed information can be found in Annex AII.5

#### LC-MS

The ionization of glycerol was made in the positive mode of turbo-electrospray ionization at atmospheric pressure. In order to detect the precursor ion of glycerol in the first mass analyser and the corresponding fragment ion in the second analyser, multiple reaction monitoring (MRM) mode have been employed (cf. section 2.1.3). Detailed information can be found in Annex AII.4. The limit of detection of the LC-MS method was calculated by using the calibration curve method according to DIN 32645. The resulting value was 200 µg/L.

The UV tests as well as the LC-MS method were developed and adapted to the requirements of this study, verified and realized by S. Wiese, T. Teutenberg and J. Türk.

#### Quantitative glycerol measurements

The filtrate of the suspension was analysed directly without derivatisation by means of the enzymatic UV test as well as the LC-MS method.

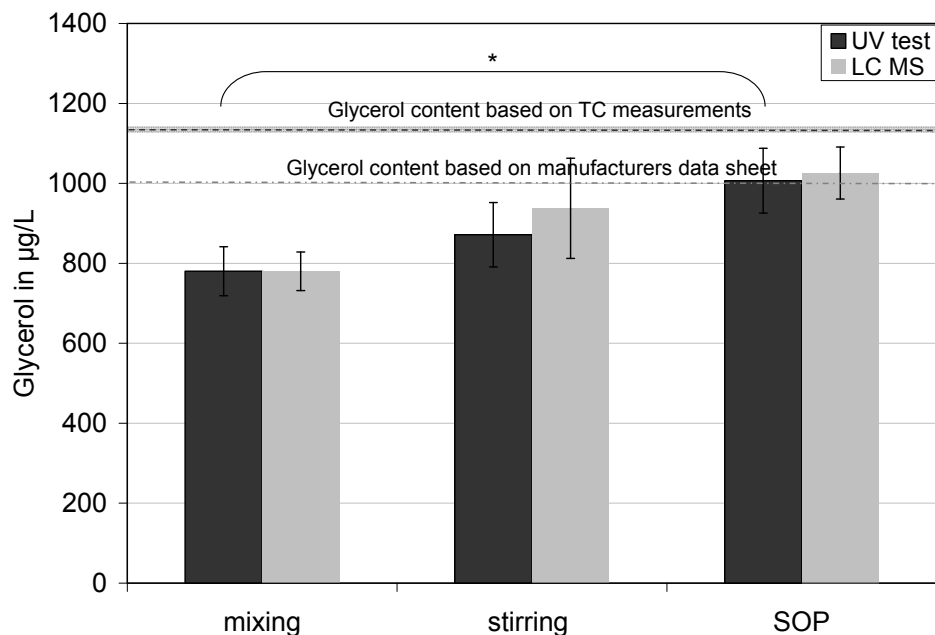


Figure 4: Quantitative measurements of the glycerol content of 100 mg/L NM104 suspension preparation using an enzymatic UV test and LC-MS measurements. The dashed lines indicate the glycerol content based on the manufactures data and based on own OC (organic carbon) measurements (incl. 75er and 25er percentile) using a sunset EC/OC (elemental and organic carbon) analyser; n = 3.

Chemical analysis of the glycerol concentration indicates that the addition of water and subsequent mixing (non-recurring manual shaking) lead to a removal of around 65% ± 9% of the glycerol from the surface of the NM104, if the OC measurements of the glycerol content were used as basis for the calculation. No significant different results were found between moderate stirring for 1 minute and the established SOP. By using the established SOP (1 min sonication (ultrasonic probe) followed by 1 hour of moderate stirring) 88% ± 8% of glycerol was removed from the surface (Figure 4).

Given these high degrees of glycerol release from the nanomaterial surface removal and the good solubility of glycerol in water, we can assume that the deviations between the three dispersion procedures are due to energy effects. Based on the results it was shown that with increasing energy input the glycerol release increased. With the established SOP nearly all glycerol was removed from the nanomaterial surface. Therefore no further analysis of the glycerol concentration was conducted in the following tests.

### Aluminium from NM104 in supernatant

After suspension preparation with the established SOP, due to the release of nearly all glycerol from the material surface, it seems that the residual coating of the NM104 material is an Al<sub>2</sub>O<sub>3</sub> layer which contributes with 6 weight-% to the total material mass according to the information from the manufacturer. Any damage of this layer is considered to



increase the Aluminium concentration in the bulk liquid, which was measured with ICP-OES. The (lower) limit of detection (LOD) of the (used) ICP-OES is reported with 1 µg/L, which corresponds to < 0.05% of the used aluminium amount. Values for the deionised water employed in this study lay below this limit. If the Al<sub>2</sub>O<sub>3</sub> coating would completely detached from the TiO<sub>2</sub> surface (100 mg/L) and dissolved in the suspension media the Al<sup>3+</sup>-concentration would amount to  $2 \times 27 / 102 \times 0.06 \times 100 \text{ ppmw} = 3.18 \text{ ppmw}$ , which corresponds to an Al<sup>3+</sup> concentration of 3180 µg/L.

The solubility of Al<sub>2</sub>O<sub>3</sub> in neutral conditions is rather low. Roelofs & Vogelsberger (2006) report the following experimental values for the maximum concentration of dissolved Al<sup>3+</sup>-species:

- < 20 µg/L, when  $5.5 \leq \text{pH} \leq 8$
- 73 µg/L, when pH = 5 and 100 µg/L when pH = 9
- 515 µg/L, when pH = 4.5

The pH of the stock suspension after SOP dispersion was 6.9. Theoretically based on the low solubility of Al<sup>3+</sup> at this pH, only a maximum amount of 20 µg/L could be dissolved from the surface of the ENM.

In the supernatant of suspensions which were prepared according to the established SOP no aluminum above the LOD could be detected.

### **Zeta potential of NM104 when dispersed according to SOP**

The zeta potential can provide an indication about the actual surface of the analysed nanomaterial, due to this, these measurement offer a further way of determining changes of surface coating. The electric charging of an Al<sub>2</sub>O<sub>3</sub> surface differs from that of a TiO<sub>2</sub> surface. This is most prominently visible in the isoelectric point (IEP, pH-value where the zeta potential becomes zero). For TiO<sub>2</sub> particles suspended in aqueous suspensions Kosmulski, (2006) cited experimental IEP values ranging between pH 5.1 - 7.6, 50% of the data were larger than 5.7 and smaller than 6.3. The variation of the IEP is rather large and due to the fact that the crystal modifications, the electrolytes and the measurement methods did considerably vary among the reviewed papers. However, for Al<sub>2</sub>O<sub>3</sub> particles (alpha and gamma modification, varying electrolyte) Kosmulski (2006) reported IEP values in the range from pH 8 to 9.5 (with 50% lying between pH 8.0 and pH 8.8). Similarly, Shin et al. (2006) gave values for the IEP of alpha-Al<sub>2</sub>O<sub>3</sub> that fall in the range of pH 8 - 9. Hence the IEPs of the Al<sub>2</sub>O<sub>3</sub> coating and of the TiO<sub>2</sub> core material are quite distinct; they may thus serve as an indirect indication of the surface coating.

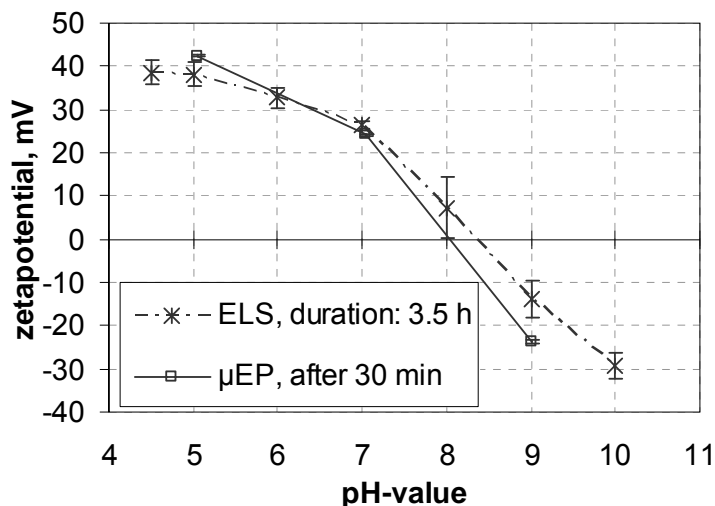


Figure 5: Zeta potential measurements of 100 mg/L NM104 in DI water, suspension preparation based on SOP; two measurement techniques were applied ELS and  $\mu$ EP; n = 3.

Figure 5 shows the pH dependency of the zeta potential for NM104 when dispersed according to the SOP. Results of two measurement techniques, electrophoretic light scattering (ELS) and microelectrophoresis ( $\mu$ EP), are reported. The curves are averages from three independent sample preparations and the standard deviation for each data point is plotted as error bar. The IEP was observed in the pH range from 8 to 9. For pH values where the IEP of the TiO<sub>2</sub> core is expected (i.e. around pH 6, see above), the measured zeta potentials are significantly larger than zero.

The IEP is in the range of that for an Al<sub>2</sub>O<sub>3</sub> surface. Hence, the zeta potential measurements confirm the conclusion of the LC-MS and UV tests, that nearly all of the glycerol was transferred from the surface into the suspension media (cf. section 3.4.2) and the aluminium oxide was the surface layer of the ENMs.

### SEM / EDX of NM104 when dispersed according to the SOP

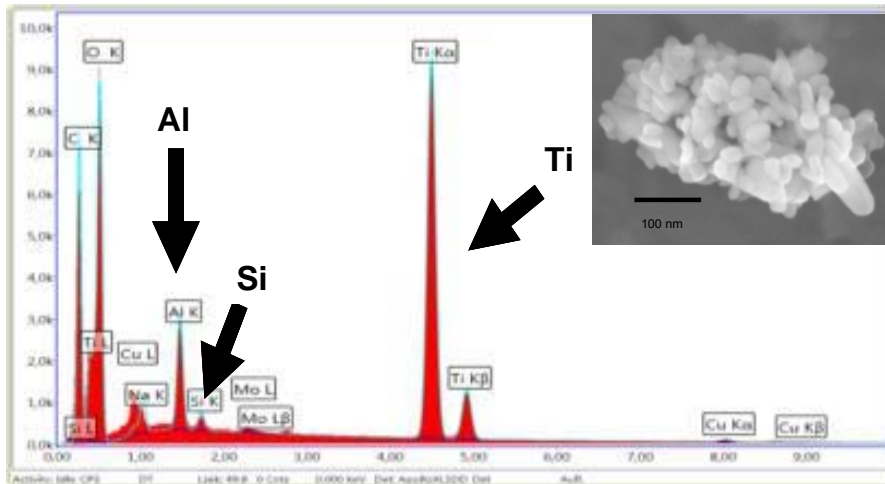


Figure 6: SEM / EDX scan of the dry powder of NM104.

In Figure 6 SEM / EDX scans of the untreated powder of the material are presented. Beside titanium and aluminium also silicon was detected although no silicon was used for the functionalisation. It is conceivable that during the manufacturing process or during the sample preparation steps (glass vessels) contamination with silicon may occur.

After suspension preparation based on the established SOP an aliquot of the suspension was analysed with SEM / EDX. Therefore 5  $\mu$ L of the suspension were pipetted to a copper grid, dried and analysed without any washing procedure. Consequently any dissolved, non-volatile species can be found on the background substrate and on the materials if present in high concentration.

A typical result of SEM / EDX for NM104 after treatment according to the SOP is shown in Figure 7 which refers to the chemical composition of the substrate and the materials, respectively.

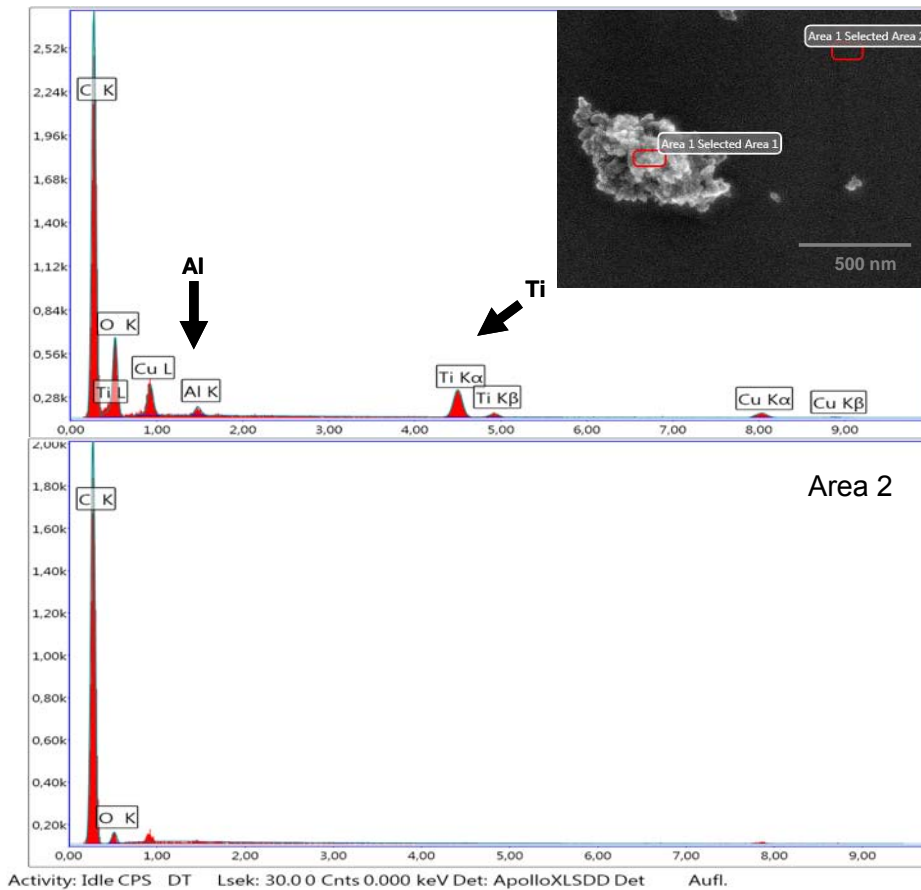


Figure 7: SEM / EDX scan of the NM104 suspension (preparation based on SOP). Background C-Tab and Cu mesh. The scan of Area 1 (upper diagram) shows the EDX analysis of titanium agglomerates, whereas area 2 showed the EDX results for an area close to the agglomerate (background).

After samples preparation agglomerates from < 100 nm up to > 750 nm were observed with SEM. The corresponding EDX scans of the agglomerates reveal the presence of titanium and aluminium (area 1 upper diagram). The height of the peaks is not directly transferable to the amount of the material, therefore only a qualitative conclusion about the chemical composition of the material can be made. Furthermore it is possible that re-adsorption of previously desorbed aluminium has occurred during sample preparation (drying, contraction).

### 3.4.3 Results - Surface coating stability of NM103 (UV Titan M262)

#### Dimethicone from NM103 in supernatant

For the experiments with NM103 the same sample preparation as for the NM104 was conducted to generate comparable results. Differently to NM104, the NM103 materials are covered by hydrophobic layer of dimethicone (C<sub>2</sub>H<sub>6</sub>OSi)<sub>n</sub>. The dimethicone release was measured by ICP-OES measurements of the silicon content in the filtrate of the suspensions. Therefore a specific measuring protocol was established (Annex - AII.7). Briefly after

suspension preparation the suspension was centrifuged (2700G for 10 min). The supernatant was then filtered using a 0.22 µm nylon filter to differentiate between solid and liquid phase. To minimize contamination (silicon release of the glass vessels), all suspension preparation steps were conducted in Teflon vessels and the digestion was done in platinum cups.

Based on the results of the NM104 two different suspension preparation steps were conducted, with the lowest and the highest external energy input (mixing and SOP). In Figure 8 the results of the chemical analysis are presented as measured silicon concentration.

Based on the ICP-OES data silicon concentration in the stock suspension of  $0.00057 \times 100 \text{ ppmw} = 0.57 \text{ ppmw}$  was observed. This corresponds to a total Si<sup>4+</sup> content of 570 µg/L, which is similar to the manufacturer's data (dimethicone  $0.02 \times 100 \text{ ppmw} = 2 \text{ ppmw} \times \text{Si } 28.09/74.15 \times 2 \text{ ppmw} = 758 \text{ µg/L}$ ). The lower limit of detection (LOD) for Si<sup>4+</sup> is reported with 1.5 µg/L. However, the experimental blank value for the deionised water used in this study was 80 µg/L.

The results indicate that the addition of water caused in the removal of around 95% ± 5% of the silicon from the surface of the NM103. By using the established SOP 86% ± 12% of the silicon was removed from the surface, based on the silicon concentration of the basic material. No significant differences between mixing and SOP were observed and due to the confidence interval of the background concentration of 86% it is conceivable that nearly all of the dimethicone coating was released during sample preparation.

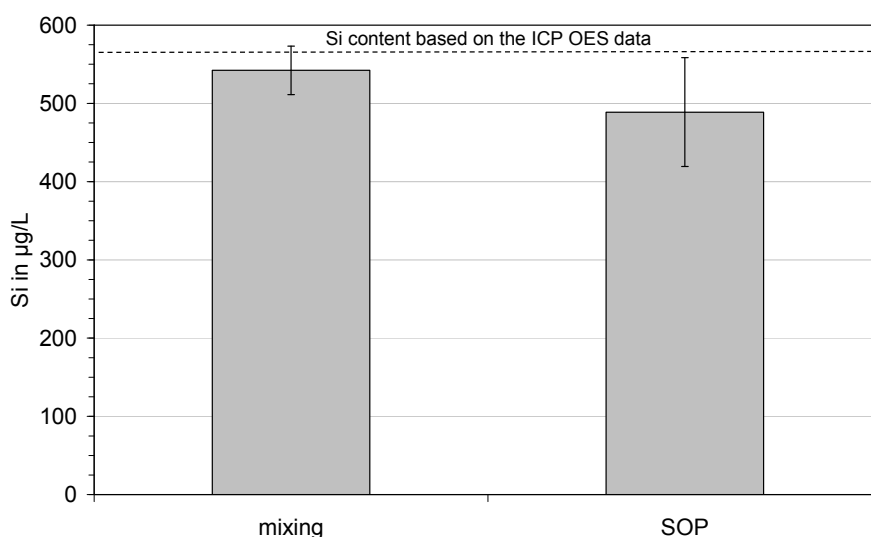


Figure 8: Average of ICP-OES measurements of the silicon content of 100 mg/L NM103 after dispersion by mixing and after standard operation procedure (SOP - 1 min sonication, 60 min stirring). The line indicate the silicon concentration based on ICP-OES measurements of the dry powder of the material; error bars = standard deviation, n = 3.

The results of the ICP-OES analysis of the supernatant of NM103 show that the majority of the dimethicone layer is dissolved when the powder is suspended in aqueous media and

subsequently dispersed. This finding is supported by the observation that the hydrophobic NM103 becomes wetted after approximately 15 min when brought onto a water surface without any energy input.

### Aluminium from NM103 in supernatant

The filtrate of the suspension was also analysed to its aluminium content. As mentioned above in section 3.4.1 also for this material no aluminium oxide above the LOD (1 µg/L) was dissolved from the surface of the material.

### Zeta potential of NM103 when dispersed according to the SOP

The pH dependency of the zeta potential of the NM103 stock suspension was measured with ELS for two series of measurements (conducted in the mid and at the end of the project phase), in which independently prepared stock suspensions were analysed Figure 9.

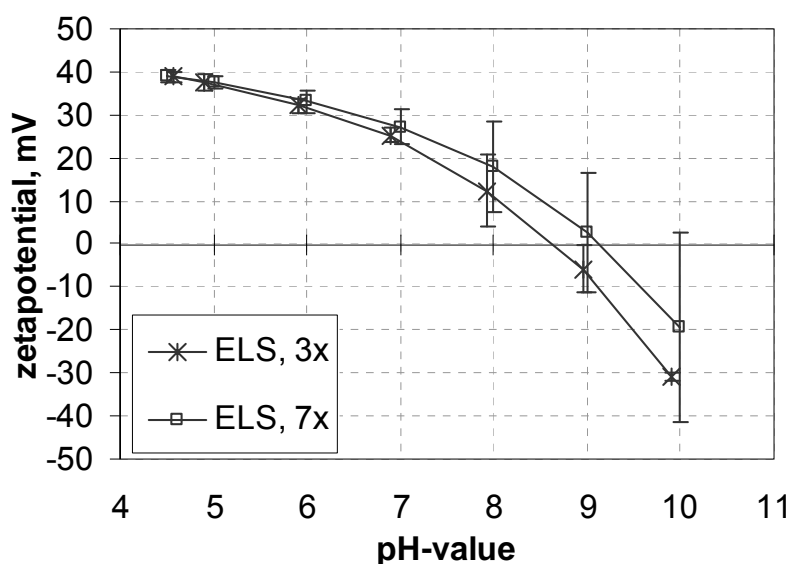


Figure 9: Two zeta potential test series of 100 mg/L NM103 in DI water, suspension preparation based on SOP, error bars = standard deviation; n = 3.

The zeta potential measurements in DI water show the isoelectric point (IEP) of NM103 to be detected between pH 8 and 9.5 in the same range as for NM104 after suspension preparation based on the established SOP. The detected IEP is comparable with the IEP of alpha aluminium oxide (Rubio-Hernández et al., 2006; Shin et al., 2006; Kosmulski 2006) and significantly different from that of the TiO<sub>2</sub> core (pH 6; see discussion in section 3.4.2). Also for pH values at 4.5 (last measured value) close to the IEP of dimethicone (polydimethylsiloxan) around 4.1 (Roth et al., 2008), significant larger values than zero were measured.

Hence, the zeta potential measurements confirm the conclusion of the chemical measurements, that nearly all of the dimethicone was transferred into the suspension media

(cf. section 3.4.3) and do not influence the zeta potential (the IEP around 4.1). The IEP is in the range of that for an Al<sub>2</sub>O<sub>3</sub> surface.

### SEM / EDX of NM103 when dispersed according to the SOP

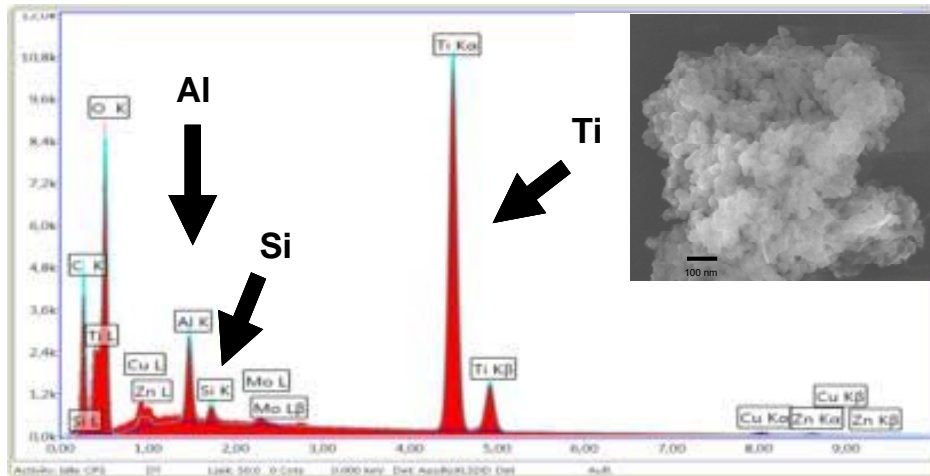


Figure 10: SEM / EDX scan of the dry powder of NM103.

In Figure 10 SEM / EDX scans of the untreated powder of NM103 are presented. Beside titanium and aluminium, silicon was detected, which may originate from the hydrophobic surface functionalisation, but possibly also be due to contamination. The sample preparation was the same as the one described for NM104 (cf. section 3.4.1).

After sample preparation according to the SOP agglomerates ranging from < 100 nm up to > 750 nm were observed (Figure 11) which is comparable to NM104. However, in contrast to the hydrophilic NM104 the EDX scans of the agglomerates detected silicon in addition to titanium and aluminium (scan 2). As discussed before, we cannot exclude an artefact due to re-adsorption of released silicon during dispersion and subsequent sample preparation for the SEM analysis.

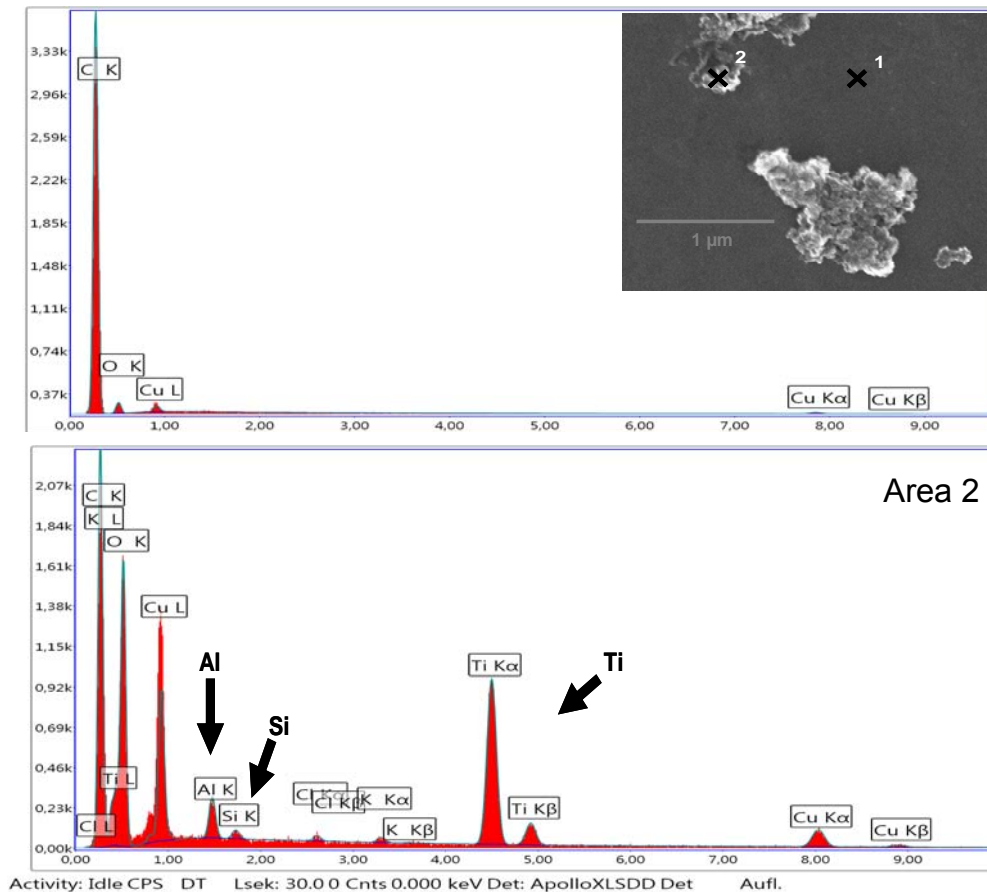


Figure 11: SEM / EDX scan of the NM103 suspension (preparation based on SOP). Background C-Tab and Cu mesh. The scan of Area 1 (upper diagram) showed the EDX results for an area close to the agglomerate (background). Area 2 (lower diagram) shows the EDX analysis of a titanium agglomerate.

### 3.4.4 Further surface properties of NM103 & NM104

#### Specific surface area

Beside the presented measurements a method for the detection of the specific surface areas of the nanomaterials in liquid was tested in the framework of this project. The method determines the amount of water molecules being in the layers directly around a particle by nuclear magnetic resonance spectroscopy. The relaxation time of water in contact to the particle surface is different to that of “free” water and can be quantified. This surface area would have been additional information to the size distribution measurements by DLS and would have been a good indicator of changes in the state of agglomeration.

The draw back of this method is that it requires a stable and high concentrated suspension of the material of at least 1 weight-%. For the both tested TiO<sub>2</sub> nanomaterials no stable suspensions could be prepared. Due to the sedimentation process no reproducible measurements could be conducted (Annex AIII.7)



### Particle induced reactive oxygen species (ROS) and “surface reactivity”

Three different approaches were applied. In a first approach the hydroxyl radical generation (OH<sup>•</sup>) potential was detected (Table 3). Briefly, 50 µL of the particle suspension is mixed with 100 µL DMPO (0.05 M) and 50 µL of H<sub>2</sub>O<sub>2</sub> (0.5 M), incubated in a dark, shaking water bath for 15 min at 37 °C. The presence of hydrogen peroxide (H<sub>2</sub>O<sub>2</sub>) and 5,5-dimethyl-1-pyrroline-N-oxide (DMPO) in this method is especially sensitive for the detection of hydroxyl radicals (OH<sup>•</sup>) generated via Fenton-type reaction according to Shi et al. (2003). The signal intensity expressed as arbitrary unit (AU) of the DMPO-OH adduct was measured by EPR. As blank value dH<sub>2</sub>O was measured. Based on the mean of the blank (n = 3) a limit of detection (LOD) is calculated (MV blank + 3\*standard deviation (SD) of the blank) and used for the data evaluation.

Table 3: Hydroxyl radical generation (OH<sup>•</sup>) potential in arbitrary unit (AU) of the coated titanium dioxide nanomaterials NM103 and NM104 and the uncoated P25 as photocatalytic material, suspension preparation based on SOP, pH 5; ± standard deviation of n = 3.

DMPO	NM103	NM104	P25	Blank (dH <sub>2</sub> O)	LOD
Mean in AU (not blank corrected)	1833 ± 632	1490 ± 23	2407 ± 579	2298 ± 54	2460
OH <sup>•</sup> generation	No	No	No	No	-

For none of the tested materials a hydroxyl radical generation was detected without UV irradiation.

The second analysis method, using CPH as the spin probe, showed a “surface reactivity” for the same materials. 50 µL of particle suspensions was mixed with 50 µL of the spin probe 1-hydroxy-3-carboxy-2,2,5,5-tetramethylpyrrolidine hydrochloride (CPH) (1 mM), mixed with the chelator desferroxamin (0.1 mM) and incubated for 10 min at 37 °C. The ability to split H<sup>+</sup> from the CPH molecule was measured. Due to the, with time increasing, blank EPR signal (dH<sub>2</sub>O) caused by an auto-oxidation of the spin probe (CPH) the results are expressed as blank corrected. The correction was done using the linear increase (R<sup>2</sup> > 0.95) of the blank signal with time. Values higher than the time dependent blank values in respect to the standard deviation are named as reactive.

The suspension was prepared using the established SOP Table 4 and an alternative preparation with 1 min mixing without sonication Table 5 to get information about the energy effect on the surface functionality.

Table 4: Surface reactivity in arbitrary unit (AU) of the coated titanium dioxide nanomaterials NM103 and NM104 and the uncoated P25 as photocatalytic material, suspension preparation based on SOP; n = 3.

CPH	NM103	NM104	P25
Mean in AU (blank corrected)	510	3322	1624
	580	1699	1446
Reactivity	No	Yes	No

With CPH a surface reactivity of NM104 was detected, whereas NM103 or P25 showed no reactivity.

To get information about the influence of the energy input on the surface reactivity an alternative suspension preparation with only 1 min mixing using a vortex mixer was conducted. The suspensions showed no reactivity neither NM103 nor NM104.

Table 5: Surface reactivity in arbitrary unit (AU) of the coated Titan materials NM103 and NM104, suspension preparation with 1 min mixing, n = 3.

CPH	NM103	NM104
Mean in AU (blank corrected)	330	-1049
	452	378
Reactivity	No	No

NM103 showed no hydroxyl radical generation and no surface reactivity independent on the type of suspension preparation.

NM104 showed no hydroxyl radical generation but a preparation dependent surface reactivity, with no reactivity for low energy and reactivity for a higher energy input. Based on the results we conclude that the higher energy input modified the surface of the NM104 whereas the other material NM103 is not affected. It is conceivable that higher amount of dimethicone of NM103 compared with glycerol of NM104 was still adsorbed at the surface of the material after suspension preparation, which affected the surface reactivity. But this conclusion could not be confirmed by ToF SIMS analysis AIII.1. Samples of NM103 which were analysed prior and after suspension preparation showed after preparation no dimethicone at the surface. It is conceivable that the aluminium oxide surface shows some differences (oxidation states, functional groups) which could cause the reactivity. But this could not be clarified in this study and should be confirmed in further studies.

In the third approach the photo catalytic activity (hydroxyl radical generation) without H<sub>2</sub>O<sub>2</sub> with and without UV irradiation was measured. For the measurement 30 µL of the particle suspension (final conc. 5 mg/L) is mixed with 30 µL DMPO (final conc. 0.05 M), analysed by EPR after irradiation with UV-light (UV Energy saving lamp Omnilux 25 Watt E27 3U 230V/50Hz AC, 6000 UV K, 22000 lm) for 10 min and compared to not irradiated samples. In addition to the analysis with NM104 and NM103 the photo catalytic active P25 (not coated) was used as positive control.

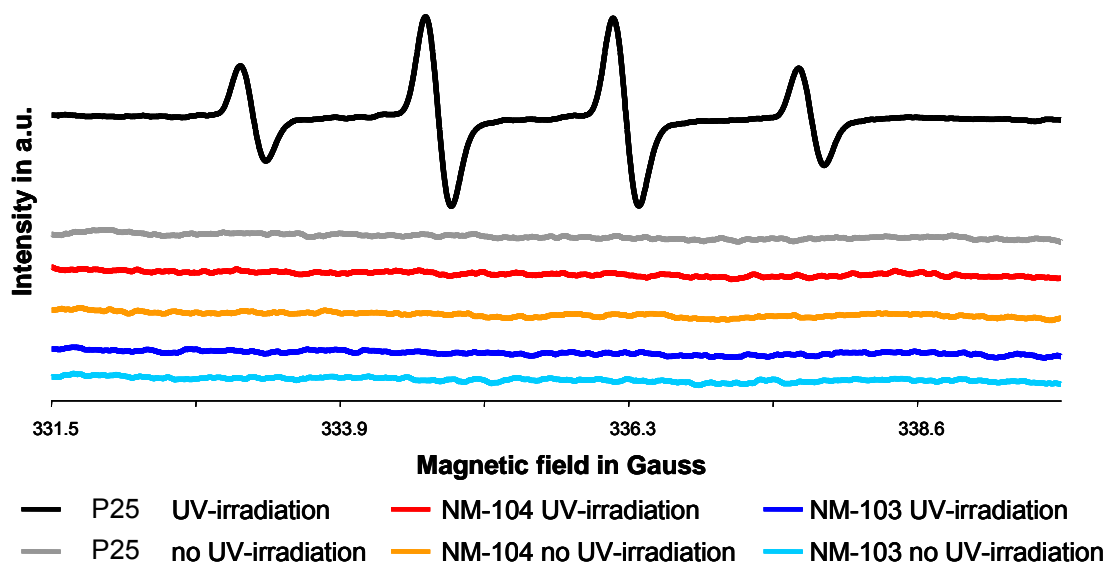


Figure 12: Hydroxyl radical generation of the coated titanium dioxide material NM104, NM103 and the uncoated P25 with and without UV irradiation, suspension preparation based on SOP, pH 5; mean values of n = 3.

No hydroxyl radical generation was detected for the coated titanium dioxide materials with or without UV irradiation, independent on the type of suspension preparation (mixing or SOP). Also with a high energy input (ultrasonic homogenizer), only measured for NM104, no hydroxyl radical generation was detected (Annex AIII.6) whereas the photo catalytic active material P25 showed a hydroxyl radical generation with UV irradiation. We conclude that the Al<sub>2</sub>O<sub>3</sub> was stable and not affected by the suspension preparation steps.

### 3.5 Summary and conclusion stability surface coating

The coating stability of the hydrophilic NM104 and the hydrophobic NM103 was observed by varying pH and different preparation steps. Both materials showed a comparable behaviour once they were dispersed in aqueous media. After mixing with water the outermost coating, which controls the interaction of the material with the liquid, was released from the surface. In summary about 86% ± 12% to 88% ± 8% of this coating layer of the titanium dioxide materials (glycerol and silicon) was removed during suspension preparation according to the SOP. No aluminium above the detection limit of the ICP-OES in-

strument was observed (LOD: 1 µg/L) in the supernatant of the suspensions. And also the zeta potential indicated that the aluminium oxide was the surface layer of the ENMs which interacts with the environment, because the detected IEP of the suspended materials was in the range of the zeta potential of aluminium oxide (pH 8 - 9) and not of the TiO<sub>2</sub> core (pH 5.5 - 7). This result was affirmed by the measurement for the ROS formation potential. With EPR measurements no ROS formation even when the sample was illuminated was detected. These results were also detected if a strong energy input was used for the suspension preparation (sonication). These results are an indication that the aluminium coating was still intact after the preparation steps.

The results of our study agree with findings of other studies. Labile et al. 2010 analysed the degradation of hydrophobic coated TiO<sub>2</sub> (polydimethylsiloxan (PDMS) and aluminium oxide) as function of time and UV irradiation. They detected a release of the PDMS layer during sample preparation whereas the aluminium oxide coating was less affected.

Auffan et al. 2010 also analysed the altering of the PDMS and aluminium oxide coating as function of time and UV irradiation with similar outcomes.

For the tested coated titanium dioxide materials of our study we conclude that the aluminium oxide is still present at the surface of the TiO<sub>2</sub> core and can affect the behaviour of the materials in the environment as residual surface.

### **3.6 Influence of pH, ionic strength and natural organic matter concentration on the interfacial properties**

The quantification of TiO<sub>2</sub> nanomaterial in different environmental media is very difficult and partly not feasible. Information about environmental behaviour and exposure concentration are still scarce (Kaegi et al., 2008; Kiser et al., 2008). The fate and behaviour in the environment is affected by the surface chemistry and the environmental conditions (i.e. pH, ionic strength, redox chemistry, type and concentration of natural organic matter (NOM, here using Aldrich Humic Acid), and temperature (French et al. 2009; Domingos et al. 2009; Guzman et al. 2006). Therefore the zeta potential of the two coated TiO<sub>2</sub> materials was measured while varying pH, the ionic strength of the suspension media and / or the natural organic matter (NOM) content. This study mainly uses solutions of CaCl<sub>2</sub>, because Ca<sup>2+</sup>-ions are the dominant cationic species in many aqueous environmental systems. Additionally, humic acids were used as typical representatives of natural organic matter.

The objective of the following investigations was to identify possible effects of environmental parameter on the surface coating and generally on the interfacial properties of the coated nanomaterials. Concerning the results of the two previous sections we con-

clude that the hydrophilic / hydrophobic coating with glycerol / dimethicone is mostly removed from the surface, while the Al<sub>2</sub>O<sub>3</sub> coating is virtually not affected by dispersion in deionised water. Possible effects of the environment are thus related to the Al<sub>2</sub>O<sub>3</sub> layer; the following scenarios are conceivable:

- Dissolution of the Al<sub>2</sub>O<sub>3</sub> – this is unlikely in most systems with an pH > 4 because of the relatively low solubility and dissolution rate of Al(III)-ions in the range  $4 \leq \text{pH} \leq 9$  (Roelofs & Vogelsberger, 2006, cf. section 3.4.2). In contrast, complete degradation of the Al<sub>2</sub>O<sub>3</sub> coating by dissolution cannot be excluded for pH < 4, since the solubility of Al<sub>2</sub>O<sub>3</sub> tremendously increases with H<sup>+</sup>-concentration. However, any layer of adsorbed or covalently bound material (e.g. multivalent cations, NOM) has an adverse effect on the surface dissolution. Thus, in natural aqueous media the Al<sub>2</sub>O<sub>3</sub> coating may remain unaffected even for very low pH-values. Anyway, the ENM behaviour at pH < 4 could not be explored (in detail) within this study.
- Slow re-crystallisation of the surface (e.g. formation of β-Al(OH)<sub>3</sub> (Bayerite), Lefevre et al., 2002), which is significant after several days to weeks, the type of transformation / the resulting aluminium phase is i.a. affected by the pH (Carrier et al., 2007).
- Specific adsorption of (multivalent) ions (James & Healy, 1972) and surface active substances like humic acids
- Surface precipitation of hardly soluble hydroxides (James & Healy, 1972)

Hence, the focus of the experimental investigation was to detect any influence of the solute concentration on the interfacial properties and if they are constant over time. The interfacial properties are quantified indirectly via zeta potential curves ( $\zeta$  as function of pH), for which an ELS instrument and a  $\mu$ EP instrument were employed.

### 3.6.1 NM in CaCl<sub>2</sub> solutions

#### Zeta potential curves of freshly prepared suspensions

The zeta potential measurements with ELS were conducted immediately after suspension preparation (nanomaterial content: 100 ppmw). The measurements started at pH 4.5 and during the measurement the pH was first stepwise adjusted to pH 10 and afterwards back to pH 4.5. The results for the two nanomaterials, NM103 & NM104, are listed in Table 6 and Table 7 respectively.

Table 6: Zeta potential measurements of NM103 suspensions with varying pH (4.5 - 10) and CaCl<sub>2</sub> concentration (0.0001M, 0.001M and 0.01M); IEP = isoelectric point; n = 3.

NM103	DI water		0.0001M CaCl <sub>2</sub>		0.001M CaCl <sub>2</sub>		0.01M CaCl <sub>2</sub>	
	Zeta Potential (mV)	SD	Zeta Potential (mV)	SD	Zeta Potential (mV)	SD	Zeta Potential (mV)	SD
4.5	37.7	1.8	34.6	3.3	37.3	0.2	40.9	0.7
5	32.1	1.8	34.8	2.7	39.5	1.7	40.6	0.4
6	25.3	1.6	30.8	2.6	37.3	1.9	38.2	0.4
7	12.3	8.4	26.4	1.2	31.4	2.7	33.2	1.0
8	-5.8	5.5	14.0	5.9	18.7	5.5	26.3	0.3
9	-30.8	0.8	-0.5	9.8	9.8	5.3	19.3	1.3
10	-24.4	2.1	-16.0	4.8	4.9	4.0	19.2	2.6
9	-11.9	3.8	-13.4	4.0	3.1	4.2	15.9	1.9
8	12.6	2.0	-7.1	6.6	5.3	4.5	12.3	1.9
7	23.9	4.7	10.7	4.9	15.7	5.0	20.5	0.2
6	35.1	0.9	24.6	1.8	28.0	3.8	29.3	1.0
5	37.0	0.0	32.1	0.4	36.4	1.7	37.9	0.5
4.5	0.0	0.0	33.8	0.5	37.6	1.6	39.2	0.6
IEP	8 ... 7		9.5 ... 8.5					

 Table 7: Zeta potential measurements of NM104 suspensions with varying pH (4.5 - 10) and CaCl<sub>2</sub> concentration (0.0001M, 0.001M and 0.01M); IEP = isoelectric point; n = 3.

NM104	DI water		0.0001M CaCl <sub>2</sub>		0.001M CaCl <sub>2</sub>		0.01M CaCl <sub>2</sub>	
	Zeta Potential (mV)	SD	Zeta Potential (mV)	SD	Zeta Potential (mV)	SD	Zeta Potential (mV)	SD
4.5	38.6	2.8	37.2	2.9	38.8	2.5	40.5	1.1
5	38.1	2.7	36.4	2.2	39.9	1.4	40.4	1.7
6	32.7	2.5	32.7	2.6	35.1	2.2	38.1	1.8
7	26.3	1.1	25.5	4.0	27.0	2.3	32.4	2.3
8	7.2	7.1	16.6	4.3	19.6	2.2	25.1	2.3
9	-13.8	4.2	3.5	3.9	8.0	0.7	19.7	3.4
10	-29.1	3.0	-13.4	0.6	3.7	0.6	20.0	1.3
9	-24.5	1.3	-9.6	1.5	2.8	0.9	14.6	1.8
8	-9.8	5.6	-1.0	2.9	5.6	2.1	10.8	2.6
7	10.1	5.6	16.0	3.7	17.0	1.7	17.9	2.6
6	25.0	3.4	25.9	1.5	28.5	0.8	28.5	1.8
5	35.0	1.4	32.9	2.0	37.3	0.9	37.3	0.8
4.5	35.7	0.5	34.6	0.6	39.3	0.5	38.9	0.3
IEP	8.5 ... 8		9.5 ... 8.5		-		-	

In Figure 13 the zeta potential for both nanomaterials and for all CaCl<sub>2</sub> concentrations are shown. The two TiO<sub>2</sub> nanomaterials revealed a very similar behaviour with regard to the interfacial properties. Additionally with increasing Ca<sup>2+</sup> concentration a charge reversal in the basic pH-range was observed and no IEP could be detected. The separate graphical analysis of the different measurements can be found in Annex III.

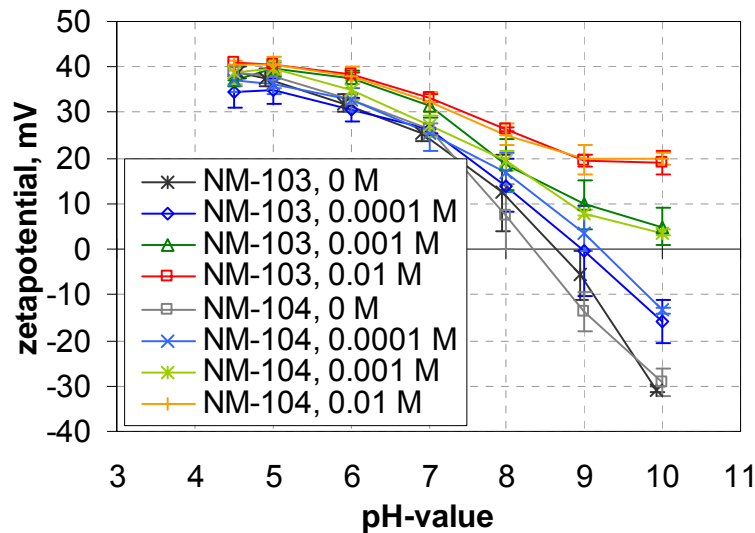


Figure 13: Zeta potential for NM103 and NM104 in CaCl<sub>2</sub> solution, ELS (continuous titration from acid to basic); n = 3.

During the titration from pH 4.5 to pH10 and back to pH 4.5 with the ELS a hysteresis in the zeta potential curves was observed for all measured samples. In detail the hysteresis is shown in (Figure 14) for DI water and in Figure 3 for DI and 0.001M CaCl<sub>2</sub> solution.

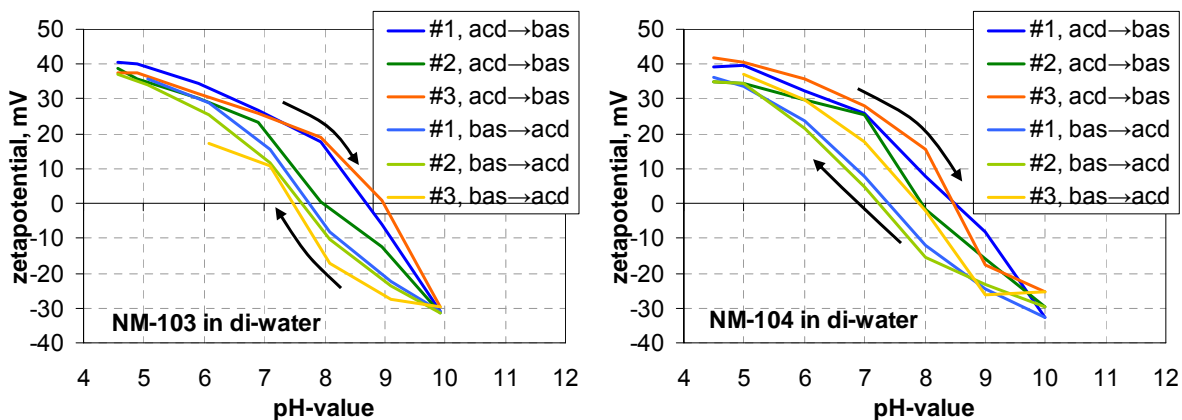


Figure 14: Zeta potential as function of pH for NM103 (left) and NM104 (right) dispersed according to the SOP in DI-water, measured with ELS (continuous titration: acid → basic → acid), 3 independent sample preparations.

It is conceivable that the short equilibration time could have led to this observation, because the  $\mu$ EP measurements without a titrator mode, which allows a longer equilibration time, did not show the hysteresis effect (Figure 15).

The hysteresis is reproducible and can be observed for all examined nanomaterials and all electrolyte concentrations employed. The duration for one complete hysteresis curve (from pH 4 to pH 10 to pH 4) takes approx. 3.5 hours.

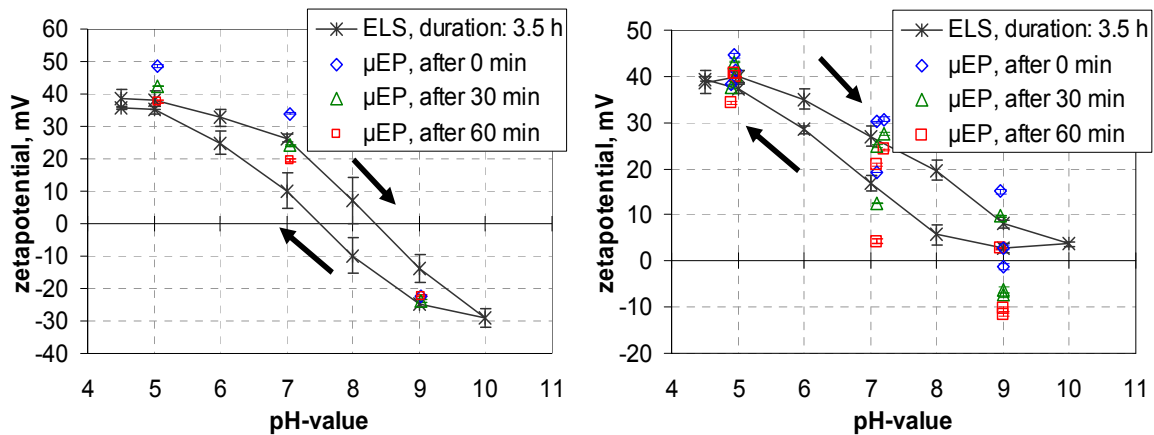


Figure 15: Zeta potential as function of pH for NM104, dispersed according to the SOP in DI-water (left) and in 0.001 M CaCl<sub>2</sub>, measured with  $\mu$ EP (discrete titration), 3 independent sample preparations.

With the  $\mu$ EP instrument the pH is adjusted by the operator and the equilibration time (sample age after pH switch) was controlled. The existence of kinetic effects could be confirmed for almost all samples; it confirms the real nature of the observed hysteresis in ELS. The curves for the two directions of titration differ considerably (hysteresis) for all suspension samples. This could be explained by equilibration time effects relaxation or “aging” of the interface. Test with the  $\mu$ EP instrument for selected samples indeed showed a significant systematic impact of sample age on the measured zeta potential. The trend of this time effect agrees with the direction of the hysteresis (Figure 16).

The hysteresis of the curves is reproducible and leads to the same zeta potentials in acid milieu (first titration direction from acid to basic).



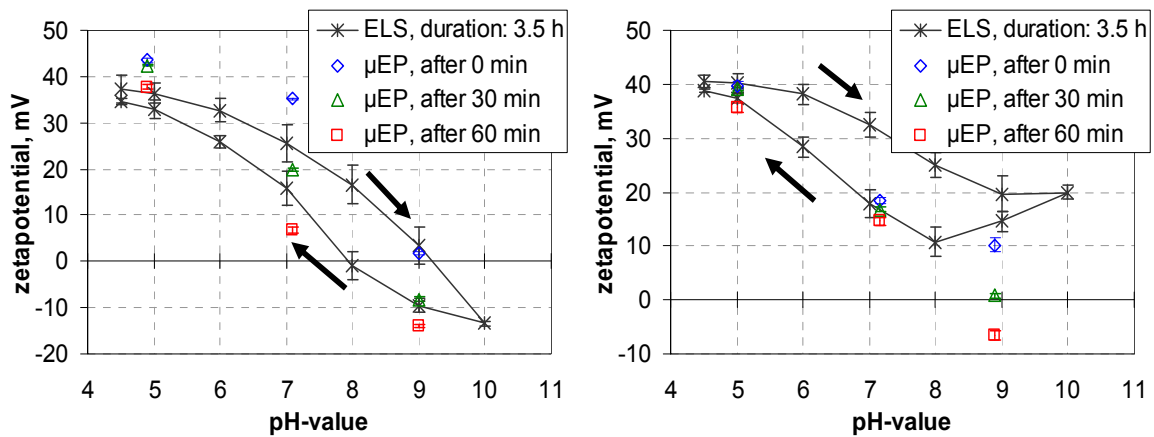


Figure 16: Zeta potential as function of pH for NM104 in 0.0001 M CaCl<sub>2</sub> (left) and 0.01 M CaCl<sub>2</sub> (right), ELS (continuous titration acid → basic (upper measurements points) and back from basic → acid (lower measurement points) μEP (discrete titration), n = 3.

### 3.6.2 Aging of suspensions in CaCl<sub>2</sub> solutions

The hysteresis of the ELS results and the time dependency of the μEP results as illustrated in Figure 16 led to more detailed study of the aging of the suspensions. In Figure 17 zeta potential measurements directly and after 24 h and 48 h respectively measured with μEP and ELS were shown for NM104 dispersed in 0.001 M CaCl<sub>2</sub>. The aging of the suspension was observed for both employed electrophoretic instruments (Figure 17).

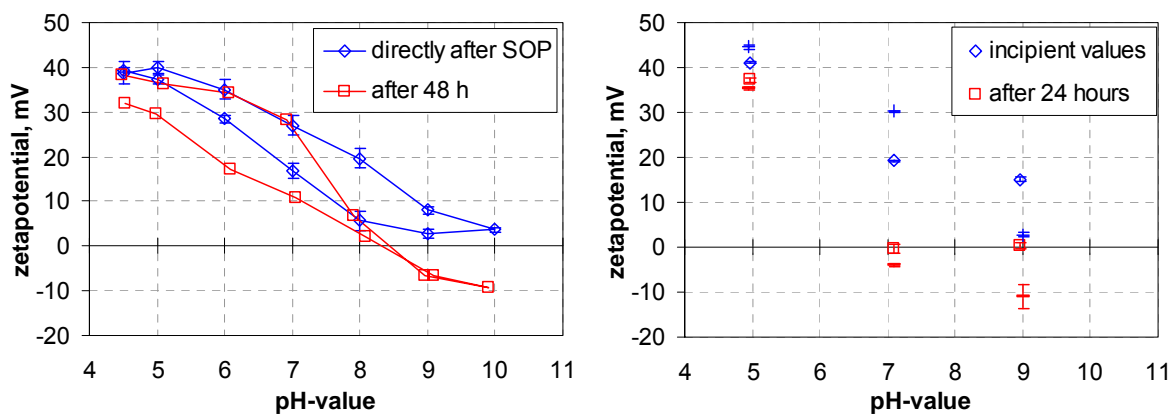


Figure 17: Zeta potential as function of pH for NM104 in 0.001 M CaCl<sub>2</sub>, measured with ELS (continuous titration acid → basic → acid; left) and μEP (discrete titration; right) on a freshly prepared and an aged suspension, n = 3.

The addition of 0.001 M CaCl<sub>2</sub> shifted the IEP to pH values above 10. Measurements after 24 h or 48 h showed already a shift of the IEP through a pH of approx. 7. In any case, the aging seems more pronounced for neutral and basic milieus than for acid milieus. In order to understand the relevance and nature of aging appropriate experiments were con-

ducted with both nanomaterials for different aqueous solutions. Detailed results can be found in Annex AIII.8. Briefly the results show a significant aging of the interface for almost all electrolyte solutions, yet with qualitative differences between the dominant cation. While in 0.0001 M and 0.001 M CaCl<sub>2</sub> solution the IEPs fall below 7, which is much lower than the IEP of Al<sub>2</sub>O<sub>3</sub>, the IEPs of deionised water and 0.001 M NaCl solution keep unchanged.

Hence, we can probably distinguish between a general and an ion-specific "aging" effect. The former may indicate a steady increase of the ionic strength due to the dissolution of atmospheric CO<sub>2</sub> which forms HCO<sub>3</sub><sup>-</sup> in neutral and additionally CO<sub>3</sub><sup>2-</sup> in basic media. Besides, the pH is shifted to its equilibrium value (for deionised water: 5.6). Changes in these fundamental suspension parameters do inevitably affect the electric double layer, thus the zeta potential. Additionally, an ion-specific effect exists, that explains for the different impact of Na and Ca salts. According to the introductory remarks in 3.6 and to the zeta potential curves of the freshly prepared suspensions, it is quite certain that specific adsorption of Ca<sup>2+</sup> ions on the aluminium oxide occurs. Aging of such interfaces/surfaces thus indicate a change of the Ca-phase on the surface, i.e. a chemical reaction with the aluminium oxide surface or with solutes e.g. HCO<sub>3</sub><sup>-</sup> and/or the formation of a surface precipitate that contains Ca. However, this could not be explored within this study.

Parallel to the zeta potential measurement all samples were analysed with regard to particle size distribution by means of DLS (Annex AIII.11). Almost all samples show a noticeable agglomeration and due to this an increase in mean particle size ( $x_{cum}$ ). In some cases close to the IEP no DLS measurements were possible.

### **3.6.3 NM in DOC solutions**

#### **Zeta potential curves of freshly prepared suspensions**

Zeta potential measurements with suspensions containing dissolved organic carbon (DOC) were conducted in DI water. The results are listed in Table 8 for NM103 and Table 9 for NM104, respectively. The corresponding graphs are presented in Annex AIII.11. For all pH values all measured zeta potentials are negative, virtually independent from pH and DOC concentration. Thus it seems that the DOC is strongly attracted to the nanomaterial surface over the total pH range considered and led to a sterical stabilisation of the TiO<sub>2</sub> agglomerates in suspension.

Table 8: Zeta potential measurements of NM103 (UV Titan M262) suspensions with varying pH (4.5 – 10) and DOC content (2.5 mg/L, 5mg/L and 10 mg/L); IEP = isoelectric point; n = 3.

NM103	DI water		2.5 mg/L NOM		5 mg/L NOM		10 mg/L NOM		
	pH	Zeta potential (mV)	SD	Zeta potential (mV)	SD	Zeta potential (mV)	SD	Zeta potential (mV)	SD
	4.5	38.8	1.3	-13.3	2.7	-18.8	2.1	-20.0	3.0
	5	37.7	1.8	-15.3	3.9	-18.8	1.2	-18.3	1.9
	6	32.1	1.8	-20.9	1.6	-23.3	3.7	-20.4	1.7
	7	25.3	1.6	-27.8	2.5	-26.9	3.1	-23.4	2.2
	8	12.3	8.4	-29.0	2.7	-26.3	5.7	-24.1	3.6
	9	-5.8	5.5	-29.3	3.4	-24.7	7.1	-22.0	3.9
	10	-30.8	0.8	-27.2	6.2	-23.6	7.9	-22.1	3.7
	9	-24.4	2.1	-28.4	4.6	-23.8	6.7	-22.4	4.2
	8	-11.9	3.8	-30.3	2.8	-26.7	4.7	-25.8	3.0
	7	12.6	2.0	-33.7	1.1	-30.8	3.5	-29.0	0.8
	6	23.9	4.7	-30.3	0.4	-28.6	2.4	-26.3	1.3
	5	35.1	0.9	-12.5	7.4	-24.4	2.0	-23.9	1.9
	4.5	37.0	0.0	-6.4	1.7	-19.1	2.8	-22.6	1.0
IEP	9 ... 8		-		-		-		

Table 9: Zeta potential measurements of NM104 (UV Titan M212) suspensions with varying pH (4.5 – 10) and DOC content (2.5 mg/L, 5 mg/L and 10 mg/L); IEP = isoelectric point; n = 3.

NM104	DI water		2.5 mg/L NOM		5 mg/L NOM		10 mg/L NOM		
	pH	Zeta potential (mV)	SD	Zeta potential (mV)	SD	Zeta potential (mV)	SD	Zeta potential (mV)	SD
	4.5	38.6	2.8	-12.5	3.2	-22.8	1.3	-23.2	0.2
	5	38.1	2.7	-9.2	4.1	-21.2	3.5	-20.4	0.3
	6	32.7	2.5	-20.2	0.8	-22.6	2.5	-25.5	3.1
	7	26.3	1.1	-27.8	3.7	-25.5	1.7	-26.7	0.6
	8	7.2	7.1	-31.7	4.8	-29.6	0.8	-24.5	0.8
	9	-13.8	4.2	-32.3	3.6	-25.6	5.6	-22.6	1.2
	10	-29.1	3.0	-30.9	5.8	-21.1	3.2	-21.9	1.8
	9	-24.5	1.3	-32.4	3.0	-24.5	3.9	-23.2	1.5
	8	-9.8	5.6	-34.0	2.6	-28.6	3.3	-26.7	0.6
	7	10.1	5.6	-34.7	4.1	-30.2	1.3	-29.6	0.4
	6	25.0	3.4	-31.5	2.0	-29.1	2.4	-28.1	1.3
	5	35.0	1.4	-17.6	3.8	-25.0	0.9	-26.0	0.5
	4.5	35.7	0.5	-12.4	3.9	-21.8	1.2	-23.9	1.0
IEP	8 .. 8.5		-		-		-		

Natural surface waters are a complex mixture of different substances like humic acids, fulvic acids, monovalent and multivalent ions. To get information about the behaviour in natural systems a suspension with one DOC and CaCl<sub>2</sub> concentration was prepared. Zeta potential measurements of suspensions containing 5 mg/L dissolved organic carbon (DOC) and 0.001M CaCl<sub>2</sub> are presented in Table 10 for NM104.

Table 10: Zeta potential measurements of NM104 (UV Titan M212) suspensions in 5 mg/L DOC and 0.001M CaCl<sub>2</sub> solution with varying pH (4.5 - 10); IEP = isoelectric point; n = 3.

NM104	5 mg/L NOM + 0.001M CaCl <sub>2</sub> solution	
	Zeta Potential (mV)	SD
pH		
4.5	-12.1	2.7
5	-11.7	2.0
6	-13.0	1.1
7	-15.0	0.8
8	-16.4	1.3
9	-16.8	2.1
10	-18.0	2.2
9	-17.7	1.9
8	-16.6	2.2
7	-15.2	2.9
6	-13.8	2.7
5	-8.6	1.4
4.5	-6.3	2.5
IEP	-	

In Figure 18 the two separate measurements for NM104 and 0.001M CaCl<sub>2</sub> solution and 5 mg/L DOC were compared with the measurements of the mixed media. The effect of the DOC on the stability and zeta potential of the NM104 suspension was also detected but less pronounced if a mixture of DOC and CaCl<sub>2</sub> was used Figure 18. Comparable results were also detected for NM103, the detailed results can be found in Annex AIII.12. Comparable results with the effect of DOC alone were observed for the mixed media. The results indicate that the sterical stabilisation of the adsorbed DOC is stronger than the destabilisation effect of the increased ionic strength at the tested concentrations.

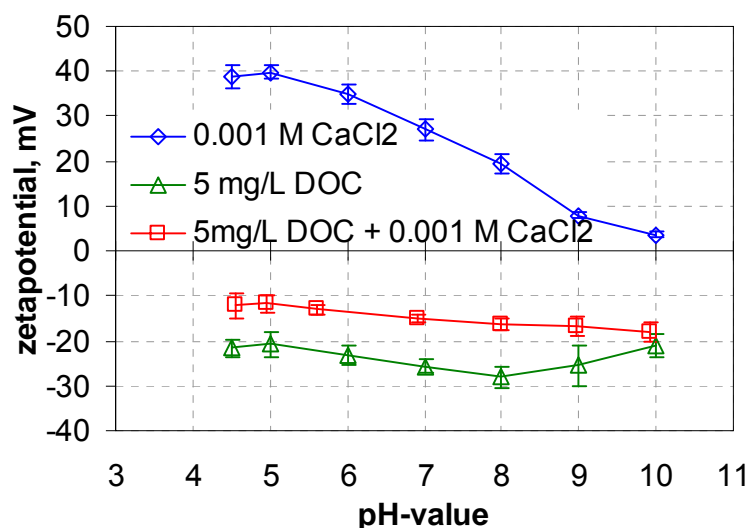


Figure 18: Zeta potential measurements of NM104 in DOC solution with 0.001 M CaCl<sub>2</sub> background, ELS (continuous titration from acid to basic); error bars = standard deviation; n = 3.

### 3.6.4 Aging of suspensions in DOC-solutions

The adsorbed DOC molecules are the determinant species of the surface charge of the materials in the suspension, as described above. In contrast to the electrolyte suspension medium (section 3.6.2), no significant aging was observed when the nanomaterials were suspended in DOC solutions. Hence no changes of interfacial properties can be assumed. The aging of the CaCl<sub>2</sub> suspension medium was probably caused by the dissolution of atmospheric CO<sub>2</sub> which leads to an increased ionic strength, which inevitably affected the electric double layer of the particles and thereby the zeta potential. It is assumed that the dissolution of atmospheric CO<sub>2</sub> also occurred for the DOC suspension, but did not change the zeta potential significantly.

## 3.7 Résumé for the environmental behaviour

The behaviour of the two coated TiO<sub>2</sub> materials was observed in different liquid media with varying CaCl<sub>2</sub> and DOC concentration. It was shown that Ca<sup>2+</sup>-ions have a significant impact on the interfacial properties, in particular in media with alkaline pH (pH 8 – 10). While in deionised water both nanomaterials possess an IEP in the pH range of 8 to 9 (which corresponds to the IEP of Al<sub>2</sub>O<sub>3</sub>), there is no IEP below pH 10 when particles are freshly suspended in CaCl<sub>2</sub> solution (> 0.001 M). These results agree with results from the literature (von der Kammer et al., 2010; Sharma et al., 2009). It was also shown that bivalent ions (here Ca<sup>2+</sup>) have a higher influence on agglomeration than monovalent ions (here Na<sup>+</sup>) comparable results were also observed by von der Kammer et al. (2010) and Labile et al. (2010). Even more, when the nanomaterials remain dispersed for more than 1 hour in the CaCl<sub>2</sub> solution, an additional gradual change of the interface is observed, which shifts the IEP back to lower pH values, even to pH < 7. While the first process can

be related to the specific adsorption of hydrolysed Ca<sup>2+</sup> ions on the material surface, the second process could not be identified within this project.

A different situation occurs when the nanomaterials are suspended in aqueous systems containing DOC – here Aldrich Humic Acid (AHA). The surface charge still becomes negative (Hyung et al., 2007, Domingos et al., 2009, Sharma, 2009, von der Kammer et al., 2010) also if CaCl<sub>2</sub> was presented. The DOC adsorbs on the surface and controls the interfacial properties, sterical stabilisation, independently from the pH (at least for  $\geq 2.5$  mg/L). Different results were found by Domingos et al., 2009. In the presence of Suwannee River Fulvic Acid and Ca<sup>2+</sup> larger agglomerates of TiO<sub>2</sub> nanomaterials were observed. It is conceivable that the type of the DOC affected the behaviour. Schwyzer et al. (2011) detected a higher stabilisation effect of humic acid compares with fulvic acids. Based on the results of this study it was shown that tested DOC (here Aldrich Humic Acid) has a large stabilizing effect for the investigated nanomaterials under tested conditions. In media with increasing ionic strength and due to the negative zeta potential another behaviour is expected e.g. decreased adsorption on negatively charged surfaces due to electrostatic as well as steric repulsion. However, in natural environments additional conditions with opposite behaviour can occur which affected the fate and behaviour, which has to be considered for a further estimation.

No qualitative differences between the two materials NM103 and NM104 were observed which confirms the previous conclusion that the hydrophilic and hydrophobic layers are removed and therefore not relevant for the nanomaterial properties, once they are dispersed in aqueous media.

The Al<sub>2</sub>O<sub>3</sub> coating of the two materials is the residual surface, which influenced the behaviour of the two materials in the environment.

Based on the findings of this study, the assumption of the previous project (Kuhlbusch et al., 2012) - which studied the mobility of different TiO<sub>2</sub> nanomaterials in soils i. a. NM103 - that not the hydrophobic TiO<sub>2</sub> with “complete” coating was tested but a altered TiO<sub>2</sub> with Al<sub>2</sub>O<sub>3</sub> at the surface, was confirmed. It is conceivable that due to the higher IEP of Al<sub>2</sub>O<sub>3</sub> (pH 8 – 9) compared with TiO<sub>2</sub> (pH 5.5 - 7) a lower degree of agglomeration of the material in the system occurred which could have influenced the mobility in the system. However the coated titanium dioxide nanomaterial showed only a slightly higher mobility compared with the other two uncoated materials. Therefore it is concluded that the positive zeta potential of the nanomaterials linked with the negative charge of the soil matter have a higher influence on ENM mobility in the tested soil types compared to the ENM size.

## 4 Soil experiments

### 4.1 Background

Man-made substances can reach soil ecosystems directly via application (e.g. agrochemicals) or indirect via waste water, sewage sludge, or air wet / dry deposition. Information on their mobility and movement into deeper soil layers or on the mobilisation of other substances in the presence of ENMs, as it was observed for different TiO<sub>2</sub> nanomaterials (Zhang et al., 2007; Fang et al., 2011), is still lacking. It is known that pollutants and other substances can adsorb to the surface of nanomaterials (Pan & Xing 2008, Hofmann & von der Kammer 2009, Fang et al. 2011), which directly can affect the mobility of these substances.

In this study the possible mobilisation effect to copper sulphate (CuSO<sub>4</sub>) and <sup>14</sup>C marked triclocarban (TCC) by TiO<sub>2</sub> nanomaterials had to be investigated. This investigation included the design of an appropriate approach based on a prior study (Kuhlbusch et al., 2012).

### 4.2 Materials and Method

Based on the OECD test guideline 312 glass columns with an inner diameter of 12 cm and a height of 20 cm were filled to a height of 11 cm with three different air-dried, sterilised and sieved natural soils, which equates to an amount of 1200 g – 1500 g soil matter.

The basic test design was to compare the mobility of Cu<sup>2+</sup> and TCC by comparing concentrations of these elements in the soil columns and eluate with and without the presence of the nanomaterial. A core sample of the column was extracted for chemical analysis. Therefore the outer ring of the soil column was separated (1cm), followingly called 'border sample'. This procedure allows the detection of possible preferential material transport along the glass column walls.

The tests were run in duplicate (soils with TiO<sub>2</sub>) with one reference system (without TiO<sub>2</sub>) for the <sup>14</sup>C marked TCC experiments. The core as well as the border sample were analysed for the TCC experiments. For CuSO<sub>4</sub> the tests were run in triplicate, for the test (with TiO<sub>2</sub>) and for the reference systems (without TiO<sub>2</sub>). The latter analysis was only conducted for the core and not for the border sample.

The pollutant and the nanomaterial were separately applied to the soil column to avoid any a priori attachment of the pollutant onto the nanomaterial and to be more realistic. The precharge of the soils with a known amount of the pollutant was done by spiking only the upper most 2 cm of the soil column with the pollutant. The nanomaterial was added afterwards in form of a suspension.

### 4.3 Selection of pollutant

Two particular different pollutants were chosen to represent two substantial different classes of pollutants. Copper (Cu) was chosen as a representative metal as a ubiquitous soil contaminant, which is still used in agriculture. Furthermore an organic molecule with toxicological relevance, namely Triclocarban (TCC) was chosen as the second pollutant. The quantitative measurement of this compound was enhanced by radioactive marking. The mobility of metals and metal ions in soils are e.g. dependent on the pH or soil organic matter. The soil pH affects the surface potential of the reactive solid phases as well as the availability of protons for adsorption sites. E.g. Alva et al. (2005) showed that the organic matter concentration affected the mobility of positively charged molecules in soils by providing pH dependent negative surface potential. Copper compounds and organic molecules with copper are widely used in pesticides and fertilizers. Due to the pH dependent mobility (mobile pH < 5.5) copper accumulation may occur in natural soils, which can lead to a high concentration of copper in an accumulation zone. In agricultural soils up to 1000 mg/kg copper was detected (Alva et al., 2005; Flores-Velez, L.M. et al., 1996).

The applications of copper as pesticide or fertilizer, lead to direct release into the environment and hence the soil ecosystems. Copper is toxic for some organisms (EC<sub>50</sub>, 48h, *Daphnia magna*: 0.02 mg/L\*, LC<sub>50</sub>, 96h, *Onchorhynchus mykiss*: 0.03 mg/L\*, LC<sub>50</sub>, acute toxicity, *Daphnia magna*: 111 µg/L (Fan et al., 2009)) and therefore information about the mobility in ecosystems is important for risk assessments. The ecotoxicity of Cu can be correlated with the adsorption to co-substrates as was shown in recent studies. They showed that TiO<sub>2</sub> nanomaterials can increase the bioavailability of copper for aquatic organisms, like carp or daphnia, due to an increased bioaccumulation (Zhang et al. 2007; Sun et al., 2009; Fan et al., 2011). This led to an increase of the toxicity of copper for *Daphnia magna* with LC<sub>50</sub> of 42 µg/L with TiO<sub>2</sub> ENMs compared to 111 µg/L without TiO<sub>2</sub> nanomaterials.

Only little information about environmental concentrations of TiO<sub>2</sub> ENMs is available. Gottschalk et al. (2009) used the few experimental data to calculate the concentration of TiO<sub>2</sub> ENMs in environmental compartments. For sewage sludge an amount of around 130 mg/kg and if sewage sludge is applied to agricultural soils a concentration of around 89 µg/kg of TiO<sub>2</sub> was estimated. With the application of sewage sludge which contains TiO<sub>2</sub> nanomaterials, both substances TiO<sub>2</sub> ENMs and Cu (from e.g. pesticide use) can come together in agricultural soils. Therefore copper was chosen for this study as a soil pollutant.

---

\* [www.carlroth.com](http://www.carlroth.com) – safety datasheet CuSO<sub>4</sub>



Triclocarban (TCC, or 3,4,4'-trichlorocarbanilide, CAS 101-20-2) is an organic antimicrobial compound used in many products like cosmetics and pesticides. Although personal care products only contain between 0.1 and 0.3% of TCC (Clarke & Smith, 2011) and its use as a biocide is forbidden in the EU, it is still applied in many products. Therefore, it belongs to the so-called "high production volume substances". Since nano-TiO<sub>2</sub> is also used in personal care products, e.g. in sunscreens, both chemicals might have the same environmental entry pathways. Their possible concomitant appearance is of course very interesting for this project, dealing with the mutual influence of TCC and nano-TiO<sub>2</sub> on the fate, behaviour and mobility of one another. In a recent review, concerning the environmental importance of emerging pollutants, TCC was listed as a "priority substance" (Clarke & Smith, 2011). It is lipophilic (Log K<sub>ow</sub> of 4.9; Ying et al., 2007), poorly photodegradable, highly resistant to biodegradation, not leaching, and hence, highly stable in soil (half-life of 108 d; Kwon et al., 2010). Its persistency and consequent tendency to accumulate can explain the fact that TCC was found in different environmental media. It was for example detected in sewage sludge (51 mg/kg; Heidler et al., 2006) at biologically relevant concentrations (median lethal concentration for earthworms, LC50 for *Eisenia fetida*: 40 mg/kg soil, Snyder et al., 2011). Further TCC concentrations were reported for biosolids retrieved from a waste water treatment plant, and soil, amounting to 5 - 10 mg/kg and to 1 - 65 µg/kg, respectively (Cha & Cupples, 2009; 2010). Heidler, Sapkota et al. (2006) suggested that 75% of TCC used in the US is spread to fields. TCC was detected in all 25 investigated wastewater treatment plants (Heidler and Halden 2009). It was found in both the inflow and the outflow of sewage treatment plants (Sapkota et al., 2007) and 30% of the compound was shown to be distributed from the water phase to the sediment of aquatic systems (UBA AT 2011). However, the fact that TCC was shown to be distributed to soils through application of sewage sludge onto fields was the main reason for its selection for the leaching experiments in the frame of this project. Next to its environmental relevance, another criterion for the choice of TCC was the commercial availability of its <sup>14</sup>C-labeled isotope. Working with radioanalytics allows easy tracking of the compound in complex matrices. Finally, this compound could be selected for the parallel project (FKZ 3710 65 413), dealing with combinatory ecotoxicological effects, because of its biological activity. This allows a more profound interpretation of the result of both projects by comparing ecotoxicological and fate data.

#### 4.4 Titanium dioxide nanomaterial selection

The possible pollutant carrier effect of a TiO<sub>2</sub> nanomaterial in soils had to be investigated in this study. Therefore a pristine, non coated TiO<sub>2</sub> material which is also part of the OECD Sponsorship program was chosen. This minimises and eliminates possible effects of surface functionalisations which could cover the effect and alter the behaviour of the Ti-

core, as it was shown in this study for the two coated TiO<sub>2</sub> nanomaterials and the aluminium oxide coating. The tested nanomaterial should ideally also be mobile in soil columns. Based on the results of a prior project (Kuhlbusch et al., 2012) where no mobility of the pristine nanomaterials was detected in the tested soil types due to their positive zeta potential, DLS and zeta potential measurements of other pristine TiO<sub>2</sub> nanomaterials were conducted. Consequently three different TiO<sub>2</sub> nanomaterials were tested, P25, PC105 and Hombikat UV100. The detailed results are presented in Annex - AIV.5. Briefly, all materials showed a positive zeta potential at pH 5, with P25 having the smallest particle mode (< 250 nm) in suspension. Hence, even though not perfect, P25 was chosen for the carrier effect experiments.

#### 4.5 Nanomaterial suspension

The carrier effect of a P25 was tested. Therefore the nanomaterial was suspended in deionised (DI) water with a pH of 5\*. The suspension protocol based on the standard operation procedure, which was established in a previous study (Kuhlbusch et al., 2012). The whole detailed description can be found in Annex AII.1. Briefly 250 mg of P25 were weighted in a beaker glass and filled up with 100 mL deionised (DI) water (pH 5). Subsequent the suspension was sonicated by using an ultrasonic homogeniser (Bandelin SONO-Plus HD 2200, VST 70, pulse 0.2/0.8) for 10 minutes. The prepared 100 mL suspension (2.5 g/L P25) was then directly applied on the top of the test soil columns.

#### 4.6 Soils

Three different natural reference soils with varying pH, texture and effective cationic exchange capacity (CEC<sub>eff</sub>), were investigated in this study (Figure 19):

- A01 - Dystric Cambisol (loamy sand, medium acid, very light humic) – average pH 5.67 and CEC<sub>eff</sub>: 38 mmolc/kg.
- A02 - Stagnic Luvisol (silt loam, sub-acid, light humic) – average pH 6.63 and CEC<sub>eff</sub>: 133 mmolc/kg.
- G03 - Eutric Cambisol (silt loam, medium acid, medium humic) – average pH 5.64 and CEC<sub>eff</sub>: 136 mmolc/kg.

---

\* pH was measured before and after suspension preparation; pH adjusted with 0.1 M NaOH and 0.1 M HCl,

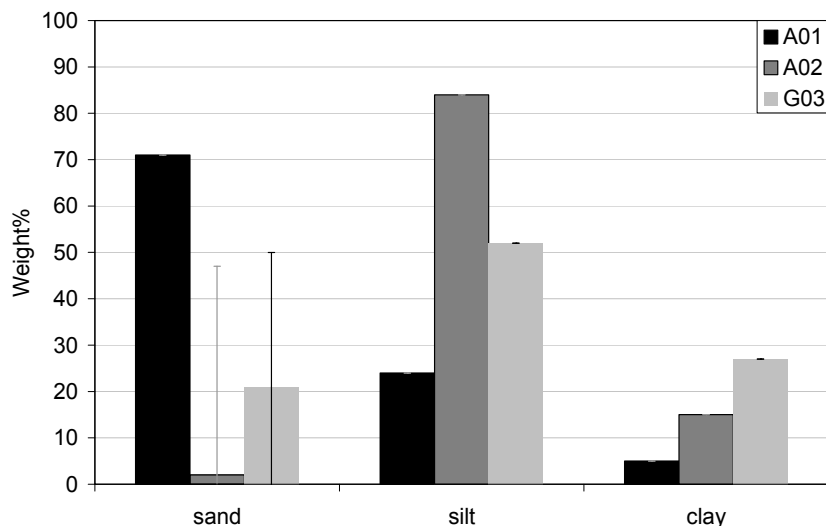


Figure 19: Texture of the tested soil types; [www.refesol.de](http://www.refesol.de).

The reference soils were provided by the Fraunhofer Institute in Schmallenberg, Germany ([www.refesol.de](http://www.refesol.de)). Before use, all soils were air dried for 48 h at 21 °C and sieved through a 2 mm mesh. Detailed information for the test soils can be found in Annex - AIV.1.

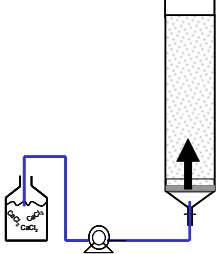
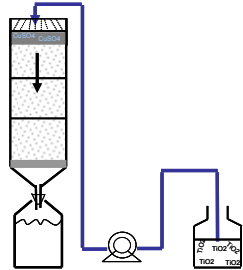
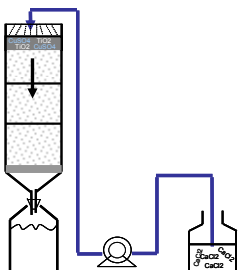
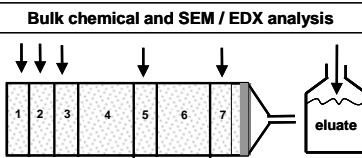




#### 4.6.1 Soil spiking

Hundred gram of the used soil (100 g ± 1 g) were spiked with 750 mg CuSO<sub>4</sub> and 200 µg TCC respectively. The CuSO<sub>4</sub> was diluted in 12 mL DI water before the water was added to the dry soil. Afterwards the soil suspension was shaken for 1 h. After shaking the soil was dried at 70 °C for 1 h. The spiked dry soil was then applied ontop of the 11 cm high unspiked soil in the column using a 2 mm mesh.

#### 4.7 Study design

The main steps of the soil transport tests are summarised in Table 11. More detailed information about the study design (SOP) can be found in Annex II - AII.8 Standard operation procedure – Carrier effects of nanoscale particles in soil columns

Table 11: Overview of the study and experiment design.

1.	2.	3.	4.
<p>Columns were filled with the reference soils. Afterwards the soils were pre-wetted with a 0.01 M CaCl<sub>2</sub> solution from the bottom to the top, to displace the air in the soil pores.</p>	<p>100 g of the soil were spiked with the test substance - <sup>14</sup>C marked TCC or CuSO<sub>4</sub>. The spiked soil was applied as separate layer on the top of the column.</p> <p>Afterwards 100 mL of the P25 suspension (2.5 g/L) was directly applied on the top of the column → total of 250 mg TiO<sub>2</sub>.</p>	<p>Then a 0.01 M CaCl<sub>2</sub> solution (200 mm / 48 h) was continuously applied to the top of the column.</p> <p>The eluate was sampled time- resolved over the test duration of 48 h.</p>	<p>After 48 h the columns were sectioned in seven segments for the copper experiment:</p> <p>Segment 1: top layer,                      Segment 2: 1 - 2 cm,                      Segment 3: 2 - 3 cm,                      Segment 4: 4 - 7 cm,                      Segment 5: 7 - 8 cm,                      Segment 6: 8 - 11 cm,                      Segment 7: 11 - 12 cm.</p> <p>Representative samples were analysed with SEM and EDX for the copper experiments.</p> <p>The segments were air dried, homogenised by grinding and segment 1, 2, 3, 5 and 7 were quantitatively analysed to their copper content with ICP-OES.</p> <p>For the TCC experiment the columns were sectioned in twelve 1 cm wide segments for the TCC experiment. The samples were burned in a scintillation counter and the amount of <sup>14</sup>C was detected.</p>
			 <p style="text-align: center;"><b>Bulk chemical and SEM / EDX analysis</b></p>
			

## 4.8 Results

### 4.8.1 Physical-chemical properties of P25 suspension

The carrier function of TiO<sub>2</sub> (P25) nanomaterials in soil columns spiked with copper sulphate and TCC was analysed in this study. Before the P25 suspension with a pH of 5 was applied to the soil column the size and zeta potential of the suspension was measured.

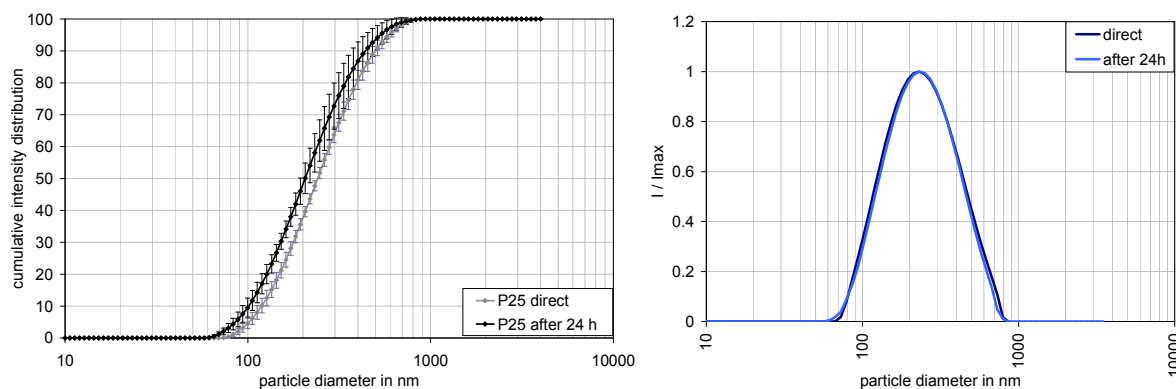


Figure 20: Cumulative intensity (left diagram) and particle size distribution (right diagram) of the particle diameter weighted in scattering intensity measured with DLS for P25 suspended in DI water at pH 5 directly after dispersion and 24 h later; error bars = standard deviation; mean value of  $n = 9$ .

The average particle size at pH 5 was 220 nm with a standard deviation of 5.84, a PDI of 0.207 (Figure 20) and a median of 241 nm (min: 234 nm, max: 250 nm) with a zeta potential  $> 15$  mV around 34 mV (min: 27.6 mV, max: 41.1 mV). The isoelectric point (IEP) of the P25 suspension was detected around pH 6.5 – 7.5 Table 12.

Table 12: Averages and standard deviation of zeta potential measurements of P25 (2.5 g/L) in 100 mL DI water; 10 min sonication (ultrasonic homogeniser);  $n = 3$ .

P25	DI water	
pH	Zeta potential (mV)	Standard deviation
4.5	36.0	7.8
5	33.6	4.9
6	19.3	9.4
7	-0.2	8.6
8	-21.6	8.4
9	-28.0	0.5

Hundred millilitres of the characterised P25 suspension were applied on the top of the soil columns of the test system for the carrier experiences.

#### 4.8.2 Mobilisation of copper sulphate by P25

For the mobilisation experiments six columns were filled with one soil type and all columns were spiked with 750 mg copper sulphate CuSO<sub>4</sub>.

1. Three columns were tested without P25 as comparison system to derive information about the copper mobility in the tested soil type.
2. Further three columns were additionally treated with P25 as test system to get information about the mobilisation effect of the titanium material on copper sulphate.

All columns were treated with the same amount of ~ 1800 mL of 0.01M CaCl<sub>2</sub> solution for 48 hours. After the experiments the soil columns of the three soil types (A01 = Dystric cambisol, A02 = Stagnic Luvisol, G03 = Eutric Cambisol) were sectioned in seven different segments – AII.8.

Segment 1, 2, 3, 5 and 7 were separated, homogenised (grinded). Compared with the results of the previous study (Kuhlbusch et al., 2012) the transport of TCC along the glass column wall was not extremely higher compared with the core samples (presented in section 4.8.4). Therefore only the core samples were analysed by ICP-OES for their copper content. The tests systems were additionally analysed for their titanium concentration. The analysed segments showed a thickness of about 1 cm which equates to an average amount of 120 g ± 20 g soil. The segments 4 and 6 were not analysed and showed a thickness of 3 cm which equates to an average amount of 360 g ± 60 g soil. The average copper and titanium background concentration of the soil types are 9 ± 4 mg/kg copper and 3135 ± 943 mg/kg titanium, detailed information are presented in Annex IV - AIV.4. The ICP-OES measurements for the reference system without P25 are presented in Figure 21.

As expected a generally low mobility of the copper was detected for all soil types. Nevertheless a soil type dependency of the copper mobility was observed  $G03 \geq A01 > A02$ . It is known, that copper shows a pH dependent mobility with increasing mobility for decreasing pH, whereas at a pH > 5.5 no mobility is expected (Fjällborg & Dave, 2003, Scheffer & Schachtschabel, 1992). In this study the soil type with the highest pH and the highest cation exchange capacity (CEC) showed as expected the lowest mobility (soil type A02 - highest copper concentration in segment 1), whereas for the other two soil types with a lower pH (soil type G03 and A01) a comparatively higher mobility was observed (Figure 21).

The low mobility of the copper is confirmed by the eluate analysis. In the eluate of the soils only a low copper concentration was observed independent on the soil type ranging from 4 µg/L to 180 µg/L (with a coefficient of variance (CV) of 0.1 – 0.7). Less than 0.005% of the total amount of copper introduced to the system was detected in the eluate inde-

pendent on the soil type and due to this the amount of leached chemical was therefore negligible.

All the determined concentrations were in the range of the experimental uncertainties of the measurements and the background concentration of the soils ranging from 9 µg/L to 60 µg/L with a CV of 0.02 – 0.8%).

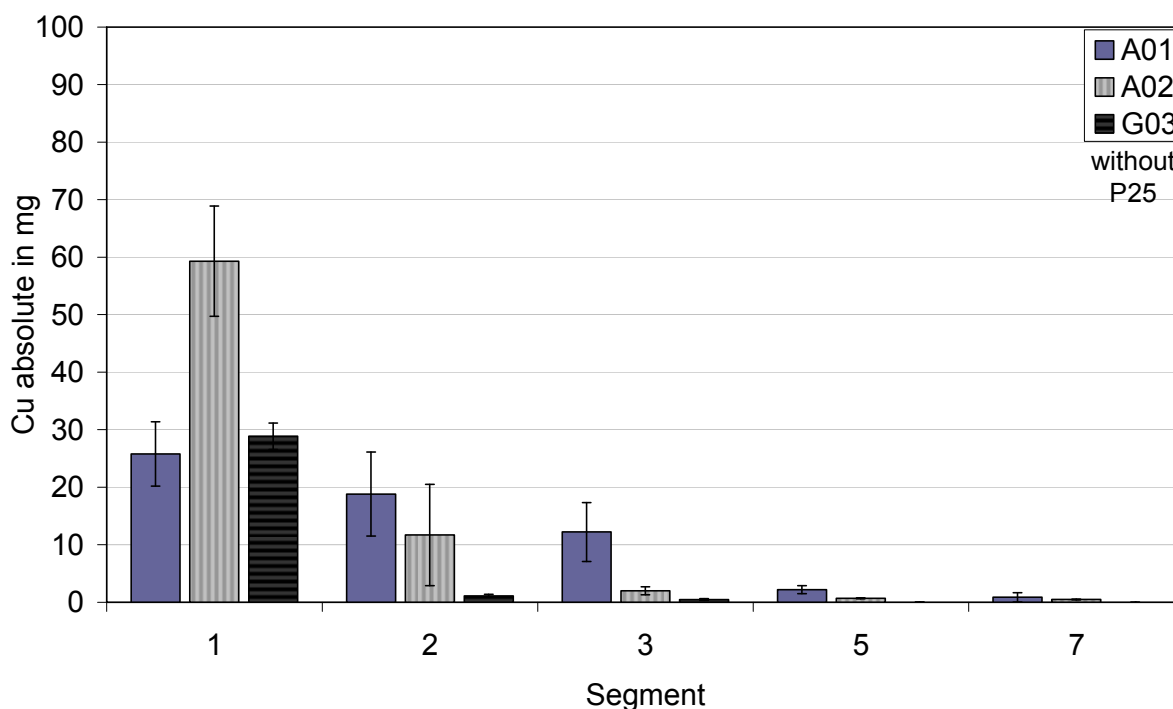


Figure 21: Average Copper concentration of the different segments of the three different soil types, without P25; n = 3. An average amount of 186 mg Cu (SD: 270) were applied to the soils, all presented values are background corrected.

It has to be generally noted that the copper recovery in these experiments has to be significant below 100% since only a) segments and b) the core of the columns were analysed.

For the test system with P25 an even lower mobility in comparison with the reference system was observed (higher copper concentrations in segment 1) whereas the mobility in the soil types showed the same ranking G03 ≥ A01 > A02 (Figure 22). The low mobility of the copper is confirmed by the eluate analysis. As it was observed for the reference system in the eluate of the soils of the test system also only a low copper concentration could be observed independent on the soil type. A copper concentration ranging from 4 µg/L to 80 µg/L with a CV of 0.1 – 1.0% was detected. Although less than 0.008% of the total amount of copper introduced to the system was detected in the eluate. Again, all measurement values are in the range of the lower detection limit.

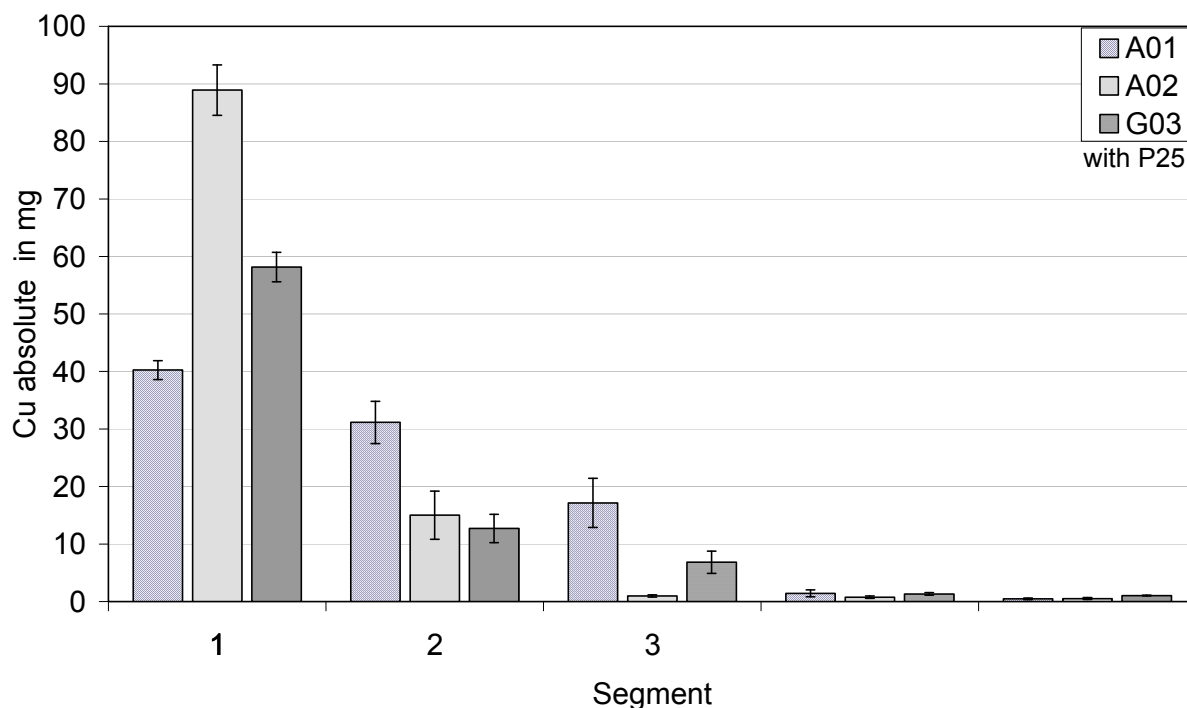


Figure 22: Average copper concentration of the different segments of the three different soil types, with P25; n = 3. An average amount of 186 mg Cu (SD: 270) were applied to the soils, all presented values are background corrected.

### 4.8.3 Titanium dioxide

For the transport experiments with copper sulphate and P25 also information about the transport behaviour of P25 can be derived from the results.

#### Eluate

The time resolved samples of the eluate were also analysed for their Ti concentration. With the ICP-OES measurements (LOD for Ti 0.12 µg/L) a minimum of <0.001% of the added TiO<sub>2</sub> could be detected. The titanium concentration in the eluate was also influenced by the soil background concentration. Exemplarily for soil type G03 a high variability ranging from 0.5 µg/L to 80 µg/L with an average concentration of 13.8 µg/L (SD: 22.2) was observed. The detected titanium concentrations were all in the range of the average background concentration plus the threefold standard deviation (cf. section AIV.8). Therefore a low mobility of P25 within the soil column was expected.

#### Soil

No titanium above the natural background concentrations (ranging from 1800 - 3800 mg/kg Ti, cf. section AIV.4 - Figure 70) was determined in the different segments. This is as expected, due to the low amount of titanium added to the system. However with SEM / EDX a transport of isolated TiO<sub>2</sub> agglomerates was detected down to the last segment of the columns for all soil types (soil type A01 Figure 23, soil type A02



Figure 24 and soil type G03 Figure 25). Further SEM / EDX scans of different segments of the soil types are shown in Annex AIV.8. The results of this study are in good agreement with the results of the previous study (Kuhlbusch et al., 2012). Both studies showed a low mobility of the added TiO<sub>2</sub> ENM, which can be explained by the positive zeta potential of P25 in suspension at pH 5 and a negative one for the soils. But both studies also showed the transport of isolated agglomerates of the nanomaterial.

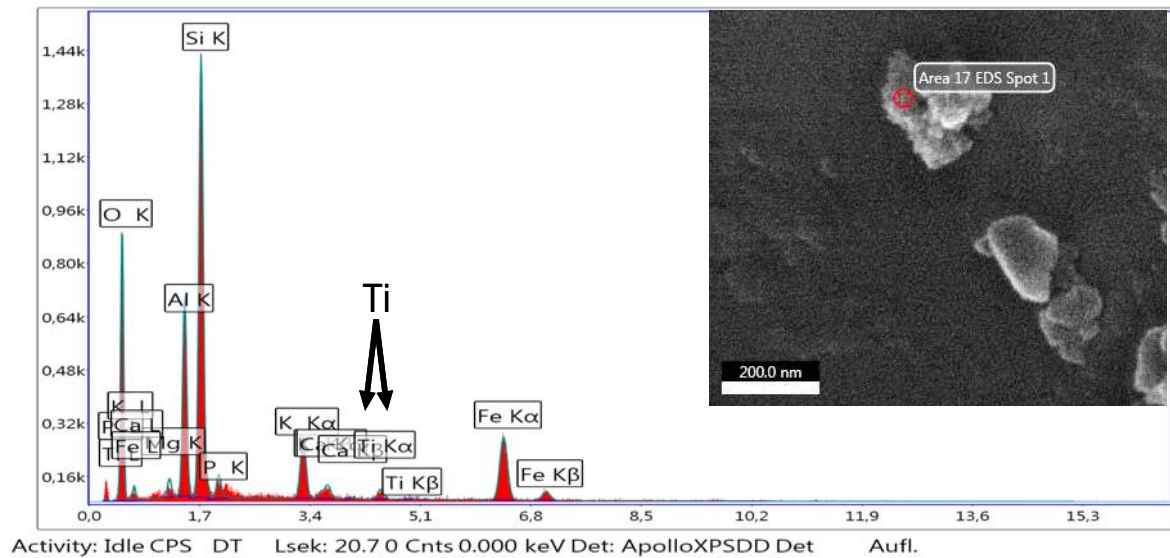


Figure 23: SEM and EDX Scan of segment 7 of column one of soil type A01.

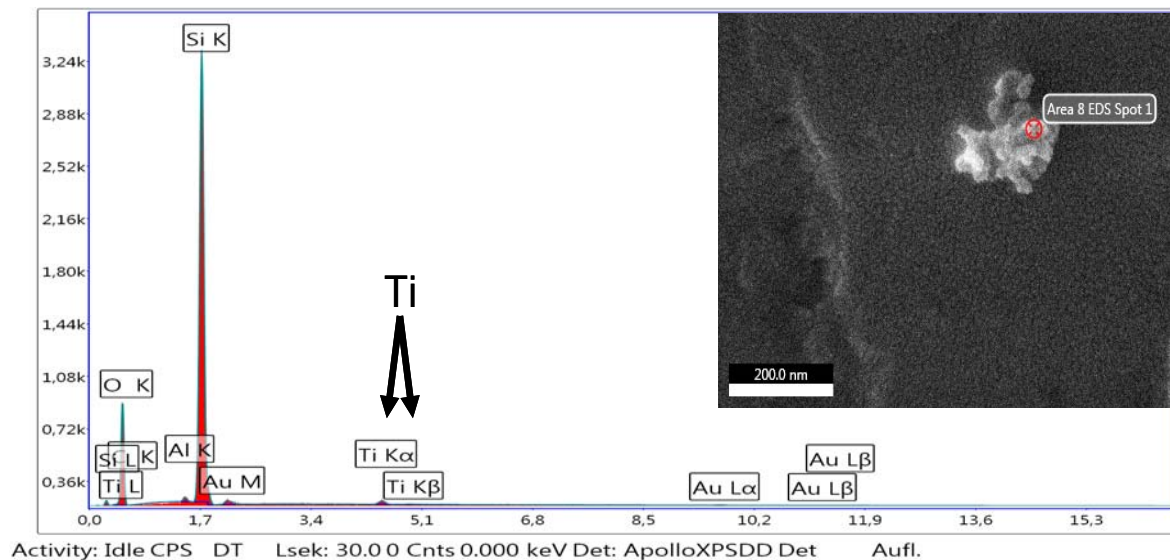


Figure 24: SEM and EDX Scan of segment 7 of column two of soil type A02.

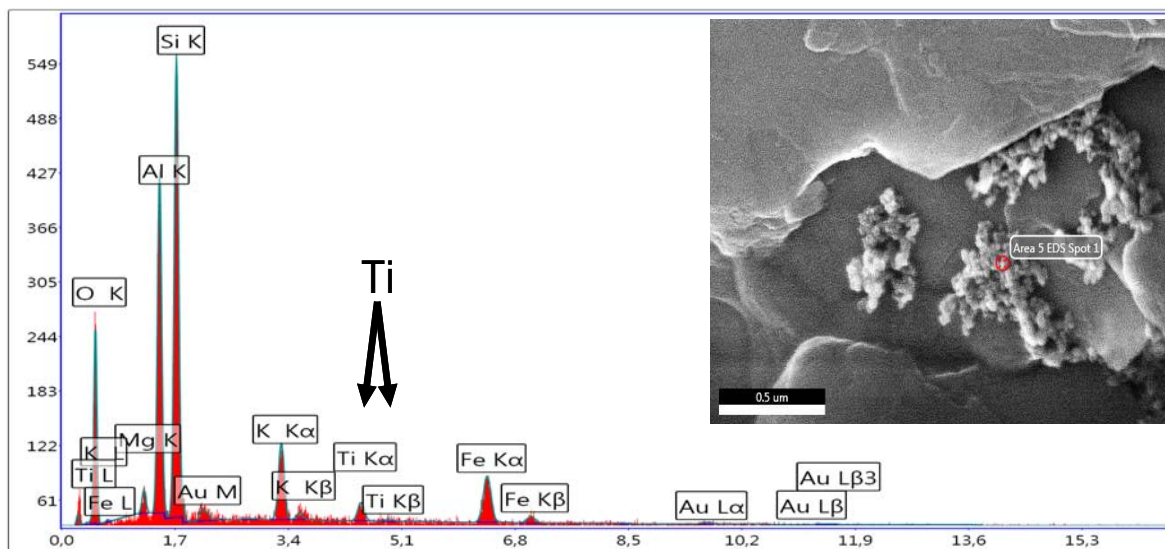


Figure 25: SEM and EDX Scan of segment 7 of column two of soil type G03.

#### 4.8.4 Mobilisation of Triclocarban by P25

The upper segment (100 g or ~ 1 cm) of the soil column was spiked with 0.2 mg <sup>14</sup>C-TCC in order to obtain a nominal TCC concentration of 2 mg/kg soil. Measurements of the radioactivity in subsamples revealed that the actual concentration ranged between 85 – 110% of this value.

To compare the soil transport of TCC in presence of TiO<sub>2</sub> to the transport in absence of this nanomaterial, a setup with three columns was designed. To two of the TCC-spiked soil columns, 100 mL of TiO<sub>2</sub> suspension at a concentration of 2.5 g/L was applied. The third TCC-containing column presented a reference system without TiO<sub>2</sub>.

After 48 h of irrigating the soil, less than 0.005% of the total amount of TCC introduced to the system was detected in the eluate. The amount of leached chemical was thus negligible in all soils, as was shown above to be the case for copper as well.

After the experiments the soil columns were sectioned in 12 different segments. The TCC concentrations were determined in the core and the border zone of these sections separately, in order to detect possible preferential material transport along the border of the column. In Figure 26 the TCC concentrations in the core samples of columns with and without TiO<sub>2</sub> after 48 h off irrigation are presented. Only in the first four centimetres from the top of the column, a concentration above the LOD could be determined. Segment 5 – 11 were therefore merged.

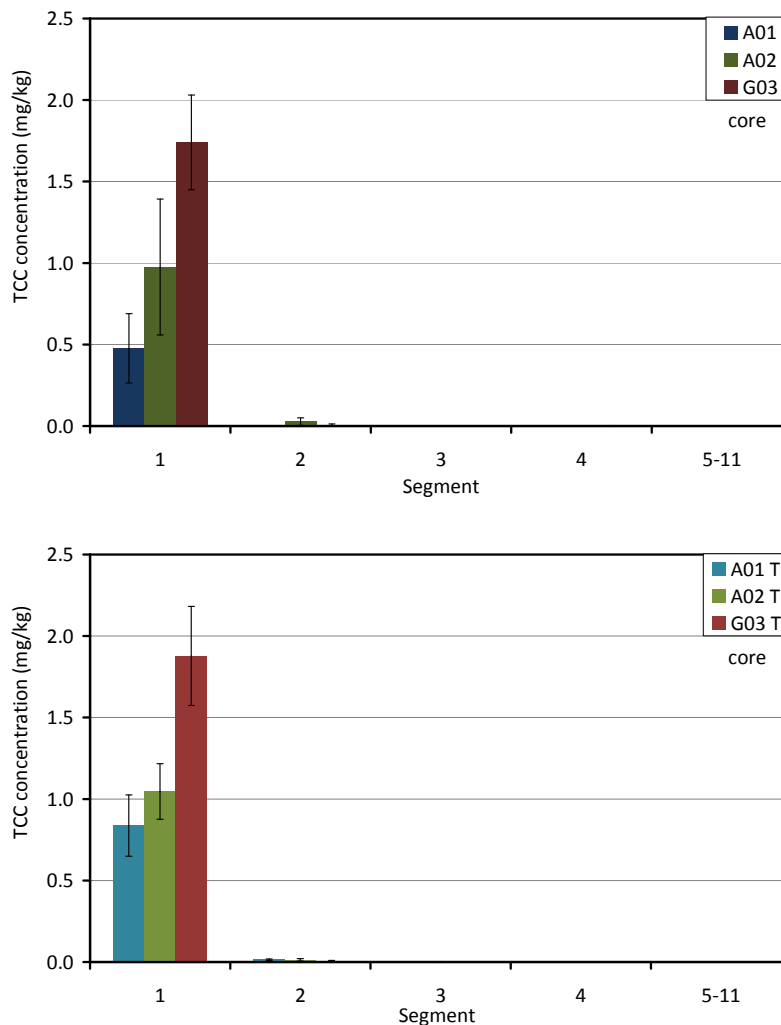


Figure 26: Triclocarban (TCC) concentration in the middle (core) of five segments (0-1, 1-2, 2-3, 3-4, and 5-11 cm) of columns filled with three different soil types (A01, A02, and G03) in absence of P25 (n = 1) upper figure and presence of P25 (Ti; n = 2) lower figure, after application of TCC to the upper segment and 48 h of surface sprinkling; error bars = SD of 3 sub samples of the corresponding segment.

At the end of the test, differences in the TCC concentration of the first segment of the different soil types were observed, although the initial concentrations were similar in all soils. TCC was least mobile in soil G03 and most mobile in soil A01. TCC concentrations in the presence or absence of P25 in soil types A02 and G03 did not significantly differ. TCC was however significantly less mobile when the nanomaterial was available in soil A01 compared to when it was not present.

Analyses of soil samples of the 1 cm region close to the glass wall in the different segments led to the same conclusions (Figure 27). TCC did not leach from the first segment of soil G03 to the same extent as in both other test soils. A negative influence of the nano-TiO<sub>2</sub>-material on the mobility of TCC was again only observed in soil A01.

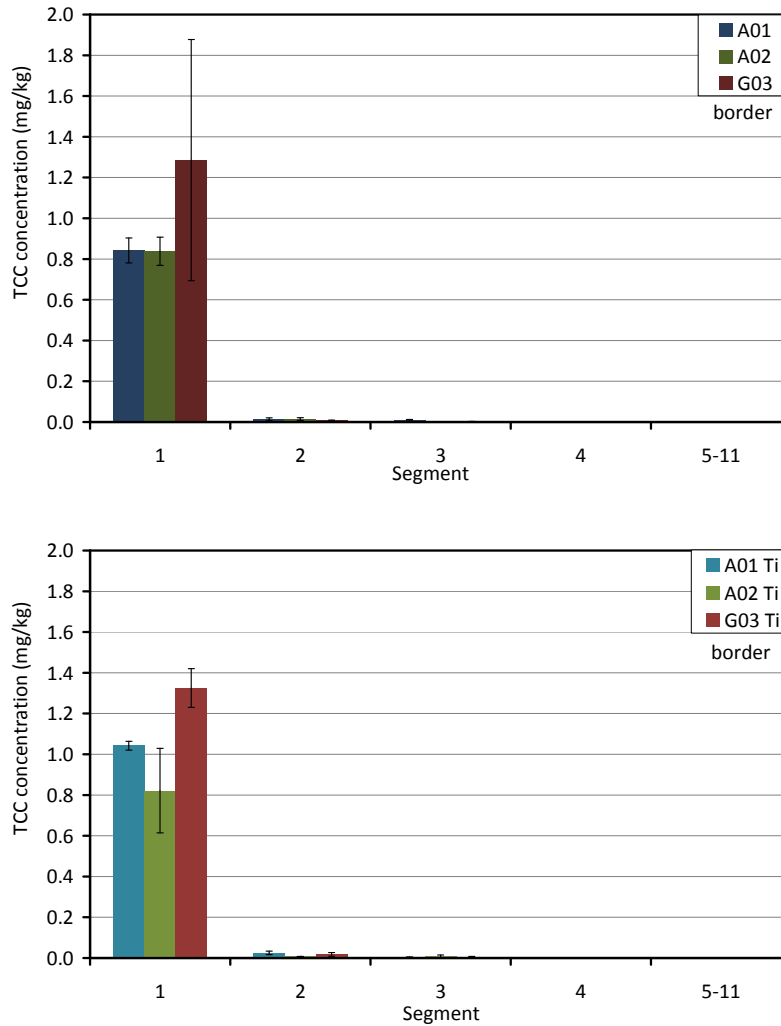


Figure 27: Triclocarban (TCC) concentration at the border (outer cm) of five segments (0-1, 1-2, 2-3, 3-4, and 5-11 cm) of columns filled with three different soil types (A01, A02, and G03) in absence of P25 (n = 1) upper figure and presence of P25 (Ti; n = 2) lower figure, after application of TCC to the upper segment and 48 h of surface sprinkling; error bars = SD of 3 sub samples of the corresponding segment.

In a previous study (Kuhlbusch et al., 2012) it was observed that TiO<sub>2</sub> may preferentially be transported along the glass column wall. Here, higher TCC concentrations were measured at the border compared to in the core of the first column segment in case of soil A01, both when TiO<sub>2</sub> was not present or available. This difference was not observed in soil A02. Only in soil G03 applied with the nanomaterial, the TCC content remained higher in the core compared to in the region close to the glass wall. To avoid that possible influences of the glass column wall on TCC transport are wrongly involved in the interpretation of the results, only the data of core samples were used for the final evaluation of the test.

## 4.9 Bioavailability for Lumbricidae

As can be derived from the leaching experiments presented above, there was a significant difference between the mobility of TCC in presence vs. in absence of P25 in the upper segment of soil A01 (chapter 4.8.4, Figure 26). Therefore, this soil type was selected for tests with the earthworm *Eisenia fetida*. Since it was shown that P25 rather keeps TCC in the top segment of the soil, i.e. where earthworms are dwelling in nature, the investigation focused on the influence of nano-TiO<sub>2</sub> on the bioavailability of TCC for these organisms.

The tests were performed based on OECD guideline 317 for the testing of chemicals (Bioaccumulation in Terrestrial Oligochaetes). One earthworm was exposed to 0.1 mg <sup>14</sup>C-TCC in a beaker filled with 50 g of soil, which is the minimum amount necessary to habitat one worm. TCC was applied to the system through three different methods: 1) spiking the compound to the medium used to wet the soil, 2) spiking of 10% of the soil before mixing it with the rest, and 3) spiking of the food applied once at the beginning of the experiment. In all treatments, TCC was brought into the system using a stock solution of 1 mg TCC/mL ethanol. As for the first application technique, the solution was directly pipetted into the medium. After soil and food spiking, acetone was added to cover the solid mass and then mixed with it, in order to obtain homogeneity. The solvent was subsequently allowed to evaporate (during 24 h). For each TCC exposure setup, a parallel to which P25 was introduced was prepared (1 g/kg soil). P25 was suspended in the amount of distilled water used to bring the soil at 50% of the water holding capacity. In case of the setup, in which TCC was spiked to the medium as well, first the dispersion was made and then TCC was applied. Only 24 h later, the suspension was added to the soil in order to allow the compound and the nanomaterial to interact for one day. When the TCC-spiked medium or TiO<sub>2</sub>-dispersion was finally mixed with the soil, one worm was added to the system and no food was provided during the experiment. Similarly, the organism was introduced only after uncontaminated medium had been applied to wet the soil in case of soil spiking. For this setup, two parallel test series were run, one in which the animals were not fed, and one in which 0.5 mg food was supplied at the start. As recommended in OECD guideline 317, the organic food source consisted of dried dung. Also in case of dietary exposure, the organisms were introduced after the spiked food had been put on top of the already wetted soil. In this way, 8 different setups at five replicates were prepared (Table 13). In the first six treatments, a final concentration of 2 mg <sup>14</sup>C-TCC/kg soil was obtained. The concentration in the diet of the other two treatments amounted to 200 mg <sup>14</sup>C-TCC/kg food, present on top of the soil.

Table 13: Prepared setups to exposure the earthworm *Eisenia fetida* to 14C-labelled triclocarban (TCC) in absence or presence of nano-TiO<sub>2</sub> (P25), with five replicates for one tests.

TCC in suspension		TCC in soil				TCC in food	
Without P25	With P25	Without P25	With P25	Without P25	With P25	Without P25	With P25
No food	No food	No food	No food	Clean food	Clean food	Spiked food	Spiked food

After 14 days, the worms were collected from the soil, carefully rinsed, and transferred to little glass vessels containing a piece of wet tissue in order to allow them to purge their guts. One day later, the organisms were put in an oven at 60 °C until complete dryness, weighed, and subjected to combustion in the biological oxidizer. Similarly, the faeces were gathered, dried, and analysed. The tissue containing excretion fluids was then transferred to a liquid scintillation vial, covered with cocktail, and directly subjected to LSC. The soil (and food) was (were) thoroughly mixed and four samples were collected, dried, weighed, and combusted.

Whereas all organisms survived in the treatments without food, the worms of several replicates died when nutrition was available (Figure 28). This shows that dietary uptake of TCC leads to more pronounced negative effects on the organisms. Nevertheless, the dry weight of the remaining worms was significantly higher ( $p < 0.05$ ). However, no difference in the dry weight of worms of setups, to which TCC was applied with different techniques (soil or food spiking), was observed. Similarly, spiking via suspension or soil did not have a significant influence on the weight of unfed organisms. The presence of P25 did not seem to affect the weight of the organisms. When TCC was however the only applied chemical, a generally larger variation in the data was observed compared to when the nanomaterial was also available. However, more worms survived in both treatments, in which a diet was provided, when P25 was present than when it was left out (Figure 28).

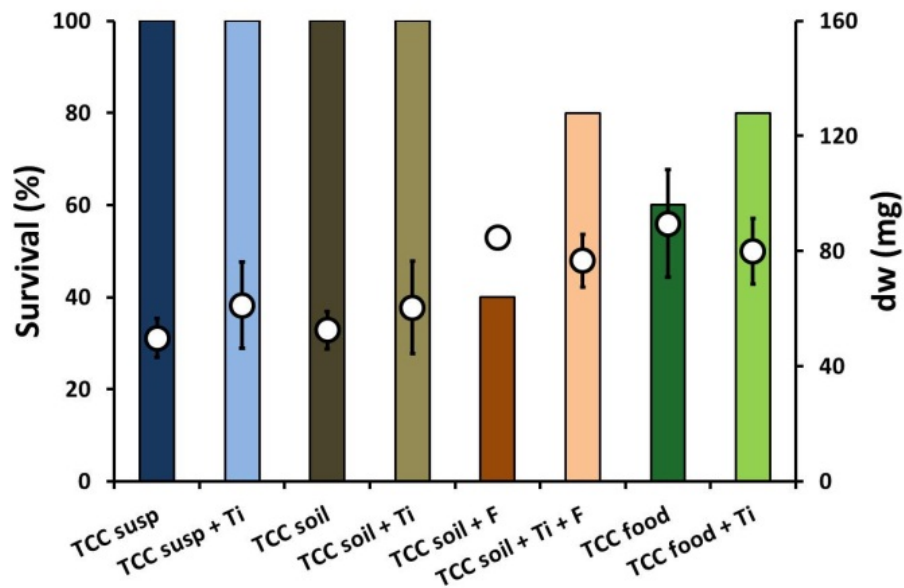


Figure 28: Survival (bars) and dry weight (dw, round data points) of earthworms (*Eisenia fetida*) exposed to triclocarban (TCC) for 14 days in soil systems spiked via different methods: via the soil water (TCC susp), via a fraction of the soil (TCC soil), and via the diet (TCC food). Treatments, in which uncontaminated food was supplied to the worms, are indicated with "+ F". The presence of P25 is indicated with "+ Ti". The whiskers represent the standard deviation on the mean weight of five replicates. The standard deviation of TC soil + F is covered by the data point; n = 5.

Mass balances were made by comparing the total amount of radioactivity in the spiked medium sampled at the beginning with the total amount in the soil at the end of the test. Recovery rates ranged between 89% and 102%. Bioaccumulation factors (BAF) were calculated by dividing the TCC concentration in the worms after they were purged by the concentration in the dry soil, when applicable including the food. Dietary exposure clearly led to the highest accumulation of TCC in the organisms, whereas worms that received unpolluted food being in a contaminated soil did not accumulate the substance (BAF < 1) (Figure 29). When no nutrition was supplied, BAFs of about 2.5 were obtained, independent of the application technique. The presence of P25 had no effect on the degree of TCC accumulation in the earthworms (Figure 29).

The fact that a higher BAF was obtained when the substance was applied via the diet (treatment "TCC food") can be explained by the fact that the TCC concentration in the food was a lot higher than in the soil. As was mentioned above, the same amount of TCC was either spiked to 0.5 g of nutrition or to 50 g of soil (treatment "TCC soil" and "TCC susp"). In the presence of unspiked food (in treatment "TCC soil + F"), the lowest BAFs were obtained, which shows that intake of this uncontaminated diet was preferred and/or that TCC absorbed from the soil was better eliminated by the earthworms. Since mortality was equal (with Ti) or even higher (without Ti) in treatment "TCC soil + F", less absorption can be ruled out making the second explanation the most feasible.

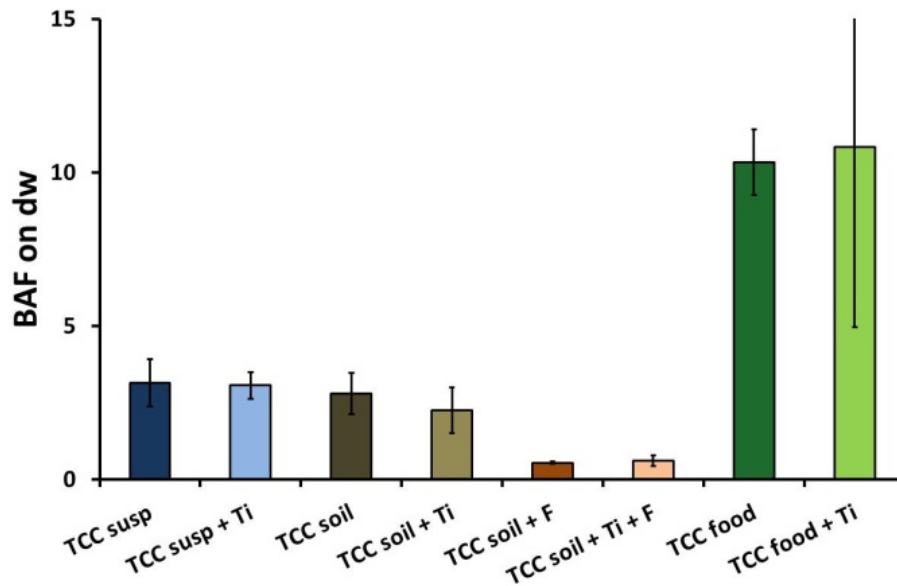


Figure 29: Bioaccumulation factors (BAF) calculated using soil and organism dry weight (dw) after exposure of earthworms (*Eisenia fetida*) to triclocarban (TCC) for 14 days in soil systems that were spiked via different methods: via the soil water (TCC susp), via a fraction of the soil (TCC soil), and via the diet (TCC food). Treatments, in which uncontaminated food was supplied to the worms, are indicated with "+ F". The presence of P25 is indicated with "+ Ti". The whiskers represent the standard deviation on the mean of five replicates.

However, when the percentage of the total radioactivity, present in the test beakers, in worms and their excretions was calculated, some more differences between the treatments were observed (Figure 30). The relative amount of radioactivity in the worms was significantly lower after soil spiking compared with suspension spiking when P25 was present and no food was provided (light blue vs. light brown bar, Figure 30, graph on the left). When food was present, the presence of P25 resulted in lower amounts of TCC in the faeces of the organisms. This influence of P25 was observed when uncontaminated food (treatment "TCC soil + F") was applied to the organisms (Figure 30), graph on the right, dark vs. light orange bar) as well as when spiked food (treatment "TCC food") was provided (Figure 30), graph on the right, dark vs. light green bar). Looking at the mortality within each of these treatments separately, more organisms survived when P25 was applied (within "TCC soil + F": 2 survived without Ti, and 4 with Ti; within "TCC food": 3 survived without Ti, and 4 with Ti present). Hence, it seems that more TCC in the faeces is linked to higher mortality.



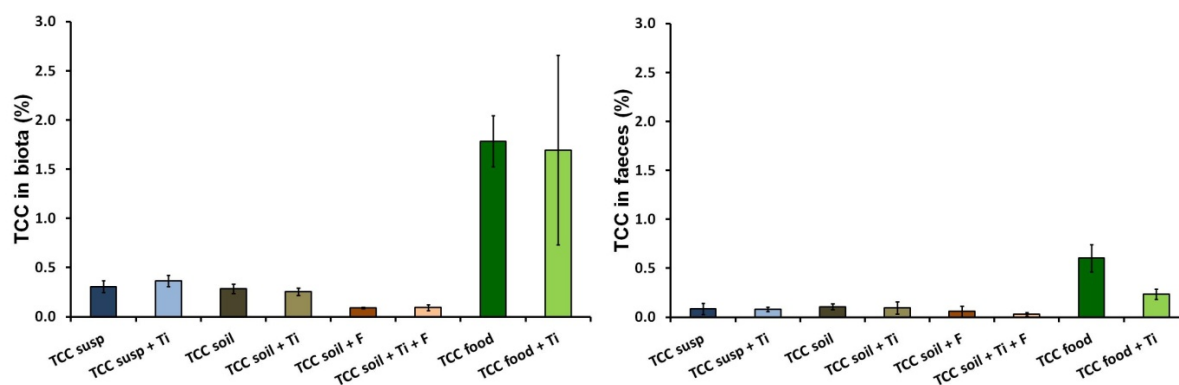


Figure 30: Percentage of the total amount of radioactivity found in earthworms (*Eisenia fetida*) and their faeces, after they were exposed to triclocarban (TCC) for 14 days in soil systems that were spiked via different methods: via the soil water (TCC susp.), via a fraction of the soil (TCC soil), and via the diet (TCC food). Treatments, in which uncontaminated food was supplied to the worms, are indicated with "+ F". The presence of P25 is indicated with "+ Ti". The whiskers represent the standard deviation on the mean of five replicates.

The results can best be discussed by comparing them to the ones of the ecotoxicological studies performed in a parallel project (UBA-project 3710 65 413 yet unpublished). In that program, both acute (14 days of exposure without feeding) and chronic (28 or 56 days of exposure with feeding) experiments were performed with the same test organism. Effects of TCC to earthworms were assessed after simultaneous application of TCC and nano-TiO<sub>2</sub> or after spiking the system with only TCC. Again, it was aimed at comparing these treatments to evaluate a possible influence of the presence of the nanomaterial on the bioavailability of TCC. It should be mentioned that other TiO<sub>2</sub> materials were tested, but at the same concentration of 1 g TiO<sub>2</sub>/kg soil, and that TCC levels were much higher than in the present study. The latter logically led to more clear effects on the organisms. In this analytical experiment, where radiolabelled TCC was used, such high concentrations could not be reached due to the high costs of the chemical, the cocktails, and the disposal of radioactive waste. In acute experiments, a dose-dependent effect of TCC on the gut content of *Eisenia fetida* was observed. At higher soil TCC contents, less faeces were present in the digestive system of the organisms (based on dry weight). It was shown that the availability of one TiO<sub>2</sub> material in the soil led to a lower degree of this effect compared to when worms were exposed to TCC alone. The mass of the gut content of worms from the present no-feeding setups did not significantly differ (data not shown). This is in agreement with the results of the parallel project, since the lowest observed effect concentration (LOEC) derived, amounted to 169 mg TCC/kg soil dry weight (here: 2 mg/kg). The gut content was however higher in the soil spiking treatment with uncontaminated food and TiO<sub>2</sub> than without TiO<sub>2</sub> (17 ± 6 vs. 12 ± 7 mg; mean ± standard deviation). Although this difference is not statistically significant, the same compensating tendency of TiO<sub>2</sub> to reduce the effect of TCC can be assumed at this lower concentration as well. Also

in the long-term experiments of the parallel project, TCC caused less severe harm to the worms when nano-TiO<sub>2</sub> was present. Mortality was significantly lower and reproduction significantly higher in combined exposure setups. This is again in agreement with the survival data obtained in the present study (Figure 28). Although no differences were observed between the BAFs of worms from the same treatments differing in the P25 availability only, the partitioning of TCC to the gut content was influenced by the nanomaterial (Figure 29). The real bioavailable fraction, i.e. the internalised, incorporated part absorbed from the digestive system, was not influenced. Combining the results of bioavailability and effect studies, it seems that the amount of TCC in the gut content is an indicator for the wellbeing of the test organism. It is assumed that this can be explained by enhanced metabolism and elimination of TCC in case the organism is affected by the compound. It seems that both the presence of uncontaminated food and TiO<sub>2</sub> are beneficial for these processes.

#### **4.10 Discussion - Mobility of TCC and copper affected by P25**

In these experiments the carrier effect of P25 with TCC and copper was analysed in three different natural soils. Based on the experiences of the previous study Kuhlbusch et al. 2012 and the results for the TiO<sub>2</sub> mobility in the soil columns in this study, only a low mobility of nano-TiO<sub>2</sub> in soils was found. Only with SEM / EDX a transport of isolated agglomerates of P25 was detected down to the last segment of the columns independent on the soil type. The low mobility of P25 is probably affected by the positive zeta potential of this material and higher heteroagglomeration with and deposition to negatively charge soil compartments (Darlington et al. 2009, Solovitch et al. 2010).

It is known that pollutants and other substances can adsorb to the surface of nanomaterials (Pan & Xing 2008, Hofmann & von der Kammer 2009, Fang et al. 2011), which directly can affect the mobility of these substance. Therefore we hypothesized that TCC as well as copper can adsorb to the surface of P25. Based on the results of the column experiments a carrier effect of P25 for the pollutants TCC or copper was not expected, due to the low mobility of the TiO<sub>2</sub> nanomaterial, but contrary, maybe accumulation could be enhanced.

It was previously shown that TCC has a low mobility and a high accumulation rate in soils (Cha & Cupples, 2010). The even lower mobility of TCC in the presence of P25 compared to its absence in soil type A01 implies interactions of TCC and the nanomaterial within the soil matrix. Nanomaterials were shown to act both as vehicles (*Trojan horses*) and scavengers for other molecules in environmental media. Both cases were previously observed, mostly in studies with carbon based materials (Cheng et al., 2004; Baun et al., 2008; Pan et al., 2008; Park et al., 2011).

The mobility of copper is dependent on the pH. A copper mobility is expected at pH < 5.5 and a high mobility at pH < 4.5 (Blume, 1990, Scheffer & Schachtschabel, 1992, Korthals et al. 1996, Fjällborg & Dave, 2006).

As expected the soil types with the lowest pH (G03 – pH 5.64 and A01 - pH 5.67) showed some copper transport whereas the soil type with the highest pH and CEC (soil type A02 - pH 6.63 and CEC 133.2 mmolc/kg) showed nearly no copper mobility independent of the presence of P25. However with P25 a lower mobility of copper was observed for all soil types and clearly for soil type G03.

An influence of the availability of nano-TiO<sub>2</sub> on the fate of inorganic substances has also been reported (e.g. Sun et al., 2007, Fang et al. 2011) and was shown in the present study with copper, but its effect on the environmental behaviour of organic chemicals remains largely unknown. Hence, this study delivers first data indicating an effect of P25 on the transport of a lipophilic compound that might enter soil systems via the same pathway as the nanomaterial.

Based on the high background concentration of titanium in natural soils and the use of unmarked materials we conclude that the bulk chemical analysis alone is not sensitive enough for the detection of the TiO<sub>2</sub> nanomaterial in the systems which were tested in this study. Therefore SEM / EDX scans have to be conducted, to derive information on the mobility of the material in the soil column and additionally information on the morphology of the transported agglomerates.

## Résumé

It can be derived from the results of the soil transport experiment that:

- P25 showed only a low mobility of single agglomerates in all tested soil types,
- the low mobility is affected by the positive zeta potential of the TiO<sub>2</sub> nanomaterial,
- TCC and copper concentrations are the highest in the first segment of all soil types,
- the TCC concentration in the top layer remained higher in soil G03 (less transport) than in soils A01 and A02,
- the TCC concentration in segments 5-11 was always below the detection limit,
- the copper concentration in the top layer remained higher in soil type A02, than in G03 and A01,
- for TCC and copper the highest mobility was observed for soil type A01 without P25,
- in the presence of P25 a tendency to lower mobilities of TCC and copper was observed for all soil types.

## 5 Summary and conclusion

Nanomaterials are nowadays used in increasing amounts in everyday products and special applications. Enhanced release of engineered nanomaterials (ENM) into the environment can hence be assumed. First experimental studies and environmental modelling exercises have been conducted during the last years (Gottschalk et al., 2010; Kuhlbusch et al. 2012; Limbach et al., 2009; Kiser et al., 2009) significantly improving our knowledge on release and environmental behaviour. Still not all necessary test procedures and information are yet available to assess the fate of ENMs in the environment. One major current lack is the knowledge on the stability of the coating of ENM, which determines the environmental behaviour. Another knowledge gap is the information of a possible carrier function of nanomaterials in soils for soil pollutants. Hence methodologies to study coating stability as well as carrier effects were developed and tested for three different TiO<sub>2</sub> nanomaterials, as one of the most used ENM in products, in soils and aqueous media. More precisely,

- The first part of the study dealt with a method development for the stability testing of the coating of two different functionalised TiO<sub>2</sub> nanomaterials. The stability was analysed covering different environmental conditions like pH, ionic strength and dissolved organic carbon concentration.
- The second part of this study analysed the carrier function of P25 for the two different substances, copper and <sup>14</sup>C trichloroethane, in three different soil types.

The surface of a material determines its behaviour in the environment (e.g. isoelectric point, adsorption capacity, and repulsion). Hence changes of surface properties and especially of coatings and their stability are of importance. A method determining surface coating stability was developed and tested with two coated titanium dioxide nanomaterials.

Changes of surface coating can be determined in different ways: a) by quantifying the released coating material in e.g. the suspension media, b) by quantifying the coating material on the nanomaterial prior and after exposure to stress conditions, and c) indirectly by determining changes in the behaviour of the ENM, e.g. changes in particle size distributions, the isoelectric point (IEP). The above endpoints were analysed for the suspension of ENMs in deionised water with as little energy input as well as for conditions as can be expected in the environment (pH, IS, DOC) or for test procedures applied in the laboratory to study environmental behaviour. This concept for testing surface coating stability can be applied to any ENMs but the analytical methods have to be chosen according to the material and media tested. The combined information from the studies are then discussed and interpreted in view of surface coating stability.

The two ENM chosen for evaluation were the hydrophobic coated NM103 (UV Titan M262) and the hydrophilic coated NM104 (UV Titan M212). The materials are produced with two layers of coatings: an Al<sub>2</sub>O<sub>3</sub> layer for averting photo-oxidation (around 6 weight-%) and a second layer of dimethicone / glycerol molecules (around 1 – 2 weight-%) on top of the Al<sub>2</sub>O<sub>3</sub> layer to ensure hydrophobic / hydrophilic behaviour.

First tests of coating stability were done using stirring of the nanomaterial in deionised water. Measurements revealed that about 88% ± 8% of the glycerol of the NM104 and 95% ± 5% of the silicon of the NM103 were already dissolved by low energy input. These results were confirmed by corresponding analysis of the remaining ENM which showed no significant concentrations of dimethicone or glycerol. Aluminum concentrations, indicating possible dissolution of the inorganic coating, were below detection limit as expected due to its low solubility at pH > 4.5. Measurements of the IEP confirmed this finding with IEPs around pH 8 as expected for an alumina surface. The IEP for TiO<sub>2</sub> is expected at a significantly higher pH around 5-7.

Additionally, different suspension preparation procedures with different energy input were tested to derive further information on coating stability. Tests using mixing (without external energy input), 1 min stirring after suspending the powder, and 1 minute sonication (ultrasonic probe) followed by 1 hour of moderate stirring (SOP) were compared as methods for suspension preparation. It was shown that the release of the organic coating increased with increasing energy input. Nearly all of the second coating was removed using the established SOP. This was confirmed by SEM / EDX and by ToF SIMS analysis, which identified a TiO<sub>2</sub> core and an aluminium oxide and dimethicone coating for the basic material and a TiO<sub>2</sub> core and an aluminium oxide coating without dimethicone after suspension preparation. Glycerol could not be specified with the two techniques. The Al<sub>2</sub>O<sub>3</sub> coating was proven to be stable and independent of the type of energy input and even after longer sonication. Zeta potential measurements indicate an isoelectric point of the coated TiO<sub>2</sub> nanomaterials around pH 8-9, which is comparable with the isoelectric point of alpha aluminium oxide and different from the isoelectric point of TiO<sub>2</sub> (Kosmulski, 2006). Furthermore EPR analyses showed no ROS formation even when the material was illuminated in the UV light. This results support the previous results of an intact aluminium oxide layer on tested TiO<sub>2</sub> materials after suspension in deionised water. Therefore we conclude that the aluminium oxide coating will be the actual surface of the two materials.

Effects of different environmental conditions on the ENM behaviour were then mimicked by varying the ionic strength using Ca<sup>2+</sup> as one of the major cations in surface waters (von der Kammer et al., 2010) and the dissolved organic carbon content (here different concentrations of humic acid - AHA). Zeta potential measurements were conducted as well as

the size of the materials under these varying conditions as an indicator of possible changes in environmental behaviour.

The variation of the ionic strength (CaCl<sub>2</sub> concentration) showed an impact on the interfacial properties, in particular in basic media. No isoelectric point below pH 10 could be identified in freshly prepared suspensions (CaCl<sub>2</sub> solution > 0.001 M). With increasing ionic strength the agglomeration of the ENM increased. A gradual change of the zeta potential was observed with IEPs moving back to lower pH values. This change may be explained by low kinetics and possible uptake of CO<sub>2</sub>. The latter influences the ion balance.

A different situation occurs if the ENMs were suspended in aqueous systems containing DOC (humic acid). DOC adsorbs on the ENM surface. It seems that this adsorption is quite stable since changes in pH and ionic strength had only a small influence on the zeta potential. The surface charge was strongly negative e.g. for DOC concentrations ≥ 2.5 mg/L, also in the presence CaCl<sub>2</sub>.

The tests clearly show that coating stability can vary significantly. Stable coating can alter the environmental behaviour significantly. This is shown by the change of the IEP for Al<sub>2</sub>O<sub>3</sub> coated TiO<sub>2</sub>. The coating has an influence on the zeta potential which has influence on soil ENM interactions and hence soil transport of ENM. Influences of the ionic strength as well as of DOC on the zeta potential were clearly shown. It seems that especially DOC is of importance. The humic acid used in this study lead to a (steric) stabilisation of the ENMs and a negative zeta potential. Both lead to higher ENM mobility in negatively charged soil environments.

The possible carrier effect of P25 for soil pollutants was the second research topic to be investigated. Recent studies indicated that mobile nanomaterials can act as carrier for pollutants (Hofmann and Kammer, 2009; Fang et al., 2011). Trichlocaban (TCC) and a copper salt (CuSO<sub>4</sub>) were chosen as soil contaminants to be tested due to the relevance and analytical advantages. Three different natural soil types were employed. Only low soil mobility was observed for P25 in this study in agreement to a previous study (Kuhlbusch et al., 2012). The transport of isolated agglomerates down to the last segment of the soil column could only be observed using electron microscopy coupled with a chemical analysis (SEM / EDX) independent on the soil type. The low mobility of P25 is probably affected by the positive zeta potential of the material in the expected pH range of the soils. With the positive zeta potential a higher adsorption on negatively charged surfaces, like soil minerals, is likely, which reduces the mobility of the material in the system.

Hence no carrier effect of P25 was expected.

For copper a low and pH dependent mobility with and without P25 was detected. The soil types with the lowest pH (soil type G03 and A01) showed a significant higher mobility whereas the soil type with the highest pH and highest cation exchange capacity (soil type

A02) showed the lowest mobility. This is in agreement with previous results showing the pH dependent mobility of copper in soils, higher mobility at lower pH.

A similar soil type dependent mobility, but overall a lower mobility of copper was observed when TiO<sub>2</sub> nanomaterial was added to the first centimetre in the soil column. This may be explained by the adsorption of the copper onto the P25 surface. The low mobility of P25 would then also lead to a lower mobility for copper. Results of Fang et al. (2011) agree with this hypothesis, but it should be noted that Fang et al. tested a TiO<sub>2</sub> nanomaterial with a negative zeta potential.

Comparable results were also shown for the experiments with TCC, which was employed at very low concentrations. Radioactive labelling of TCC with <sup>14</sup>C allowed the use of these low concentrations. TCC soil mobility was lower than for copper in all tested soil types. Anyhow, the presence of P25 diminished the mobility of TCC even more but not significantly, also in the sandy soils at low pH.

Even though the results were similar for TCC and copper, it has to be noted that the results probably differ for other nanomaterials, e.g. showing increased soil pollutant mobility when ENM is added.

Overall, reduced mobility of soil pollutants may lead to an accumulation in the upper soil layers. The formation of accumulation layers with high concentrations of pollutants can be hazardous for soil organisms like lumbricidae which live in the upper soil layer.

On the other hand, ecotoxicological tests conducted in the framework of this study show that the presence of TiO<sub>2</sub> leads to higher fractions of TCC in the gut of a common earthworm and lower negative effects of the compound towards this organism. It is hypothesised that the adsorption of TCC on the TiO<sub>2</sub> surface may facilitates its excretion leading to lower negative effects. Only few similar investigations have been published so far, and hence, more research is necessary to enable some generalisations on the overall influence of (inorganic) nanomaterials on the bioavailability of organic compounds. Nevertheless, both tests, the soil leaching experiments and the bioavailability tests, proof that ENMs, here TiO<sub>2</sub> might have a significant influence on the fate of environmentally important pollutants.

## 6 Literature

- Auffan, M.; Oedeutour, M.; Rose, J.; Masion, A.; Ziarelli, F.; Borschneck, D.; Chaneac, C.; Botta, C.; Chaurand, P.; Labille, J.; Bottero, J.-Y. (2010): Structural degradation at the surface of TiO<sub>2</sub>-based nanomaterials used in cosmetics, *Environmental Science & Technology*, 44, 2689-2694.
- Baun, A.; Sorensen, S.N.; Rasmussen, R.F.; Hartmann, N.B.; Koch, C.B. (2008): Toxicity and bioaccumulation of xenobiotic organic compounds in the presence of aqueous suspensions of aggregates of nano-C-60. *Aquatic Toxicology* 86 (3), 379-387.
- Blume, H-P. (1990): Handbuch des Bodenschutzes. Ecomed Verlag, Landsberg. 686 S.
- Carrier, X.; Marceau, E.; Lambert, J.F.; Che, M. (2007): Transformations of  $\gamma$ -alumina in aqueous suspensions. 1. Alumina chemical weathering studied as a function of pH. *Journal of Colloid and Interface Science*, 308(2), 429-437.
- Cha, J.; Cupples, A.M. (2009): Detection of the antimicrobials triclocarban and triclosan in agricultural soils following land application of municipal biosolids. *Water Research* 43 (9), 2522-2530.
- Cha, J.; Cupples, A.M. (2010): Triclocarban and triclosan biodegradation at field concentrations and the resulting leaching potentials in three agricultural soils. *Chemosphere* 81 (4), 494-499.
- Chen, S.B.; Xu, M.G.; Ma, Y.B.; Yang, J.C. (2007): Evaluation of different phosphate amendments on availability of metals in contaminated soil. *Ecotoxicology and Environmental Safety*, 67: 278-285.
- Cheng, X.K.; Kan, A.T.; Tomson, M.B. (2004): Naphthalene adsorption and desorption from Aqueous C-60 fullerene. *Journal of Chemical and Engineering Data* 49 (3), 675-683.
- Clarke, B.O.; Smith, S.R. (2011): Review of 'emerging' organic contaminants in biosolids and assessment of international research priorities for the agricultural use of biosolids. *Environment International* 37 (1), 226-247.
- Darlington, T.K.; Neigh, A.M.; Spencer, M.T.; Nguyen, O.T.; Oldenburg, S.J. (2009): Nanoparticle Characteristics Affecting Environmental Fate and Transport Through Soil. *Environmental Toxicology and Chemistry*, 28 (6), 1191 – 1199.
- Delgado, A. V.; González-Caballero, F.; Hunter, R. J.; Koopal, L. K.; Lyklema, J. (2007): Measurement and interpretation of electrokinetic phenomena. *J. Colloid Interface Sci.*, 309(2), 194-224. doi:10.1016/j.jcis.2006.12.075.
- Domingos, R.F.; Tufenkji, N.; Wilkinson, K.J. (2009): Aggregation of titanium dioxide nanoparticles: role of a fulvic acid. *Environmental Science and Technology*, 43(5), 1282 - 1286.
- Düster, L.; Prasse, C.; Vogel, J.V.; Vink, J.P.M.; Schaumann, G.E. (2011): Translocation of Sb and Ti in an undisturbed floodplain soil after application of Sb<sub>2</sub>O<sub>3</sub> and TiO<sub>2</sub> nanoparticles to the surface. *Journal of Environmental Monitoring*, 13, 1204 - 1211.
- Fan, W.; Cui, M.; Liu, H.; Wang, C.; Shi, Z.; Tan, C.; Yang, X. (2011): Nano-TiO<sub>2</sub> enhances the toxicity of copper in natural water to *Daphnia magna*, *Environmental Pollution*, 159, 729-734.
- Fang, J.; Shan, X.; Wen, B.; Lin, J.; Owens, G. (2009): Stability of titania nanoparticles in soil suspensions and transport in saturated homogeneous soil columns, *Environmental Pollution*, 157(4), 1101-1109.
- Fang, J.; Shan, X.; Wen, B.; Lin, J.; Owens, G.; Zhou, S. (2011): Transport of copper as affected by titania nanoparticles in soil columns. *Environmental Pollution*, 159, 5, 1248-1256.



- Fjällborg, B; Dave, G. (2003): Toxicity of copper in sewage sludge. *Environment International*, 28, 761-769.
- Flores-Velez, L.M.; Ducaroir, J.; Jaunet, A.M.; Robert, M. (1996): Study of the distribution of copper in an acid sandy vineyard soil by three different methods. *European Journal of Soil Science.*, 47, 523-532.
- French, R.A.; Jacobson, A.R.; Kim, B.; Isley, S.L.; Penn, R.L.; Baveye, P.C. (2009): Influence of Ionic Strength, pH, and Cation Valence on Aggregation Kinetic of titanium Dioxide Nanoparticles. *Environmental Science & Technology*, 43, 1354-1359.
- Fuerstenau, D.W.; Manmohan, D.; Raghavan, S. (1981): Adsorption from Aqueous Solutions, Plenum Press, New York, 93-117
- Tewari, P.H. (Ed.). In v. d. Kammer, F.; Ottofuellin, S.; Hofmann, T. (2010): Assessment of the physico-chemical behavior of titanium dioxide nanoparticles in aquatic environments using multi-dimensional parameter testing. *Environmental Pollution*, 158, 3472-3481.
- Gottschalk, F.; Sonderer, T.; Scholz, R.W.; Nowack, B. (2009): Modeled Environmental Concentrations of Engineered Nanomaterials (TiO<sub>2</sub>, ZnO, Ag, CNT, Fullerenes) for Different Regions, *Environmental Science & Technology*, 43 (24), 9216-9222.
- Gottschalk, F.; Sonderer, T.; Scholz, R.W.; Nowack, B. (2009): Modeled Environmental Concentrations of Engineered Nanomaterials (TiO<sub>2</sub>, ZnO, Ag, CNT, Fullerenes) for Different Regions. *Environmental Science & Technology* 43 (24), 9216-9222.
- Guzman, K.A.D.; Finnegan, M.P.; Banfield, J.F. (2006): Influence of surface potential on aggregation and transport of titania nanoparticles. *Environmental Science & Technology*, 40(24), 7688-7693.
- Heidler, J.; Sapkota, A.; Halden, R.U. (2006): Partitioning, persistence, and accumulation in digested sludge of the topical antiseptic triclocarban during wastewater treatment. *Environmental Science & Technology* 40 (11), 3634-3639.
- Heidler, J.; Halden, R.U. (2009): Fate of organohalogenes in US wastewater treatment plants and estimated chemical releases to soils nationwide from biosolids recycling. *JEM Journal of Environmental Monitoring* 11 (12), 2207-2215.
- Hofmann, T. & von der Kammer, F. (2009): Estimating the relevance of engineered carbonaceous nanoparticle facilitated transport of hydrophobic organic contaminants in porous media, *Environmental Pollution*, 157, 1117-1126.
- Hunter, R. J.: Zeta potential in Colloid Sciences. Academic Press, London, 1988.
- Hyung, H.; Fortner, J. D.; Hughes, J. B.; Kim, J.H. (2007): Natural organic matter stabilizes carbon nanotubes in the aqueous phase. *Environmental Science & Technology*, 41(1), 179 - 184.
- ISO 22412:2008 Particle size analysis - Dynamic light scattering (DLS)”. Beuth-Verlag Berlin, 2008.
- James, Healy (1972): *J. Colloid Interface Sci.* 40 (1), 42-52 / 53-64 / 65-81.
- Johnson, S. B.; Scales, P. J.; Healy, T. W. (1999): The Binding of Monovalent Electrolyte Ions on alpha-Alumina. I. Electroacoustic Studies at High Electrolyte Concentrations. *Langmuir*, 15, 2836-2843. doi:10.1021/la980875f
- Kaegi, R.; Ulrich, A.; Sinnet, B.; Vonbank, R.; Wichser, A.; Zuleeg, S.; SimmLer, H.; Brunner, S.; Vonmont, H.; Burkhardt, M.; Boller, M. (2008): Synthetic TiO<sub>2</sub> nanoparticle emission from exterior facades into the aquatic environment. *Environmental Pollution*, 156, 233-239.
- Kaegi, R.; Sinnet, B.; Zuleeg, S.; Hagendorfer, H.; Mueller, E.; Vonbank, R.; Boller, M.; Burkhardt, M. (2010): Release of silver nanoparticles from outdoor facades. *Environmental Pollution*, doi:10.1016/j.envpol.2010.06.009

- Kiser, M. A.; Westerhof, P.; Benn, T.; Wang, Y.; Pérez-Rivera, J.; Hristovski, K. (2009): Titanium Nanomaterial Removal and Release from Wastewater Treatment Plants. *Environmental Science & Technology*, 43 (17), 6757 - 6763.
- Kosmulski, M. (2006): PH-dependent surface charging and points of zero charge. III. Update. *Journal of Colloid and Interface Science*, 298(2):730-741.
- Kosmulski, M. (2009): pH-dependent surface charging and points of zero charge. IV. Update and new approach, *Journal of Colloid and Interface Science*, 337, 439-448.
- Kwon, L-W.; Armbrust, K.L.; Xia, K. (2010): Transformation of Triclosan and Triclocarban in Soils and Biosolids-applied Soils. *Journal of Environmental Quality* 39 (4), 1139-1144.
- von der Kammer, F.; Ottofuellin, S.; Hofmann, T. (2010): Assessment of the physico-chemical behavior of titanium dioxide nanoparticles in aquatic environments using multi-dimensional parameter testing. *Environmental Pollution*, 158, 3472-3481.
- Koppel, D. E.(1972): Analysis of Macromolecular Polydispersity in Intensity Correlation Spectroscopy: The Method of Cumulants. *J. Chem. Phys.* 57 (11), 4814-4820.
- Korthals, G.W.; Alexiev, A.D.; Lexmond, T.M.; Kammenga, J.E.; Bongers, T. (1996): Long-term effects of copper and pH on the nematode community in an agroecosystem. *Environ Toxicol Chem*, 15, 979-985.
- Kuhlbusch, T.A.J.; Nickel, C.; Hellack, B., Gartiser, S.; Flach, F.; Schiwy, A.; Maes, H.; Schaeffer, A.; Erdinger, L.; Gabsch, S.; Stintz, M. (2012): Fate and behaviour of TiO<sub>2</sub> nanomaterials in the environment, influenced by their shape, size and surface area, *UBA Report 25/2012*, pp. 163.
- Labille, J.; Feng, J.; Botta, C.; Borschneck, D.; Sammut, M.; Cabie, M.; Auffan, M.; Rose, J.; Bottero, J.-Y. (2010): Aging of TiO<sub>2</sub> nanocomposites used in sunscreen. Dispersion and fate of the degradation products in aqueous environment. *Environmental Pollution*, 158: 3482-3489.
- Lawson, C. L.; Hanson, R.J. (1995): Solving least squares problems. In series: Classics in applied mathematics, Bd. 15. *Society for Industrial Mathematics*, Philadelphia.
- Lecoanet, H.F., Bottero, J.Y., Wiesner, M.R. (2004): Laboratory Assessment of the Mobility of Nanomaterials in Porous Media. *Environmental Science & Technology*, 38, 5164 - 5169.
- Lefèvre, G.; Duc, M.; Fedoroff, M. (2004): Effect of solubility on the determination of the protonable surface site density of oxyhydroxides. *Journal of Colloid and Interface Science*, 269(2), 274-282.  
doi: 10.1016/S0021-9797(03)00653-2
- Limbach, L.K.; Bereiter, R.; Müller, E.; Krebs, R.; Gälli, R.; Stark, W.J. (2008): Removal of Oxide Nanoparticles in a Model Wastewater Treatment Plant: Influence of Agglomeration and Surfactants on Cleaning Efficiency. *Environmental Science and Technology*, 42, 5828 - 5833.
- Lipovsky, A.; Levitski, L.; Tzitrinovich, Z.; Gedanken, A.; Lubart, R. (2012): The Different Behavior of Rutile and Anatase Nanoparticles in Forming Oxy Radicals Upon Illumination with Visible Light: An EPR Study, *Photochemistry and Photobiology*, 88(1): 14-20.
- Löfgren, S.; Zetterberg, T. (2011): Decreased DOC concentrations in soil water in forested areas in southern Sweden during 1987–2008. *Science of the Total Environment*, 409, 1916-1926.
- Mie, G. (1908): Beiträge zur Optik trüber Medien, speziell kolloidaler Goldlösungen, *Ann. Phys.* IV, 4(25), 77-445. doi:10.1002/andp.19083300302.
- Miller, T.R.; Colquhoun, D.R.; Halden, R.U. (2010): Identification of Wastewater Bacteria Involved in the Degradation of Triclocarban and its Non-Chlorinated Congener. *Journal of Hazardous Materials*.

- Nowack, B.; Bucheli, T.D. (2007): Occurrence, behaviour and effects of nanoparticles in the environment. *Environmental Pollution*, 150 (1), 5-22.
- O'Brien, R.W.; White, L.R. (1978): Electrophoretic Mobility of a Spherical Colloidal Particle. *J. Chem. Soc., Faraday Trans. 2*, 74 (9), 1607-1626, DOI: 10.1039/F29787401607
- Ottofülling, S.; von der Kammer, F.; Hofmann, T. (2011): Commercial Titanium Dioxide Nanoparticles in Both Natural and Synthetic Water: Comprehensive Multidimensional Testing and Prediction of Aggregation Behavior. *Environmental Science and Technology*, 45 (23), 10045-10052.
- Pan, B.; Xing, B.S. (2008): Adsorption Mechanisms of Organic Chemicals on Carbon Nanotubes. *Environmental Science & Technology* 42 (24), 9005-9013.
- Park, J-W.; Henry, T.B.; Ard, S.; Menn, F-M.M Compton, R.N.; Sayler, G.S. (2011): The association between nC(60) and 17 alphaethinylestradiol (EE2) decreases EE2 bioavailability in zebrafish and alters nanoaggregate characteristics. *Nanotoxicology*, 5 (3), 406-416.
- Papageorgiou, I.; Brown, C.; Schins, R.; Singh, S.; Newson, R.; Davis, S.; Fisher, J.; Ingham, E.; Case, C.P. (2007): The effect of nano- and micron-sized particles of cobalt chromium alloy on human fibroblasts in vitro. *Biomaterials* 28 (19), 2946-2958.
- Petrosa, A.R.; Jaisi, D.P.; Quevedo, I.R.; Emelimelech, M.; Tufebkji, N. (2010): Aggregation and deposition of engineered nanomaterials in aquatic environments: Role of physicochemical interaction. *Environmental Science and Technology*, 44, 6532-6549.
- Priester, J.H.; Ge, Y.; Mielke, R.E.; Horst, A.M.; Moritz, S.C.; Espinosa, K.; Gelb, J.; Walker, S.L.; Nisbe, R.M.; An, Y-J.; Schimel, J.P.; Palmer, R.G.; Hernandez-Viezca, J.A.; Zhao, L.; Gardea-Torresdey, J.L.; Holden, P.A. (2012): Soybean susceptibility to manufactured nanomaterials with evidence for food quality and soil fertility interruption, *PNAS*, August, 20; pp.6.  
<http://www.pnas.org/content/early/2012/08/14/1205431109>
- Provencher, S.W. (1982): CONTIN. A General Purpose Constrained Regularization Program for inverting noisy linear algebraic and integral Equations. *Comput. Phys. Commun.*, 27, 229-242.
- Roelofs, F. & Vogelsberger, W. (2006): Dissolution kinetics of nanodispersed  $\gamma$ -alumina in aqueous solution at different pH: Unusual kinetic size effect and formation of a new phase. *Journal of Colloid and Interface Science*, 303(2), 450-459.
- Roth, J.; Albrecht, V.; Nitschke, M.; Bellmann, C.; Simon, F.; Zschoche, S.; Michel, S.; Luhmann, C.; Grundke, K.; Voit, B. (2008): Surface Functionalization of Silicone Rubber for Permanent Adhesion Improvement, *Langmuir* 24, 12603-12611, in Kosmulski, M. (2009): pH-dependent surface charging and points of zero charge. IV. Update and new approach. *Journal of Colloid and Interface Science*, 337, 439-448.
- Rubio-Hernández, F.J.; Ayúcar-Rubio, M.F.; Velázquez-Navarro, J.F.; Galindo-Rosales, F.J. (2006): Intrinsic viscosity of SiO<sub>2</sub>, Al<sub>2</sub>O<sub>3</sub> and TiO<sub>2</sub> aqueous suspensions. *Journal of Colloid and Interface Science*, 298, 967-972.
- Sapkota, A.; Heidler, J.; Halden, R.U. (2007): Detection of triclocarban and two co-contaminating chlorocarbonylides in US aquatic environments using isotope dilution liquid chromatography tandem mass spectrometry. *Environmental research* 103,(1), 21-29.
- Scheffer, F. & Schachtschabel, P. (1992): Lehrbuch der Bodenkunde, *Spektrum Akademischer Verlag*, 13. Auflage, 593 S.
- Schwytzer, I.; Kaegi, R.; Sigg, L.; Magrez, A.; Nowack, B. (2011): Influence of the initial state of carbon nanotubes on their colloidal stability under natural conditions. *Environmental Pollution*, 159 (6), 1641-1648.

- Sharma, V.K. (2009): Aggregation and toxicity of titanium dioxide nanoparticles in aquatic environment - A Review. *Journal of Environmental Science and Health Part A*, 44, 1485–1495
- Shi, T; Schins, R.P.F.; Knaapen, A.M.; Kuhlbusch, T.; Pitz, M.; Heinrich, J.; Borm, P.J.A. (2003): Hydroxyl radical generation by electron paramagnetic resonance as a new method to monitor ambient particulate matter composition. *J. Environ. Monit*, 5, 1-8.
- Shin, Y.J.; Su, C.C.; Shen, Y.H. (2006): Dispersion of aqueous nano-sized alumina suspensions using cationic polyelectrolyte. *Materials Research Bulletin*, 41:1964-1971.
- Smoluchowski v., M. (1903) : Contribution à la théorie de l'endosmose électrique et de quelques phénomènes corrélatifs. *Bull. Int. Acad. Sci. Cracovie, Cl. Sci. Math. Nat.* 8, 182-200.
- Snyder, E.H.; O'Connor, G.A.; McAvoy, D.C. (2011): Toxicity and bioaccumulation of biosolids-borne triclocarban (TCC) in terrestrial organisms. *Chemosphere* 82 (3) :460-467.
- Solovitch, N. ; Labille, J. ; Rose, J. ; Chaurand, P. ; Borschneck, D. ; Wiesner, M. ; Bottero, J.Y. (2010): Concurrent Aggregation and Deposition of TiO<sub>2</sub> Nanoparticles in a Sandy Porous Media. *Environmental Science & Technology*, 44, 4897 - 4902.
- Sun, H.; Zhang, X.; Niu, Q.; Chen, Y.; Crittenden, J.C. (2007): Enhanced accumulation of arsenate in carp in the presence of titanium dioxide nanoparticles. *Water Air and Soil Pollution* 178 (1-4), 245-254.
- Sun, H.W.; Zhang, X.Z.; Zhang, Z.Y.; Chen, Y.S.; Crittenden, J.C. (2009): Influence of titanium dioxide nanoparticles on speciation and bioavailability of arsenite. *Environmental Pollution* 157, 1165-1170.
- TCC Consortium (2002): U.S. High Production Volume (HPV) Chemical Challenge Program. Robust Summary and Test Plan for Triclocarban, CAS 101-20-2. Prepared for the HPV Challenge Program by the TCC Consortium. December 27, 2002. *Received at Office of Pollution Prevention and Toxics*, 201-14186A.
- Wetzel, R. G. (1983): *Limnology* 2. Aufl.- Saunders Comp., Philadelphia. 763 pp. Zitiert in: H. Zimmermann-Timm: Versalzung von Gewässern. In: . Lozán, J. L. H. Graßl, P. Hupfer, L. Karbe & C.-D. Schönwiese (eds.): *WARNSIGNAL KLIMA: Genug Wasser für alle?*, 3rd ed., pp. 197-202. Climate Service Center Hamburg, 2011. [http://www.climate-service-center.de/012389/index\\_0012389.html](http://www.climate-service-center.de/012389/index_0012389.html)
- Woodrow Wilson Database (2012), available online, [http://www.nanotechproject.org/inventories/consumer/analysis\\_draft/](http://www.nanotechproject.org/inventories/consumer/analysis_draft/).
- Xu, R. (2000): Particle Characterization: Light Scattering Methods. In series: *Particle Technology Series*. Kluwer Academic Publishers, London.
- Ying, G-G.; Yu, X-Y.; Kookana, R.S. (2007): Biological degradation of triclocarban and triclosan in a soil under aerobic and anaerobic conditions and comparison with environmental fate modelling. *Environmental Pollution* 150 (3), 300-305.
- Zänker, H.; Richter, W.; Hüttig, G.; Nitsche, H.; Wiesener, W.; Mende, A. (1996): Charakterisierung der Sub-micron-Partikel in einem umweltrelevanten Wasser: Stauwasser in einer Kommunal Mülldeponie über einem Schlammteich (Tailing) der Uranerzaufbereitung in Freital/Sachsen. Forschungsbericht 155, Forschungszentrum Rossendorf e.V.
- Zhang, H.; Sun, H.; Zhang, Z.; Niu, Q.; Chen, Y.; Crittenden, J.C. (2007): Enhanced bioaccumulation of cadmium in carp in the presence of titanium dioxide Nanoparticles. *Chemosphere*, 67, 160-166.

## **Annex**

## Annex I Measurement techniques

### AI.1 Dynamic Light Scattering

#### Principle

Dynamic Light Scattering measures the fluctuation of light, which is scattered by a quiescent liquid dispersion. In the case of dispersions with small (colloidal) particles this fluctuation is due to on-going changes of the particle's positions by Brownian motion. For very low particle concentrations the signal fluctuation can be related to the effective diffusion coefficient  $D_{\text{eff}}$  of the particles or equivalently to the effective hydrodynamic diameter<sup>2</sup>  $x_{\text{h,eff}}$  (Xu 2000).

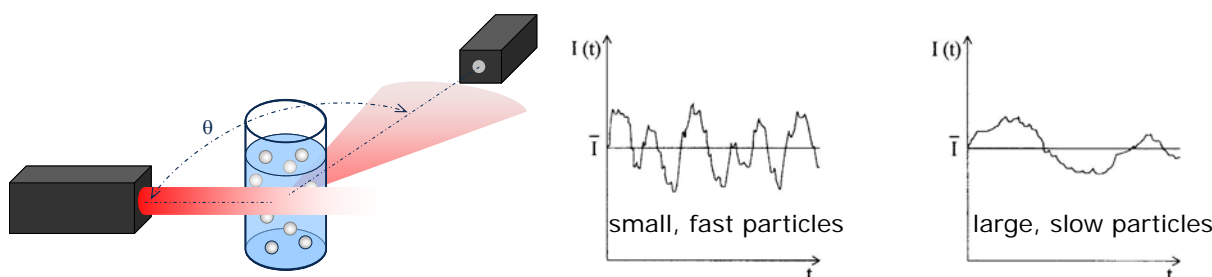


Figure 31: Dynamic light scattering: instrumental technique and time signals

The signal fluctuation is measured in the instruments and analysed via a frequency analysis or via a time-correlation function. The time-correlation function follows an exponential decay for monodisperse particle systems and can be expressed as the sum of exponential functions for polydisperse systems. Size distributions are obtained by inversion algorithms and are intrinsically weighted by the fractional scattering intensity.

#### Data interpretation

All data interpretation was done using the instrument software (DTS 4.20). It uses the measured data and analyses them in two ways: with *the method of cumulants* (Koppel 1972) and with an inversion algorithm. The former is a robust algorithm that yields a mean particle diameter ( $x_{\text{cum}}$  or z-average) and an index of polydispersity (PDI). The  $x_{\text{cum}}$  can be interpreted as the harmonic mean of the intensity weighted size distribution:

$$x_{\text{cum}}^{-1} = \int x_{\text{h,eff}}^{-1} dQ_{\text{int}} \quad (3)$$

while the polydispersity index is a normalised parameter for the variation of the effective hydrodynamic diameter:

$$PDI/x_{\text{cum}}^2 = \int (x_{\text{h,eff}}^{-1} - x_{\text{cum}}^{-1})^2 dQ_{\text{int}} = \int x_{\text{h,eff}}^{-2} dQ_{\text{int}} - x_{\text{cum}}^{-2} \quad (4)$$

<sup>2</sup> Even though the signal fluctuations in DLS measurements are mainly due to the particles translational motion, there is frequently a contribution from the particles Brownian rotation. Its significance rises with the particles asphericity and size as well as with the scattering angle. The effective hydrodynamic diameter of a particle therefore reflects its resistance to translation and to rotation (viscous drag and torque).

The method of cumulants yields average size distribution parameters only. In order to resolve the shape of an intensity weighted size distribution from the correlation functions an inversion algorithm is used. Even though the manufacturer does not reveal the details of the employed inversion algorithm it certainly contains a regularised procedure that smoothes the shape of the size distribution and impose a non-negative least square (NNLS) constraint (Lawson & Hanson 1995). A typical example of such a data analysis is the CONTIN algorithm proposed by Provencher (1982). Additionally the software requires a model for the optical properties of the diffusing particles in order to convert intensity to volume or number weighted size distributions. For this purpose Mie's solution of electromagnetic scattering on spheres is used (Mie 1908).

## **AI.2 Zeta potential**

### **Electric double layer and zeta potential**

When colloidal particles are dispersed in a liquid solvent it is very likely that they acquire a surface charge, which has to be compensated by a corresponding counter charge in the surface's vicinity. Both regions charged surface and counter-charged solvent, form the electric double layer (EDL). The charge separation between the two layers causes an electric potential between the particle surface and the bulk solvent, which is responsible for attractive or repulsive interactions between colloidal particles.

Important measurands for the characterisation of the EDL are the surface charge (density) and the electro-kinetic potential or zeta potential. The zeta potential is the electric potential at a hypothetical shear plane, which separates the mobile solvent from solvent molecules that adhere to the particle surface. The zeta potential can be probed by imposing a relative motion between bulk solvent and particle (Delgado et al. 2007).

Such a relative motion can be induced by external electric fields or by pressure gradients or bulk forces (e.g. gravity). It is possible that particles move in quiescent solvent or that the solvent flows through fixed bed of particles. A detailed description of electrokinetic phenomena is e.g. given by Hunter (1988). Zeta potential measurements on colloidal suspensions are frequently conducted via electrophoresis or by means of electroacoustics. Besides, there are recent techniques based on non-linear optics that are sensitive to interfacial changes.

### **Measurement of the zeta potential by electrophoresis**

If an electric field is applied to a suspension of charged colloidal particles the mobile ions within the double layer become spatially separated according to the sign of their charge (double layer polarisation) and the particles start to move along the lines of the electric field. This electrophoretic motion is characterised by the electrokinetic mobility  $\mu_{ek}$ :

$$\mu_{ek} = \frac{V_P}{E} \quad (5)$$

which is a function of the zeta potential  $\zeta$  and the Debye-Hückel-parameter  $\kappa$  (the inverse double layer thickness  $\kappa^{-1}$ ):

$$\mu_{ek} = \frac{2}{3} \cdot \frac{\varepsilon_r \varepsilon_0 \zeta}{\eta} \cdot f(\kappa a, \zeta) \quad (6)$$

$$\text{with } \kappa^2 = \frac{F^2}{\varepsilon_r \varepsilon_0 \cdot RT} \cdot \sum v_i^2 c_{n,i}^\infty \quad (7)$$

The double layer thickness is decisive for the retarding impact of double layer polarisation on the electrophoretic motion. Eq.6 yields simple linear relationships only for the two limiting cases of very thin double layers ( $\kappa a \rightarrow \infty$ ) and infinity thick ones ( $\kappa a \rightarrow 0$ ). The correction function  $f(\kappa a)$  then simplify to a constant value of 3/2 and 1, respectively (Smoluchowski 1903, O'Brien & White 1978).

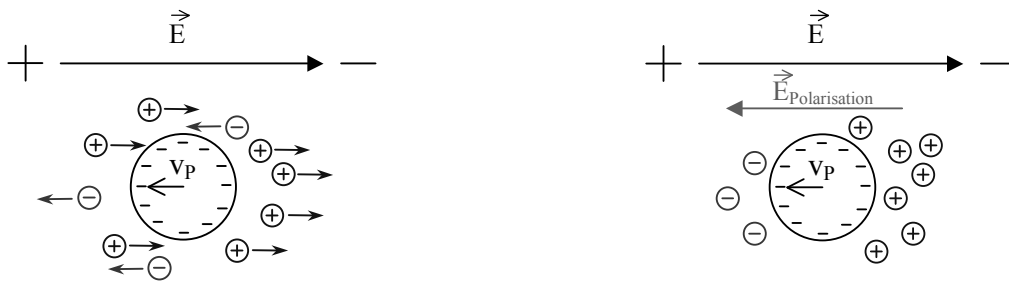


Figure 32: electrophoresis and double layer polarisation

### Instrumentation

The electrophoretic motion is either measured microscopically or by light scattering. The former way is called microelectrophoresis ( $\mu$ EP) and usually employs ultramicroscopes when dealing with colloidal particle systems. The optical instrumentation can be identical to that of dynamic ultramicroscopy (DUM), while the software has to be modified because only the displacement in the direction of the electric field is relevant. The methods yield a number weighted distribution of zeta potentials. Similar to DUM a sufficient number of trajectories has to be evaluated in order to keep the statistical uncertainty within an acceptable level. Moreover the method may be insensitive to weak scatterers within a polydisperse colloidal suspension.

An instrumental alternative to microelectrophoresis is the Electrophoretic Light Scattering (ELS). The light scattering at migrating particles leads to phase shift (Doppler effect), which can be detected by a reference-beating (superheterodyne) DLS set-up. The method yields an intensity weighted distribution of the zeta potential.



The electrophoretic motion of colloidal particles is superposed by their Brownian motion. Ideally, both can be separated because of their different space-time-correlation. In praxis, however, diffusion leads to broadening of the zeta potential distribution. In microelectrophoresis the Brownian contribution can be minimised by long observation times ( $t \gg D_t/v_p^2$ ). For ELS it becomes less pronounced at small scattering angles (Xu 2000, pp. 323).

## **Annex II - Standard operation procedure - SOPs**

### **All.1 Standard operation procedure - Preparing titanium dioxide (stock) suspension**

Date: 16th July 2012

Version: 1.0 english

Scope

Purpose

References

Requirements for the suspension stability

Instrument specification

Sample preparation

Data Evaluation / Reporting

Occupational safety

Waste disposal

Purpose

The aim of this Standard Operating Procedure is the preparation of a stable nanoscale TiO<sub>2</sub> suspension for environmental testing. The actual procedure based on an established SOP from a previous study (Kuhlbusch et al., 2012). This SOP affords reproducible results in different laboratories (comprehensible proceedings) and describes the proceedings which are suitable for preparing a stable TiO<sub>2</sub> nanomaterial suspension.

References

Kuhlbusch et al. 2012: "Fate and behaviour of TiO<sub>2</sub> nanomaterials in the environment, influenced by their shape, size and surface area". Hrsg.: Umweltbundesamt, Report 25/2012, FKZ 3710 65 417, UBA-FB 001577, ISSN 1862-4804,

## Requirements for the suspension stability

### Suspension Requirements

- The suspension must be stable at least for 24 h (a variance of 10% is accepted).
- An appropriate stability of a suspension is declared as a constant particle size distribution and / or zeta potential.

### Stability criteria

- Optical observation (no visible sedimentation of the particles).
- Size of the particles in the suspension.
- Zeta potential.
- Particle concentration.
- PH value of the suspension.
- Conductance of the suspension.

## Instrument specification

### Necessary instruments

- Sensitive analytic balance.
- Ultrasonic homogeniser with sufficient rated power (min. 200 Watt – e.g. Sonoplus HD 2200 from Bandelin GmbH & Co. KG and UDS 751 from Topas GmbH)
- Sensitive instrument detecting the particle size distribution and the zeta potential in aqueous media (e.g. dynamic light scattering instrument - Delsa-Nano C from Beckman Coulter and HPPS from Malvern Instruments)

### Necessary materials

- Tested nanomaterial
- Deionised water

### Sample preparation

- Weigh a defined amount of the nanomaterial (e.g. 50 mg of the solid material) in a 100 mL beaker glass, a variance of 1% is accepted.
- After this add deionised water (e.g. 50 ml) with pH 5.0 (variance of 10%) carefully to the material.
- Wait until the nanomaterial has become wetted and is completely submerged in the liquid phase, 10 min.
- Afterwards homogenise the suspension by continuously, moderate agitation with an overhead or magnetic stirrer by around 350 rpm for at least 15 minutes.

- Disperse the nanomaterial suspension with an ultrasonic homogeniser with 200 W power for at least 1 minute (here 1 min for surface characterisation and 10 min for analysis of the carrier function).
- The probe of the ultrasonic homogeniser should be dipped into the suspension and placed in the middle of the beaker glass with a distance between probe and bottom of the beaker glass of approximately 1 cm.
- During the sonication the beaker glass with the suspension can put in a bigger container with cold/ice water to minimize the heating of the suspension during the sonication.
- After use the probe will be cleaned with ethanol and afterwards with deionised water.
- Sonication is followed by at least 60 min of moderate stirring (overhead stirrer 350 rpm or magnetic stirrer).
- Every stock suspension was characterised to its size distribution – using a DLS instrument.

\* the sonication time must be adapted to the volume of the prepared suspension, diameter of the beaker glass, the concentration of the nanomaterials and the rated power of the ultrasonic instrument.

#### Data Evaluation / Reporting

The particle size distribution as well as the zeta potential of the TiO<sub>2</sub> suspensions was measured as stability criteria. The results were presented as harmonic means of the intensity weighted size distribution (z-average) and as measured the zeta potential. The measurement precision of the size measurements was proofed with PSL standard solutions of 20 nm ± 1 nm (Nanosphere NIST size standard) and 182 nm ± 5 nm (BS particle GmbH) as well as aluminium oxide solution for the zeta potential +50 mV ± 5 mV (Microtrac Reference material).

#### Occupational safety

Every measurement campaign must be conducted based on a risk assessment and the requirements of occupational safety regulations. When handling the nanomaterials, protective clothing and suitable gloves have to be worn at any time and the working area as well as the used materials and instruments have to be labeled. Furthermore, the laboratory regulations regarding these materials have to be followed. A fume hood has to be used whenever possible.

#### Waste disposal

Nanomaterial containing waste has to be collected and disposed of separately. It has to be differentiated between the kind of nanomaterial.

Title: Suspension preparation P25 nanomaterial	
This SOP is valid from: 16.07.2012 Version: First Version	
Responsible person of the implementation of the SOP: user  Pervious changes: first version  Information for: user safety administrator laboratory and division manager	
	date/signature
Author:	_____ Carmen Nickel
counterchecked:	_____ Dr. Frank Babick
Approved:	_____ Dr. rer. nat. T. Kuhlbusch

## All.2 Standard operation procedure - Particle size and zeta potential measurements by using Dynamic Light Scattering (DLS)

Standard operation procedure – Particle size and zeta potential measurements by using Dynamic Light Scattering (DLS)

Date: 16th July 2012

Version: 1.0 english

Scope

Purpose

Instrument specification

Measuring procedure

Data Evaluation / Reporting

Quality control

Occupational safety

Waste disposal

Purpose

The aim of this Standard Operating Procedure is intended to provide information about the size and zeta potential measurement of TiO<sub>2</sub> suspension for environmental testing and to enable reproducible results in different laboratories.

The SOP describes the procedures which are suitable for particle size and zeta potential measurements by Dynamic light scattering (DLS).

DLS is a technique to determine the size distribution profile of small particles in suspension. Performing a dynamic light scattering in aqueous media requires the knowledge of the refractive index of the particle and the particle's absorption. Furthermore the knowledge about the characteristics of the medium is necessary.

Instrument specification

Necessary instruments

- Dynamic light scattering instrument
- Liquid handling apparatus

## Used instruments

In this project dynamic light scattering instruments (HPPS, Malvern, England, Delsa-Nano C - Beckman Coulter, Krefeld, Germany) were used to measure particle size and zeta potential of coated and uncoated TiO<sub>2</sub> in an aqueous suspension.

## Measuring procedure

### **Size measurement by Dynamic Light Scattering (DLS)**

DLS is a technique to determine the size distribution profile of small particles in suspension. Performing a DLS in aqueous media requires the knowledge about the characteristics of the medium.

### **Zeta potential measurement by Electrophoretic light Scattering (ELS)**

The zeta potential can be used to assess the charge stability of a disperse system. The zeta potential is the force that controls the charge interactions in a suspension. It can be measured by applying an electric field across the dispersion. The zeta potential correlates with the magnitude of particle's migration velocity towards the electrode of the opposite charge. This can be measured with laser Doppler anemometry. With the knowledge of the dispersant viscosity and the use of Smoluchowski or Huckel theories the zeta potential can be calculated.

Preliminary results show that larger particles in the suspension have a higher impact on the size measurement than smaller particles. Hence large particles are over represented in the size measurement. The obtained results can be presented as intensities, number and volume concentrations of the particles. However the intensity data is the basic information obtained from the measurements, is least influence by assumptions and hence should be used. The cumulate analysis gives two values, the mean size of the particles ( $x_{cum}$  or z-average) and a polydispersity index (PDI). For measurement result comparisons z-average value of the diameter should preferably be used

To gain reproducible measurements the dynamic light scattering measurements were standardised in this project. All chemical properties were shared between the project partners. For Malvern products a software internal SOP was generated for the measurement. The suspensions were sampled according to the recommendations of the DLS instruments manufacturers. Suspensions were sampled from the upper water column with a pipette without homogenisation.

Malvern Instruments: Size measurement

Create a new SOP for measuring a TiO<sub>2</sub> suspension

Sample:

Material:

Name: TiO<sub>2</sub>

RI: 2.7

Absorption: 0.01

Dispersant

Dispersant: Water

Temperature: 25 °C

Viscosity: 0.8872

RI: 1.33

General Options

Sample viscosity options: use dispersant viscosity as sample

Temperature

Temperature: 25 °C

Equilibration time: 15 min

Cell

Cell type: Disposable sizing cuvette

Measurement

Measurement angle: 173 Backscatter

Measurement duration: 1\*60 sec

Measurement:

Number of Measurements: min 3 (recommended 10)

Delay between measurements: 2 sec

Advanced

Measurement duration

Extend duration for large particles: No

Measurement setting:

Positioning method: fixed position

Automatic attenuation selection: Yes

Data processing

Analysis model: General purpose



DELSA-NANO C - Beckmann Coulter

Measurement Parameter

General Conditions

File Save:	Auto
Repetition:	3 (recommended 10)
Manuel Temperature Setting:	No
Auto Print:	Manuel
Equilibrating:	Yes
Statistical Summary	Yes
Equilibration:	15 min
Waiting time:	2 sec

Size Measurements

Dust Limit	5
Upper Dust Limit	10
Lower dust Limit	100
Minimum Intensity	3000
Pinhole (µm)	50

Analysis Parameter

General

Analysis method:	CONTIN
Side cut left	0
Side cut right	0

Display

Graph x Axis:	Manual 4000 nm
Graph Y Axis	AUTO

Others

Fitting range	G2( $\tau$ )
G2( $\tau$ )max	2
G2( $\tau$ )min	1.003
Noise cut level (%)	0.3

Molecular wight Analisys Const

Molecular weight	NO
------------------	----

Cell Parameter

General

Measurement item	Size
Measurement type	Type 2
Cell name	Disposable Cuvette

Details

Correlation type	Log
Size Measurements	
Accumulation Time	70
Diluent properties	
General	
Diluent name	Water
- Properties	
RI	1.33
Viscosity	0.89
Dielectrical constant	78.3

#### Data Evaluation / Reporting

Test report according to ISO 22412:2008

The test report shall contain at least the following information:

- a) Average particle size,  $x_{cum}$  being the mean and standard deviation of at least three repeated measurements\*
- b) The PDI, being the mean and standard deviation of at least three repeated measurements
- c) If the mean values of  $x_{cum}$  and PDI are concentration dependent, this values extrapolated to infinite dilution or the value obtained at the lowest concentration
- d) All the information required for the complete identification of the sample, including details of particle shape and homogeneity
- e) The sampling method used, if known
- f) The test method used, together with reference to this International Standard
- g) The instrument type and number
- h) The dispersion conditions
  - 1) Dispersing liquid and its cleaning procedure
  - 2) Concentration of particulate material
  - 3) Dispersing agents and their concentration
  - 4) Dispersing procedure
  - 5) Sonication conditions: frequency and applied power (if necessary)
- i) The measurement conditions
  - 1) actual concentration investigated
  - 2) viscosity and refractive index of the dispersion liquid
  - 3) temperature of the sample
- j) analyst identification
  - 1) name and place of laboratory
  - 2) operator's name and initials
  - 3) date

- k) All operation details not specified in this International Standard, or regarded as optional, together with details of any incident that may have influenced the result(s).

\* ISO 13321:1996 specifies six repeated measurements. Experience with the method specified in this International Standard indicates that three measurements are sufficient.

#### Quality control

The results were presented as intensity weighted z-average in nm and the zeta potential in mV. The measurement precision of the size measurements was proofed with PSL standard solutions of 20 nm ± 1 nm (Nanosphere NIST size standard) and 182 nm ± 5 nm (BS particle GmbH) as well as aluminium oxide solution for the zeta potential +50 mV ± 5 mV (Microtrac Reference material).

#### Occupational safety

Every measurement campaign must be conducted based on a risk assessment and the requirements of occupational safety regulations. When handling the nanomaterials, protective clothing and suitable gloves have to be worn at any time and the working area as well as the used materials and instruments have to be labeled. Furthermore, the laboratory regulations regarding these materials have to be followed.

#### Waste disposal

Nanomaterial containing waste has to be collected and disposed of separately. It has to be differentiated between the kind of nanomaterial.

Title: Dynamic light scattering (DLS) and zeta potential measurements	
This SOP is valid from: 16.07.2012	
Version: First Version	
Responsible person of the implementation of the SOP: user	
Pervious changes: first version	
Information for:	user safety administrator laboratory and division manager
	date/signature
Author:	_____ Carmen Nickel
counterchecked:	_____ Dr. Frank Babick
Approved:	_____ Dr. rer. nat. T. Kuhlbusch

### All.3 Standard operation procedure - zeta potential measurements using microelectrophoresis ( $\mu$ EP)

Date: 16th July 2012

Version: 1.0 english

Scope

Purpose

Instrument specification

Measuring procedure

Occupational safety

Waste disposal

Purpose

The aim of this Standard Operating Procedure is intended to provide information about the zeta potential measurement of coated titanium dioxides for analysis of the surface characteristic and the behaviour of them in the environment. The SOP describes the procedures which are suitable for zeta potential measurements in a micro-electrophoresis cell.

Instrument specification

Necessary Instruments

- Laser Electrophoresis Video Microscope
- Liquid handling apparatus

Used instruments

In this project the Laser Electrophoresis Video Microscope ZetaView PMX100 from Particle Metrix GmbH was used to monitor the movement of particles (here coated and uncoated TiO<sub>2</sub>) in an electrophoresis cell.

## Zeta potential measurement by Microelectrophoresis ( $\mu$ EP)

### Measuring procedure

- Preparing stock suspension according to SOP – Preparing Titanium dioxide (stock) suspension (see Annex AII.1).
- After having been dispersed the stock suspension remains at rest for at least 24 hours in order to give the interface time for equilibration.
- Dilute suspension to final measurement concentration (here 2 ppmw) with deionised water or respective solution, afterwards adjust the pH value by adding acid or base. The suspensions should be prepared from the stock suspension while stirring.
- Before first characterisation, the diluted samples will be stirred and homogenised for at least one minute.
- For measurement inject the sample free from bubbles in the electrophoresis cell.
- The surface characteristic of the samples were analysed directly, 30 min, 60 min and 24 hours after dilution. During the first hour the pH was constantly monitored and adjusted, if required.
- After each measurement clean directly the electrophoresis cell with deionised water.

### Occupational safety

Every measurement campaign must be conducted based on a risk assessment and the requirements of occupational safety regulations. When handling the nanomaterials, protective clothing and suitable gloves have to be worn at any time and the working area as well as the used materials and instruments have to be labeled. Furthermore, the laboratory regulations regarding these materials have to be followed.

### Waste disposal

Nanomaterial containing waste has to be collected and disposed of separately. It has to be differentiated between the kinds of nanomaterial.

Title: Dynamic light scattering (DLS) and zeta potential measurements using micro-electrophoresis	
This SOP is valid from: 16.07.2012	
Version: First Version	
Responsible person of the implementation of the SOP: user	
Pervious changes: first version	
Information for:	user safety administrator laboratory and division manager
	date/signature
Author:	_____ André Nogowski
counterchecked:	_____ Dr. Frank Babick
Approved:	_____ Dr. rer. nat. T. Kuhlbusch

## All.4 Standard operation procedure - Liquid chromatography measurements

Date: 16th July 2012

Version: 1.0 english

Scope

Purpose

Instrument specification

Sample preparation

Data Evaluation / Reporting

Quality control measures

Potential error sources when conducting measurements

Occupational safety

Purpose

The standard work specification must be applied for chemical measurements using liquid chromatography mass spectrometry (LC-MS) of liquid samples and the quantification of glycerol concentration in liquid samples. This method was developed, adapted to the requirements of this study, verified and realized by S. Wiese, T. Teutenberg and J. Türk.

Instrument specification

For LC-MS measurements, a Shimadzu Prominence HPLC system which consists of a CBM-20A controller, a DGU-20A3 degasser, two LC-20AD pumps, an SIL-20AC auto sampler, and a CTO-20A column oven (Shimadzu, Duisburg, Germany) was coupled to a tandem mass spectrometer (3200 QTrap, AB Sciex, Darmstadt, Germany). Data acquisition and analysis were performed with Analyst Software version 1.5.2. The chromatographic separation was done on a Phenomenex Luna Amino column (150 × 2.0 mm, 3 μm) at 35°C. The mobile phase consisted of 20/80 (v/v) water/acetonitrile with 40 μmol/L cesium acetate as cationizing agent. The flow rate and the injection volume were set to 0.2 mL/min and 10 μL, respectively.

Quantification was carried out in Multiple Reaction Monitoring (MRM) mode utilising positive electrospray ionization (ESI) The ion source temperature was 50°C and ion spray voltage 5500 V. Nitrogen was used as curtain (45 psi), nebulizer (45 psi), and collision gas (medium). The dwell time was set to 200 ms. The optimized MRM parameters are depicted in Table 14.



Table 14: MRM parameter settings for glycerol.

Parameter	Value
MRM transition (Q1/Q3) <sup>a</sup> (m/z)	225 → 133
Declustering potential (DP) in V	11.0
Entrance potential (EP) in V	4.5
Collision cell entrance potential (CEP) in V	4.0
Collision energy (CE) in V	21.0
Collision cell exit potential (CXP) in V	4.0

<sup>a</sup> Q1: Precursor ion; Q3: Fragment ion.

### Sample preparation

The stability of the glycerol layer was examined for three different dispersion procedures:

- 1 min sonication followed by 1 hour of moderate stirring (see specified SOP),
- 1 minute (of magnetic) stirring after suspending the powder,
- No mechanical agitation after suspending the powder.

The released glycerol concentration was measured in the supernatant of the prepared suspensions. Therefore, after suspension preparation, the suspension was centrifuged (2700 G for 10 min) and the supernatant was afterwards filtered using a 0.22 µm nylon filter (Magna-Nylon, Roth) to separate the solid from the liquid phase. The glycerol concentration was measured in the filtrate of the suspension.

### Data Evaluation / Reporting

Measurement preparation and implementation as well as the data evaluation of the measurements must be documented.

### Quality assurance

- Comparison and (if necessary) adjustment of the instruments in the laboratory before each measurement campaign
- Reference material for the examination of the digestion method, chemical analysis and limit of detection of the applied technique
- Reference materials

The measurements were performed in triplicate for the LC-MS. In order to quantify the glycerol concentration within the samples at first a calibration curve (linear regression) was constructed. For this approach, 13 standard solutions were prepared to comprise a concentration range from 100 µg/L to 3000 µg/L glycerol. The resulting calibration curve is shown in Figure 33.

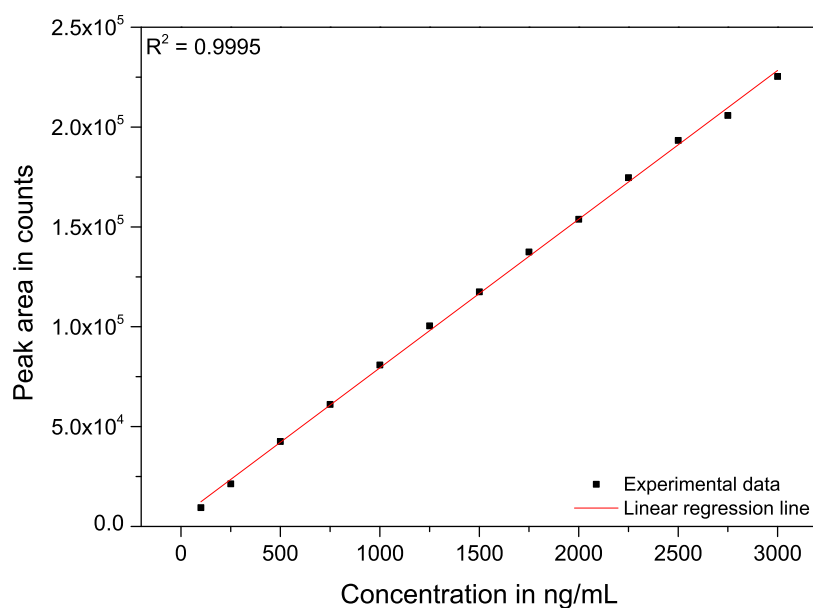


Figure 33: Calibration curve for quantitative estimation of glycerol within aqueous solutions.

The limit of detection of the LC-MS/MS method was 200 µg/L, it was calculated by using the calibration curve method according to DIN 32645.

#### Potential error sources when conducting measurements

- Re-adsorption of the previously released glycerol material.
- Loss of the material at the test vessels.

#### Occupational safety

Every measurement campaign must be conducted based on a risk assessment and the requirements of occupational safety regulations. This includes in particular the regulation of responsibilities and of the interfaces to occupational safety and health on the premises where the measurements shall be conducted. When handling the nanomaterials, protective clothing and suitable gloves have to be worn at any time and the working area as well as the used materials and instruments have to be labeled. Furthermore, the laboratory regulations regarding these materials have to be followed.

Title: LC MS measurements	
This SOP is valid from: 16.07.2012	
Version: First Version	
Responsible person of the implementation of the SOP: user	
Pervious changes: first version	
Information for:	user safety administrator laboratory and division manager
	date/signature
Author:	----- Carmen Nickel
counterchecked:	----- Dr. Steffen Wiese
Approved:	----- Dr. rer. nat. T. Kuhlbusch

## All.5 Standard operation procedure - enzymatic UV Tests

Date: 16th July 2012

Version: 1.0 english

Scope

Purpose

Test and instrument specification

Sample preparation

Data Evaluation / Reporting

Quality control measures

Potential error sources when conducting measurements

Occupational safety

Purpose

The standard work specification must be applied for chemical measurements using an enzymatic UV test for the quantification of the glycerol concentration in liquid samples. This method was developed, adapted to the requirements of this study, verified and realized by S. Wiese, T. Teutenberg and J.Türk.

Test and instrument specification

For this method a commercially available assay (R-BIOPHARM, Darmstadt, Germany) has been employed and the determination of glycerol takes place indirectly. First, glycerol is phosphorylated by means of adenosine-5'-triphosphate to L-glycerol-3-phosphate and adenosine-5'-diphosphate, a reaction which is catalyzed by glycerokinase. Afterwards, the formed adenosine-5'-diphosphate is reconverted into ATP and pyruvate by phosphoenolpyruvate. Here, the reaction was catalyzed by pyruvate kinase. Finally, in the presence of the enzyme L-lactate dehydrogenase, the formed pyruvate is reduced to L-lactate by reduced nicotinamide-adenine dinucleotide (NADH) which concurrently is oxidized to NAD. Moreover, the consumption of NADH is stoichiometric to the amount of glycerol and has been detected by means of its UV absorption at a wavelength of 340 nm using a Specord 200 UV/VIS spectrometer (spectrometer (Analytik Jena, Jena, Germany). The detected amount of the NADH was employed for the calculation of the glycerol concentration.

According to the following equation:

$$c = \frac{V \times M}{\varepsilon \times d \times v \times 1000} \times \Delta E$$

Here,  $c$  is the concentration of glycerol in g/L,  $V$  is the total test volume,  $M$  is the molar mass of glycerol,  $\varepsilon$  is molar extinction coefficient of NADH at a wavelength of 340 nm,  $d$  is the thickness of the cuvette,  $v$  is the sample volume, and  $\Delta E$  is the extinction difference between blank and sample. Except for the measured  $\Delta E$  values, all parameters of Equation 1 were held constant throughout our measurements (see Table 15).

Table 15: Overview of parameters/values required to calculate the concentration of glycerol.

Parameter	Value
$V$ in mL	3.02
$M$ in g/mol	92.1
$\varepsilon$ at 340 nm	6.3
$d$ in cm	1.0
$v$ in mL	2.0

According to the manufacturer, the limit of detection (LOD) of the enzymatic UV test is 400 µg/L glycerol.

#### Sample preparation

The stability of the glycerol layer was examined for three different dispersion procedures:

- 1 min sonication followed by 1 hour of moderate stirring see specified SOP ,
- 1 minute (of magnetic) stirring after suspending the powder
- no mechanical agitation after suspending the powder

The released glycerol concentration was measured in the supernatant of the prepared suspensions. Therefore after suspension preparation, the suspension was centrifuged (2700G for 10 min ) and the supernatant was afterwards filtered using a 0.22 µm nylon filter (Magna-Nylon, Roth) to differentiate between solid and liquid phase. The glycerol concentration was measured in the filtrate of the suspension.

#### Data Evaluation / Reporting

Measurement preparation and implementation as well as the data evaluation of the measurements must be documented.

#### Quality control measures

- Comparison and (if necessary) adjustment of the instruments in the laboratory before each measurement campaign
- Reference material for the examination of the digestion method, chemical analysis and limit of detection of the applied technique
- Reference materials

- Calibration

Potential error sources when conducting measurements

- Re-adsorption of the previously desorbed material.
- Loss of the material at the test vessels.

Occupational safety

Every measurement campaign must be conducted based on a risk assessment and the requirements of occupational safety regulations. This includes in particular the regulation of responsibilities and of the interfaces to occupational safety and health on the premises where the measurements shall be conducted. When handling the nanomaterials, protective clothing and suitable gloves have to be worn at any time and the working area as well as the used materials and instruments have to be labeled. Furthermore, the laboratory regulations regarding these materials have to be followed.

Title: Enzymatic UV tests	
This SOP is valid from: 16.07.2012	
Version: First Version	
Responsible person of the implementation of the SOP: user	
Pervious changes: first version	
Information for:	user safety administrator laboratory and division manager
	date/signature
Author:	_____ Carmen Nickel
counterchecked:	_____ Dr. Steffen Wiese
Approved:	_____ Dr. rer. nat. T. Kuhlbusch

## All.6 Standard operation procedure - radioanalytics

Date: 16th July 2012

Version: 1.0 english

Scope

Purpose

Test and instrument specification

Sample preparation

Data Evaluation / Reporting

Quality control measures

Potential error sources when conducting measurements

Occupational safety

Purpose

The standard operation procedure was applied to measure the amount of radioactivity in soil and eluate samples derived from <sup>14</sup>C labelled triclocarban (<sup>14</sup>C-TCC) leaching experiments. The solid material was combusted in a biological oxidizer to transform <sup>14</sup>C-atoms of TCC into <sup>14</sup>CO<sub>2</sub> that was trapped in a scintillation cocktail. Liquid samples were directly mixed with such cocktail. Both samples from combustion and liquid samples mixed with cocktail were subjected to liquid scintillation counting (LSC).

Instrument specification

Biological oxidizer: OX500; RJ Harvey Instruments Corporation, USA

Liquid scintillation counter: LS 5000G TD, Beckman Instruments GmbH, Germany

Sample preparation

Liquide samples:

To all samples larger than 7 mL, an equal volume of chloroform was added for liquid extraction. The organic phase was then separated from the water phase, concentrated by means of a rotary evaporator to a volume of less than 7 mL, and transferred to 20 mL polyethylene vials. After adding 13 mL of scintillation cocktail (LumaSafe Plus<sup>TM</sup>, Perkin Elmer, Germany), the number of disintegrations per minute (dpm) of radioactive atoms was determined in the liquid scintillation counter (LSC; LS 5000G TD, Beckman Instruments GmbH, Germany), recalculated to the number of disintegrations per second (dps or Bq) or the mass of the compound (specific radioactivity: 3.5 MBq/mg <sup>14</sup>C-TCC).



### Solid samples

From the core and the border sample, three subsamples of about 300 mg were taken, dried in an oven, weighed, and were combusted in a biological oxidizer (OX500; RJ Harvey Instruments Corporation, USA). The <sup>14</sup>CO<sub>2</sub> produced during oxidizing was trapped in a scintillation vial containing 15 mL of scintillation cocktail (Oxysolve C-400; Zinsser Analytic GmbH, Germany) that was subsequently subjected to LSC. The recovery of this process was determined by comparing the known radioactivity of 10 µL of a standard solution (SV) with the radioactivity measured after combusting paper cones filled with cellulose spiked with 10 µL of this standard (CV). The amount of radioactivity in samples was then calculated by subtracting blank values (BV), obtained by combusting clear cellulose, from the measured values (MV), and multiplying the result by the combustion factor, i.e.  $(SV - BV)/(CV - BV)$ , to correct for losses during the combustion process. BV, CV and SV are the mean values of at least three replicates.

### Data Evaluation / Reporting

Measurement preparation and implementation as well as the data evaluation of the measurements must be documented in a laboratory book.

### Quality control measures

- A reference material for calibrating the oxidiser is available and the combustion factor of this substance is determined in the same way as described above to evaluate the recovery.
- Calibration of the LSC is also performed by measuring a concentration series of a reference material to check the accuracy of the instrument. The instruments lower limit of detection amounts to 60 dpm or 1 Bq.

### Potential error sources when conducting measurements

Chemiluminescent compounds, e.g. in eluate samples originating from the soil column, can disturb LSC measurements. This can generally be avoided by allowing the cocktail and the sample to react overnight in the dark at 4°C. Incomplete combustion in the oxidiser or incomplete trapping of generated CO<sub>2</sub> can occur if solid samples are too large.

### Occupational safety

Every measurement campaign must be conducted based on a risk assessment and the requirements of occupational safety regulations. This includes in particular the regulation of responsibilities and of the interfaces to occupational safety and health on the premises where the measurements shall be conducted. When handling the nanomaterials, protective clothing and suitable gloves have to be worn at any time and the working area as well as the used materials and instruments have to be labeled. Furthermore, the laboratory regulations regarding these materials have to be followed.

Title: Radioanalytics	
This SOP is valid from: 16.07.2012	
Version: First Version	
Responsible person of the implementation of the SOP: user	
Pervious changes: first version	
Information for:	user safety administrator laboratory and division manager
	date/signature
Author:	_____ Dr. Hanna Maes
counterchecked:	_____ Carmen Nickel
Approved:	_____ Dr. rer. nat. T. Kuhlbusch

## **All.7 Standard operation procedure - inductively coupled plasma optical emission spectrometry (ICP-OES)**

### **All.7.1 Standard operation procedure (SOP) - ICP-OES measurements of applied substances in natural soils**

Date: 16th July 2012

Version: 1.0 english

Scope

Purpose

References

Instrument specification

Necessary materials

Digestion method

Data Evaluation / Reporting

Quality control measures

Potential error sources when conducting measurements

Occupational safety

Purpose

The standard work specification must be applied for chemical measurements using Inductively coupled plasma optic emission spectrometry (ICP-OES) of applied substances, here copper and titanium, in natural soil samples.

References

Kuhlbusch et al. 2012: "Fate and behaviour of TiO<sub>2</sub> nanomaterials in the environment, influenced by their shape, size and surface area". Hrsg.: Umweltbundesamt, Report 25/2012, FKZ 3710 65 417, UBA-FB 001577, ISSN 1862-4804,

### Instrument specification



Manufacturer: Thermo Scientific

Version: ICAP6000 series

### Necessary materials

- HF (95%)
- HNO<sub>3</sub> (65%)
- Deionised water
- Reference materials SRM 2709a “San Joaquin Soil” and BCR 196

### Digestion method

An exact amount of sediment (about 150 mg) is placed in a volumetric flask. 5 mL HF (95%, Roth supra, Ti < 1 ppb) and 8 mL HNO<sub>3</sub> (65%) were added and filled up to 25 mL with ultra pure water. The reaction vessel is placed in an automated micro-wave digestion apparatus (MLS Ethos plus) and digested by heating up to 218°C within 30 min and holding the temperature for 30 min. Samples are allowed to cool to room temperature and are filled up to a defined volume. Samples are centrifuged at 4000 rpm for 20 min, and supernatant is passed through a 0.45 µm membrane filter.

### Data Evaluation / Reporting

Measurement preparation and implementation as well as the data evaluation of the measurements must be documented in a test report.

### Quality control measures

- The homogeneity of variance was verified according to DIN 38402, part 51.
- Comparison and (if necessary) adjustment of the instruments in the laboratory before each measurement campaign
- Reference material for the examination of the digestion method, chemical analysis and limit of detection of the applied technique was verified according to DIN EN ISO 11885.

- Reference materials for the purposes of this project, SRM 2709a “San Joaquin Soil” and BCR 196 were purchased. This reference material was selected because it contains a certified value for titanium (3360 mg/kg and 2700 mg/kg) and copper (33.9 mg/kg and 69.7 mg/kg).

According to the calibration, the limit of detection (LOD) of this digestion method is around 0.12 µg/L for titanium and 0.41 µg/L for copper.

#### Potential error sources when conducting measurements

- Digestion method → incomplete digestion of minerals → different concentrations
- In any case a detailed record of measurements must be kept in which all possible disturbances are noted with time stamps.

#### Occupational safety

Every measurement campaign must be conducted based on a risk assessment and the requirements of occupational safety regulations. This includes in particular the regulation of responsibilities and of the interfaces to occupational safety and health on the premises where the measurements shall be conducted. When handling the nanomaterials, protective clothing and suitable gloves have to be worn at any time and the working area as well as the used materials and instruments have to be labeled. Furthermore, the laboratory regulations regarding these materials have to be followed.

Title: ICP-OES measurements in natural soil	
This SOP is valid from: 16.07.2012	
Version: First Version	
Responsible person of the implementation of the SOP: user	
Pervious changes: first version	
Information for:	user safety administrator laboratory and division manager
Author:	_____ date/signature Carmen Nickel
counterchecked:	_____ Fritz Luther
Approved:	_____ Dr. rer. nat. T. Kuhlbusch

## **All.7.2 Standard operation procedure (SOP) - ICP-OES measurements in the eluate of natural soils**

Date: 16th July 2012

Version: 1.0 english

Scope

Purpose

References

Instrument specification

Necessary materials

Digestion method

Data Evaluation / Reporting

Quality control measures

Potential error sources when conducting measurements

Occupational safety

Purpose

The standard work specification must be applied for chemical measurements using Inductive coupled plasma optic emission spectrometry (ICP OES) of the eluate of soil columns for the quantification of specific substances in the eluate, here TiO<sub>2</sub> and copper.

References

Kuhlbusch et al. 2012: "Fate and behaviour of TiO<sub>2</sub> nanomaterials in the environment, influenced by their shape, size and surface area". Hrsg.: Umweltbundesamt, Report 25/2012, FKZ 3710 65 417, UBA-FB 001577, ISSN 1862-4804,

### Instrument specification



Manufacturer: Thermo Scientific

Version: ICAP6000 series

### Necessary materials

- H<sub>2</sub>O<sub>2</sub> (20%)
- HNO<sub>3</sub> (65%)
- Deionised water
- Reference material NIST standard 1633c

### Digestion method

An exact volume of 10 mL amount of the eluate or suspension were filled in a volumetric flask. 5 mL HNO<sub>3</sub> (65%) and 1 mL H<sub>2</sub>O<sub>2</sub> (20%) were added and filled up to 25 mL with ultra pure water. The reaction vessel is placed in an automated micro-wave digestion apparatus (MLS Ethos plus) and digested by heating up to 218°C within 30 min and holding the temperature for 30 min. Samples are allowed to cool to room temperature and are filled up to a defined volume. Samples are centrifuged at 4000 rpm for 20 min, and supernatant is passed through a 0.45 µm membrane filter.

### Data Evaluation / Reporting

Measurement preparation and implementation as well as the data evaluation of the measurements must be documented in a test report.

### Quality control measures

- The homogeneity of variance was verified according to DIN 38402, part 51.
- Comparison and (if necessary) adjustment of the instruments in the laboratory before each measurement campaign.



- Reference material for the examination of the digestion method, chemical analysis and limit of detection of the applied technique was verified according to DIN EN ISO 11885.
- Reference materials NIST standard 1633c.

According to the calibration, the limit of detection (LOD) of this digestion method is around 0.12 µg/L for titanium and 0.41 µg/L for copper.

#### Potential error sources when conducting measurements

- Digestion method → incomplete digestion of minerals → different concentrations
- In any case a detailed record of measurements must be kept in which all possible disturbances are noted with time stamps.

#### Occupational safety

Every measurement campaign must be conducted based on a risk assessment and the requirements of occupational safety regulations. This includes in particular the regulation of responsibilities and of the interfaces to occupational safety and health on the premises where the measurements shall be conducted. When handling the nanomaterials, protective clothing and suitable gloves have to be worn at any time and the working area as well as the used materials and instruments have to be labeled. Furthermore, the laboratory regulations regarding these materials have to be followed.

Title: ICP-OES measurements in the eluate of natural soils	
This SOP is valid from: 16.07.2012	
Version: First Version	
Responsible person of the implementation of the SOP: user	
Pervious changes: first version	
Information for:	user safety administrator laboratory and division manager
	date/signature
Author:	----- Carmen Nickel
counterchecked:	----- Fritz Luther
Approved:	----- Dr. rer. nat. T. Kuhlbusch

### **AII.7.3 Standard operation procedure (SOP) - ICP-OES measurements of Aluminium and Silicon in solid samples**

Date: 16th July 2012

Version: 1.0 english

Scope

Purpose

Instrument specification

Necessary materials

Digestion method

Data Evaluation / Reporting

Quality control measures

Potential error sources when conducting measurements

Occupational safety

Purpose

The standard work specification must be applied for chemical measurements using Inductive coupled plasma optic emission spectrometry (ICP-OES) to detect aluminium and silicon concentration in dry solid samples.

Instrument specification



Manufacturer: Thermo Scientific

Version: ICAP 6000 Series

#### Necessary materials

- H<sub>2</sub>O<sub>2</sub> (30%)
- HNO<sub>3</sub> (65%)
- NaOH (solid)
- PTFE Teflon Filter 0.45 µm
- Deionised water

#### Digestion method

##### **Aluminium**

100 – 200 mg of the solid material was mixed with 9 mL HNO<sub>3</sub> (65% ROTH) and 1 mL H<sub>2</sub>O<sub>2</sub> (30% ROTH) followed by a microwave digestion (temperature program - 3 min 20 °C to 130 °C, 5 min 130 °C to 210 °C and 7 min at 210 °C). Afterwards the sample was filled up to a volume of 25 mL

##### **Silicon**

100 – 200 mg of the dry powder was placed in a platinum cup. 1000 mg NaOH (solid) was added and mixed with the powder. Afterwards the mixture was heated for 20 min at 600 °C. Afterwards 50 mL ultrapure water was added. If necessary the samples were filtered with a 0.45 µm PTFE - Teflon filter.

#### Data Evaluation / Reporting

Measurement preparation and implementation as well as the data evaluation of the measurements must be documented in a test report.

#### Quality control measures

- The homogeneity of variance was verified according to DIN 38402, part 51.
- Comparison and (if necessary) adjustment of the instruments in the laboratory before each measurement campaign
- Reference material for the examination of the digestion method, chemical analysis and limit of detection of the applied technique was verified according to DIN EN ISO 11885.

According to the calibration, the limit of detection (LOD) of this digestion method is around 1 µg/L for aluminium and 1.5 µg/L for silicon.

#### Potential error sources when conducting measurements

- Digestion method → incomplete digestion of the material
- Loss of the substances at the vessel walls

- In any case a detailed record of measurements must be kept in which all possible disturbances are noted with time stamps

#### Occupational safety

Every measurement campaign must be conducted based on a risk assessment and the requirements of occupational safety regulations. This includes in particular the regulation of responsibilities and of the interfaces to occupational safety and health on the premises where the measurements shall be conducted. When handling the nanomaterials, protective clothing and suitable gloves have to be worn at any time and the working area as well as the used materials and instruments have to be labeled. Furthermore, the laboratory regulations regarding these materials have to be followed.

Title: ICP-OES measurements of Aluminium and Silicon in solid samples	
This SOP is valid from: 16.07.2012	
Version: First Version	
Responsible person of the implementation of the SOP: user	
Pervious changes: first version	
Information for:	user safety administrator laboratory and division manager
	date/signature
Author:	----- Carmen Nickel
counterchecked:	----- Fritz Luther
Approved:	----- Dr. rer. nat. T. Kuhlbusch

## **AII.7.4 Standard operation procedure (SOP) - ICP-OES measurements of Aluminium and Silicon in liquid samples**

Date: 16th July 2012

Version: 1.0 english

Scope

Purpose

Instrument specification

Necessary materials

Sample preparation

Digestion method

Data Evaluation / Reporting

Quality control measures

Potential error sources when conducting measurements

Occupational safety

Purpose

The standard work specification must be applied for chemical measurements using Inductive coupled plasma optic emission spectrometry (ICP-OES) to detect the concentration of aluminium and silicon in liquid samples.

Instrument specification



Manufacturer: Thermo Scientific

Version: ICAP 6000 Series

Necessary materials

- HNO<sub>3</sub> (65%)
- Deionised water
- 0.22 µm nylon filter

### Sample preparation

The stability of the aluminium and silicon coating was examined for three different dispersion procedures:

- SOP, which includes 1 min sonication followed by 1 hour of moderate stirring,
- 1 minute (of magnetic) stirring after suspending the powder
- No mechanical agitation after suspending the powder

The suspension was centrifuged (2700G for 10 min). The supernatant was then filtered using a 0.22 µm nylon filter (Magna-Nylon, Roth) to differentiate between solid and liquid phase. Afterwards the desorbed aluminium and / or silicon concentration was measured in the filtrate of the suspension.

### Digestion method

Six millilitres of the supernatant was mixed with 0.8 mL HNO<sub>3</sub> (69%) followed by microwave digestion (temperature program - 3 min 20 °C to 130 °C, 5 min 130 °C to 210 °C and 7 min at 210 °C). Afterwards the samples were cooled down to room temperature for 90 min.

### Data Evaluation / Reporting

Measurement preparation and implementation as well as the data evaluation of the measurements must be documented in a test report.

### Quality control measures

- The homogeneity of variance was verified according to DIN 38402, part 51.
- Comparison and (if necessary) adjustment of the instruments in the laboratory before each measurement campaign
- Reference material for the examination of the digestion method, chemical analysis and limit of detection of the applied technique was verified according to DIN EN ISO 11885.

According to the calibration, the limit of detection (LOD) of this digestion method is around 1 µg/L for aluminium and 1.5 µg/L for silicon.

### Potential error sources when conducting measurements

- Separation of glycerol with the bulk material during centrifugation or filtration
- Loss of the substances at the vessel walls
- In any case a detailed record of measurements must be kept in which all possible disturbances are noted with time stamps.

### Occupational safety

Every measurement campaign must be conducted based on a risk assessment and the requirements of occupational safety regulations. This includes in particular the regulation



of responsibilities and of the interfaces to occupational safety and health on the premises where the measurements shall be conducted. When handling the nanomaterials, protective clothing and suitable gloves have to be worn at any time and the working area as well as the used materials and instruments have to be labeled. Furthermore, the laboratory regulations regarding these materials have to be followed.

Title: ICP-OES measurements in liquids	
This SOP is valid from: 20.07.2012	
Version: First Version	
Responsible person of the implementation of the SOP: user	
Pervious changes: first version	
Information for:	user safety administrator laboratory and division manager
	date/signature
Author:	----- Carmen Nickel
counterchecked:	----- Fritz Luther
Approved:	----- Dr. rer. nat. T. Kuhlbusch

## **All.8 Standard operation procedure - Carrier effects of nanoscale particles in soil columns**

Date: 16th July 2012

Version: 1.0 english

Scope

Purpose

References

Instrument specification

Necessary materials

Sample preparation

Digestion method

Data Evaluation / Reporting

Quality control measures

Potential error sources when conducting measurements

Occupational safety

Waste disposal

Purpose

The aim of this Standard Operating Procedure is to provide information about the quality of leaching experiments, dealing with carrier transport of an environmental pollutant in the presence of TiO<sub>2</sub> nanomaterials in soils, and performed within the Project 3710 65 414. The SOP describes suitable proceedings to assess the influence of nanomaterials on the fate and behaviour of environmental pollutants in soil columns.

References

OECD Guideline 312, Leaching in soil columns, 2004.

### Measurement Strategy

The carrier effect experiments were conducted in glass columns filled with reference soil. The test procedure based on the OECD guideline 312, 2004.

The amount of the test substance and the nanomaterial were quantified using chemical analysis, like ICP-OES or LC MS measurements of the eluate as well as the soil itself. In the end also SEM / EDX scans of different samples of the soil columns were conducted, to get information about the morphology as well as transport behaviour of isolated agglomerates whose concentration are too low for the chemical analysis.

It must be taken into account that some substances occur ubiquitously and may influence the measurements or the tested concentration of nanoscale product materials. TiO<sub>2</sub> for example showed a high background concentration in natural soils up to 4 g/kg (cambic rendzina, refesol, 2012).

### Instruments

- ICP-OES or comparable instruments for a quantitative detection
- SEM / EDX or comparable visual instruments
- Szintillation counter - Radioanalyses of soil and eluate samples to quantify the distribution of the organic compound

### Necessary materials

- Three glass columns (inner diameter 12 cm, height 20 cm)
- Silane-treated glass wool
- Reference soil types ([www.refesol.de](http://www.refesol.de))
- Electrolyte (10 mmol/L CaCl<sub>2</sub>, pH7)
- Peristaltic pump tubing (e.g. 0.030 inch ID), silicone tubing and matching connections
- Glass vials, Schott bottles, beakers
- Spatula
- CuSO<sub>4</sub> (750 mg / 12 ml)
- <sup>14</sup>C-TCC
- 2 mm stainless steel meshes

### Test performance

Preparatory work – wet spiking of the soil

Hundred gram of the test soil type (100 g ± 1 g) were spiked with 750 mg (± 2 mg) CuSO<sub>4</sub> and 200 µg <sup>14</sup>C-TCC respectively.

The CuSO<sub>4</sub> was diluted in 12 mL DI water before the water was added to the dry soil. Afterwards the soil suspension was shaken for 1 h. After shaking the soil was dried at 70 °C for 1 h. The dry soil was then applied to the soil column using a 2 mm mesh 100 g (± 1 g) of the soil type were.

#### Experiment realisation

Glass columns (inert material) were packed with air dried, sieved soil (< 2 mm) to a height of 11 cm. The soil was added to the column in small portions with a spoon. The soil weight of the duplicate test columns should be similar (< 10% variance).

Afterwards the soil was pre-wetted with a 0.01 M CaCl<sub>2</sub> solution from the bottom to the top. Until the 0.01 M CaCl<sub>2</sub> solution reached a height of 2 cm above the top of the soil. Afterwards the soil was allowed to drain by gravity.

Thereafter 100 g of the spiked soil (Cu or TCC) were homogeneous sieved (using a 2 mm mesh) to the top of the soil, presenting the upper segment.

For the test system with TiO<sub>2</sub> 100 mL of the TiO<sub>2</sub> suspension with pH 5 (prepared according to the SOP for TiO<sub>2</sub> suspension preparation in DI water), a total amount of 250 mg TiO<sub>2</sub>, was directly applied to the soil column surface. For the reference system the same amount of 100 mL DI water with pH 5 were directly applied to the soil column surface, respectively.

After the suspension or the DI water was applied, 0.01M CaCl<sub>2</sub> solution (42 mL / min) was continuously sprinkled to the soil for 48h.

The eluate was collected in different time periods, after 1h, 2h, 3h, 20h and 48h.

Afterwards the soil columns were sectioned into an adequate amount but a minimum of three different samples to get information about the mobility of the applied substances.

#### For the copper experiments

Seven samples were chemically analysed by ICP-OES to get information about the mobility of the copper and TiO<sub>2</sub> in the test system and the copper in the reference system.

#### from the top of the column

Segment 1 – top layer,

Segment 2 – 1 - 2 cm,

Segment 3 – 2 - 3 cm,

Segment 4 – 4 - 7 cm,

Segment 5 – 7 - 8 cm,

Segment 6 – 8 - 11 cm,

Segment 7 – 11 - 12 cm.

The test was performed in triplicate for the test and reference system.

For the <sup>14</sup>C-labelled triclocarban, <sup>14</sup>C-TCC experiment

Twelve samples each with a height of 1 cm were analysed by radio analysis.

For each soil type, at least three of these setups were prepared.

At two of the columns 100 mL of a TiO<sub>2</sub> suspension (after the SOP for TiO<sub>2</sub> suspension preparation in DI water) at a concentration of 2.5 g/L and a pH of 5 was applied.

To the surface of the third column, i.e. the TCC reference system, the same volume of DI water (pH 5) was applied.

Ten minutes later, irrigation with 0.01 M CaCl<sub>2</sub> solution was started and continued for 48 h at a constant flow of 42 mL/min. In this time frame, the eluate was collected at different time intervals.

### Sampling

Eluate samples were taken at small time intervals directly after the beginning of the experiment, i.e. when the raining event was started. Afterwards, more volume was collected from longer time periods. Fourteen samples were taken in total, i.e. after 10', 20', 30', 1 h, 2 h, 3 h, 6 h, 18 h, 22 h, 26 h, 30 h, 42 h, 45 h und 48 h.

For copper after a preliminary test not all fourteen samples were analysed for the further study. It was conducive that 5 samples were analysed, after 1 h, 2 h, 3 h, 20 h and 48 h.

A core sample of the column was extracted for chemical analysis. Therefore an outside margin was separated (1 cm) and only the inner sample was used for the analysis, in order to detect possible preferential material transport along the glass column wall.

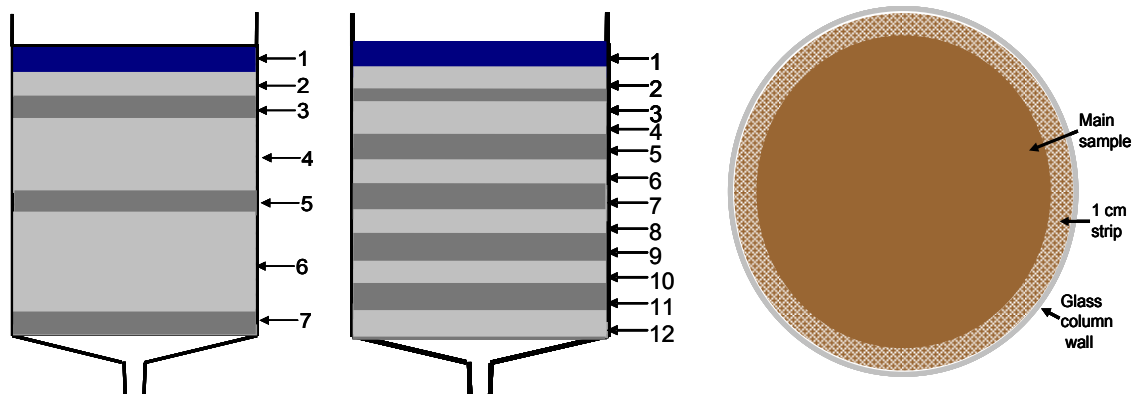


Figure 34: Simplified graphic description of the segment sampling for the copper experiments left, <sup>14</sup>C TCC experiments in the middle.

### Termination of measurement

The measurements must be terminated in accordance with the corresponding SOPs for the measurement instruments. The measurement results should preferably be stored redundantly. Potential product contaminations on the instrument surfaces must be wiped off before packaging, for example using moist cloths.

### Data Evaluation / Reporting

Measurement preparation and implementation as well as the data evaluation of the measurements must be documented in a test report (see TRGS 402).

#### Analysis of the particle number concentrations

The recovery of the added copper or titanium was calculated as absolute values in mg/kg in relation to the sample quantity, due to the subsample extraction.

The recovery of the added <sup>14</sup>C-TCC was calculated as the detected concentration in relation to the added concentration.

#### Quality control measures

- Comparison and (if necessary) adjustment of the instruments in the laboratory before each measurement campaign
- Reference material for the examination of the digestion method, chemical analysis and limit of detection of the applied technique

#### Potential error sources when conducting measurements

- Digestion method → incomplete digestion of minerals → different concentrations
- Digestion method and salt content → interferences with some instruments like ICP MS
- In any case a detailed record of measurements must be kept in which all possible disturbances are noted with time stamps.

#### Occupational safety

Every measurement campaign must be conducted based on a risk assessment and the requirements of occupational safety regulations. This includes in particular the regulation of responsibilities and of the interfaces to occupational safety and health on the premises where the measurements shall be conducted. When handling the nanomaterials, protective clothing and suitable gloves have to be worn at any time and the working area as well as the used materials and instruments have to be labeled. Furthermore, the laboratory regulations regarding these materials have to be followed.

#### Waste disposal

Nanomaterial containing waste has to be collected and disposed of separately. It has to be differentiated between the kind of nanomaterial.

Title: Carrier effect of nanomaterials in soil columns	
This SOP is valid from: 16.07.2012	
Version: First Version	
Responsible person of the implementation of the SOP: user	
Pervious changes: first version	
Information for:	user safety administrator laboratory and division manager
	date/signature
Author:	_____ Carmen Nickel
counterchecked:	_____ Dr. rer. nat. Hanna Maes
Approved:	_____ Dr. rer. nat. T. Kuhlbusch



## Annex III Results of the Coating Characterisation

### AIII.1 Basic characterisation of NM104 and NM103

For the basic characterisation of the two materials FTIR, LEIS and TOF SIMS analysis were conducted from the dry powder to get information about the basic chemical formation of the ENMs.

#### AIII.1.1 Fourier transform infrared spectroscopy (FTIR) measurements of the powder of both coated titanium dioxide nanomaterials

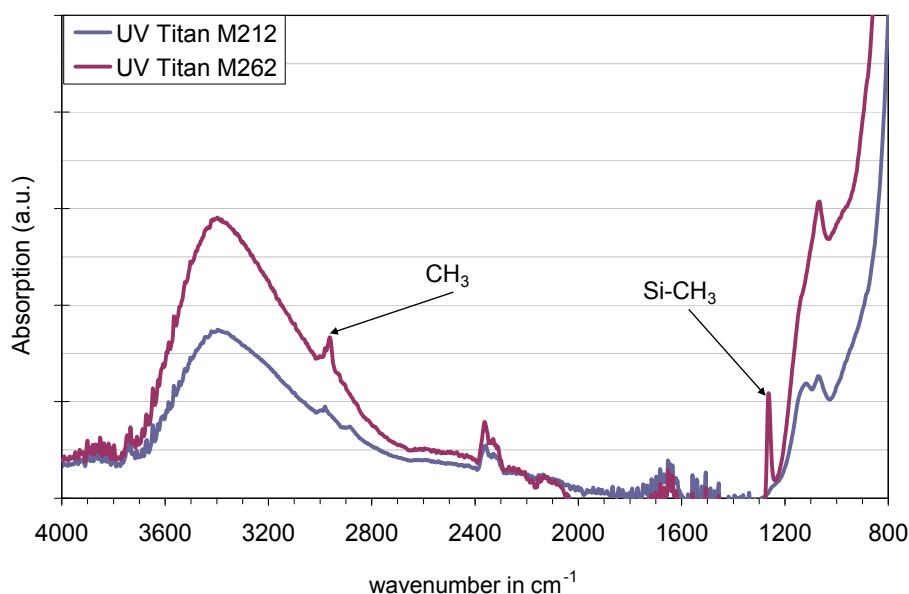


Figure 35: FTIR spectrum of the dry powder of the two coated titanium dioxide nanomaterials.

With FTIR measurements of the dry powder the typical dimethicone peaks for Si-CH<sub>3</sub> and CH<sub>3</sub> were detected for the original NM103 material. For NM104 none of these peaks can be detected.

The dry materials were also suspended in DI water after the established SOP and the supernatant (after filtration with 0.22 μm Nylon filter) was analysed. In the supernatant no observation of the glycerol or dimethicone was possible. It is conceivable that the concentration in suspension was below the limit of detection of the instrument.

#### AIII.1.2 Low energy ion scattering (LEIS) measurements of the two materials

LEIS measurements of the first atomic layer of the two materials (dry powder) were conducted (Figure 36) by TASCAN GmbH to derive information about the surface of the two materials. An ION-TOF-Qtac100 Leis instrument was used. For the analysis a thin layer of the dry powder was applied on a sample holder with an area of 10 mm<sup>2</sup>. As primary ion 3 keV He<sup>+</sup> was used. An area of 2 x 2 mm was analysed. The 3 keV He<sup>+</sup> spectra were detected with 180s and 5 nA (140 x 10<sup>12</sup> ions / cm<sup>2</sup>).

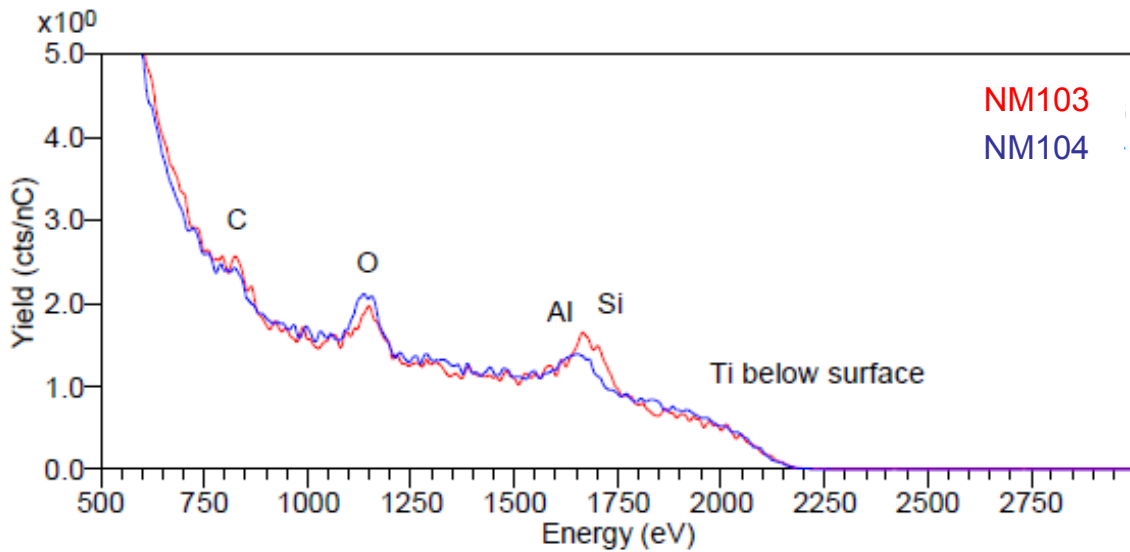


Figure 36: Detailed 3 keV He<sup>+</sup> Leis spectrum of NM103 and NM104

The measurements indicate that the coating for both materials covered the Ti core completely. This was shown in more detail in Figure 37. Differences between the two materials were also observed, NM103 showed a high Si, C and O concentration at the surface, whereas NM104 showed a high concentration of C, O and Al and a low concentration of Si.

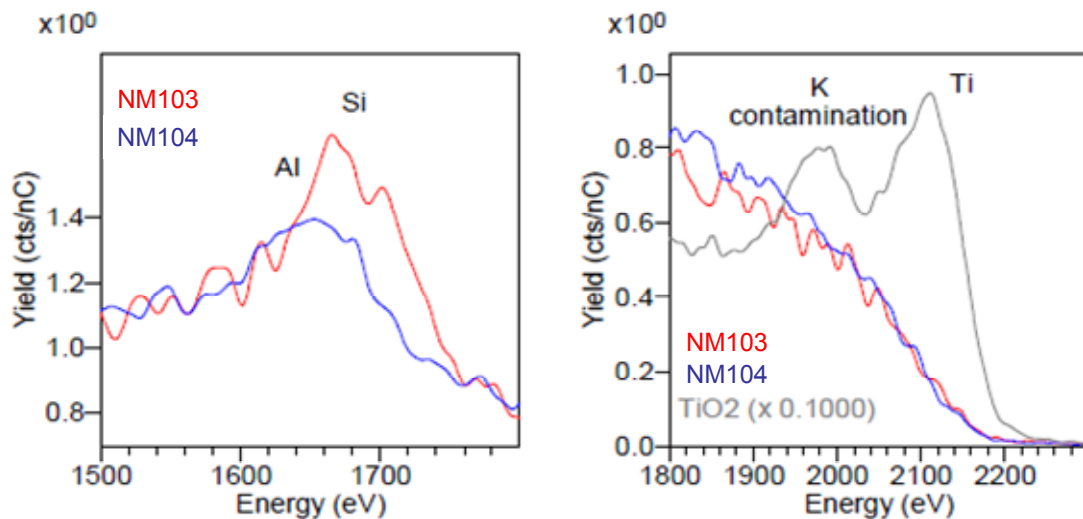


Figure 37: Details of the 3 keV He<sup>+</sup> Leis spectrum of the Al, Si (left diagram) and Ti region (right diagram) for NM103 and NM104. In the Ti region a Ti reference spectrum (with K contamination) is shown.

### AIII.1.3 Time of Flight Secondary Ion Mass Spectrometry (ToF SIMS) analysis of the powder of both coated titanium dioxide nanomaterials

The ToF SIMS measurements were conducted by nanoAnalytics to derive information about the chemical composition at the surface of the two coated TiO<sub>2</sub> nanomaterials. For both materials titanium and aluminium was identified with ToF SIMS analysis. Also SO<sub>x</sub>

and aluminium oxide was identified. In Table 16 the detected materials which were identified at the surface of the materials are presented. But also some differences could be identified.

Table 16: Relative intensities of the detected substances, - = no detection, + = detection in the range of LOD, ++ = low, +++ = medium and ++++ = high intensity.

	NM103	NM104
Alkaline / alkaline earth		
Calcium	++	++
Potassium	++	++
Magnesium	++	++
Sodium	+++	+++
anion		
Formate (COOH)	++	+++
CN-/CNO-	++	++
NO <sub>x</sub> -	++	++
PO <sub>x</sub> -	+	+
SO <sub>x</sub> -	++++	++++
Fatty acids		
>C13	+	+
Metalloid		
Silicon	+++	+
Siliconoxide	+++	-
Halogen		
Fluorine	+++	+++
Chlorine	++	+++
Bromine	++	++
Cation		
C <sub>2</sub> H <sub>5</sub> O <sup>+</sup>	+++	+++
C <sub>8</sub> H <sub>5</sub> O <sub>3</sub> <sup>+</sup>	+++	+++
Metal		
Aluminium	++++	++++
Aluminiumoxide	+++	+++
Aluminiumoxidesulfate	+++	+++
Titanium / titandioxide	++++	++++
Silicon		
Polydimethylsiloxan	+++	-
Sundries		
Octylphenoethoxylate	++	++
Sulphur	++	++

Only for the material NM103, the organic coating, in this case polydimethylsiloxan (PDMS) was detected without any doubt (Table 16 and Figure 38 and Figure 39). Glycerol could not be clearly identified. It is conceivable, that for substances with short chain length (e.g. glycerol) identification with TOF SIMS is not specific enough. Moreover both TiO<sub>2</sub> nanomaterials showed spectra for C<sub>x</sub>H<sub>y</sub> groups, which is an integral part of both organic coating. The aluminium of the inorganic coating and the titanium of the core were measured for both materials.

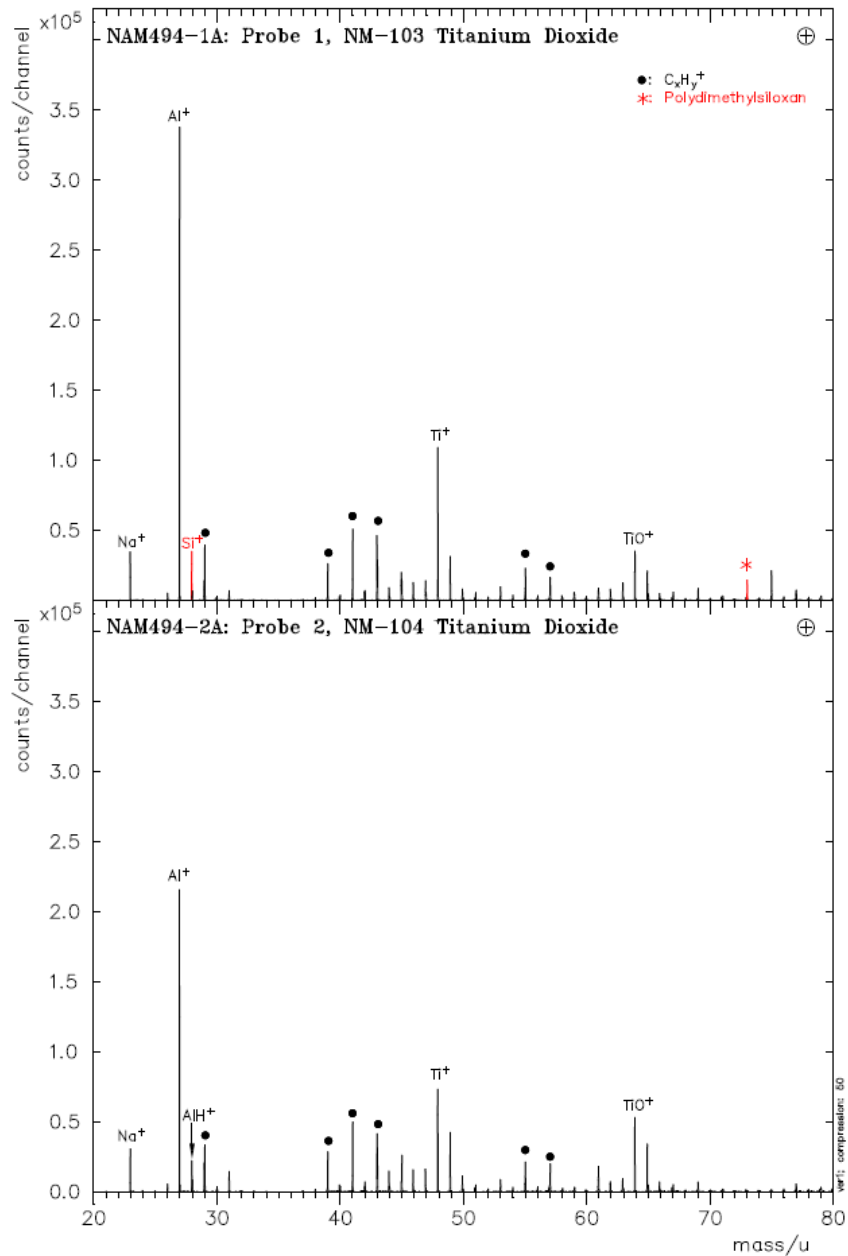


Figure 38: Detail TOF SIMS spectrum of positive secondary ions

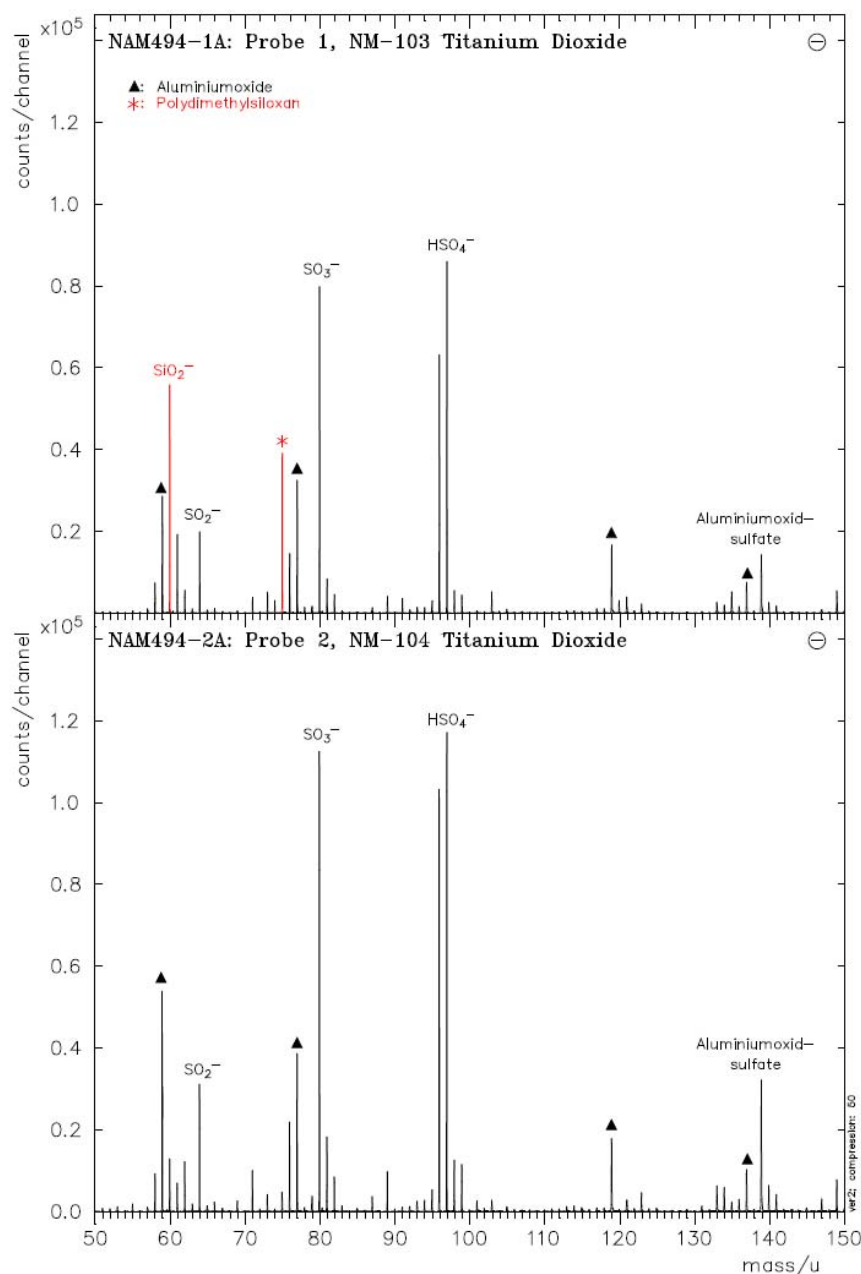


Figure 39: Detail TOF SIMS spectrum of negative secondary ions

For the NM103 material, ToF SIMS measurements were also conducted for samples which were prepared after the established SOP to derive information about the surface chemistry of the materials after suspension preparation. Therefore the dispersed material was centrifuged (15 min, 2700G) to differentiate between the solid and the liquid phase. The supernatant was pipeted until an amount of 2 mL was still in the sample. Afterwards the sample was washed with 50 mL deionised water and shaken and centrifuged again. The supernatant was again pipeted until an amount of 2 mL was still in the sample. The remaining sample was dried until no water was left. The dry sample was then homogenised using an agate mortar and analysed. The results are presented in Figure 40.

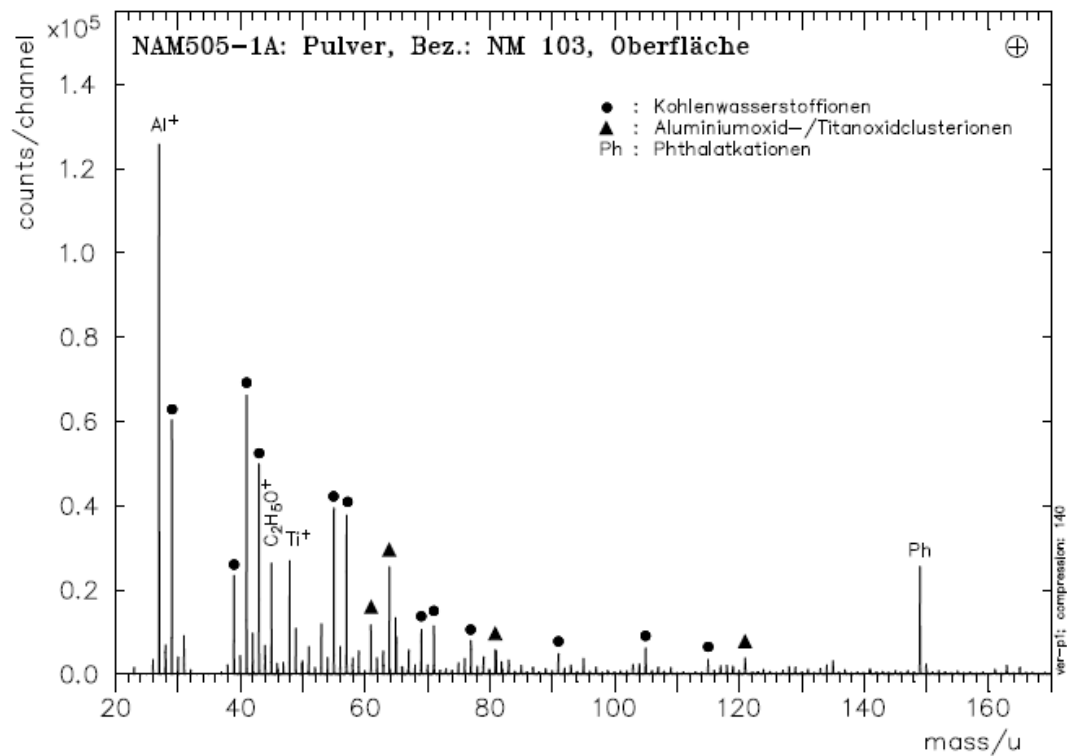


Figure 40: Typical TOF SIMS spectrum of positive secondary ions

Titanium and aluminium was identified, but no dimethicone was detected. These findings underline the results of the ICP-OES analyses. These finding indicate that nearly all dime-  
thicone was removed during suspension preparation and the aluminium oxide coating  
was presented at the surface.

### AIII.2 Comparison measurement and validation of the enzymatic UV test and the LC-MS analysis

For this approach the concentration levels 500, 1000, 1500, and 2000 µg/L have been investigated. The measurements were performed three times and five times for the LC-MS and the UV test, respectively. Moreover, for both analytical methods the same fresh standard solutions were employed. Method validation results are summarized in Table 17.

As can be seen, the recovery rates range between 97% and 108% which means that the experimentally obtained concentration levels of glycerol are in good agreement with the nominal values. Moreover, the results in Table 17 underline that both analytical methods yield similar concentrations of glycerol in aqueous solutions.

Table 17: Overview of validation results for the enzymatic UV test and the LC-MS/MS method.

QC	LC-MS/MS method (n = 3)			Enzymatic UV test (n = 5)		
	Nominal conc. in µg/L	Actual conc. in µg/L	Recovery rate in %	Nominal conc. in µg/L	Actual conc. in µg/L	Recovery rate in %
1	500	540 ± 10	108	500	530 ± 20	106
2	1000	970 ± 30	97	1000	1020 ± 40	102
3	1500	1470 ± 30	98	1500	1480 ± 10	99
4	2000	1960 ± 40	98	2000	1950 ± 10	98



### AIII.3 Dispersibility tests of NM104 and NM103

Different suspension preparation procedures were tested to generate stable suspension.

Table 18: Median, Minimum and Maximum of the z-average and zeta potential; n = 3.

	NM104 (UV Titan M212)		NM103 (UV Titan M262)	
	Median in nm (min; max)		Median in nm (min; max)	
	direct	after 96 h	direct	after 96 h
Stirring	1100 (450; 4500)	350 (240; 550)	806 (327; 1480)	350 (260; 450)
zeta potential	-	-	+ 12 mV	-
sonication in a waterbath	280 (175; 567)	209 (189; 242)	367 (231; 862)	323 (282; 502)
zeta potential	+ 43 mV	+ 6 mV	+ 24 mV	+ 9 mV
sonication using a probe	344 (218; 1097)	192 (184; 207)	249 (181; 699)	189 (174; 215)
zeta potential	+ 43 mV	+ 29 mV	+ 30 mV	+ 30 mV

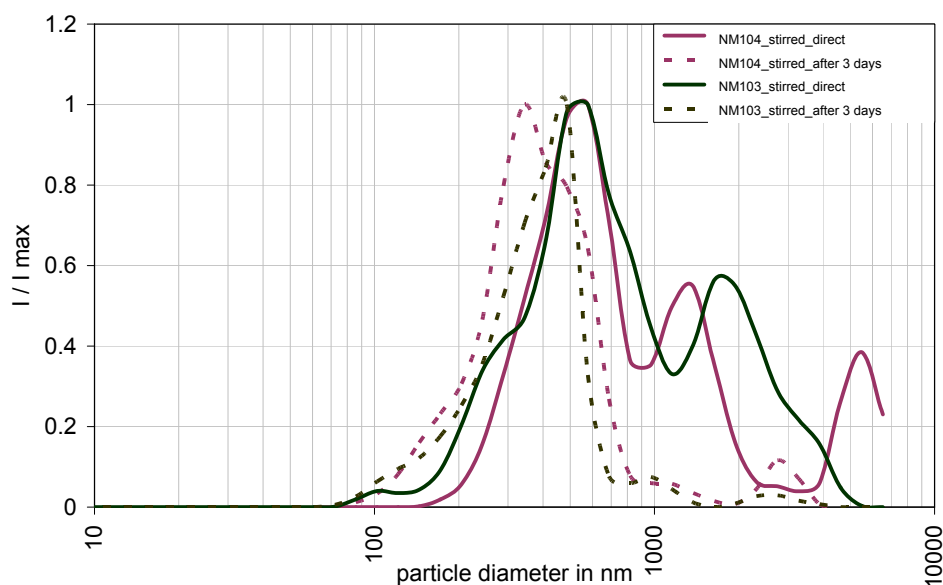


Figure 41: Normalised intensity particle distribution of NM103 and NM104 after 10 min stirring directly (solid line) and after 96 h (dashed line).

Only with stirring no stable suspension could be prepared and agglomeration of the materials was visually observed. Due to this only for NM103 zeta potential measurements

could be conducted with +12 mV. For the other materials no zeta potential measurements were possible.

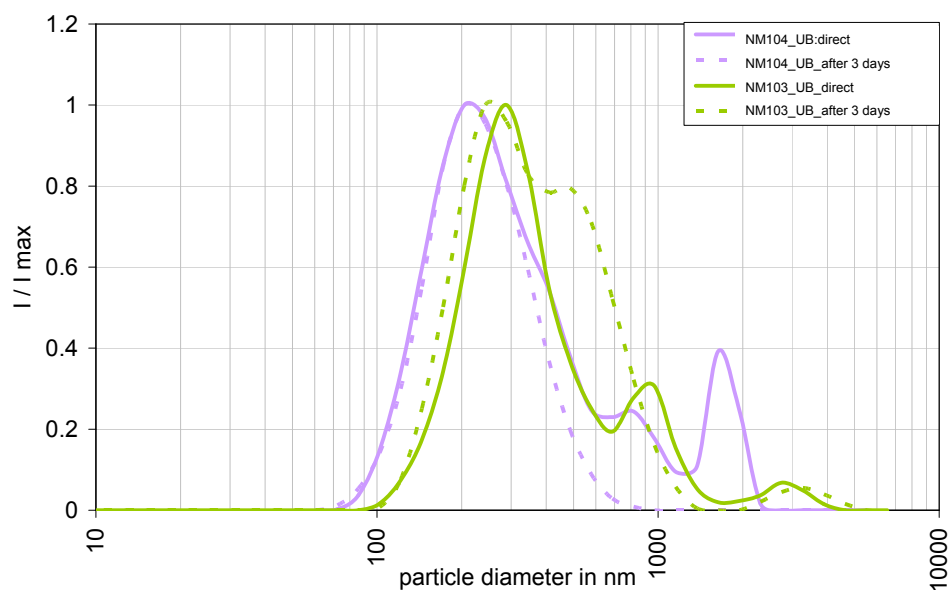


Figure 42: Normalised Intensity particle distribution of NM103 and NM104 after 10 min sonication using a waterbath (UB) directly (solid line) and after 96 h (dashed line).

After suspension preparation with sonication using a waterbath the size and the zeta potential of the suspension could be measured Figure 42. The zeta potential was around +43 mV for NM104 and +24 mV for NM103. After 96 h the zeta potential decreased dramatically and was between +6 mV and +9 mV for both materials.

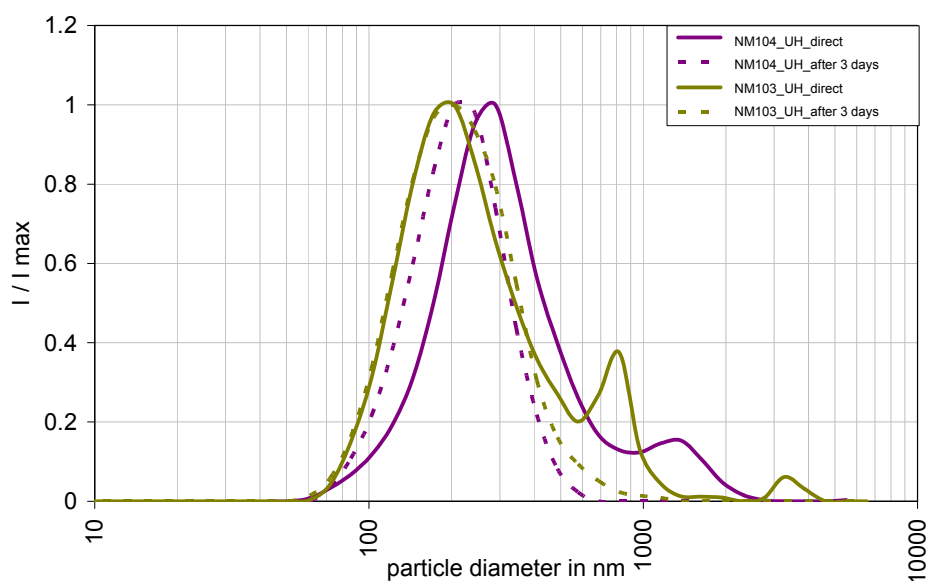


Figure 43: Normalised Intensity particle distribution of NM103 and NM104 after 10 min sonication using an ultrasonic homogeniser (UH) directly (solid line) and after 96 h (dashed line).

After suspension preparation with an ultrasonic probe stable suspension of the two materials could be prepared. Size (Figure 43) and zeta potential measurements were conducted. The zeta potential for both materials was > +30 mV for both materials directly and after 96 h, which is an indication for stable suspensions.

Sufficient stability is warranted if the suspension (e.g. 50 mg TiO<sub>2</sub> material / 50 mL deionised water in a 100 mL beaker glass) was sonicated for at least 1 minute.

Table 19: DLS results for differently prepared NM suspensions; powders suspended in deionised water and dispersed with sonication using a probe (200 W), with overhead stirrer (~350 rpm) and with sonication in a waterbath (120 W, stirred, fixed position of the sample); measurement precision: n = 10 measurements per sample.

dispersion technique	NM104		1000 ppmw		NM103	
	100 ppmw		1000 ppmw		1000 ppmw	
	x <sub>Cumr</sub> , nm	PDI	x <sub>Cumr</sub> , nm	PDI	x <sub>Cumr</sub> , nm	PDI
1 min probe	206.1 ± 4.13	0.302 ± 0.037	205.0 ± 5.62	0.287 ± 0.029	246.5 ± 5.76	0.366 ± 0.015
2 min probe	202.6 ± 3.68	0.326 ± 0.034	194.1 ± 2.78	0.252 ± 0.010	217.7 ± 4.78	0.371 ± 0.027
4 min probe	179.8 ± 4.89	0.260 ± 0.022	182.4 ± 1.30	0.244 ± 0.016	184.6 ± 2.91	0.351 ± 0.024
10 min probe	164.9 ± 1.29	0.242 ± 0.018	163.2 ± 2.19	0.211 ± 0.016	163.0 ± 2.45	0.317 ± 0.020
1 h overhead stirrer	611.0 ± 35.7	0.372 ± 0.076	-	-	-	-
30 min waterbath + overhead stirrer	224.2 ± 3.61	0.288 ± 0.025	-	-	-	-

#### AI.4 Stability of the stock suspensions from NM103 & NM104

Table 20: Evolution of the size distribution of stock suspensions (1000 ppmw) over a period of 30 days as measured with DLS

sample age	NM103, 1000ppm		NM104, 1000ppm	
	x <sub>Cumr</sub> , nm	PDI	x <sub>Cumr</sub> , nm	PDI
1 hour	246.5 ± 5.8	0.366 ± 0.015	204.9 ± 5.6	0.287 ± 0.029
1 day	245.8 ± 5.7	0.372 ± 0.026	204.3 ± 4.3	0.284 ± 0.021
3 days	253.0 ± 8.0	0.383 ± 0.024	208.6 ± 4.3	0.287 ± 0.023
5 days	253.2 ± 5.6	0.383 ± 0.024	203.1 ± 2.6	0.277 ± 0.032
7 days	252.2 ± 7.7	0.382 ± 0.021	204.0 ± 3.1	0.264 ± 0.026
30 days	258.0 ± 9.4	0.396 ± 0.047	224.0 ± 6.0	0.294 ± 0.029

## AIII.5 Zeta potential measurements of NM103 and NM104

### AIII.5.1 Hysteresis of ELS measurements

Table 21: Zeta potential of NM103 in deionised water, measured with ELS, titration from acid → basic → acid, 3 independent samples and average result

pH	#1	#2	#3	averaging	
	ζ, mV	ζ, mV	ζ, mV	ave(ζ), mV	s(ζ) mV
4.56	40.5	38.7	37.3	38.8	1.3
4.9	40	35.6	37.46	37.7	1.8
5.9	34.5	30.3	31.5	32.1	1.8
6.9	26.9	23.1	25.77	25.3	1.6
7.93	17.6	0.43	19	12.3	8.4
8.95	-5.8	-12.5	1.02	-5.8	5.5
9.91	-31.1	-31.6	-29.81	-30.8	0.8
9.09	-22.2	-23.8	-27.32	-24.4	2.1
8.09	-8.2	-10.4	-17.05	-11.9	3.8
7.09	15.4	11.5	10.83	12.6	2.0
6.07	28.7	25.4	17.48	23.9	4.7
5.06	36	34.2		35.1	0.9
4.57		37		37.0	0.0

Table 22: Zeta potential of NM104 in deionised water, measured with ELS, titration from acid → basic → acid, 3 independent samples and average result

pH	#1	#2	#3	averaging	
	ζ, mV	ζ, mV	ζ, mV	ave(ζ), mV	s(ζ) mV
4.5	39.1	34.9	41.8	38.6	2.8
5	39.6	34.3	40.4	38.1	2.7
6	32.4	29.8	35.9	32.7	2.5
7	25.7	25.4	27.9	26.3	1.1
8	7.8	-1.8	15.6	7.2	7.1
9	-8	-15.75	-17.7	-13.8	4.2
10	-32.5	-29.7	-25.2	-29.1	3.0
9	-24.3	-23.1	-26.2	-24.5	1.3
8	-11.8	-15.4	-2.1	-9.8	5.6
7	8	4.6	17.8	10.1	5.6
6	23.6	21.7	29.6	25.0	3.4
5	33.7	34.5	36.9	35.0	1.4
4.5	36.2	35.1		35.7	0.5

Table 23: Zeta potential of NM104 in 0.001 M CaCl<sub>2</sub>, measured with ELS, titration from acid → basic → acid, 3 independent samples and average result

pH	#1	#2	#3	averaging	
	ζ, mV	ζ, mV	ζ, mV	ave(ζ), mV	s(ζ) mV
4.5	33.8	40.9	37	37.2	2.9
5	33.8	39.2	36.3	36.4	2.2
6	30.2	36.3	31.7	32.7	2.6
7	20.7	30.4	25.5	25.5	4.0
8	11.1	21.6	17.2	16.6	4.3
9	-0.6	8.7	2.3	3.5	3.9
10	-13.8	-13.8	-12.6	-13.4	0.6
9	-11.7	-8.5	-8.5	-9.6	1.5
8	-4.5	2.7	-1.1	-1.0	2.9
7	11.5	20.5	15.9	16.0	3.7
6	23.9	27.2	26.7	25.9	1.5
5	30.3	35.1	33.4	32.9	2.0
4.5	33.8	35.3	34.7	34.6	0.6

### AIII.6 EPR measurements of the two coated TiO<sub>2</sub> nanomaterials NM104 and NM103

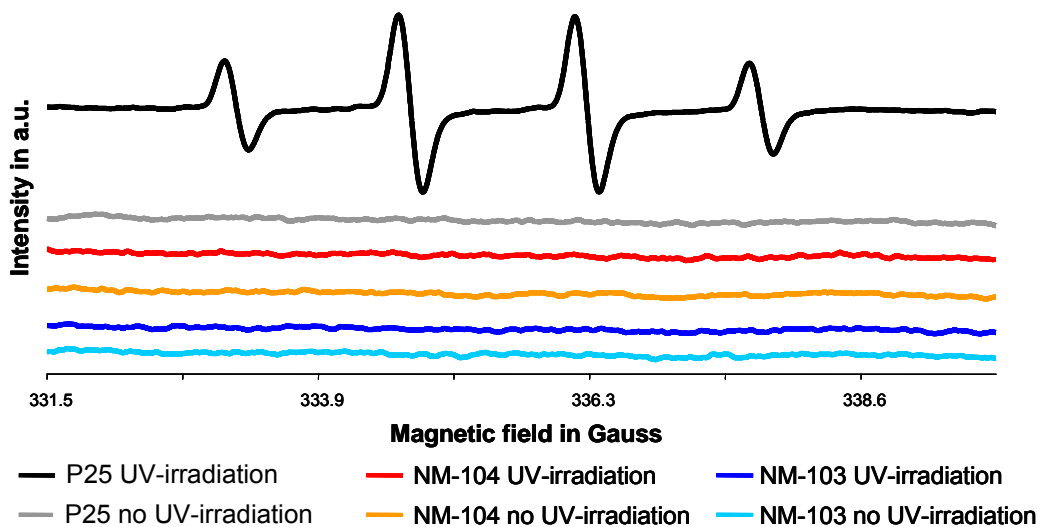


Figure 44: EPR measurements of 100 mg/L NM104, NM103 and P25 as positive control. Suspension preparation based on established SOP, with and without 5 min UV irradiation; n=3. Note: Exemplarily one measurement is shown (n = 3 was tested and no differences were detected).

The influence of the suspension preparation procedure was exemplarily tested for NM104. The material was suspended in DI water using an ultrasonic homogenizer (pulse 0.2 / 0.8, 200 W) for 30 and 60 min. The OH· generation was measured with and without 5 min UV irradiation; n =3.

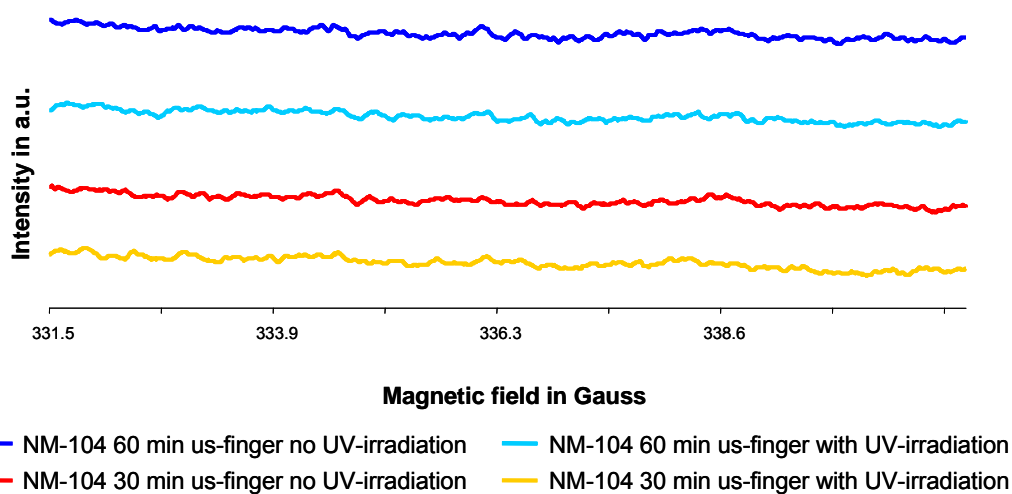


Figure 45: EPR measurements of 100 mg/L NM104 after suspension preparation using an ultrasonic homogenizer (pulse 0.2/0.8, 200 W) with and without 5 min UV irradiation; n =3.

The OH generation of the photocatalytic active material P25 was tested by different suspension preparation steps; established SOP and 1 min vortexing.

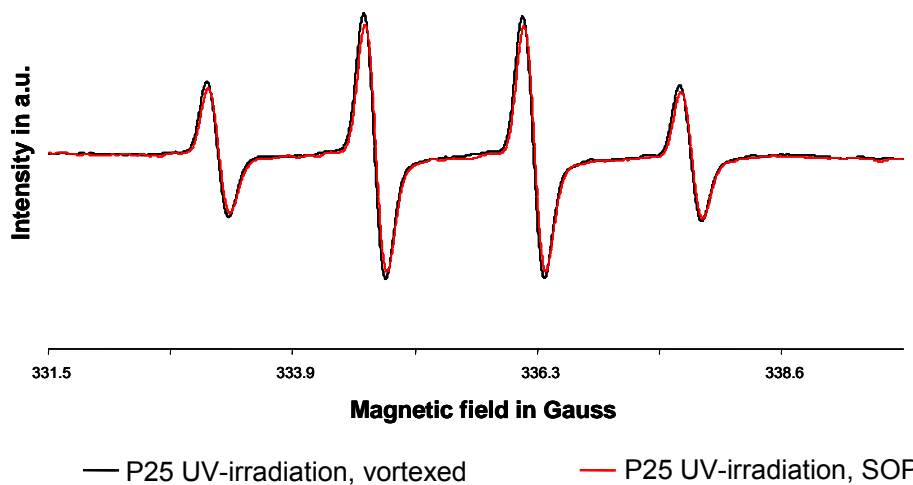


Figure 46: EPR measurements of 100 mg/L P25 as positive control. Suspension preparation based on established SOP and 1 min vortexing, with 5 min UV irradiation; n = 3.

It was shown that the suspension preparation step did not show any effect on the OH· generation potential of the tested Materials. Independent of the preparation step OH· generation was observed for P25 whereas for NM104 no OH· generation was detected.

### AIII.7 NMR measurements of NM104 and NM103

For solid materials the most common method of particle surface area determination is the nitrogen (N<sub>2</sub>) gas adsorption method by Brunnauer-Emmett-Teller (BET). For particles in suspension the most applied direct but not routine method is the cost and very time intensive titration method. Consequently, it is still a goal to detect the particle surface area in suspension by a more convenient technique. As such a promising technique the high resolution nuclear magnetic (NMR) spectroscopy is assumed to detect the wetted particle surface area in suspensions. A commercial instrument - the Acorn Area™ - using low resolution NMR is now available (US Patent, 7,417,426, 2008) and was used for particle surface area detection in this study. In principle, this technique is detecting the different behaviour - in our case the relaxation time - of liquid in contact (or bound) to a particle surface or liquid without particles (blank or particle free suspension) in a magnetic field. If the surrounding liquid is bound to the particle surface the relaxation time is shorter compared to the particle free liquid. This relaxation time is detected and calculated to the surface area after energy input leading to a temporary shift in the magnetic orientation of the sample and its relapse to their initial energy level.

However, the surface area determination by NMR has certain limitations – in particular for NMs – that have to be considered and became evident in this study. The main limiting factors are the minimum particle concentration of 1 weight-% and the required high stability of the suspension. Such high concentration stability cannot be ensured for the tested TiO<sub>2</sub> NM without additives. Consequently, a visual sedimentation was observed. This leads finally to a movement of particles in the measurements vessels and it was actually not feasible to perform reliable measurements.



Mobility, fate and behaviour of TiO<sub>2</sub> nanomaterials in different environmental media

material	preparation / comment	size by manufacturer in nm	used concentration in weight-%	by manufacturer BET surface area in m <sup>2</sup> /g	detected specific surface area in m <sup>2</sup> /g by NMR	Mean value in m <sup>2</sup> /g	SD in m <sup>2</sup> /g	median in m <sup>2</sup> /g	min in m <sup>2</sup> /g	max in m <sup>2</sup> /g
Polystyrene (PSL)	1 min vortexing	246	2.0	???	13	16	8	14	8	37
					23					
					8					
					12					
					13					
					14					
					17					
					15					
					16					
					12					
					14					
					37					
Polystyrene (PSL)	1 min vortexing	182	0.2	???	92	110	90	92	29	382
					81					
					119					
					100					
					116					
					74					
					110					
					91					

Mobility, fate and behaviour of TiO<sub>2</sub> nanomaterials in different environmental media

					59					
					29					
					65					
					382					
P25	ultrasonication by homogeniser otherwise visually sedimentation	???	2.5	???	30	115	102	116	22	204
					22					
					202					
					204					
NM104	ultrasonication by homogeniser otherwise visually sedimentation	???	1.0	???	81	109	27	111	81	134
					111					
					134					
NM103	ultrasonication by homogeniser otherwise visually sedimentation	???	1.0	???	11	9	5	11	3	12
					12					
					3					

No reproducible measurements could be conducted (high standard deviation of the measurements). It is conceivable that agglomeration in the suspension occurred due to the higher concentration of the suspension (1 g/L).

### AIII.8 Zeta potential measurements of NM104 and NM103 as function of pH in deionised water as basic characterisation

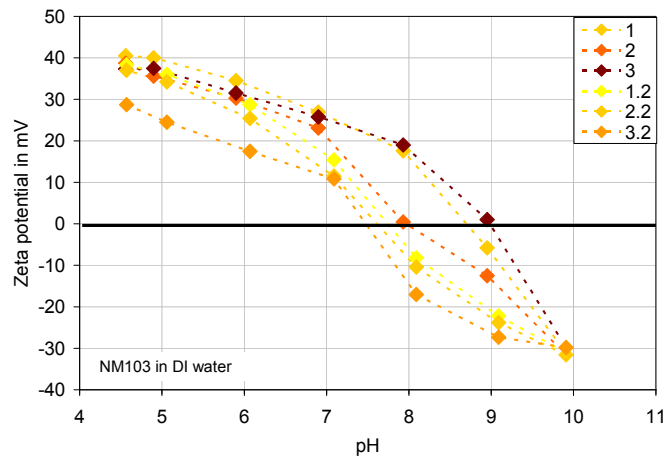


Figure 47: Zeta potential measurements three separate measurements of NM103 in DI water. The pH was varied in a first step from 4.5 to pH 10 (measurements 1 - 3) and in a second step back from pH 10 to pH 4.5 (measurements 1.2 - 3.2).

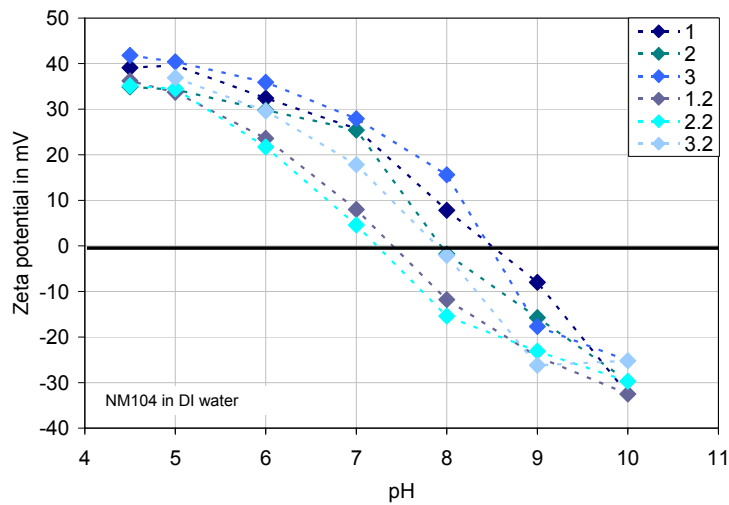


Figure 48: Zeta potential measurements of three separate measurements of NM104 in DI water. The pH was varied in a first step from 4.5 to pH 10 (measurements 1 - 3) and in a second step back from pH 10 to pH 4.5 (measurements 1.2 - 3.2).

### AIII.9 Zeta potential measurements in environmental like media

#### AIII.9.1 Zeta potential measurements of NM103 and NM104 in environmental like media - variation of ionic strength

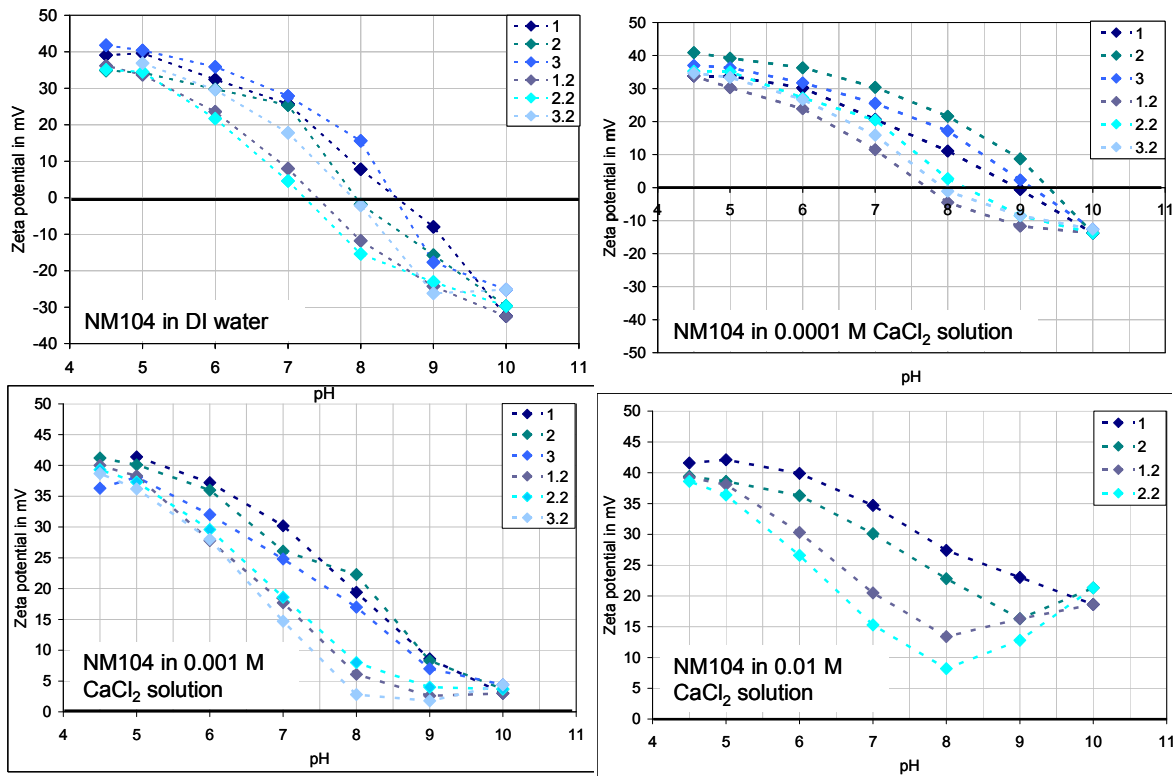


Figure 49: Zeta potential measurements of three separate measurements for NM104 in DI water (top left) with 0.0001M CaCl<sub>2</sub> solution (top right), 0.001M CaCl<sub>2</sub> solution (bottom left) and 0.01M CaCl<sub>2</sub> solution (bottom right). The pH was varied in a first step from 4.5 to pH 10 (measurements 1 - 3) and in a second step back from pH 10 to pH 4.5 (measurements 1.2 - 3.2).

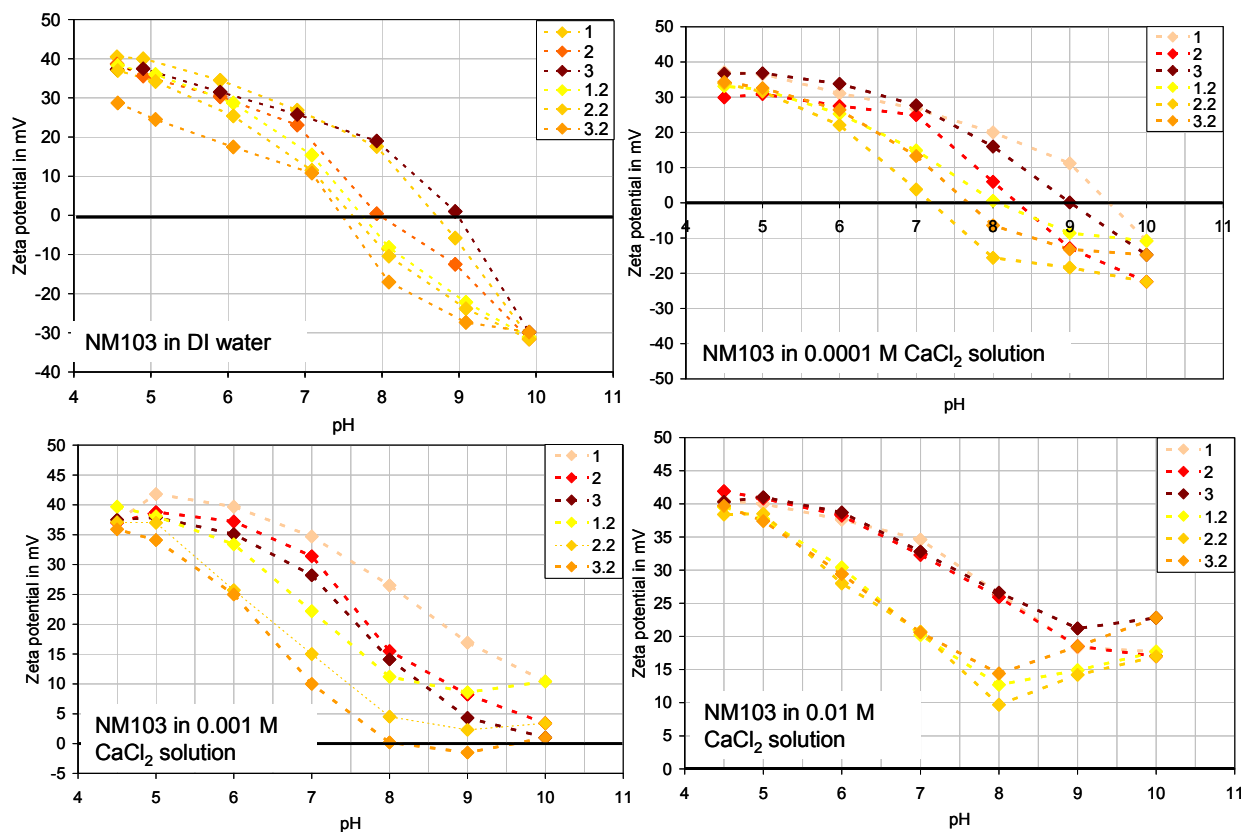


Figure 50: Zeta potential measurements of three separate measurements of NM103 in DI water (top left), with 0.0001M CaCl<sub>2</sub> solution (top right), 0.001M CaCl<sub>2</sub> solution (bottom left) and 0.01M CaCl<sub>2</sub> solution (bottom right). The pH was varied in a first step from 4.5 to pH 10 (measurements 1 - 3) and in a second step back from pH 10 to pH 4.5 (1.2 - 3.2).

Based on the results of the direct measurements it was observed that with increasing ionic strength the IEP was shifted to a higher pH. For the two highest concentrations no IEP could be detected. No significant differences between the two materials were observed.

The aging of the suspension was observed at three different pH values (5, 7, 9) with  $\mu$ EP, after 30 min, 60 min and 24h.

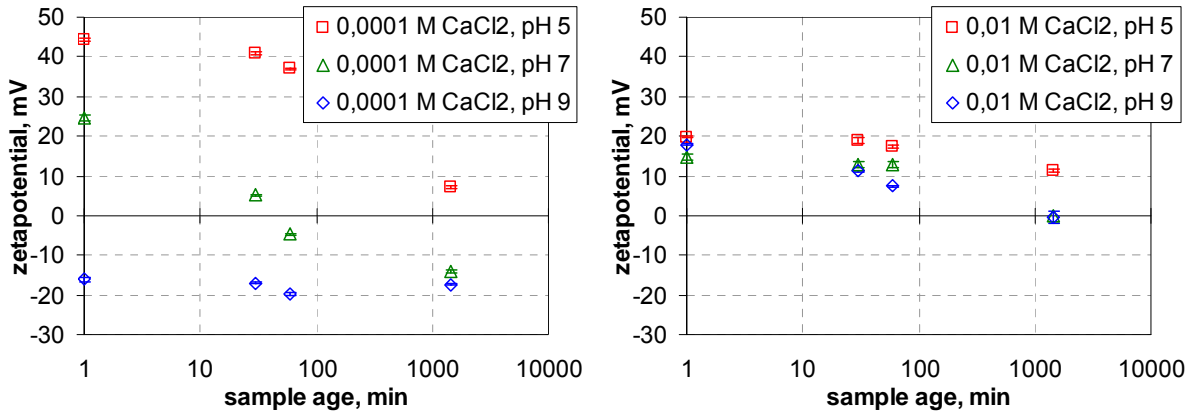


Figure 51: Evolution of zeta potential values for NM103 in 0.0001 M CaCl<sub>2</sub> and 0.01 M CaCl<sub>2</sub>, measured with μEP.

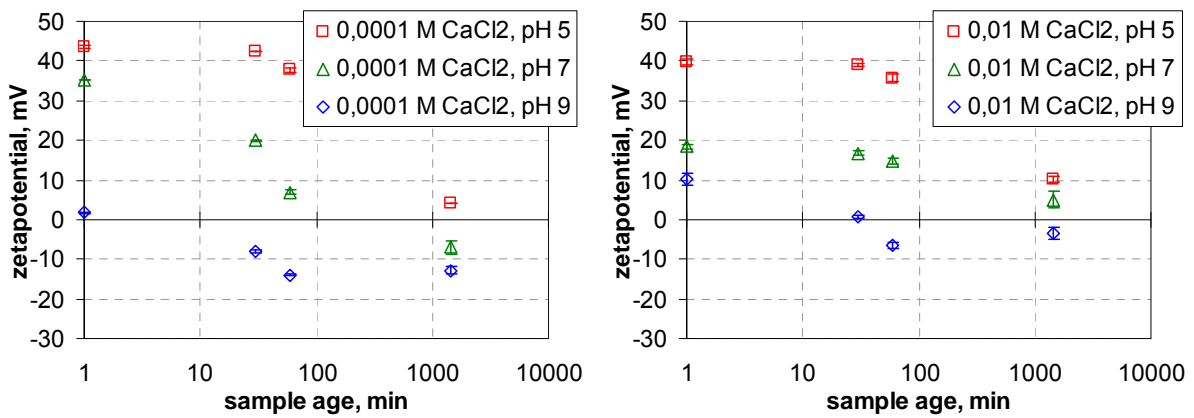


Figure 52: Evolution of zeta potential values for NM104 in 0.0001 M CaCl<sub>2</sub> and 0.01 M CaCl<sub>2</sub>, measured with μEP.

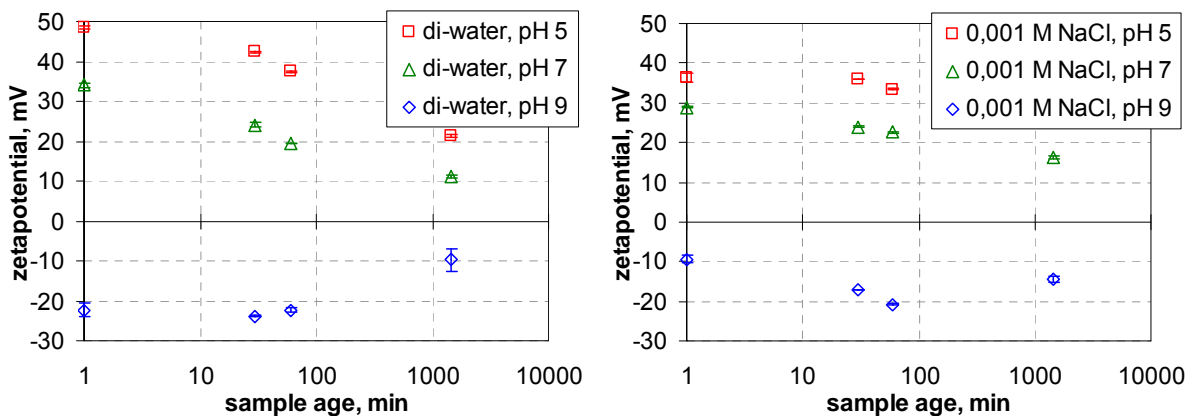


Figure 53: Evolution of zeta potential values for NM104 in DI-water and 0.001 M NaCl, measured with μEP.

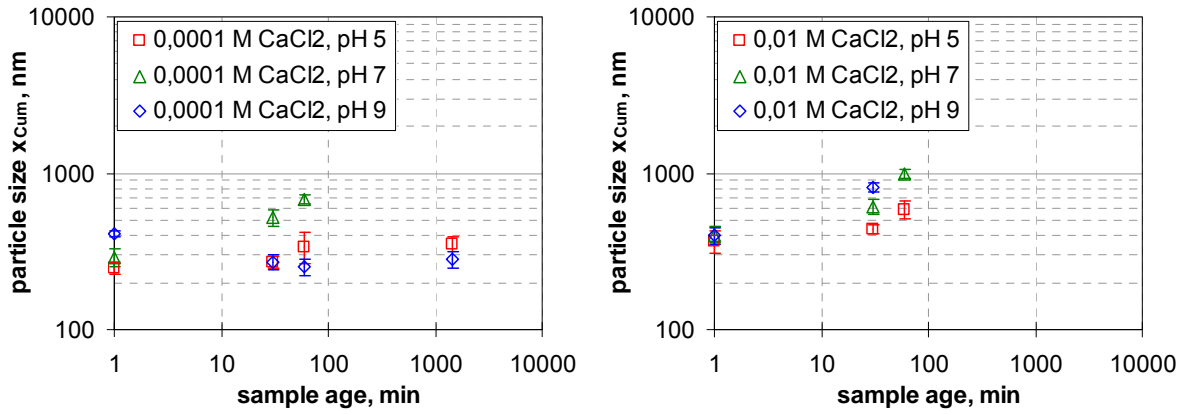


Figure 54: Evolution of average particle size ( $x_{cum}$ ) for NM103 in 0.0001 M CaCl<sub>2</sub> and 0.01 M CaCl<sub>2</sub>, measured with DLS.

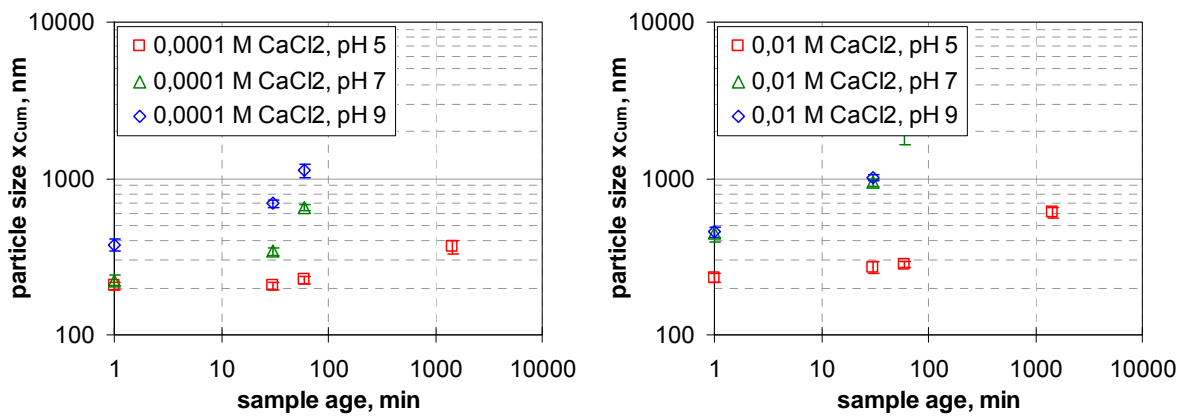


Figure 55: Evolution of average particle size ( $x_{cum}$ ) for NM104 in 0.0001 M CaCl<sub>2</sub> and 0.01 M CaCl<sub>2</sub>, measured with DLS.

The influence of divalent and monovalent ions on the agglomeration size in suspension and zeta potential was exemplarily tested for NM104 by using monovalent ions, here sodium chloride.

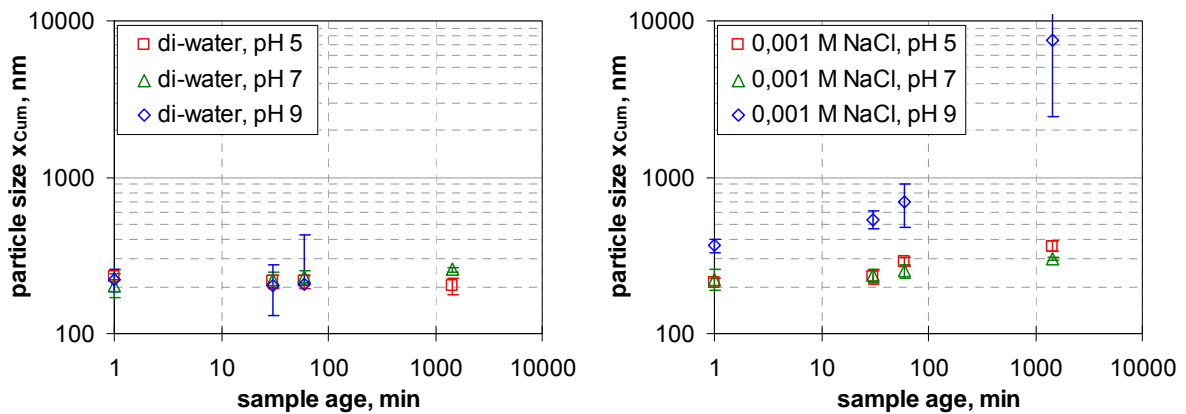


Figure 56: Evolution of average particle size ( $x_{cum}$ ) for NM104 in DI-water and 0.001 M NaCl, measured with DLS.

Table 24: Zeta potential of NM103 in aqueous CaCl<sub>2</sub> solutions, measured with ELS, titration from acid → basic → acid, averages from 3 independent samples.

pH	DI-water		0.0001 M CaCl <sub>2</sub>		0.001 M CaCl <sub>2</sub>		0.01 M CaCl <sub>2</sub>	
	ζ, mV	s(ζ) mV	ζ, mV	s(ζ) mV	ζ, mV	s(ζ) mV	ζ, mV	s(ζ) mV
4.5	38.8	1.3	34.6	3.3	37.3	0.2	40.9	0.7
5	37.7	1.8	34.8	2.7	39.5	1.7	40.6	0.4
6	32.1	1.8	30.8	2.6	37.3	1.9	38.2	0.4
7	25.3	1.6	26.4	1.2	31.4	2.7	33.2	1.0
8	12.3	8.4	14.0	5.9	18.7	5.5	26.3	0.3
9	-5.8	5.5	-0.5	9.8	9.8	5.3	19.3	1.3
10	-30.8	0.8	-16.0	4.8	4.9	4.0	19.2	2.6
9	-24.4	2.1	-13.4	4.0	3.1	4.2	15.9	1.9
8	-11.9	3.8	-7.1	6.6	5.3	4.5	12.3	1.9
7	12.6	2.0	10.7	4.9	15.7	5.0	20.5	0.2
6	23.9	4.7	24.6	1.8	28.0	3.8	29.3	1.0
5	35.1	0.9	32.1	0.4	36.4	1.7	37.9	0.5
4.5	37.0	0.0	33.8	0.5	37.6	1.6	39.2	0.6

 Table 25: Zeta potential of NM104 in aqueous CaCl<sub>2</sub> solutions, measured with ELS, titration from acid → basic → acid, averages from 3 independent samples.

pH	DI-water		0.0001 M CaCl <sub>2</sub>		0.001 M CaCl <sub>2</sub>		0.01 M CaCl <sub>2</sub>	
	ζ, mV	s(ζ) mV	ζ, mV	s(ζ) mV	ζ, mV	s(ζ) mV	ζ, mV	s(ζ) mV
4.5	38.6	2.8	37.2	2.9	38.8	2.5	40.5	1.1
5	38.1	2.7	36.4	2.2	39.9	1.4	40.4	1.7
6	32.7	2.5	32.7	2.6	35.1	2.2	38.1	1.8
7	26.3	1.1	25.5	4.0	27.0	2.3	32.4	2.3
8	7.2	7.1	16.6	4.3	19.6	2.2	25.1	2.3
9	-13.8	4.2	3.5	3.9	8.0	0.7	19.7	3.4
10	-29.1	3.0	-13.4	0.6	3.7	0.6	20.0	1.3
9	-24.5	1.3	-9.6	1.5	2.8	0.9	14.6	1.8
8	-9.8	5.6	-1.0	2.9	5.6	2.1	10.8	2.6
7	10.1	5.6	16.0	3.7	17.0	1.7	17.9	2.6
6	25.0	3.4	25.9	1.5	28.5	0.8	28.5	1.8
5	35.0	1.4	32.9	2.0	37.3	0.9	37.3	0.8
4.5	35.7	0.5	34.6	0.6	39.3	0.5	38.9	0.3



Table 26: Zeta potential of NM103 in 0.0001 M CaCl<sub>2</sub>, measured with  $\mu$ EP, independent samples for each pH value, averages from 3 repeated measurements.

pH	after 0 min		after 30 min		after 60 min		after 24 hours		
	$\zeta$ , mV	s( $\zeta$ ) mV	$\zeta$ , mV	s( $\zeta$ ) mV	$\zeta$ , mV	s( $\zeta$ ) mV	pH	$\zeta$ , mV	s( $\zeta$ ) mV
5	44.39	0.32	40.84	0.35	37.03	0.13	5.05	7.26	0.36
7.1	24.66	0.66	5.07	0.08	-4.74	0.23	6.6	-14.13	0.44
9	-16.12	0.66	-17.04	0.20	-19.77	0.38	7.1	-17.42	0.18

 Table 27: Zeta potential of NM103 in 0.001 M CaCl<sub>2</sub>, measured with  $\mu$ EP, independent samples for each pH value, averages from 3 repeated measurements.

pH	after 0 min		after 30 min		after 60 min		after 24 hours		
	$\zeta$ , mV	s( $\zeta$ ) mV	$\zeta$ , mV	s( $\zeta$ ) mV	$\zeta$ , mV	s( $\zeta$ ) mV	pH	$\zeta$ , mV	s( $\zeta$ ) mV
5	39.16	0.29	39.10	0.04	38.90	0.39	5.1	35.54	0.26
6.1	36.30	0.29	35.97	0.32	35.73	0.30	6.1	26.67	0.40
6.9	34.23	0.03	31.80	0.23	27.76	0.25	6.7	17.56	0.70
8.1	35.78	0.27	30.93	0.18	24.50	0.37	7	20.08	0.18
9	20.60	0.25	16.77	0.32	10.29	0.43	7	-11.29	0.39

 Table 28: Zeta potential of NM103 in 0.01 M CaCl<sub>2</sub>, measured with  $\mu$ EP, independent samples for each pH value, averages from 3 repeated measurements.

pH	after 0 min		after 30 min		after 60 min		after 24 hours		
	$\zeta$ , mV	s( $\zeta$ ) mV	$\zeta$ , mV	s( $\zeta$ ) mV	$\zeta$ , mV	s( $\zeta$ ) mV	pH	$\zeta$ , mV	s( $\zeta$ ) mV
5.06	19.85	0.34	18.97	0.81	17.32	0.43	5.11	11.27	0.45
7.08	14.72	0.65	12.95	0.71	12.86	0.79	7.18	-0.15	1.38
9.2	17.91	0.27	11.21	0.21	7.36	0.17	7.18	-0.39	1.53

 Table 29: Zeta potential of NM103 in 0.001 M CaCl<sub>2</sub>, dispersed with 10 min us-homogenizer instead of 1 min as in SOP, measured with  $\mu$ EP, independent samples for each pH value, averages from 3 repeated measurements.

pH	after 0 min		after 30 min		after 60 min		after 24 hours		
	$\zeta$ , mV	s( $\zeta$ ) mV	$\zeta$ , mV	s( $\zeta$ ) mV	$\zeta$ , mV	s( $\zeta$ ) mV	pH	$\zeta$ , mV	s( $\zeta$ ) mV
4.93	48.01	0.60	46.75	0.43	45.27	0.14	5.16	24.15	0.40
7.02	38.41	0.20	37.36	0.33	32.63	0.41	6.73	2.22	0.09
8.95	28.64	0.35	21.85	0.24	17.55	0.46	7.08	-6.69	0.19

Table 30: Zeta potential of NM104 in 0.0001 M CaCl<sub>2</sub>, measured with  $\mu$ EP, independent samples for each pH value, averages from 3 repeated measurements.

pH	after 0 min		after 30 min		after 60 min		after 24 hours		
	$\zeta$ , mV	s( $\zeta$ ) mV	$\zeta$ , mV	s( $\zeta$ ) mV	$\zeta$ , mV	s( $\zeta$ ) mV	pH	$\zeta$ , mV	s( $\zeta$ ) mV
4.9	43.52	0.43	42.37	0.13	37.74	0.46	5	4.25	0.01
7.1	35.23	0.16	19.89	0.27	6.86	0.60	6.67	-6.96	1.79
9	1.72	0.31	-8.12	0.37	-13.95	0.30	7.1	-12.76	0.78

 Table 31: Zeta potential of NM104 in 0.001 M CaCl<sub>2</sub>, measured with  $\mu$ EP, independent samples for each pH value, averages from 3 repeated measurements, series A.

pH	after 0 min		after 30 min		after 60 min		after 24 hours		
	$\zeta$ , mV	s( $\zeta$ ) mV	$\zeta$ , mV	s( $\zeta$ ) mV	$\zeta$ , mV	s( $\zeta$ ) mV	pH	$\zeta$ , mV	s( $\zeta$ ) mV
4.97	41.13	0.21	40.17	0.10	39.81	0.18	5.1	37.21	0.54
7.1	19.17	0.10	12.53	0.12	4.19	0.43	6.8	-0.46	1.01
8.96	15.09	0.47	9.71	0.18	2.67	0.27	7.46	0.28	0.70

 Table 32: Zeta potential of NM104 in 0.001 M CaCl<sub>2</sub>, measured with  $\mu$ EP, independent samples for each pH value, averages from 3 repeated measurements, series B.

pH	after 0 min		after 30 min		after 60 min		after 24 hours		
	$\zeta$ , mV	s( $\zeta$ ) mV	$\zeta$ , mV	s( $\zeta$ ) mV	$\zeta$ , mV	s( $\zeta$ ) mV	pH	$\zeta$ , mV	s( $\zeta$ ) mV
4.91	38.14	0.14	37.59	0.29	34.25	0.45	5.27	28.78	0.09
7.2	30.69	0.52	27.62	0.31	24.08	0.06	6.52	20.76	0.49
9	-1.39	0.67	-6.39	0.68	-11.63	0.39	7.12	-7.49	1.06

 Table 33: Zeta potential of NM104 in 0.001 M CaCl<sub>2</sub>, measured with  $\mu$ EP, independent samples for each pH value, averages from 3 repeated measurements, series C.

pH	after 0 min		after 30 min		after 60 min		after 24 hours		
	$\zeta$ , mV	s( $\zeta$ ) mV	$\zeta$ , mV	s( $\zeta$ ) mV	$\zeta$ , mV	s( $\zeta$ ) mV	pH	$\zeta$ , mV	s( $\zeta$ ) mV
4.95	44.61	0.51	43.08	0.20	40.59	0.46	5.13	35.42	0.36
7.1	30.19	0.16	24.82	0.37	20.85	0.26	6.7	-4.00	0.39
9	2.82	0.47	-7.38	0.47	-10.45	0.55	7.08	-10.90	2.66

Table 34: Zeta potential of NM104 in 0.01 M CaCl<sub>2</sub>, measured with  $\mu$ EP, independent samples for each pH value, averages from 3 repeated measurements.

pH	after 0 min		after 30 min		after 60 min		after 24 hours		
	$\zeta$ , mV	s( $\zeta$ ) mV	$\zeta$ , mV	s( $\zeta$ ) mV	$\zeta$ , mV	s( $\zeta$ ) mV	pH	$\zeta$ , mV	s( $\zeta$ ) mV
5.01	39.79	0.79	39.08	0.40	35.74	0.89	4.88	10.11	0.74
7.15	18.43	0.60	16.82	0.42	14.64	0.69	6.61	5.03	2.05
8.9	10.20	1.35	0.77	0.50	-6.50	0.85	7.65	-3.43	1.39

 Table 35: Zeta potential of NM104 in 0.001 M NaCl, measured with  $\mu$ EP, independent samples for each pH value, averages from 3 repeated measurements.

pH	after 0 min		after 30 min		after 60 min		after 24 hours		
	$\zeta$ , mV	s( $\zeta$ ) mV	$\zeta$ , mV	s( $\zeta$ ) mV	$\zeta$ , mV	s( $\zeta$ ) mV	pH	$\zeta$ , mV	s( $\zeta$ ) mV
4.9	36.33	0.15	36.03	0.25	33.43	0.21	5.2	29.67	0.25
6.9	28.90	0.20	24.00	0.20	22.53	0.15	6.8	16.20	0.36
9	-9.37	1.10	-17.13	0.12	-20.73	0.15	7.5	-14.50	0.66

 Table 36: Zeta potential of NM104 in 0.001 M CaCl<sub>2</sub>, dispersed with 10 min us-homogenizer instead of 1 min as in SOP, measured with  $\mu$ EP, independent samples for each pH value, averages from 3 repeated measurements.

pH	after 0 min		after 30 min		after 60 min		after 24 hours		
	$\zeta$ , mV	s( $\zeta$ ) mV	$\zeta$ , mV	s( $\zeta$ ) mV	$\zeta$ , mV	s( $\zeta$ ) mV	pH	$\zeta$ , mV	s( $\zeta$ ) mV
4.88	44.72	0.12	43.57	0.41	42.22	0.40	5.09	33.38	0.33
6.98	39.80	0.30	36.45	0.20	32.85	0.04	6.69	-3.97	0.42
8.94	24.62	0.12	20.06	0.04	13.41	0.71	7.1	-4.66	0.61

### AIII.10 Agglomeration in environmental media - DLS

Table 37: Mean particle size ( $x_{Cum}$ ) of NM103 in 0.0001 M CaCl<sub>2</sub>, measured with DLS, independent samples for each pH value, averages from 3 repeated measurements.

pH	after 0 min		after 30 min		after 60 min		after 24 hours		
	$x_{Cum}$ , nm	$s(x_{Cum})$ , nm	$x_{Cum}$ , nm	$s(x_{Cum})$ , nm	$x_{Cum}$ , nm	$s(x_{Cum})$ , nm	pH	$x_{Cum}$ , nm	$s(x_{Cum})$ , nm
5	248	22.2	269	22.6	338	76.9	5.05	355	39
7.1	291	40.6	521	63.5	676	43.5	6.6	0	0
9	410	16.5	272	31.9	253	30.2	7.1	281	34.1

Table 38: Mean particle size ( $x_{Cum}$ ) of NM103 in 0.001 M CaCl<sub>2</sub>, measured with DLS, independent samples for each pH value, averages from 3 repeated measurements.

pH	after 0 min		after 30 min		after 60 min		after 24 hours		
	$x_{Cum}$ , nm	$s(x_{Cum})$ , nm	$x_{Cum}$ , nm	$s(x_{Cum})$ , nm	$x_{Cum}$ , nm	$s(x_{Cum})$ , nm	pH	$x_{Cum}$ , nm	$s(x_{Cum})$ , nm
5	329	70.7	304	51.5	288	45.8	5.1	393	68.5
6.1	231	18.3	277	37.6	259	31.3	6.1	252	45.6
6.9	249	17.2	311	53.5	334	42.6	6.7	430	110
8.1	274	48.6	287	27.1	334	25.6	7	617	90.9
9	287	28.1	424	42.5	923	129	7	1170	98.1

Table 39: Mean particle size ( $x_{Cum}$ ) of NM103 in 0.01 M CaCl<sub>2</sub>, measured with DLS, independent samples for each pH value, averages from 3 repeated measurements.

pH	after 0 min		after 30 min		after 60 min		after 24 hours		
	$x_{Cum}$ , nm	$s(x_{Cum})$ , nm	$x_{Cum}$ , nm	$s(x_{Cum})$ , nm	$x_{Cum}$ , nm	$s(x_{Cum})$ , nm	pH	$x_{Cum}$ , nm	$s(x_{Cum})$ , nm
5.06	367	60.4	438	31.3	587	75.5	5.11	0	0
7.08	405	48.3	613	67.4	995	69.7	7.18	0	0
9.2	399	46	807	52.8	0	0	7.18	0	0

Table 40: Mean particle size ( $x_{Cum}$ ) of NM103 in 0.001 M CaCl<sub>2</sub>, dispersed with 10 min us-homogenizer instead of 1 min as in SOP, measured with DLS, independent samples for each pH value, averages from 3 repeated measurements.

pH	after 0 min		after 30 min		after 60 min		after 24 hours		
	$x_{Cum}$ , nm	$s(x_{Cum})$ , nm	$x_{Cum}$ , nm	$s(x_{Cum})$ , nm	$x_{Cum}$ , nm	$s(x_{Cum})$ , nm	pH	$x_{Cum}$ , nm	$s(x_{Cum})$ , nm
4.93	158	8.55	165	11.7	174	11.8	5.16	219	26.7
7.02	162	17.1	192	15.6	221	30.7	6.73	471	66.1
8.95	174	13.4	356	24.9	638	35.6	7.08	0	0

 Table 41: Mean particle size ( $x_{Cum}$ ) of NM104 in 0.0001 M CaCl<sub>2</sub>, measured with DLS, independent samples for each pH value, averages from 3 repeated measurements.

pH	after 0 min		after 30 min		after 60 min		after 24 hours		
	$x_{Cum}$ , nm	$s(x_{Cum})$ , nm	$x_{Cum}$ , nm	$s(x_{Cum})$ , nm	$x_{Cum}$ , nm	$s(x_{Cum})$ , nm	pH	$x_{Cum}$ , nm	$s(x_{Cum})$ , nm
4.9	205	9.71	206	10.3	225	13.4	5	364	33.4
7.1	223	17.6	341	18	651	29.6	6.67	0	0
9	375	30.3	690	37.3	1130	113	7.1	0	0

 Table 42: Mean particle size ( $x_{Cum}$ ) of NM104 in 0.001 M CaCl<sub>2</sub>, measured with DLS, independent samples for each pH value, averages from 3 repeated measurements, series A.

pH	after 0 min		after 30 min		after 60 min		after 24 hours		
	$x_{Cum}$ , nm	$s(x_{Cum})$ , nm	$x_{Cum}$ , nm	$s(x_{Cum})$ , nm	$x_{Cum}$ , nm	$s(x_{Cum})$ , nm	pH	$x_{Cum}$ , nm	$s(x_{Cum})$ , nm
4.97	198	6.03	205	7.91	214	4.15	5.1	213	21.5
7.1	275	21.5	566	60.6	0	0	6.8	0	0
8.96	304	32.1	610	30.1	1210	253	7.46	1890	369

 Table 43: Mean particle size ( $x_{Cum}$ ) of NM104 in 0.001 M CaCl<sub>2</sub>, measured with DLS, independent samples for each pH value, averages from 3 repeated measurements, series B.

pH	after 0 min		after 30 min		after 60 min		after 24 hours		
	$x_{Cum}$ , nm	$s(x_{Cum})$ , nm	$x_{Cum}$ , nm	$s(x_{Cum})$ , nm	$x_{Cum}$ , nm	$s(x_{Cum})$ , nm	pH	$x_{Cum}$ , nm	$s(x_{Cum})$ , nm
4.91	219	28.5	223	24.6	217	14.5	5.27	227	14.8
7.2	215	16	250	31.2	279	25.2	6.52	321	16.2
9	378	43.1	812	78.3	0	0	7.12	0	0

Table 44: Mean particle size ( $x_{Cum}$ ) of NM104 in 0.001 M CaCl<sub>2</sub>, measured with DLS, independent samples for each pH value, averages from 3 repeated measurements, series C.

pH	after 0 min		after 30 min		after 60 min		after 24 hours		
	$x_{Cum}$ , nm	$s(x_{Cum})$ , nm	$x_{Cum}$ , nm	$s(x_{Cum})$ , nm	$x_{Cum}$ , nm	$s(x_{Cum})$ , nm	pH	$x_{Cum}$ , nm	$s(x_{Cum})$ , nm
4.95	206	17.8	204	14.9	215	14.1	5.13	225	26.4
7.1	239	27.4	282	17.7	366	19	6.7	1290	96.3
9	359	30.7	681	52	0	0	7.08	0	0

 Table 45: Mean particle size ( $x_{Cum}$ ) of NM104 in 0.01 M CaCl<sub>2</sub>, measured with DLS, independent samples for each pH value, averages from 3 repeated measurements.

pH	after 0 min		after 30 min		after 60 min		after 24 hours		
	$x_{Cum}$ , nm	$s(x_{Cum})$ , nm	$x_{Cum}$ , nm	$s(x_{Cum})$ , nm	$x_{Cum}$ , nm	$s(x_{Cum})$ , nm	pH	$x_{Cum}$ , nm	$s(x_{Cum})$ , nm
5.01	232	14.8	272	24.3	281	11.7	4.88	607	44.1
7.15	443	50.8	939	47.8	2170	527	6.61	0	0
8.9	454	31.7	1020	43.8	0	0	7.65	0	0

 Table 46: Mean particle size ( $x_{Cum}$ ) of NM104 in 0.001 M NaCl, measured with DLS, independent samples for each pH value, averages from 3 repeated measurements.

pH	after 0 min		after 30 min		after 60 min		after 24 hours		
	$x_{Cum}$ , nm	$s(x_{Cum})$ , nm	$x_{Cum}$ , nm	$s(x_{Cum})$ , nm	$x_{Cum}$ , nm	$s(x_{Cum})$ , nm	pH	$x_{Cum}$ , nm	$s(x_{Cum})$ , nm
4.9	213	10.6	231	23.3	287	19.8	5.2	362	26.4
6.9	223	35.4	235	24.4	252	23.8	6.8	301	6.47
9	365	36	537	73.4	694	219	7.5	7520	5070

 Table 47: Mean particle size ( $x_{Cum}$ ) of NM104 in 0.001 M CaCl<sub>2</sub>, dispersed with 10 min us-homogenizer instead of 1 min as in SOP, measured with DLS, independent samples for each pH value, averages from 3 repeated measurements.

pH	after 0 min		after 30 min		after 60 min		after 24 hours		
	$x_{Cum}$ , nm	$s(x_{Cum})$ , nm	$x_{Cum}$ , nm	$s(x_{Cum})$ , nm	$x_{Cum}$ , nm	$s(x_{Cum})$ , nm	pH	$x_{Cum}$ , nm	$s(x_{Cum})$ , nm
4.88	164	7.51	168	13.7	177	6.9	5.09	180	8.26
6.98	162	4.45	179	10.2	192	11.3	6.69	301	16.7
8.94	166	4.68	388	17.8	772	27.1	7.1	0	0

### All.11 Zeta potential measurements of NM104 and NM103 in environmental like media - variation of dissolved organic carbon (DOC) concentration

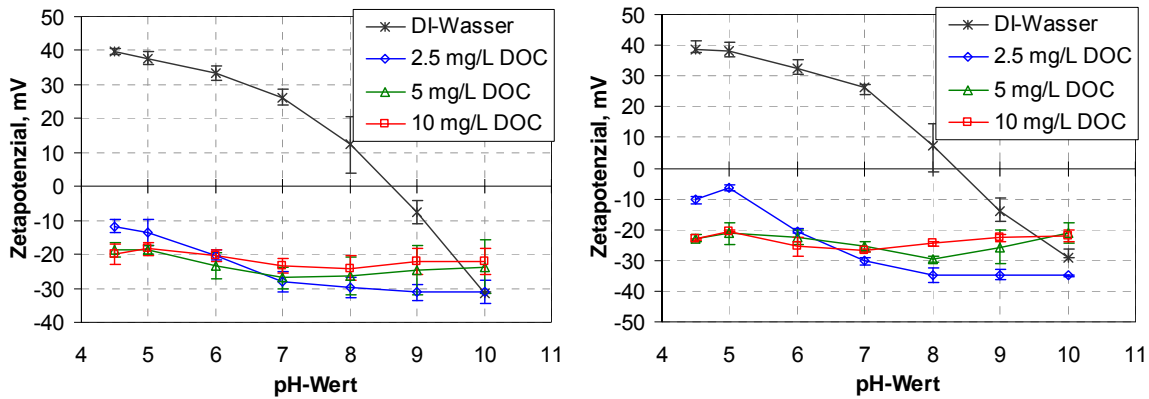


Figure 57: Zeta potential vs. pH for NM103 (left) and NM104 (right) in DOC solution, ELS (continuous titration from acid to basic).

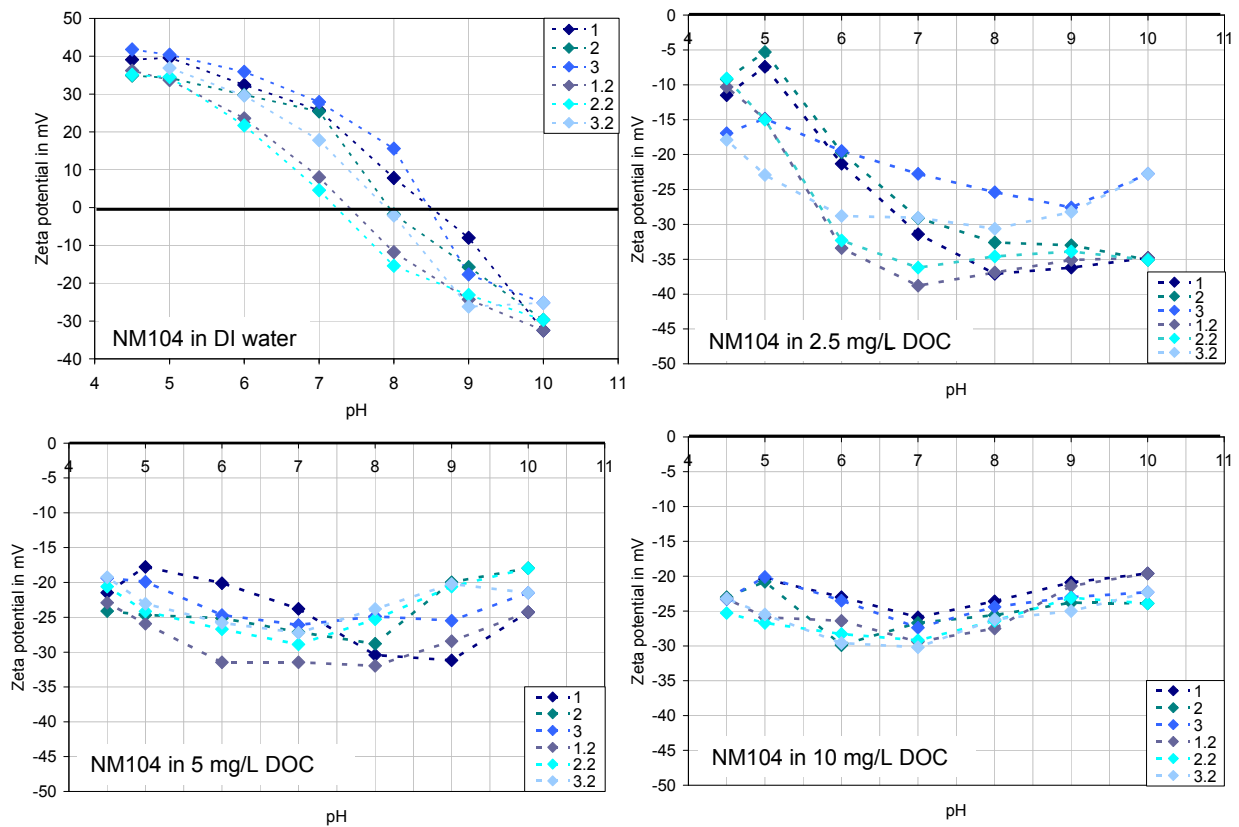


Figure 58: Zeta potential of three separate NM104 measurements in DI water (top left), with 2.5 mg/L DOC solution (top right), 5 mg/L DOC solution (bottom left) and 10 mg/L DOC solution (bottom right). The pH was varied in a first step from 4.5 to pH 10 (measurements 1 - 3) and in a second step back from pH 10 to pH 4.5 (measurements 1.2 - 3.2).

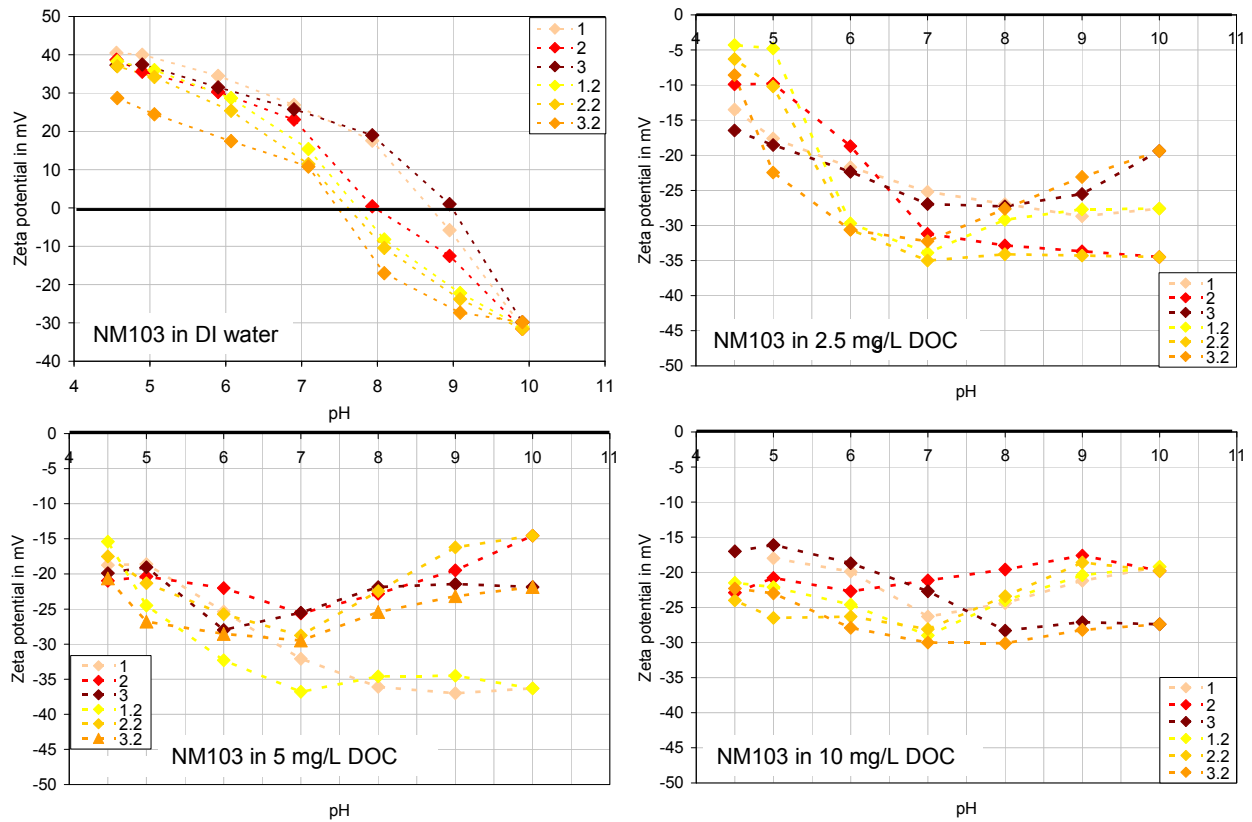


Figure 59: Zeta potential of three separate NM103 measurements in DI water (top left) with 2.5 mg/L DOC solution (top right), 5 mg/L DOC solution (bottom left) and 10 mg/L DOC solution (bottom right). The pH was varied in a first step from 4.5 to pH 10 (measurements 1 - 3) and in a second step back from pH 10 to pH 4.5 (measurements 1.2 - 3.2).

Based on the results of the direct measurements it was observed that with NOM here DOC (Aldrich humic Acid) no IEP was detected and the materials showed a negative zeta potential. No significant differences between the two materials were observed.

The aging of the suspension was observed at three different pH values (5, 7, 9) with  $\mu$ EP, after 30 min, 60 min and 24 h.



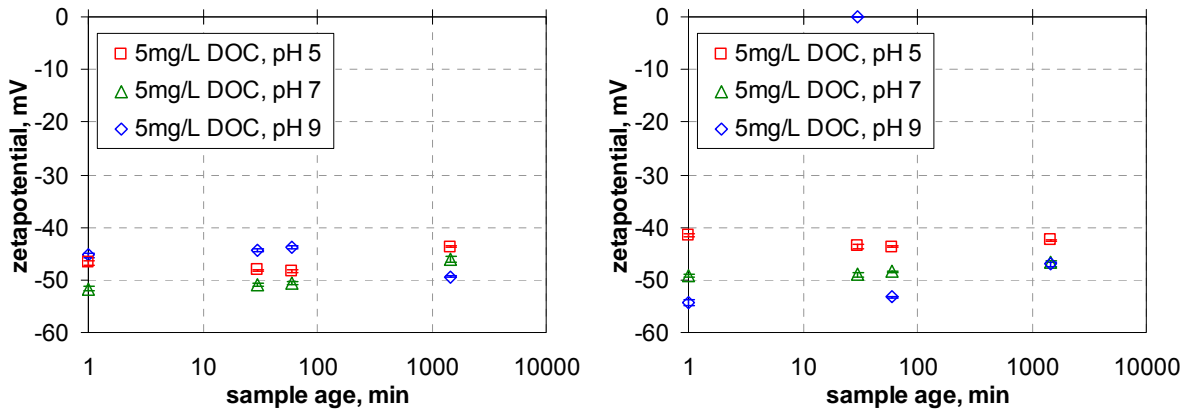


Figure 60: Evolution of zeta potential values for NM103 (left) and NM104 (right) in aqueous solution of 5 mg/L DOC, measured with  $\mu$ EP.

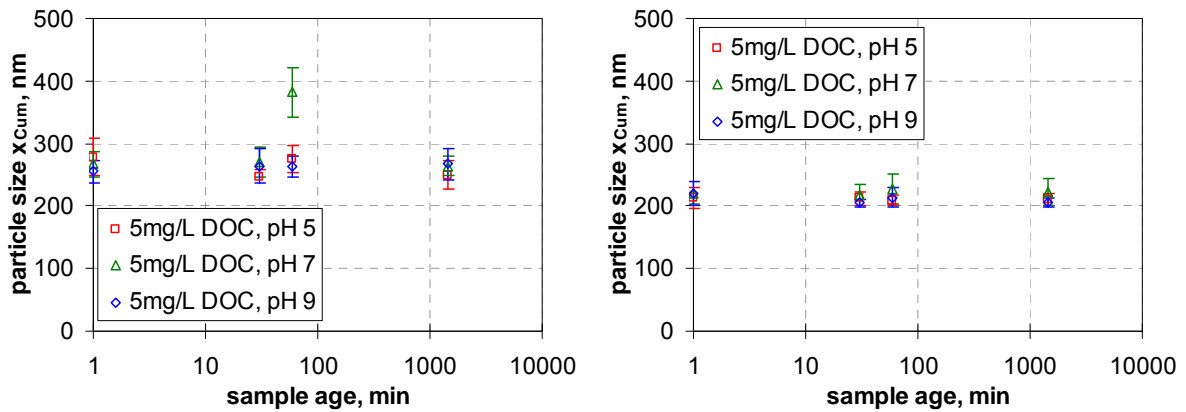


Figure 61: Evolution of average particle size ( $x_{cum}$ ) for NM103 (left) and NM104 (right) in aqueous solution of 5 mg/L DOC, measured with DLS.

In opposite to the electrolyte solutions there is no significant aging of the interfacial properties when the nanomaterials are suspended in DOC solution. Even more, the strong negative charging of the surfaces yield high suspension stability for the total pH range considered.

Table 48: Zeta potential of NM103 in aqueous solutions of DOC, measured with ELS, titration from acid → basic → acid, averages from 3 independent samples.

pH	DI-water		2.5 ppmw DOC		5 ppmw DOC		10 ppmw DOC	
	ζ, mV	s(ζ) mV	ζ, mV	s(ζ) mV	ζ, mV	s(ζ) mV	ζ, mV	s(ζ) mV
4.5	38.8	1.3	-13.3	2.7	-18.8	2.1	-20.0	3.0
5	37.7	1.8	-15.3	3.9	-18.8	1.2	-18.3	1.9
6	32.1	1.8	-20.9	1.6	-23.3	3.7	-20.4	1.7
7	25.3	1.6	-27.8	2.5	-26.9	3.1	-23.4	2.2
8	12.3	8.4	-29.0	2.7	-26.3	5.7	-24.1	3.6
9	-5.8	5.5	-29.3	3.4	-24.7	7.1	-22.0	3.9
10	-30.8	0.8	-27.2	6.2	-23.6	7.9	-22.1	3.7
9	-24.4	2.1	-28.4	4.6	-23.8	6.7	-22.4	4.2
8	-11.9	3.8	-30.3	2.8	-26.7	4.7	-25.8	3.0
7	12.6	2.0	-33.7	1.1	-30.8	3.5	-29.0	0.8
6	23.9	4.7	-30.3	0.4	-28.6	2.4	-26.3	1.3
5	35.1	0.9	-12.5	7.4	-24.4	2.0	-23.9	1.9
4.5	37.0	0.0	-6.4	1.7	-19.1	2.8	-22.6	1.0

Table 49: Zeta potential of NM104 in aqueous solutions of DOC, measured with ELS, titration from acid → basic → acid, averages from 3 independent samples.

pH	DI-water		2.5 ppmw DOC		5 ppmw DOC		10 ppmw DOC	
	ζ, mV	s(ζ) mV	ζ, mV	s(ζ) mV	ζ, mV	s(ζ) mV	ζ, mV	s(ζ) mV
4.5	38.6	2.8	-12.5	3.2	-21.6	1.9	-23.2	0.2
5	38.1	2.7	-9.2	4.1	-20.8	2.9	-20.4	0.3
6	32.7	2.5	-20.2	0.8	-23.3	2.3	-25.5	3.1
7	26.3	1.1	-27.8	3.7	-25.7	1.4	-26.7	0.6
8	7.2	7.1	-31.7	4.8	-28.0	2.3	-24.5	0.8
9	-13.8	4.2	-32.3	3.6	-25.5	4.6	-22.6	1.2
10	-29.1	3.0	-30.9	5.8	-21.2	2.6	-21.9	1.8
9	-24.5	1.3	-32.4	3.0	-23.1	3.8	-23.2	1.5
8	-9.8	5.6	-34.0	2.6	-27.0	3.5	-26.7	0.6
7	10.1	5.6	-34.7	4.1	-29.2	1.7	-29.6	0.4
6	25.0	3.4	-31.5	2.0	-28.0	2.5	-28.1	1.3
5	35.0	1.4	-17.6	3.8	-24.4	1.2	-26.0	0.5
4.5	35.7	0.5	-12.4	3.9	-20.9	1.5	-23.9	1.0

Table 50: Zeta potential of NM103 in 2.5 ppmw DOC, measured with μEP, independent samples for each pH value, averages from 3 repeated measurements.

pH	after 0 min		after 30 min		after 60 min		after 24 hours		
	ζ, mV	s(ζ) mV	ζ, mV	s(ζ) mV	ζ, mV	s(ζ) mV	pH	ζ, mV	s(ζ) mV
4.95	-41.85	1.01	-42.52	0.63	-42.82	0.60	5	-39.41	0.32
7.1	-43.51	0.14	-43.19	0.09	-42.68	0.20	6.57	-41.77	0.75
9.2	-44.75	1.93	-42.84	0.99	-41.47	0.51	6.72	-42.97	0.21

Table 51: Zeta potential of NM103 in 5 ppmw DOC, measured with μEP, independent samples for each pH value, averages from 3 repeated measurements.

pH	after 0 min		after 30 min		after 60 min		after 24 hours		
	ζ, mV	s(ζ) mV	ζ, mV	s(ζ) mV	ζ, mV	s(ζ) mV	pH	ζ, mV	s(ζ) mV
4.9	-46.73	0.49	-48.13	0.20	-48.26	0.26	4.86	-43.66	0.26
7.15	-51.67	0.47	-50.85	0.36	-50.64	0.33	6.24	-45.99	0.54
8.9	-45.24	0.40	-44.37	0.22	-43.74	0.24	7.23	-49.45	0.17

Table 52: Zeta potential of NM103 in 10 ppmw DOC, measured with  $\mu$ EP, independent samples for each pH value, averages from 3 repeated measurements.

pH	after 0 min		after 30 min		after 60 min		after 24 hours		
	$\zeta$ , mV	s( $\zeta$ ) mV	$\zeta$ , mV	s( $\zeta$ ) mV	$\zeta$ , mV	s( $\zeta$ ) mV	pH	$\zeta$ , mV	s( $\zeta$ ) mV
5.08	-42.00	0.25	-43.69	0.76	-44.53	0.31	5.25	-42.91	1.26
6.92	-47.85	0.82	-48.47	0.45	-47.97	0.39	6.42	-45.82	0.03
8.94	-46.99	0.72	-45.82	1.00	-47.52	0.16	7.06	-41.35	0.07

 Table 53: Zeta potential of NM104 in di-water, measured with  $\mu$ EP, independent samples for each pH value, averages from 3 repeated measurements.

pH	after 0 min		after 30 min		after 60 min		after 24 hours		
	$\zeta$ , mV	s( $\zeta$ ) mV	$\zeta$ , mV	s( $\zeta$ ) mV	$\zeta$ , mV	s( $\zeta$ ) mV	pH	$\zeta$ , mV	s( $\zeta$ ) mV
5.05	48.59	0.45	42.43	0.18	37.49	0.21	5.33	21.34	0.27
7.04	34.03	0.52	24.15	0.40	19.44	0.16	6.28	11.06	0.45
9.02	-22.27	1.52	-23.79	0.19	-22.29	0.50	6.92	-9.76	2.80

 Table 54: Zeta potential of NM104 in 2.5 ppmw DOC, measured with  $\mu$ EP, independent samples for each pH value, averages from 3 repeated measurements.

pH	after 0 min		after 30 min		after 60 min		after 24 hours		
	$\zeta$ , mV	s( $\zeta$ ) mV	$\zeta$ , mV	s( $\zeta$ ) mV	$\zeta$ , mV	s( $\zeta$ ) mV	pH	$\zeta$ , mV	s( $\zeta$ ) mV
4.8	-42.00	0.40	-43.58	0.14	-43.92	0.15	5.3	-46.53	0.24
6.9	-45.58	0.63	-45.57	0.33	-45.75	0.31	6.5	-46.96	0.40
9	-48.18	1.05	-46.09	1.43	-44.74	0.73	7.5	-42.75	0.39

 Table 55: Zeta potential of NM104 in 5 ppmw DOC, measured with  $\mu$ EP, independent samples for each pH value, averages from 3 repeated measurements.

pH	after 0 min		after 30 min		after 60 min		after 24 hours		
	$\zeta$ , mV	s( $\zeta$ ) mV	$\zeta$ , mV	s( $\zeta$ ) mV	$\zeta$ , mV	s( $\zeta$ ) mV	pH	$\zeta$ , mV	s( $\zeta$ ) mV
4.8	-41.58	0.26	-43.59	0.45	-43.72	0.08	4.9	-42.50	0.23
7.2	-49.21	0.25	-48.96	0.39	-48.38	0.11	6.5	-46.53	0.08
9	-54.34	0.61	k.A.	k.A.	-53.21	0.14	6.7	-47.03	0.45

Table 56: Zeta potential of NM104 in 10 ppmw DOC, measured with  $\mu$ EP, independent samples for each pH value, averages from 3 repeated measurements.

pH	after 0 min		after 30 min		after 60 min		after 24 hours		
	$\zeta$ , mV	s( $\zeta$ ) mV	$\zeta$ , mV	s( $\zeta$ ) mV	$\zeta$ , mV	s( $\zeta$ ) mV	pH	$\zeta$ , mV	s( $\zeta$ ) mV
4.91	-39.94	0.42	-40.05	1.08	-43.55	0.73	5.65	-41.99	0.39
7.03	-46.68	2.93	-44.51	3.66	-47.37	2.17	6.86	-46.36	0.50
8.9	-49.76	0.29	-48.35	3.20	-52.33	6.38	7.44	-44.91	0.58

## Agglomeration in environmental media - DLS

Table 57: Mean particle size ( $x_{Cum}$ ) of NM103 in 2.5 ppmw DOC, measured with DLS, independent samples for each pH value, averages from 3 repeated measurements.

pH	after 0 min		after 30 min		after 60 min		after 24 hours		
	$x_{Cum}$ , nm	$s(x_{Cum})$ , nm	$x_{Cum}$ , nm	$s(x_{Cum})$ , nm	$x_{Cum}$ , nm	$s(x_{Cum})$ , nm	pH	$x_{Cum}$ , nm	$s(x_{Cum})$ , nm
4.95	276	54.8	257	21.6	248	25.7	5	291	68.6
7.1	263	44.3	258	45.8	243	38.7	6.57	263	47.5
9.2	256	38.6	261	27.5	245	40.6	6.72	247	26.6

Table 58: Mean particle size ( $x_{Cum}$ ) of NM103 in 5 ppmw DOC, measured with DLS, independent samples for each pH value, averages from 3 repeated measurements.

pH	after 0 min		after 30 min		after 60 min		after 24 hours		
	$x_{Cum}$ , nm	$s(x_{Cum})$ , nm	$x_{Cum}$ , nm	$s(x_{Cum})$ , nm	$x_{Cum}$ , nm	$s(x_{Cum})$ , nm	pH	$x_{Cum}$ , nm	$s(x_{Cum})$ , nm
4.9	278	29.6	247	10.4	276	21.5	4.86	250	23.7
7.15	267	19.4	270	23.9	382	40.2	6.24	264	15.7
8.9	255	18	264	28.1	263	16.3	7.23	267	24.8

Table 59: Mean particle size ( $x_{Cum}$ ) of NM103 in 10 ppmw DOC, measured with DLS, independent samples for each pH value, averages from 3 repeated measurements.

pH	after 0 min		after 30 min		after 60 min		after 24 hours		
	$x_{Cum}$ , nm	$s(x_{Cum})$ , nm	$x_{Cum}$ , nm	$s(x_{Cum})$ , nm	$x_{Cum}$ , nm	$s(x_{Cum})$ , nm	pH	$x_{Cum}$ , nm	$s(x_{Cum})$ , nm
5.08	262	39.1	238	33.4	247	22.8	5.25	247	32.2
6.92	264	38.3	264	29.8	241	26	6.42	246	22.8
8.94	256	15.5	249	38.8	237	29.2	7.06	286	21.5

Table 60: Mean particle size ( $x_{Cum}$ ) of NM104 in di-water, measured with DLS, independent samples for each pH value, averages from 3 repeated measurements.

pH	after 0 min		after 30 min		after 60 min		after 24 hours		
	$x_{Cum}$ , nm	$s(x_{Cum})$ , nm	$x_{Cum}$ , nm	$s(x_{Cum})$ , nm	$x_{Cum}$ , nm	$s(x_{Cum})$ , nm	pH	$x_{Cum}$ , nm	$s(x_{Cum})$ , nm
5.05	230	10.6	215	23.3	215	19.8	5.33	202	26.4
7.04	204	35.4	223	24.4	230	23.8	6.28	256	6.47
9.02	222	36	203	73.4	206	219	6.92	0	5070

Table 61: Mean particle size ( $x_{Cum}$ ) of NM104 in 2.5 ppmw DOC, measured with DLS, independent samples for each pH value, averages from 3 repeated measurements.

pH	after 0 min		after 30 min		after 60 min		after 24 hours		
	$x_{Cum}$ , nm	$s(x_{Cum})$ , nm	$x_{Cum}$ , nm	$s(x_{Cum})$ , nm	$x_{Cum}$ , nm	$s(x_{Cum})$ , nm	pH	$x_{Cum}$ , nm	$s(x_{Cum})$ , nm
4.8	213	7.92	218	11.1	212	13.8	5.3	226	19.9
6.9	220	16.4	215	18	222	20.7	6.5	214	9.51
9	215	7.22	220	18.1	213	8.96	7.5	218	19.6

 Table 62: Mean particle size ( $x_{Cum}$ ) of NM104 in 5 ppmw DOC, measured with DLS, independent samples for each pH value, averages from 3 repeated measurements.

pH	after 0 min		after 30 min		after 60 min		after 24 hours		
	$x_{Cum}$ , nm	$s(x_{Cum})$ , nm	$x_{Cum}$ , nm	$s(x_{Cum})$ , nm	$x_{Cum}$ , nm	$s(x_{Cum})$ , nm	pH	$x_{Cum}$ , nm	$s(x_{Cum})$ , nm
4.8	213	16.2	212	10.9	209	8.57	4.9	211	9.81
7.2	221	17.1	217	18.3	227	23.5	6.5	222	21.6
9	220	18.9	205	6.29	214	14.9	6.7	206	7.32

 Table 63: Mean particle size ( $x_{Cum}$ ) of NM104 in 10 ppmw DOC, measured with DLS, independent samples for each pH value, averages from 3 repeated measurements.

pH	after 0 min		after 30 min		after 60 min		after 24 hours		
	$x_{Cum}$ , nm	$s(x_{Cum})$ , nm	$x_{Cum}$ , nm	$s(x_{Cum})$ , nm	$x_{Cum}$ , nm	$s(x_{Cum})$ , nm	pH	$x_{Cum}$ , nm	$s(x_{Cum})$ , nm
4.91	199	11.2	204	12.8	205	11.7	5.65	210	12.8
7.03	216	16.8	206	8.12	212	17.9	6.86	208	9.28
8.9	209	12.4	216	20.6	207	9.6	7.44	220	23.3

### AIII.12 Zeta potential measurements of NM104 and NM103 in environmental like media - in a mixture of CaCl<sub>2</sub> and dissolved organic carbon (DOC)

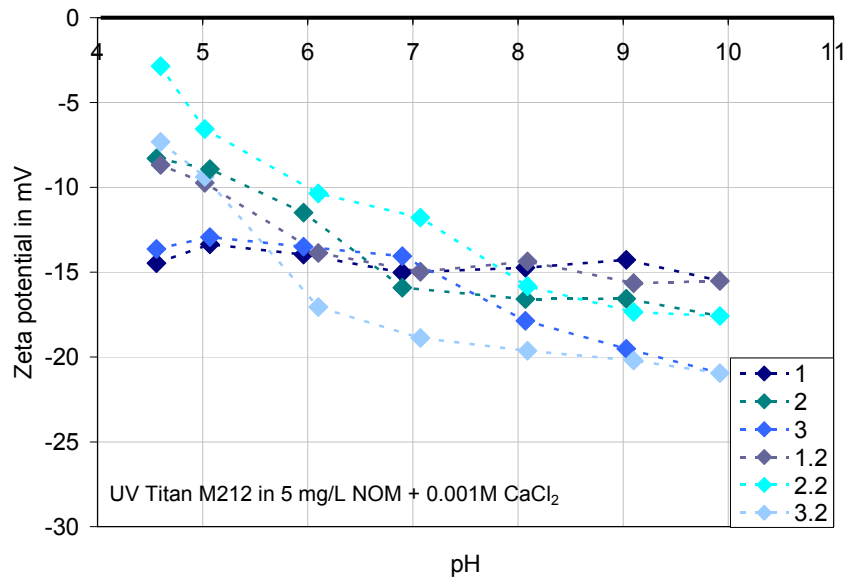


Figure 62: Zeta potential measurements of NM104 in 5 mg/L NOM and 0.001M CaCl<sub>2</sub> solution. The pH was varied in a first step from 4.5 to pH 10 and in a second step back from pH 10 to pH 4.5.

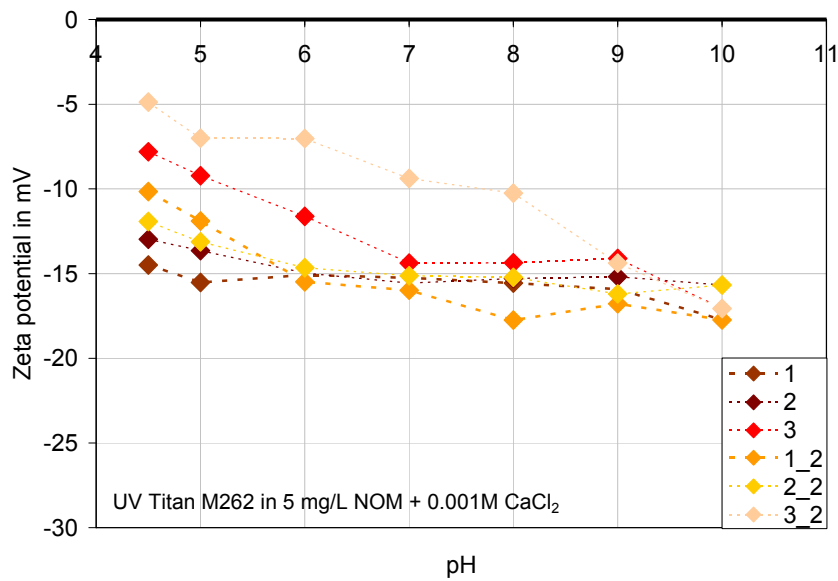


Figure 63: Zeta potential measurements of NM103 in 5 mg/L NOM and 0.001M CaCl<sub>2</sub> solution. The pH was varied in a first step from 4.5 to pH 10 and in a second step back from pH 10 to pH 4.5.



## Annex IV Results of the soil experiments

### AIV.1 Detailed analysis data of the employed soils

Table 64: Detailed analysis data of the used soils - Soil A01 Dystric Cambisol - AV = Average, COV = coefficient of variation. A = field.

Dystric Cambisol - A01			
	AV	COV	Unit
Sand	71	5.8	(weight-%)
Silt	24	13.8	(weight-%)
Clay	5	19	(weight-%)
pH	5.67	4	
OC	0.93	24.7	(%)
N	882	11.5	(mg/kg)
CEC <sub>eff</sub>	37.9	25.8	(mmolc/kg)
Fe <sub>ox</sub>	1.57	15.3	(mmolc/kg)
Al <sub>ox</sub>	0.95	6.5	(mmolc/kg)
Watercapacity*	264		(mL/kg)

eff = effective, ox = oxalate, \* only IME laboratory

Table 65: Detailed analysis data of the used soils - Soil A02 Stagnic Luvisol - AV = Average, COV = coefficient of variation. A = field.

Stagnic Luvisol - A02			
	AV	COV	Unit
Sand	2	45	[weight-%]
Silt	84	1.6	[weight-%]
Clay	15	8.7	[weight-%]
pH	6,63	2.4	
OC	1.3	4.9	[%]
N	1500	2	[mg/kg]
CEC <sub>eff</sub>	133.2	6.8	[mmolc/kg]
Fe <sub>ox</sub>	3.54	16.2	[mmolc/kg]
Al <sub>ox</sub>	0.69	0.8	[mmolc/kg]
Watercapacity*	419		[mL/kg]

eff = effective, ox = oxalate, \* only IME laboratory

Table 66: Detailed analysis data of the used soils - Soil G03 Eutric Cambisol - AV = Average, COV = coefficient of variation. A = field.

Eutric Cambisol - G03			
	AV	COV	Unit
Sand	21	29	[weight-%]
Silt	52	8.3	[weight-%]
Clay	27	9.8	[weight-%]
pH	5,64	1.2	
OC	3,85	4.5	[%]
N	4179	9.1	[mg/kg]
CEC <sub>eff</sub>	135.8	6.3	[mmolc/kg]
Fe <sub>ox</sub>	6.66	19.4	[mmolc/kg]
Al <sub>ox</sub>	2.32	4.4	[mmolc/kg]
Watercapacity*	768		[mL/kg]

eff = effective, ox = oxalate, \* only IME laboratory

#### AIV.2 Quality assurance ICP-OES measurements of the soil samples

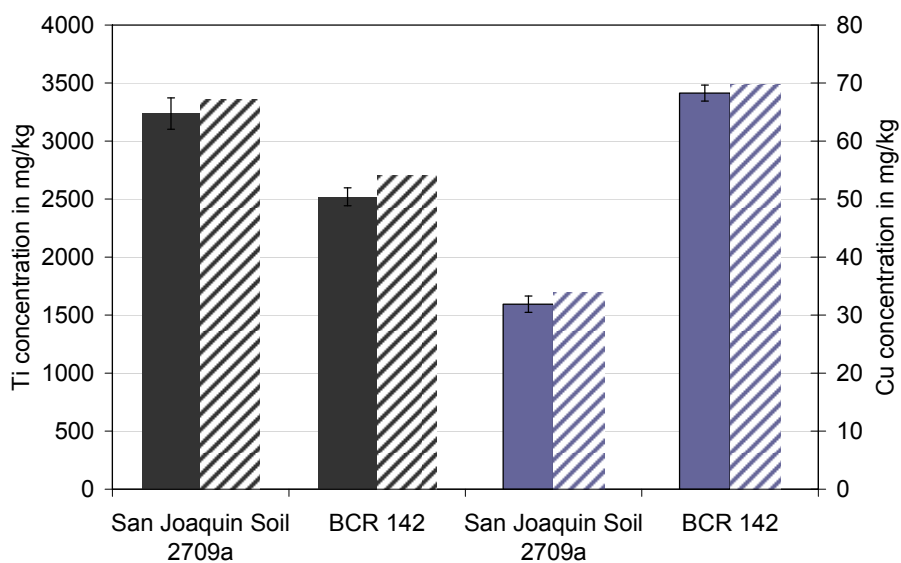


Figure 64: Measured (full bars) and default values (dashed bars) of Ti concentration and Cu concentration of two reference soils: error bars = standard deviation; n = 8. The certified value for Ti is 3360 mg/kg and for Cu 33.9 mg/kg for San Joaquin soil 2709a and 2700 mg/kg for Ti and 69.7 mg/kg for Cu for BCR.

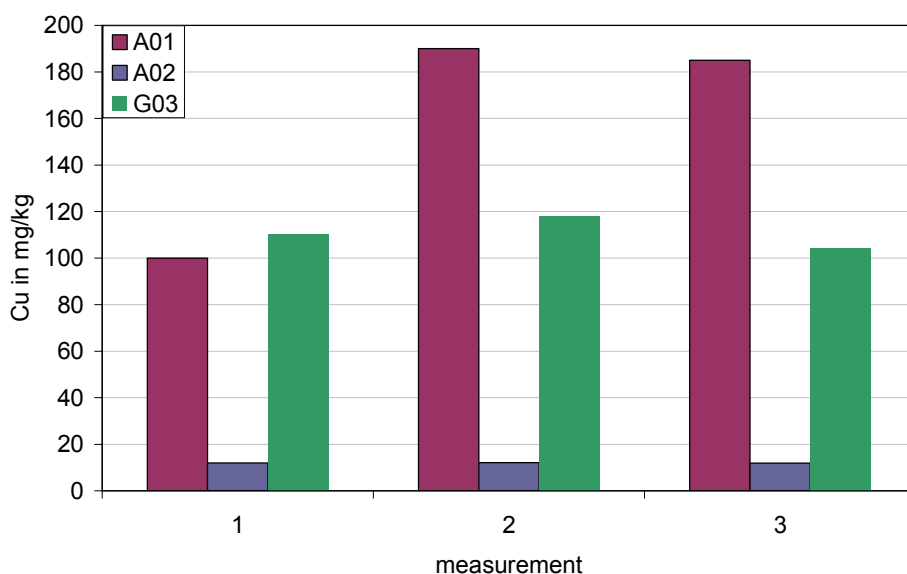


Figure 65: Determination of the reproducibility of the digestion method and ICP-OES measurements of the copper concentration in one segment of the three soil types.

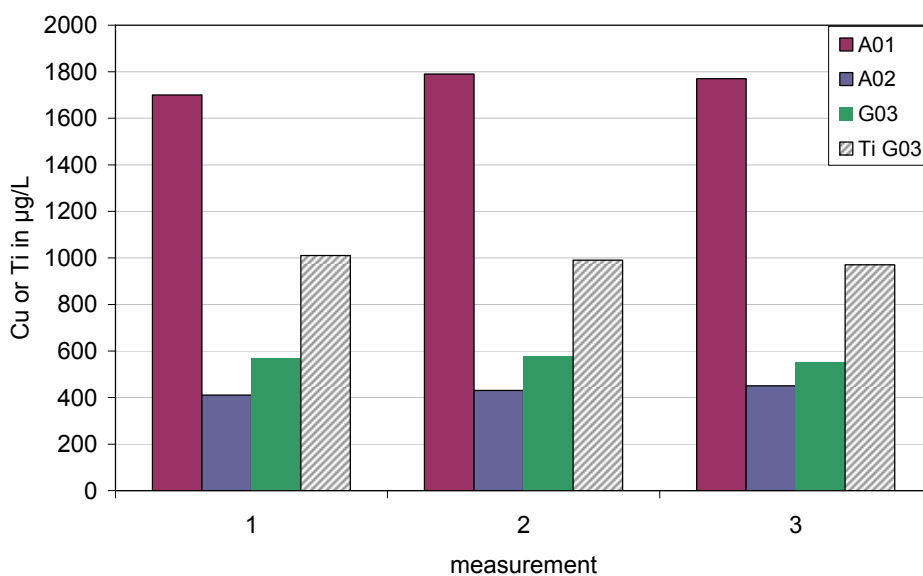


Figure 66: Determination of the reproducibility of the digestion method and ICP-OES measurements of the copper (full bars) and Ti (dashed bars) concentration in the eluate of the three soil types.

### AIV.3 Breakthrough curves of the tested soil types

Breakthrough experiments are commonly performed a priori to define or test possible transport processes in general. Consequently before the leaching experiments were conducted with the nanomaterials, breakthrough curves of the soils A01, A06 and A04 with a 0.1 M NaCl solution were performed.

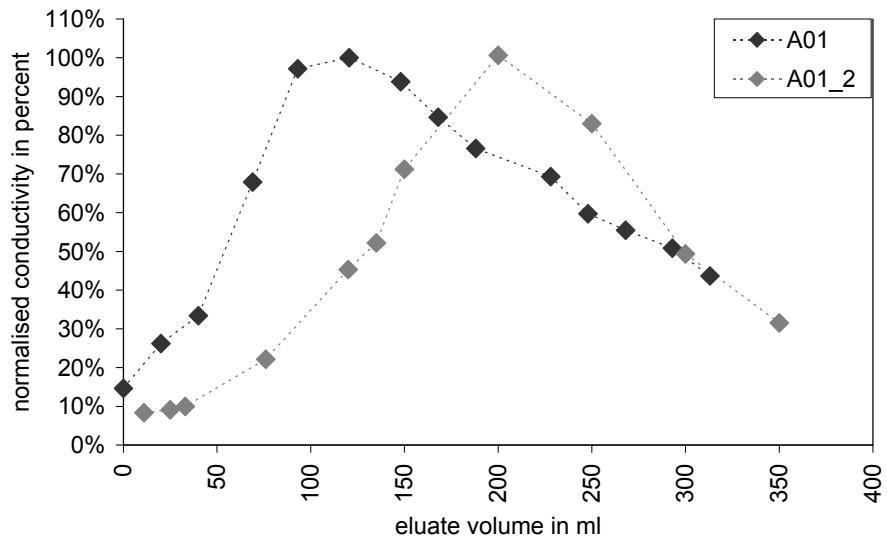


Figure 67: Breakthrough curve of soil type A01 - Dystric Cambisol normalized to the initial conductivity in percent conducted in both laboratories (IUTA and RWTH).

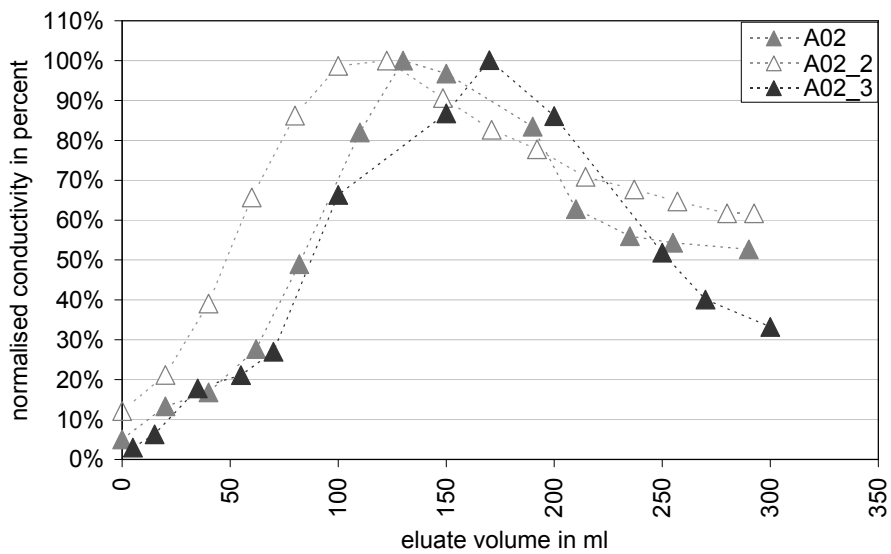


Figure 68: Breakthrough curve of soil type A02 - Stagnic Luvisol normalized to the initial conductivity in percent conducted in both laboratories (IUTA and RWTH).

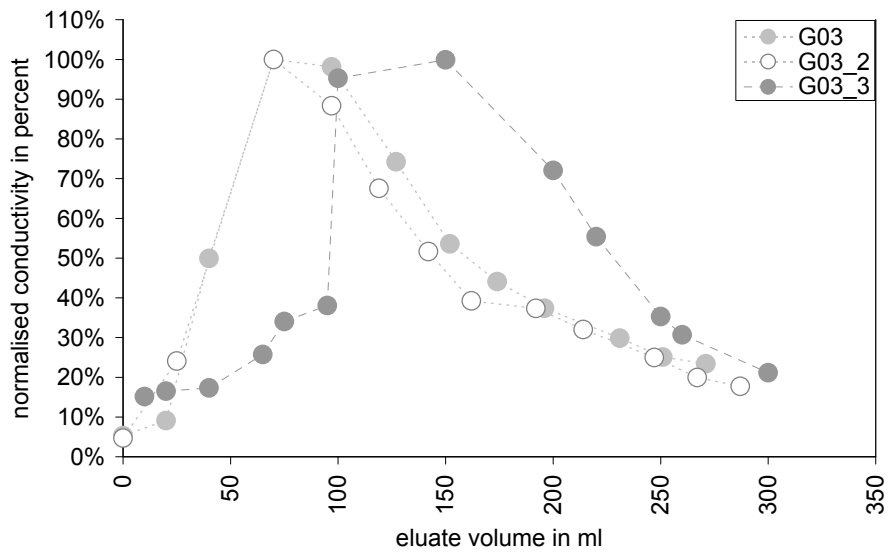


Figure 69: Breakthrough curve of soil type G03 - Eutric Cambisol normalized to the initial conductivity in percent conducted in both laboratories (IUTA and RWTH).

#### AIV.4 Background concentration of Ti and Cu in the tested soil types

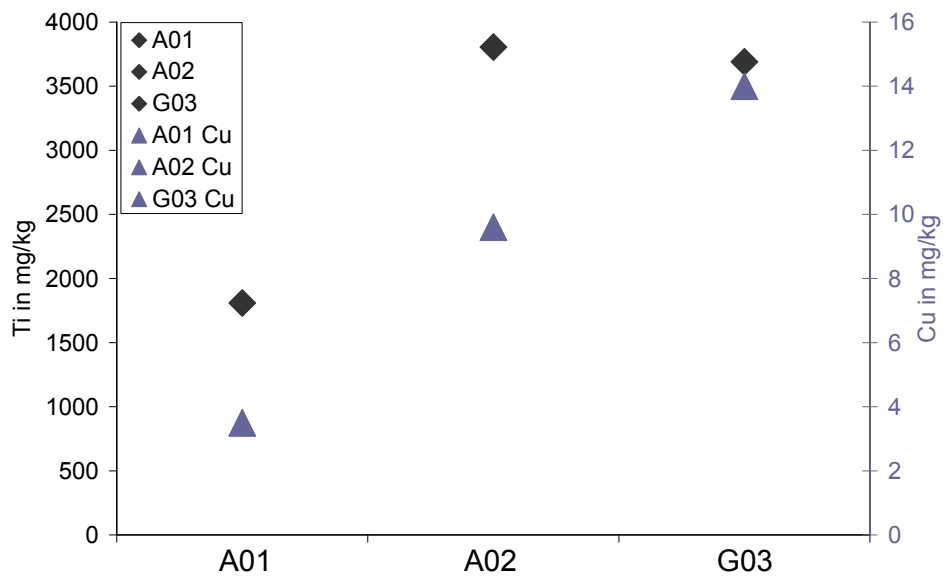


Figure 70: Background concentration of Ti diamonds and Cu triangle for the three tested soil types, n = 2.

### AIV.5 Results Zeta potential measurements different TiO<sub>2</sub> materials in DI water, 0.01M CaCl<sub>2</sub> solution and soil eluate

zeta potential were analysed with  $\mu$ EP

Table 67: Zeta potential of TiO<sub>2</sub> in deionised Water as function of time after dilution of the stock suspension. Measurements were conducted 1 day after suspension preparation, zeta potential was analysed with  $\mu$ EP. NM101 = Hombikat UV100, NM102 = PC105.

Sample	zeta potential			pH	DLS*	
	1.	2.	3.		z-average	Pdl
	mV	mV	mV	-	nm	-
NM-101 Nr. 1423				5.9	1.560	0.299
After 24h	18.0	18.5	19.4			
After 24h and 20 min	19.9	20.3	20.7			
40 min	18.7	18.9	18.9			
60 min	22.6	22.5	23.5	5.1		
120 min	23.3	22.4	22.8			
NM-102				4.6	710	0.356
After 24h	8.6	12.6	15.5			
After 24h and 20 min	27.3	27.4	28.2			
40 min	30.0	29.6	29.5			
60 min	30.7	30.2	30.1	4.8		
120 min	29.4	29.1	29.0			
P25 Nr. 0084				4.5	248	0.260
After 24h	16.7	21.2	24.7			
After 24h and 20 min	36.4	35.6	36.2			
40 min	38.1	37.2	37.4			
60 min	38.6	38.9	38.6	5.0		
120 min	40.0	39.7	38.7			

\* Measurements were conducted with a concentration of 100 ppm

Table 68: Zeta potential of TiO<sub>2</sub> in deionised water. Measurements were conducted 1 day after suspension preparation and 1 h after dilution, zeta potential was analysed with  $\mu$ EP. NM101 = Hombikat UV100, NM102 = PC105

sample	zeta potential			pH		DLS*	
	1.	2.	3.			z-average	Pdl
	mV	mV	mV	-	$\mu$ S/cm	nm	-
NM-101.Nr. 1423				5.9	13.7	1.560	0.299
... diluted	22.6	22.5	23.5	5.1	1		
NM-101.Nr. 1423				5.9	15.5	1.030	0.412
... diluted	22.0	21.9	21.9	4.9	1		
NM-101.Nr. 1423				5.9	15.5	1.140	0.368
... diluted	23.7	24.0	24.1	4.7	1		
NM-102				4.6	10.8	710	0.356
... diluted	30.7	30.2	30.1	4.8	1		
NM-102				4.9	9.7	915	0.478
... diluted	30.0	29.0	29.0	4.7	1		
NM-102				4.3	8.9	898	0.431
... diluted	27.4	27.8	28.1	4.7	1		
P25 Nr. 0084				4.5	8.3	248	0.260
... diluted	38.6	38.9	38.6	5.0	1		
P25 Nr. 0084				3.8	13.5	223	0.243
... diluted	41.8	41.5	41.8	4.6	1		
P25 Nr. 0083				4.3	11.9	228	0.246
... diluted	32.5	32.3	32.5	5.0	1		

\*Measurements were conducted with a concentration of 100 ppm

Table 69: Zeta potential of TiO<sub>2</sub> in 0.01 M CaCl<sub>2</sub>-solution as function of time after dilution of the stock suspension with 0.01 M CaCl<sub>2</sub>-solution. NM101 = Hombikat UV100, NM102 = PC105. Measurements were conducted 1 day after suspension preparation, zeta potential was analysed with  $\mu$ EP.

Sample	zeta potential			pH		DLS*	
	1.	2.	3.			z-average	Pdl
	mV	mV	mV	-	$\mu$ S/cm	nm	-
NM-101 Nr. 1423 - diluted				6.1	2.119	2.300	0.263
after 1 day	17.7	16.2	16.9	5.9	2.114		
20 min	16.6	18.1	17.8				
40 min	13.3	15.8	16.2				
60 min	15.0	16.3	16.5	5.8	2.146		
120 min	14.0	12.6	14.6				
NM-102				5.2	2.125	2.260	0.234
after 1 day	19.7	24.1	24.1	5.7	2.084		
20 min	21.6	20.2	23.3				
40 min	21.2	22.0	23.3				
60 min	19.6	20.4	22.1	5.6	2.156		
120 min	21.4	20.3	21.0				
P25. Nr. 0083				5.1	2.123	2.940	0.140
after 1 day	13.9	14.9	15.8	5.7	2.071		
20 min	14.4	17.1	23.2				
40 min	26.1	25.7	26.7				
60 min	22.4	22.1	25.0	5.7	2.118		
120 min	24.5	26.8	26.3				

\* Measurements were conducted with a concentration of 100 ppm



## AIV.6 Results carrier function triclocarban

### AIV.6.1 Soil Type A01

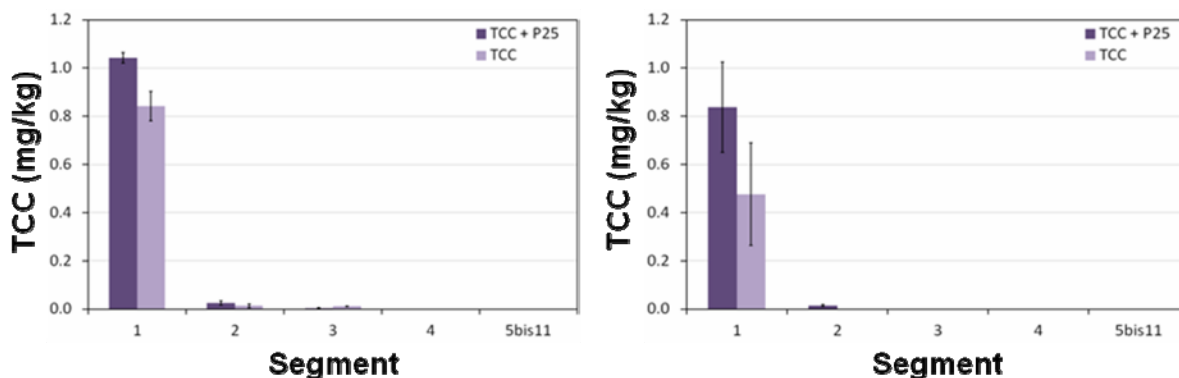


Figure 71: Triclocarban (TCC) concentration at the wall (outer cm, left) and in the core (right) of 1 cm soil segments taken from columns filled with soil of type A01 in absence of TiO<sub>2</sub> (n = 1) and presence (n = 2) of TiO<sub>2</sub> (P25). Analyses were performed 48 h after the upper segment of the soil column had been spiked with TCC and had been subjected to continuous surface sprinkling in that time frame. The whiskers represent the standard deviation on the mean of replicates and soil subsamples (3).

### AIV.6.2 Soil Type A02

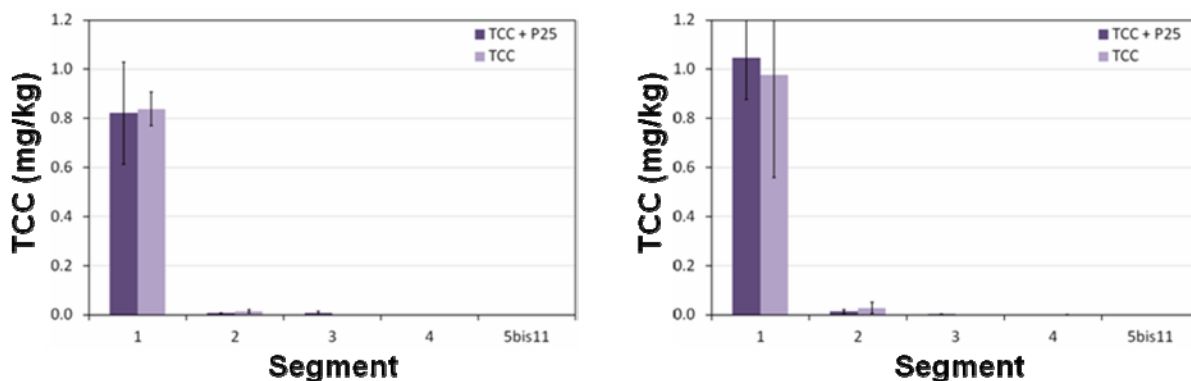


Figure 72: Triclocarban (TCC) concentration at the wall (outer cm, left) and in the core (right) of 1 cm soil segments taken from columns filled with soil of type A02 in absence of TiO<sub>2</sub> (n = 1) and presence (n = 2) of TiO<sub>2</sub> (P25). Analyses were performed 48 h after the upper segment of the soil column had been spiked with TCC and had been subjected to continuous surface sprinkling in that time frame. The whiskers represent the standard deviation on the mean of replicates and soil subsamples (3).

AIV.6.3 Soil Type G03

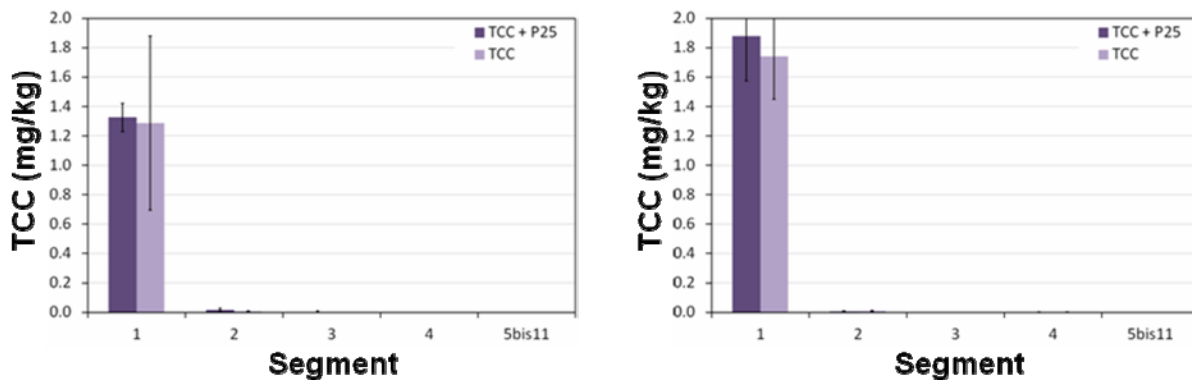


Figure 73: Triclorcarban (TCC) concentration at the wall (outer cm, left) and in the core (right) of 1 cm soil segments taken from columns filled with soil of type A02 in absence of TiO<sub>2</sub> (n = 1) and presence (n = 2) of TiO<sub>2</sub> (P25). Analyses were performed 48 h after the upper segment of the soil column had been spiked with TCC and had been subjected to continuous surface sprinkling in that time frame. The whiskers represent the standard deviation on the mean of replicates and soil subsamples (3).

## AIV.7 Results carrier function copper sulphate

### AIV.7.1 Soil type A01

Detected Cu in the different soil segments of soil type A01

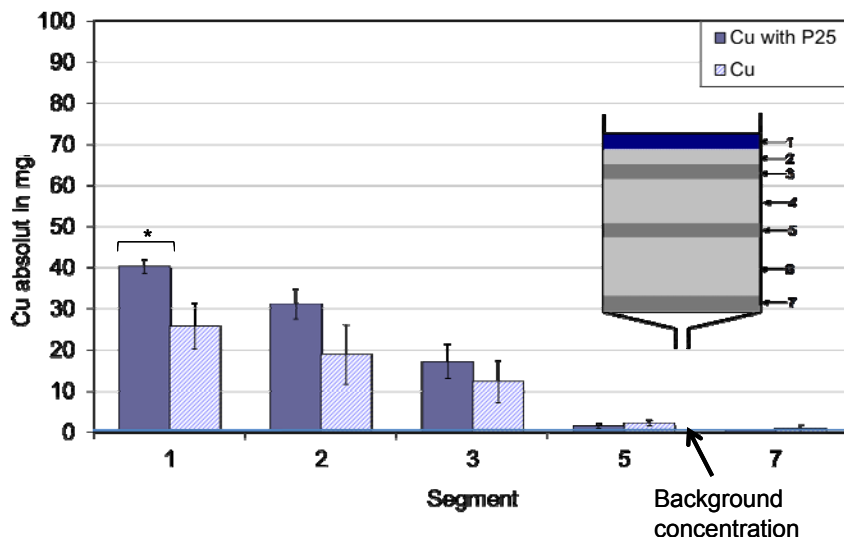


Figure 74: ICP-OES results of the copper concentration of the five different segments of the three columns. Reference system without P25 and test system with P25, soil type A01; n = 3.

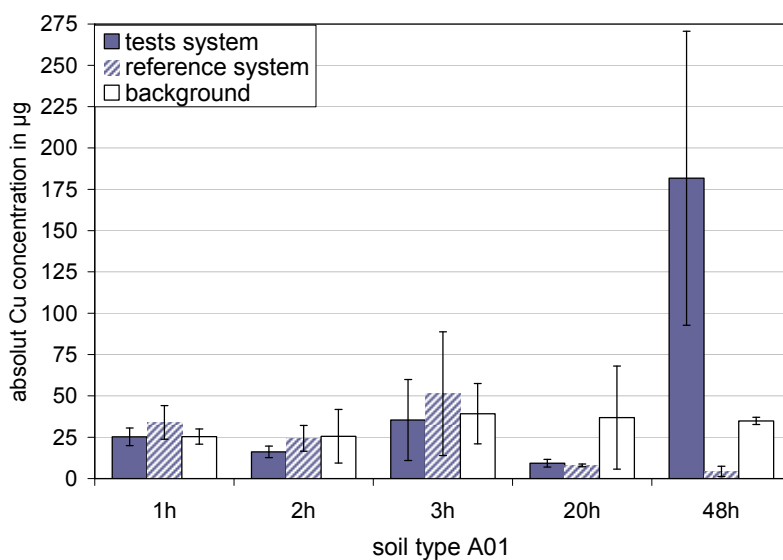


Figure 75: ICP-OES results of the copper concentration of the eluate at the five different time points of soil type A01, of the test system with P25, the reference system without P25 and the background; n = 3. An average amount of 186 mg Cu (SD 270) were applied to the soils.

### AIV.7.2 Soil type A02

Detected Cu in the different soil segments of soil type A02

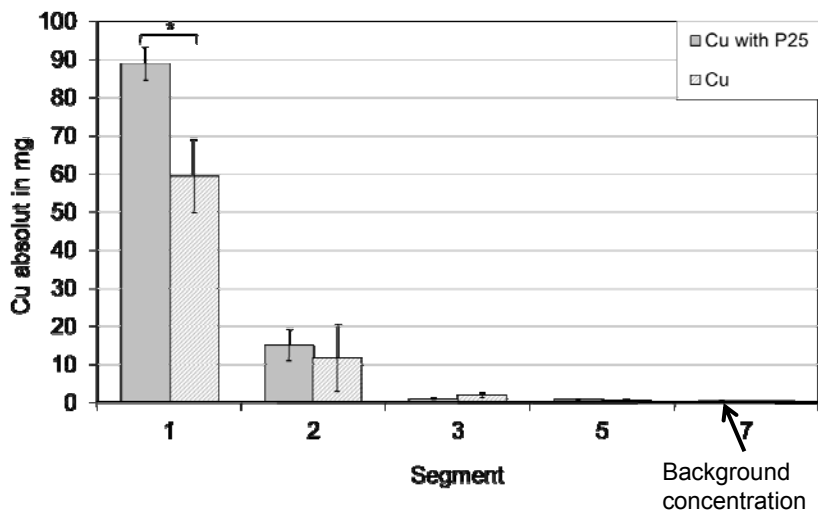


Figure 76: ICP-OES results of the copper concentration of the five different segments of the three columns. Reference system without P25 and test system with P25, soil type A02

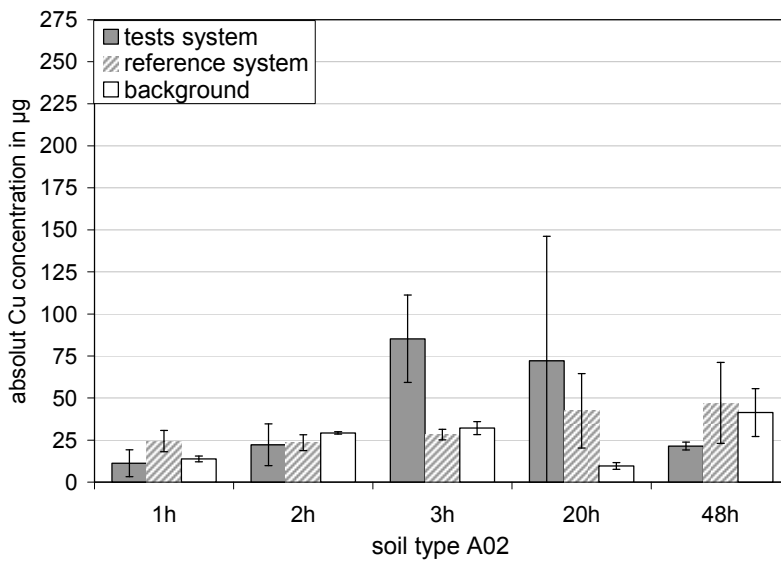


Figure 77: ICP-OES results of the copper concentration of the eluate at the five different time points of soil type A02, of the test system with P25, the reference system without P25 and the background; n = 3. An average amount of 186 mg Cu (SD: 270) were applied to the soils.

### AIV.7.3 Soil type G03

Detected Cu in the different soil segments of soil type G03

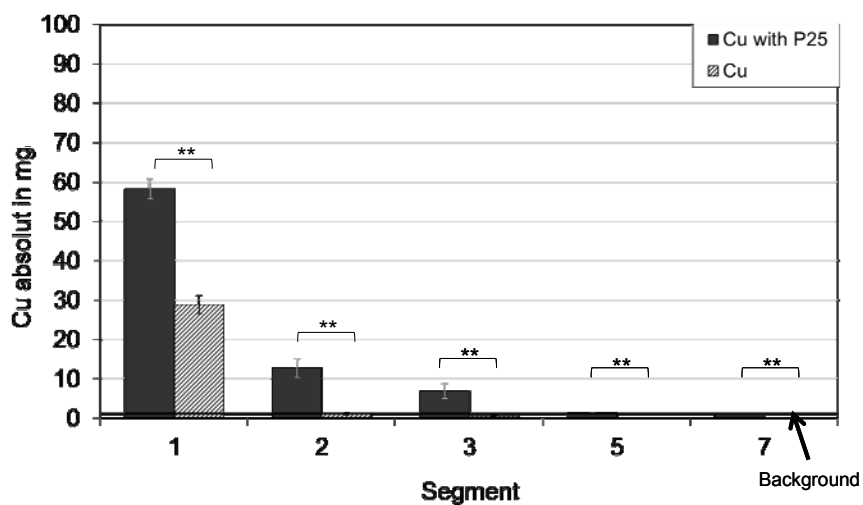


Figure 78: ICP-OES results of the copper concentration of the five different segments of the three columns. Reference system without P25 and test system with P25, soil type G03.

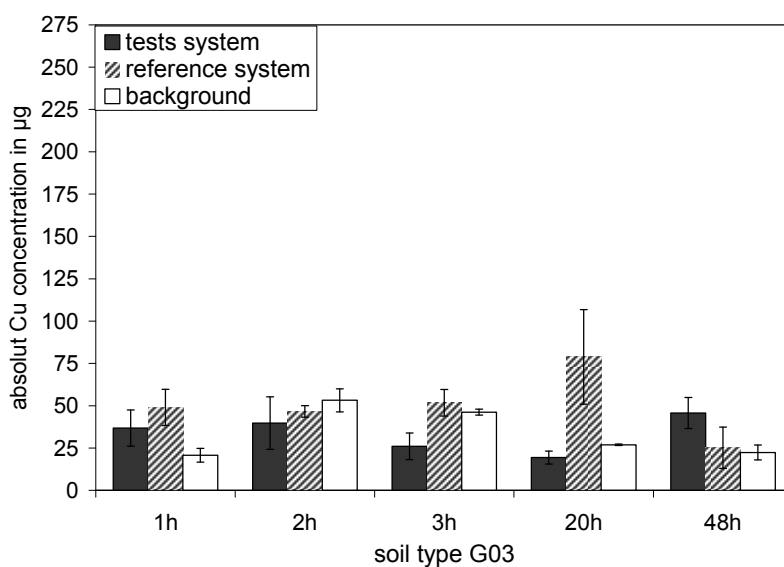


Figure 79: ICP-OES results of the copper concentration of the eluate at the five different time points of soil type G03, of the test system with P25, the reference system without P25 and the background; n = 3. An average amount of 186 mg Cu (SD: 270) were applied to the soils.

#### AIV.7.4 Eluate

Detected Cu in the eluate of the three soil types collected at 5 different time points

Table 70: Detection of Cu in the reference system without P25. Values are presented as percent of the added copper. The eluat was collected at different time points. Sample 1 = after 1h, sample 2 = after 2 h, sample 3 = after 3 h, sample 4 = after 18 h, sample 5 = after 48 h, ± = Standard Deviation; n = 3.

Without P25	Recovery in %		
Sample	A01	A02	G03
1	0.014% ± 0.005%	0.006% ± 0.003%	0.020% ± 0.006%
2	0.009% ± 0.004%	0.012% ± 0.003%	0.021% ± 0.002%
3	0.019% ± 0.020%	0.046% ± 0.002%	0.014% ± 0.004%
4	0.005% ± 0.000%	0.039% ± 0.012%	0.010% ± 0.015%
5	0.098% ± 0.002%	0.012% ± 0.013%	0.025% ± 0.007%

Table 71: Detection of Cu in the test system with P25. Values are presented as percent of the added copper. The eluat was collected at different time points. Sample 1 = after 1h, sample 2 = after 2 h, sample 3 = after 3 h, sample 4 = after 18 h, sample 5 = after 48 h, ± = Standard Deviation; n = 3.

With P25	Recovery in %		
Sample	A01	A02	G03
1	0.018% ± 0.003%	0.013% ± 0.004%	0.026% ± 0.006%
2	0.013% ± 0.002%	0.013% ± 0.007%	0.025% ± 0.008%
3	0.028% ± 0.013%	0.015% ± 0.014%	0.028% ± 0.004%
4	0.004% ± 0.001%	0.023% ± 0.040%	0.042% ± 0.002%
5	0.002% ± 0.048%	0.025% ± 0.001%	0.014% ± 0.005%

## AIV.8 Results titanium transport ICP-OES and SEM / EDX scans

### AIV.8.1 Soil type A01

#### Detected Ti in the different soil segments of soil type A01

With the ICP-OES measurements no significant transport of the titanium in the different segments of the soil columns could be detected. But with SEM / EDX scans transport of isolated agglomerates down to the last segments of the soil could be detected.

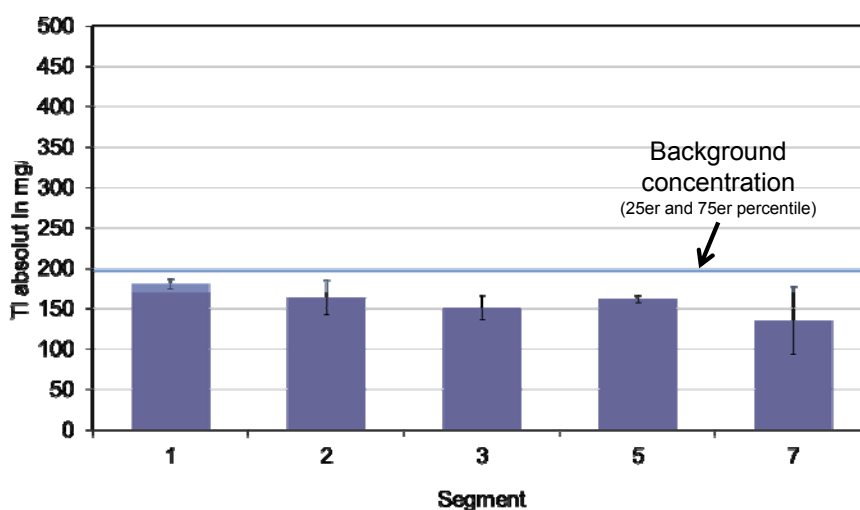


Figure 80: Ti concentration of the different segments of the soil type A01. The blue line shows the background concentration of the soil type; n = 3.

### AIV.8.2 Soil type A02

#### Detected Ti in the different soil segments of soil type A02

With the ICP-OES measurements no significant transport of the titanium in the different segments of the soil columns could be detected. But with SEM / EDX scans transport of isolated agglomerates down to the last segments of the soil could be detected.

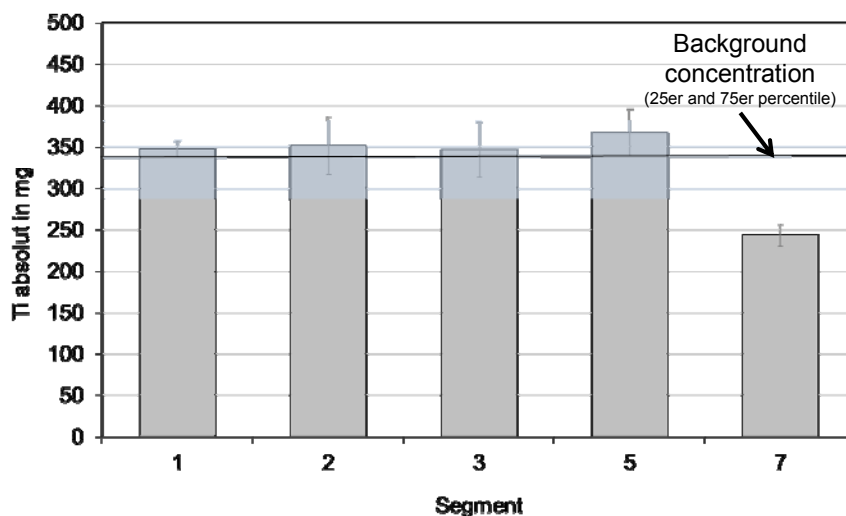


Figure 81: Ti concentration of the different segments of the soil type A02. The blue line shows the background concentration of the soil type; n = 3.

### AIV.8.3 Soil type G03

#### Detected Ti in the different soil segments of soil type G03

With the ICP-OES measurements in column 1 and column 2 a transport was indicated, but the detected concentration was in the range of the uncertainties of the measurements. With SEM / EDX scans transport of isolated agglomerates down to the last segments of the soil could be detected.

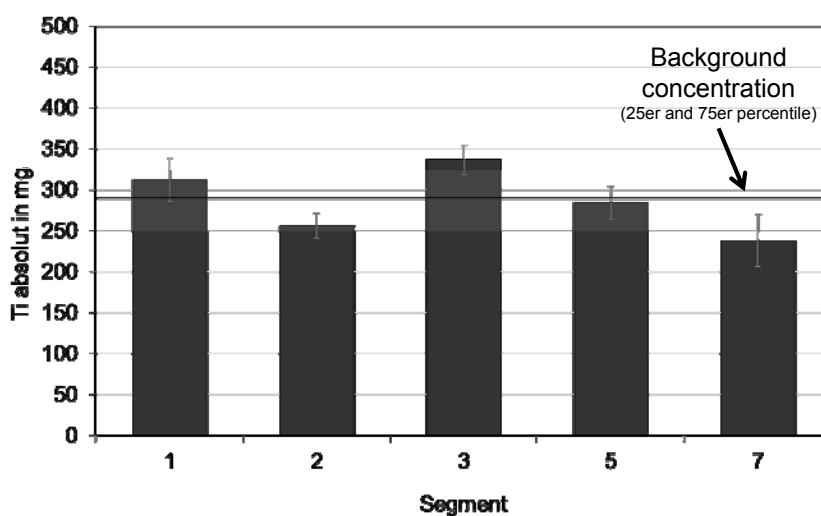


Figure 82: Ti concentration of the different segments of the soil type G03. The blue line shows the background concentration of the soil type; n = 3.



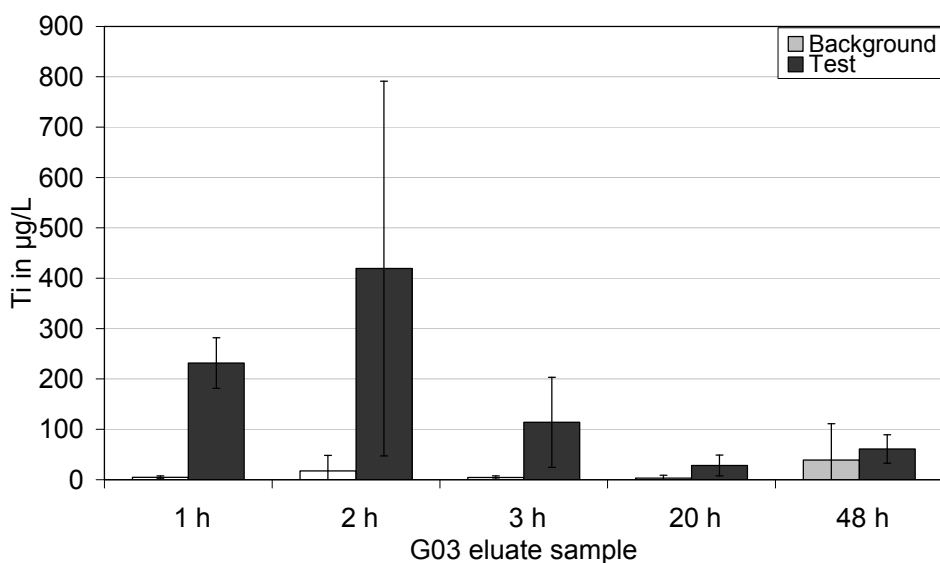


Figure 83: Titanium concentration in the eluate of the test and the background sample for soil type G03. Background, n = 2, test n = 3, error bars = min and max.

#### AIV.8.4 Eluate

#### Detected Ti in the eluate of the three soil types collected at 5 different time points

Table 72: Detection of P25 in the eluate of the three different soil types, Values are presented as percent of the added TiO<sub>2</sub>, The eluate was collected at different time points. Sample 1 = after 1h, sample 2 = after 2 h, sample 3 = after 3 h, sample 4 = after 18 h, sample 5 = after 48 h, ± = Standard Deviation; n = 5.

P25	Recovery in %		
	A01	A02	G03
Sample 1	<0.001% ± <0.001%	<0.001% ± <0.001%	0.021% ± 0.01%
Sample 2	<0.001% ± <0.001%	<0.001% ± <0.001%	0.052% ± 0.041%
Sample 3	0.001% ± 0.001%	<0.001% ± <0.001%	0.011% ± 0.008%
Sample 4	0.002% ± 0.001%	<0.001% ± <0.001%	0.010% ± 0.008%
Sample 5	0.001% ± 0.001%	<0.001% ± <0.001%	0.035% ± 0.014%

## AIV.9 SEM / EDX scans of different soil segments

### AIV.9.1 Soil type A01

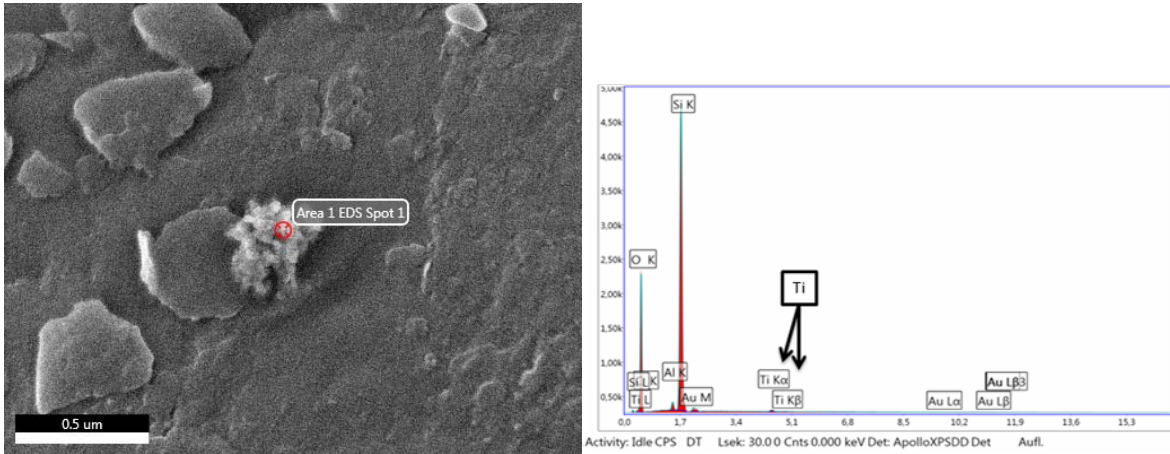


Figure 84: Soil type A01, column three, segment one.

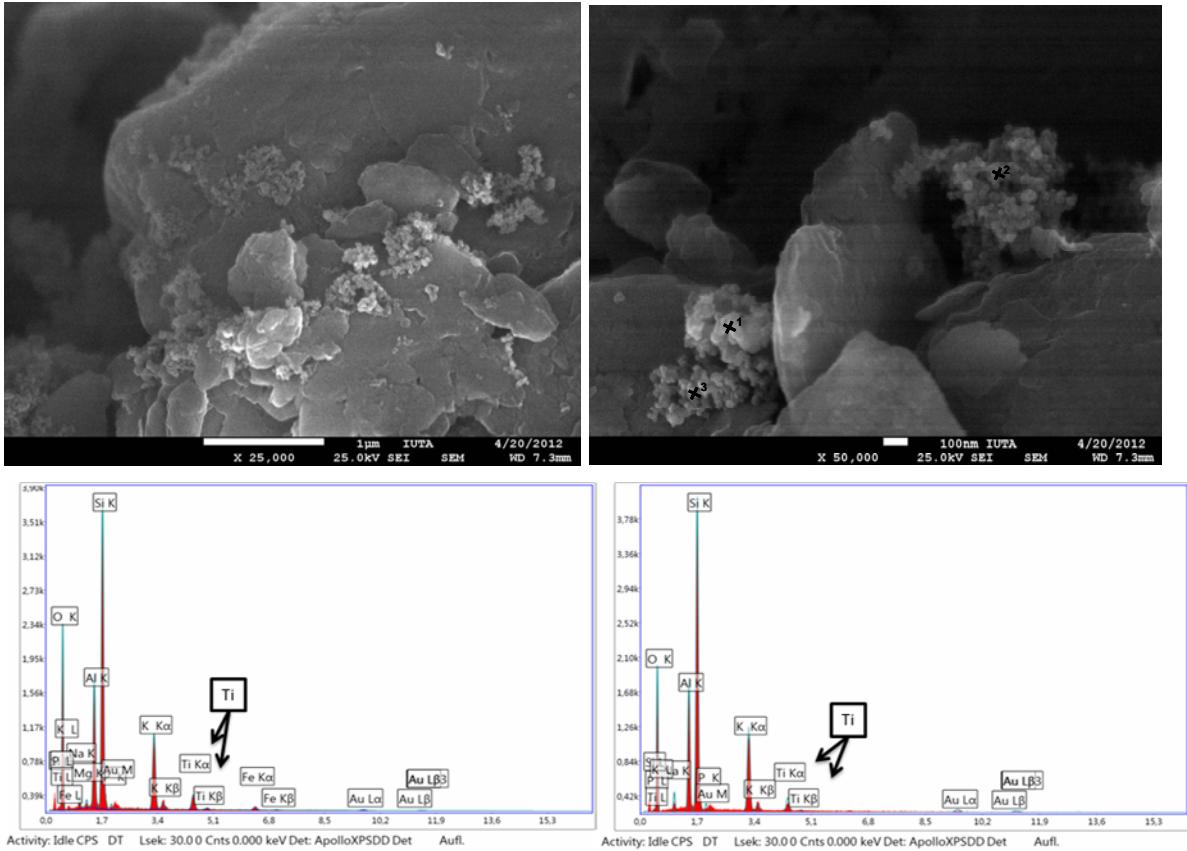


Figure 85: Soil type A01, column two, segment one.

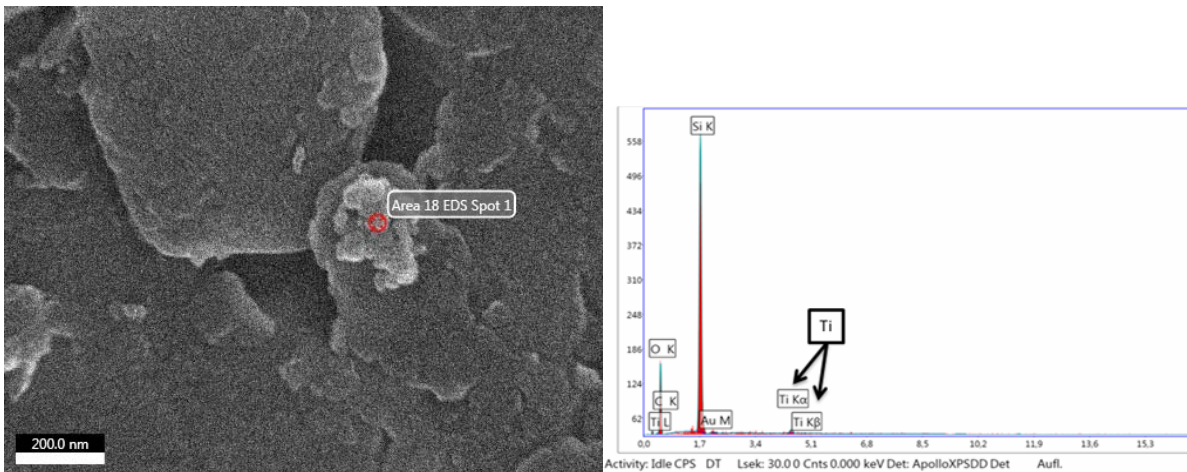


Figure 86: Soil type A01, column one, segment one.

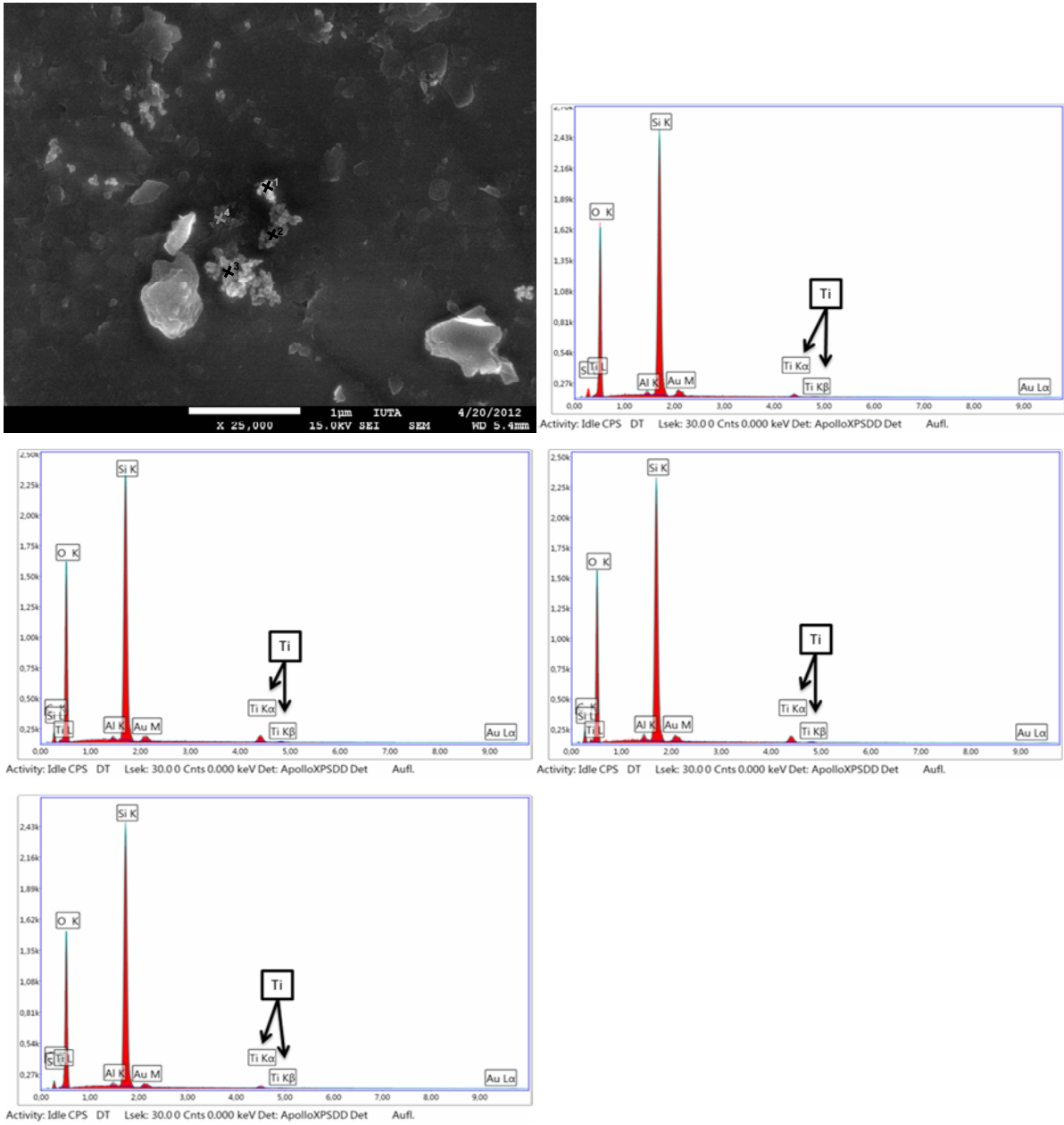


Figure 87: Soil type A01, column one, segment one.

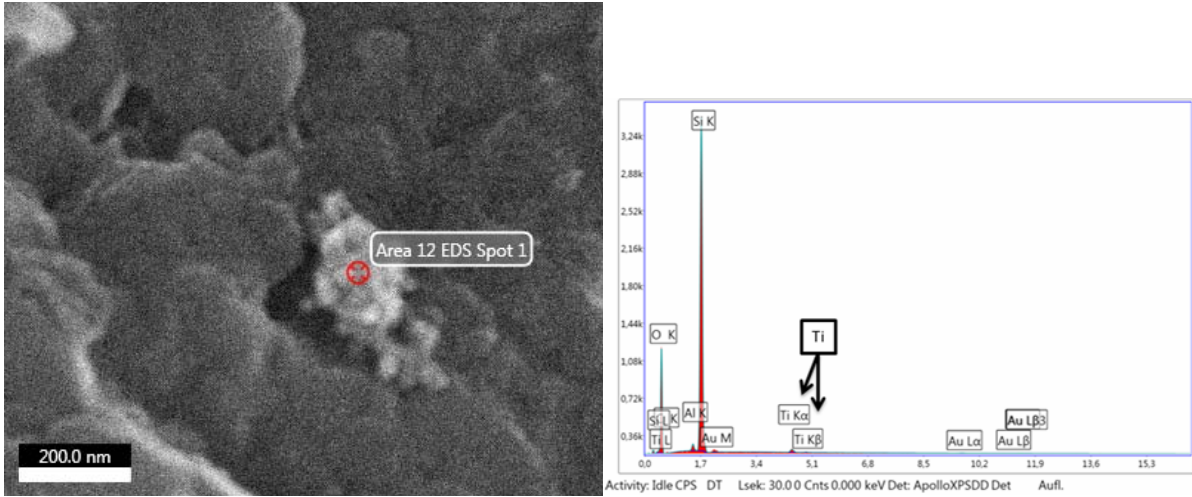


Figure 88: Soil type A01, column one, segment two.

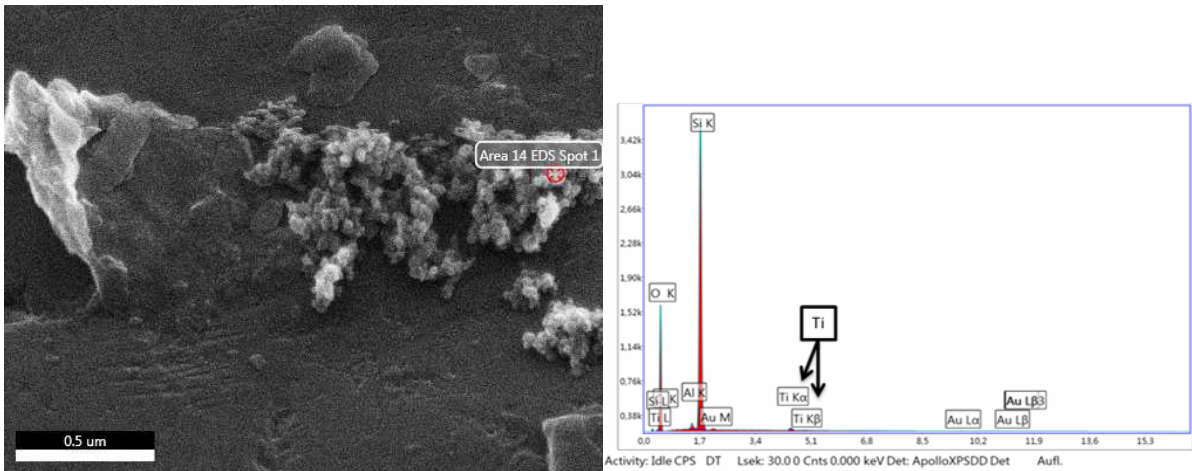


Figure 89: Soil type A01, column two, segment two.

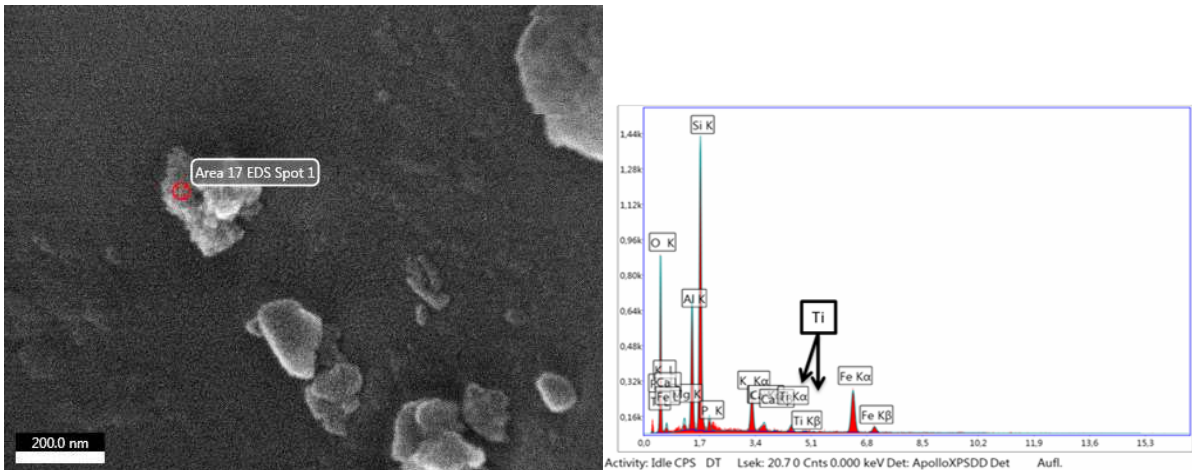


Figure 90: Soil type A01, column one, segment seven.

AIV.9.2 Soil type A02

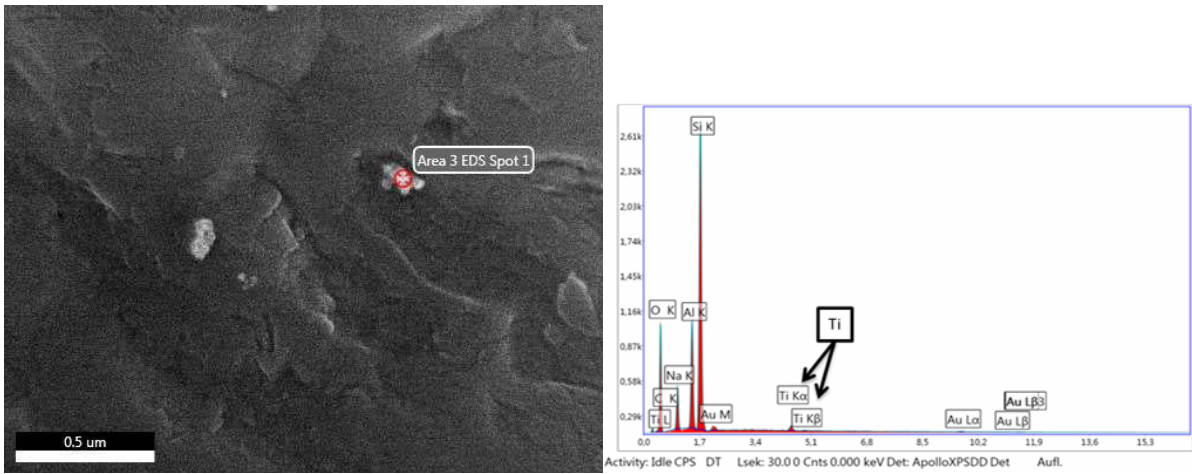


Figure 91: Soil type A02, column one, segment one.

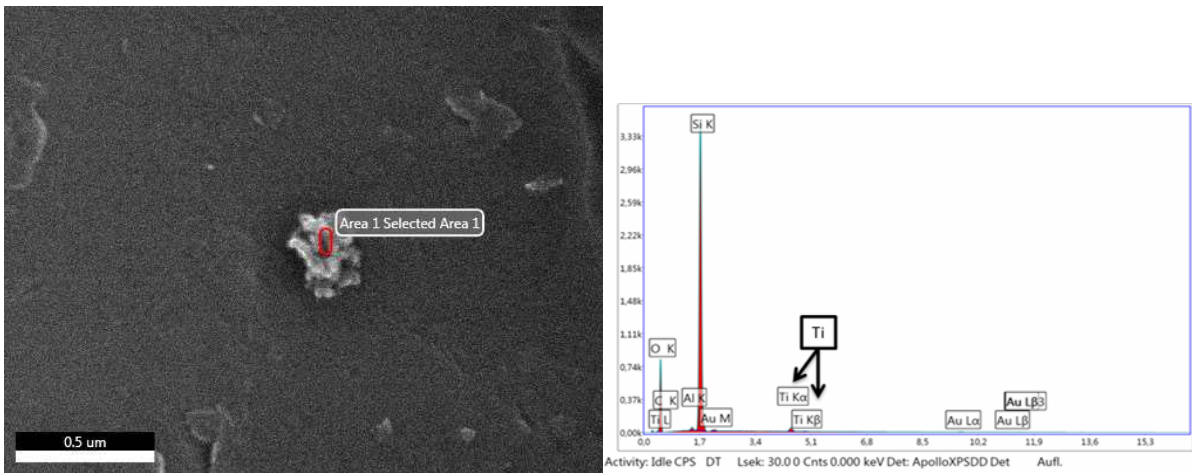


Figure 92: Soil type A02, column two, segment one.

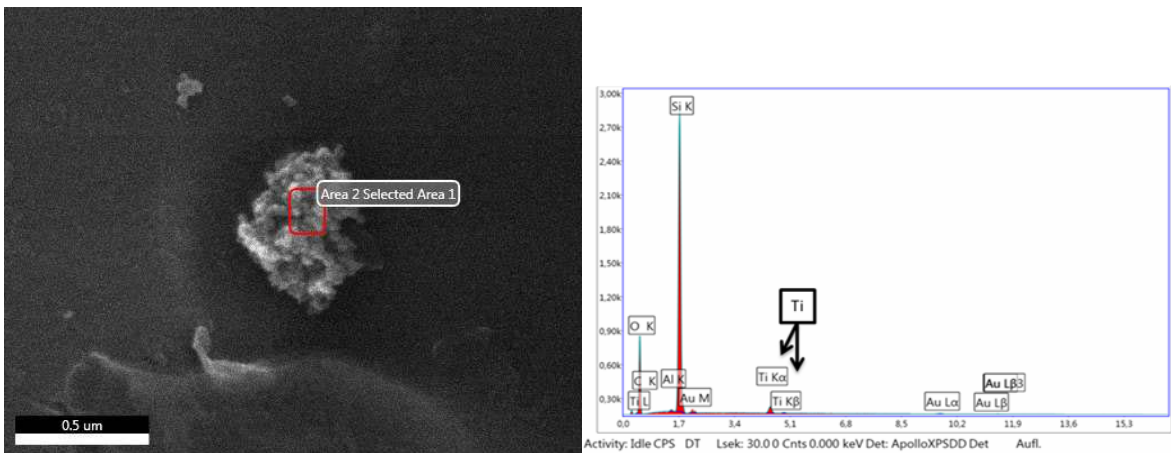


Figure 93: Soil type A02, column two, segment one.

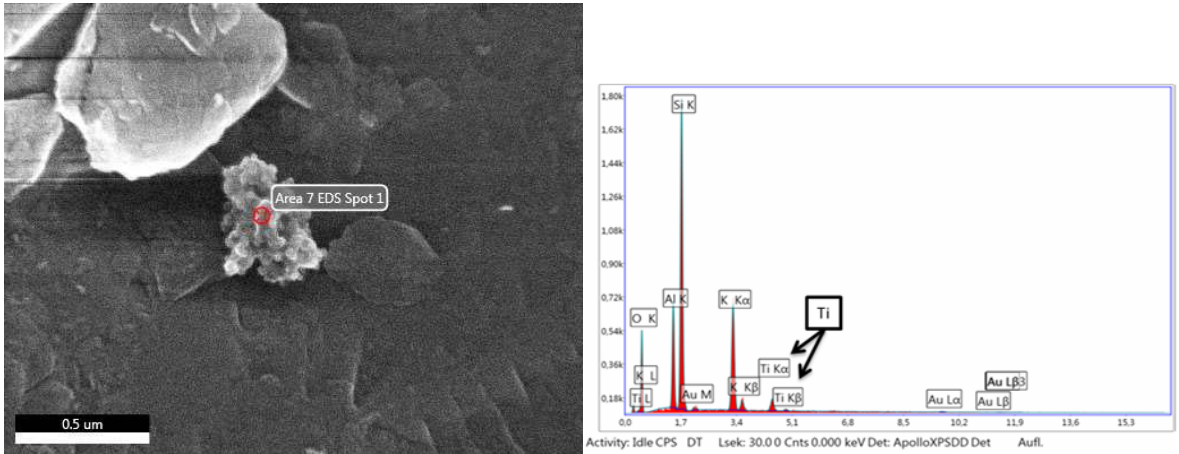


Figure 94: Soil type A02, column three, segment one.

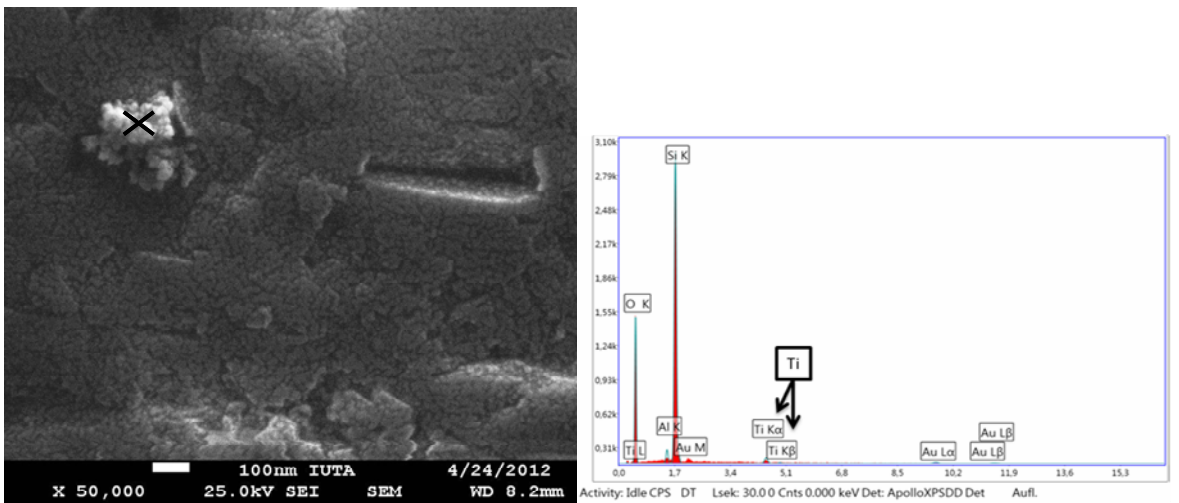


Figure 95: Soil type A02, column one, segment two.

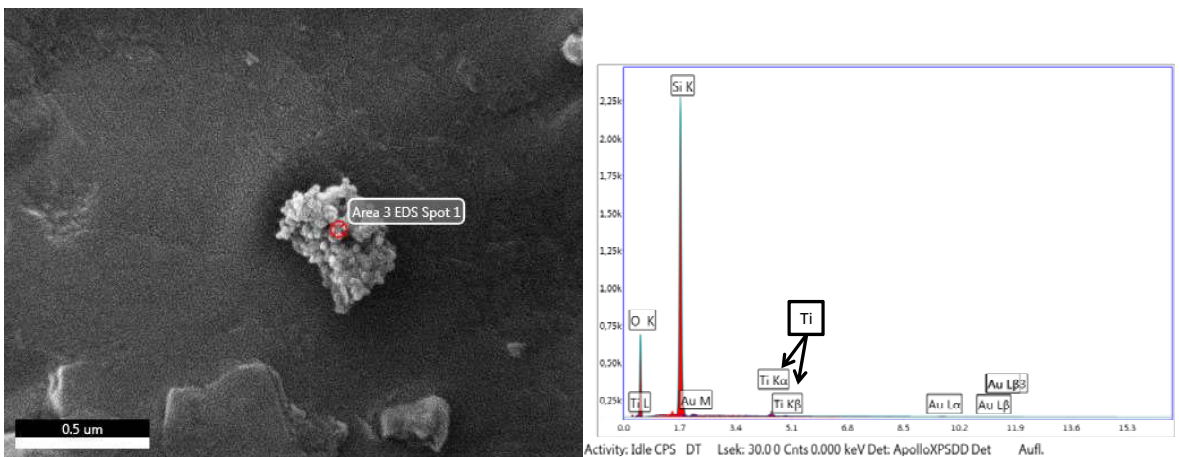


Figure 96: Soil type A02, column two, segment two.

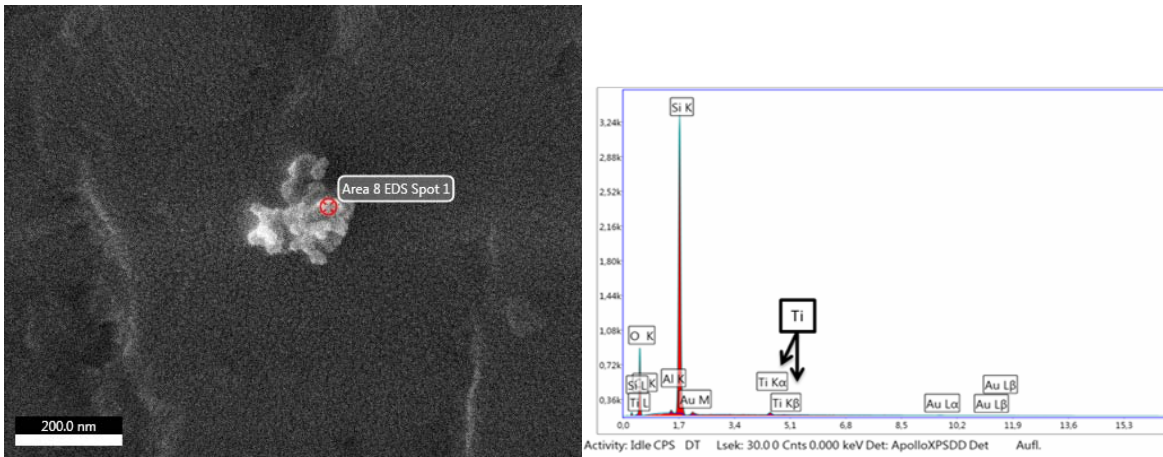


Figure 97: Soil type A02, column two, segment seven.

### AIV.9.3 Soil type G03

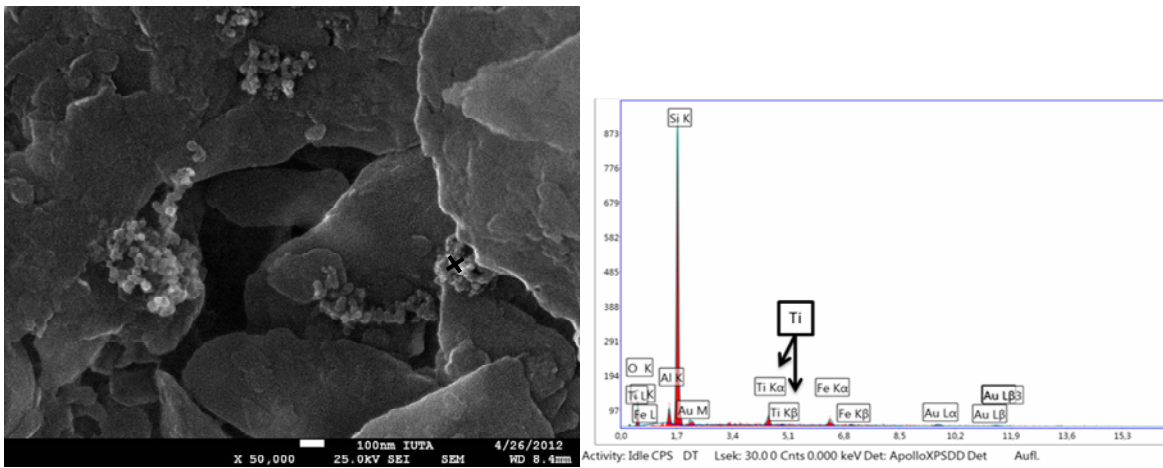


Figure 98: Soil type G03, column one, segment one.

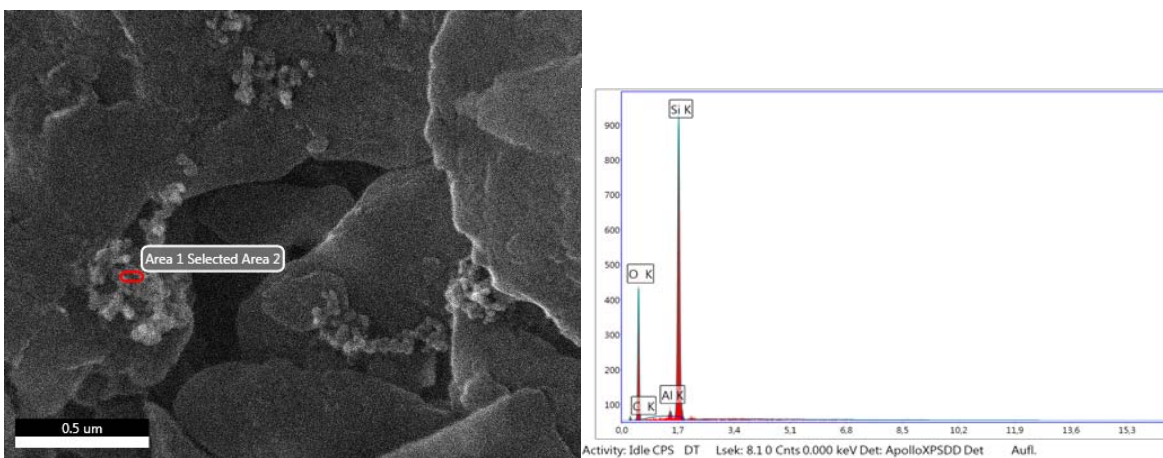


Figure 99: Soil type G03, column one, segment one, negative control.



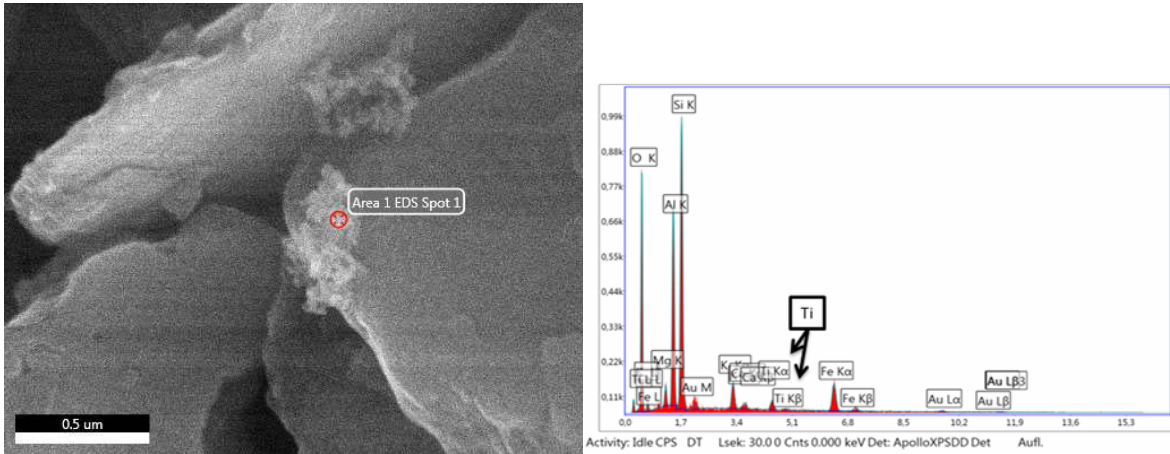


Figure 100: Soil type G03, column two, segment one.

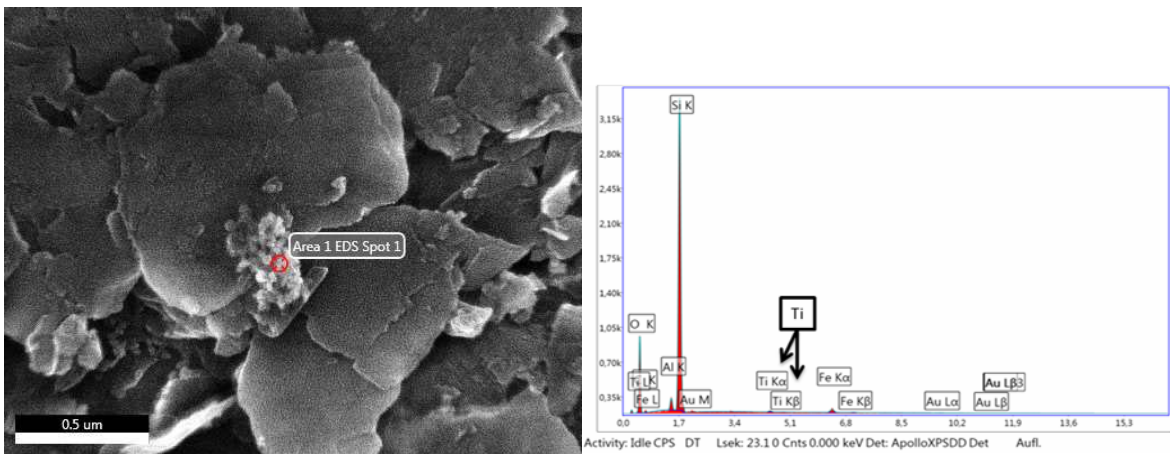


Figure 101: Soil type G03, column three, segment one.

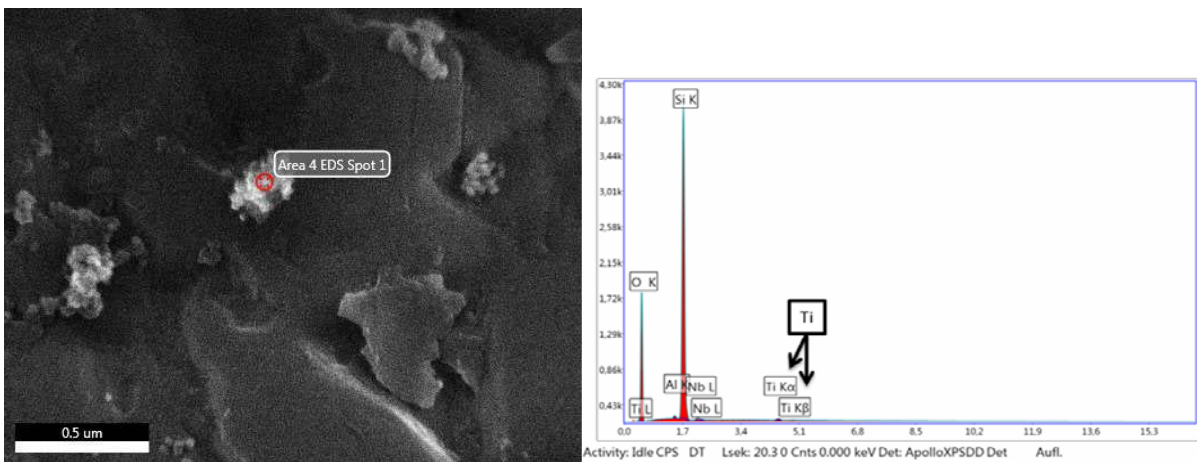
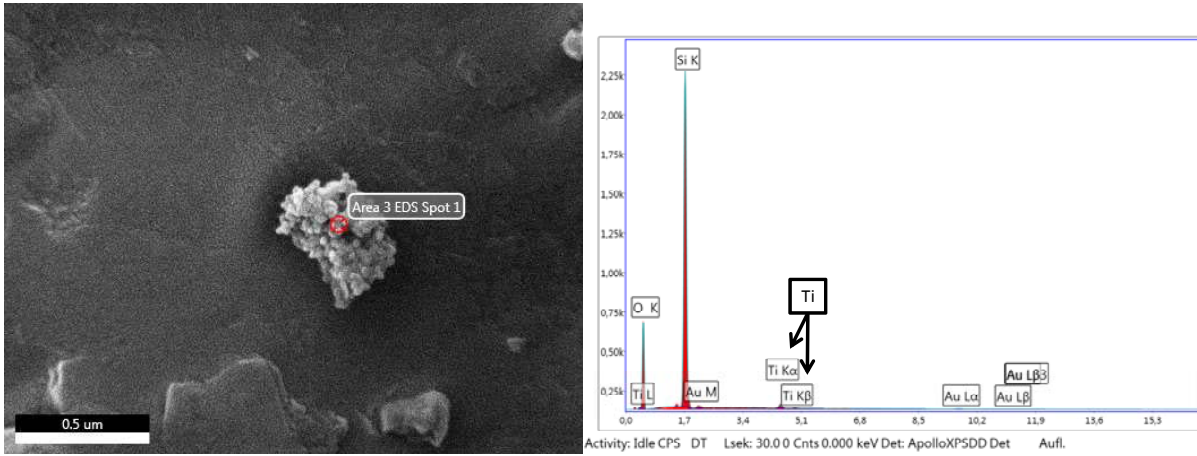


Figure 102: Soil type G03, column three, segment one.

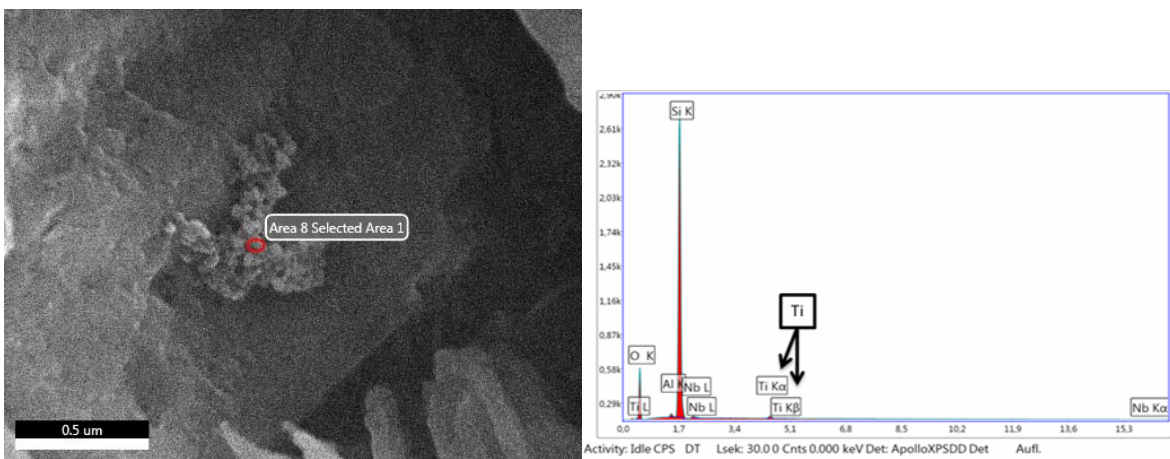


Figure 103: Soil type G03, column one, segment two.

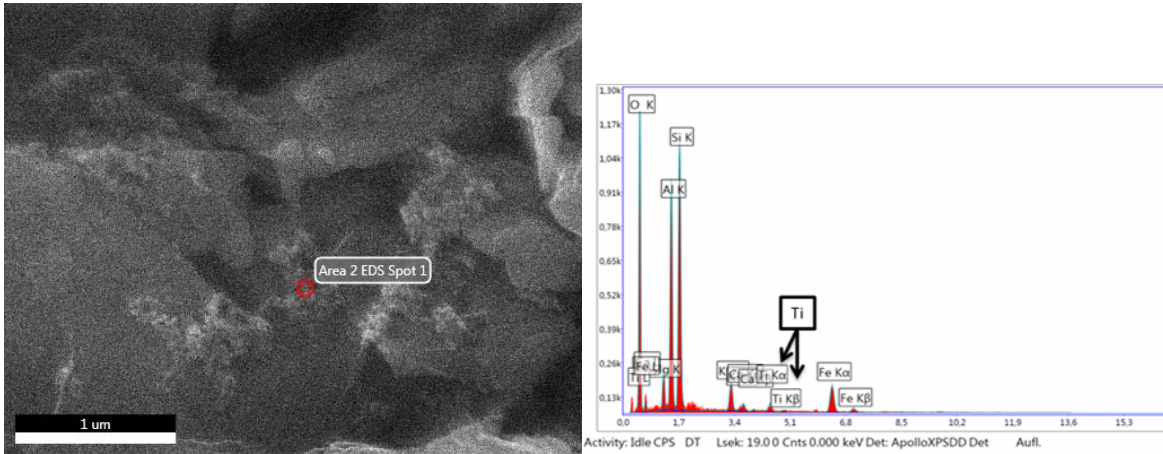


Figure 104: Soil type G03, column three, segment two.

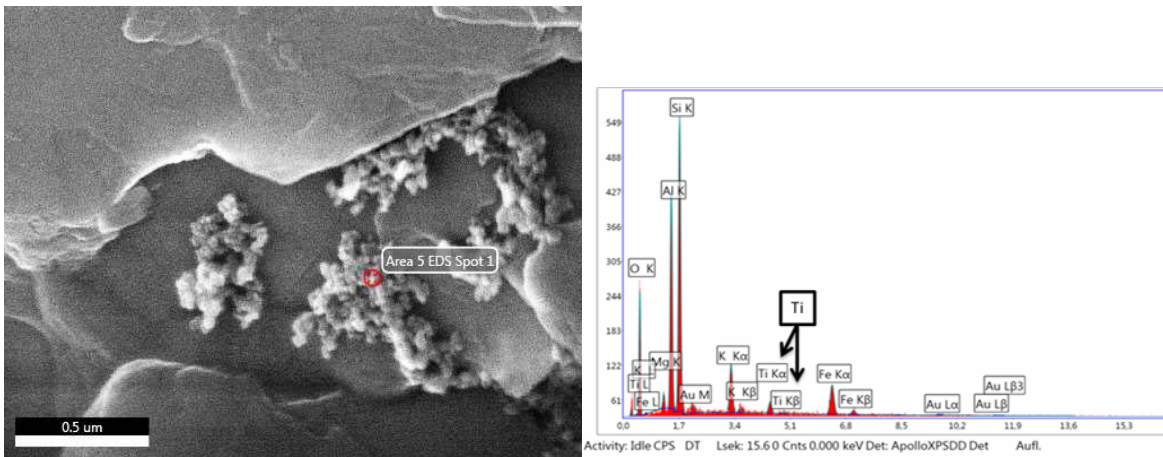


Figure 105: Soil type G03, column two, segment seven.